Bangor University

DOCTOR OF PHILOSOPHY

Prediction of the coverage and performance of the Datatrak low-frequency tracking system

Williams, Alwyn Idris

Award date:
2004

Awarding institution:
Bangor University

Link to publication

Prediction of the Coverage and Performance of the Datatrak Low-Frequency Tracking System

Thesis submitted in candidature for the degree of

Doctor of Philosophy

April 2004

Alwyn Idris Williams

• PRIFYSGOL CYMRU •
UNIVERSITY OF WALES

BANGOR

1884

School of Informatics

University of Wales

Bangor

United Kingdom

Acknowledgements

Summary

The Siemens Datatrak Automatic Vehicle Location System (AVLS) has been in operation for almost two decades. It provides a unique, reliable, and secure vehicle tracking solution for security applications such as cash-in-transit vehicles. There are several parts to an AVLS, one of which is the navigation system that actually determines the location of a vehicle.

Datatrak have developed and operate a navigation system based on a network of low powered, low frequency (LF), transmitters around the area of interest. It also provides the timing requirements for the whole system. Designing a new network is fraught with complex issues that need to be resolved to ensure optimum use is made of the design. Until recently, most of the design work to establish the coverage and performance of the network had been made by manual means, using the vast experience of engineers and rules-of-thumb as guidance. This costs time and money.

This research reviews the methods used by the engineers with a view to improving them using computer modelling techniques. Some of the coverage and performance factors have already been computer-modelled in recent research studies. These principles have, for the first time, been applied to the Datatrak system.

However, the results of this research go further than those of computer models of other LF navigation systems. The amount of uncertainty in the position fix can now be predicted using novel techniques. Further, Datatrak engineers have never been able to predict accurately the actual propagation delays between transmitters and receivers. This shortcoming has been overcome by applying to Datatrak novel techniques recently developed for predicting Loran-C Additional Secondary Factors (ASFs). The model has then been further developed to predict for the first time the absolute accuracy of the positions, plus the 'confidence factor', a measure of how well multiple measurements align. This unique model will enable Datatrak engineers to see which areas need more attention. All this can be done before the first mast has been erected.

The final implementation of the model is a Windows-based software suite that will enable Datatrak engineer to control the model easily and apply different scenarios.

Abbreviations

ADC	Analogue-to-Digital Converter
AM	Amplitude Modulation
ASF	Additional Secondary Factor
ASIC	Application-Specific Integrated Circuit
AVLS	Automatic Vehicle Location System
BANDPASS	Bangor Datatrak Performance Analysis Software Suite
BBC	British Broadcasting Corporation
BR IFIC	Bureau des Radiocommunications, International Frequency Information Circular
CF	Confidence Factor
CS	Commercial Service
DGPS	Differential Global Positioning System
DMA	Direct Memory Access
DSB	Double Sideband
DTED	Digital Terrain Elevation Database
ERP	Effective Radiated Power
ESA	European Space Agency
ETS	European Telecommunications Standard
EU	European Union
FDR	Frequency Dependent Rejection
FM	Frequency Modulation
FSK	Frequency-Shift Keying
GDR	Groundwave-to-Disturbance Ratio
GMT	Greenwich Mean Time
GNSS	Global Navigation Satellite System
GPRS	General Packet Radio Service
GPS	Global Positioning System
GSM	Global System for Mobile Communication
HDOP	Horizontal Dilution of Precision
ID	Interval Distance
IF	Intermediate Frequency
IFL	International Frequency List

IP	Ingress Protection
ITU	International Telecommunication Union
LEO	Low Earth Orbit
LF	Low Frequency
LHS	Left-Hand Side
LO	Local Oscillator
LOP	Line of Position
MEO	Medium Earth Orbit
MF	Medium Frequency
MSDOS	Microsoft Disk Operating System
NIMA	National Imagery and Mapping Agency
OS	Open Service
PD	Propagation Delay
PEP	Peak Envelope Power
PF	Primary Factor
PPP	Public-Private Partnership
PRN	Pseudo-Random Noise
PSD	Power Spectral Density
QPSK	Quadrature Phase Shift Keying
RC	Resistor/Capacitor
RHS	Right-Hand Side
RMS	Root Mean Squared
SA	Selective Availability
SF	Secondary Factor
SGR	Skywave-to-Groundwave Ratio
SIM	Subscriber Identity Module
SIR	Signal-to-Interference Ratio
SMS	Short Message Service
SNR	Signal-to-Noise Ratio
SPO	Station Phase Offset
SSB	Single Sideband
SSB-SC	Single Sideband, Suppressed Carrier
TD	Time Difference

TOA	Time of Arrival
UHF	Ultra High Frequency
UK	United Kingdom
US	United States
USGS	United States Geological Survey
VHF	Very High Frequency
VL	Virtual Locator
VLF	Very Low Frequency
WGS84	World Geodetic System 1984
WHDOP	Weighted Horizontal Dilution of Precision

List of Symbols

ϕ	Instantaneous groundwave phase disturbance
λ	Free space wavelength
μ	Scaling factor
ϕ_i	Latitude of ith point
λ_i	Longitude of ith point
ϕ_{new}	New latitude
λ_{new}	New longitude
ϕ_o	Original latitude
λ_o	Original longitude
ε_r	Complex permittivity
$\varepsilon_X, \varepsilon_Y, \varepsilon_Z$	Rotational factors
$\varepsilon_{linkbias,N_s}$	Link bias error for N_s^{th} station
$\varepsilon_{V_p,i-1,i}$	V_p error between the ith-1 and i^{th} stations in chain
ε_{V_p}	Link bias error
a	Mean radius of earth
A	Directional cosines matrix
a_{axis}	Semi-major axis length
A_{dB}	Attenuation of groundwave signal in dB
A_{gain}	Antenna gain of interferer antenna structure
A_i	Attenuation of groundwave signal in the ith section
A_{PS}	Area of power spectrum
b	Interferer bandwidth
b_{axis}	Semi-minor axis length
$B_{i,j}$	i^{th} and j^{th} coefficient in calculating F_{am}
$b_{j,k}$	j^{th} and k^{th} coefficient for calculation of F_{am}
$b_{receiver}$	Bandwidth of receiver
c	Speed of light in vacuum
C	Field strength of groundwave signal 1 km from 1 kW transmitter
$C(N,I)$	Range factor
CF	Confidence factor

c_i	i^{th} groundwave propagation curve polynomial
C_i	i^{th} calculated range
C_{sky}	Skywave field strength constant
d	Range from transmitter in km
d_m	Magnitude of disturbance vector
D_m	Disturbance vector
D	Interval distance
d_c	Chord distance
d_i	Length of ith section in Millington's method
D_ℓ	Lower decile of atmospheric noise field strength
D_u	Upper decile of atmospheric noise field strength
D_x	Magnitude of disturbance vector in x direction
D_y	Magnitude of disturbance vector in y direction
E	Measured field strength in mV/m
$E(ND,ID)$	Effective surface impedance
$E[X^n]$	n^{th} moment of the probability distribution of the random variable X
E_{1kW}	Annual median night-time field strength of 1 kW transmitter in dB-µV/m
e^2	Eccentricity squared
$E_{atmospheric}$	Median atmospheric noise field strength
E_{block}	Blocking field strength of Locator
$E_{Datatrak}$	Datatrak signal field strength
E_{edge}	Skywave field strength at edge of network boundary
E_{ground}	Groundwave field strength
E_I	Field strength of interferer signal in space
E_{Ieff}	Effective interferer field strength in dB-µV/m
E_{max}	Maximum skywave field strength
$E_{noisefloor}$	Mk4 Locator noise floor
$E_{primary}$	Field strength of primary factor
E_{sea}	Attenuation of signal over seawater
E_{sky}	Median skywave field strength
$E_{vehicle}$	Median vehicle noise field strength
f	Interferer frequency

F	Signal frequency
f_0	RC Filter cut-off frequency
f_1	Highest Datatrak centre frequency in given network
f_{1-}	Frequency of the highest Datatrak centre frequency with negative phase modulation
f_{1+}	Frequency of the highest Datatrak centre frequency with positive phase modulation
f_2	Lowest Datatrak centre frequency in given network
f_{2-}	Lowest Datatrak centre frequency with negative phase modulation
f_{2+}	Lowest Datatrak centre frequency with positive phase modulation
f_a	Frequency range within interferer bandwidth
f_{AA}	Nearest frequency to multiple of sampling frequency
f_{ADC}	Nearest frequency to multiple of over-sampling frequency
F_{am}	Noise strength given in dB above thermal noise
f_c	Interferer centre frequency
FDR_{dB}	Frequency-dependent rejection in dB
FDR_{side}	Frequency-dependent rejection of sidebands in dB
f_e	Flattening of ellipsoid
f_{MHz}	Signal frequency in MHz
f_r	Receiver tuned frequency
F_s	ADC Sampling frequency
$f_{\Delta t}$	Difference between interferer frequency and tuned frequency
g	Magnitude of groundwave vector
$G(r)$	Complex attenuation factor at calculation point at range r
$G(R)$	Complex attenuation factor at receiver
G_{AA}	Anti-aliasing filter frequency response
G_{ant}	Antenna gain factor in dB
G_{basic_sea}	Basic sea gain
G_{DF}	Trigger/Data digital filter frequency response
GDR_{dB}	Groundwave-to-disturbance ratio in dB
Gnd_{dB}	Groundwave field strength for a 1 kW transmitter
G_{NF}	Navigation digital filter frequency response
G_{RC}	RC Filter frequency response

G_s	Sea gain in dB
G_{static}	Frequency response of the static, front-end, filters of Mk4 Locator
h	Ionosphere height
H	Covariance matrix
$H(f)$	Frequency response of the Mk4 Locator
$HDOP$	Horizontal dilution of precision
$HDOP_{min}$	Minimum HDOP value
H_{ij}	Element in i^{th} column and j^{th} row in matrix H
I	Iteration counter
j	Imaginary number operator
k	Dielectric constant
k_{geo}	Geomagnetic latitude variable
K_i	i^{th} coefficient in calculating F_{am}
L_a	Ionospheric loss factor
ld	Logarithm of range in km.
m	Harmonic order
M	Number of millicycles
n	Number of measurements
N	Number of iterations
N_i	Curvature radius in the prime vertical at the ith point
N_s	Number of slaves in chain
O_i	i^{th} observed range
p	Slant propagation distance
P	Total interferer power within its bandwidth
$p(f)$	Power spectrum of interfering signal at the equivalent intermediate frequency
$P(f)$	Power spectrum of interfering signal
$P_{carrier}$	Normalised interferer carrier power
$P_n(f)$	Normalised interferer power spectrum
P_r	Radiated power in kW
$PSD_{gradient}$	Gradient of power spectral density as a function of frequency
PSD_{peak}	Peak power spectral density
$P_{sideband}$	Normalised interferer sideband power

P_{Watts}	Radiated power in Watts
r	Range from transmitter to calculation point
R	Range of receiver from transmitter
$\bar{R}$	Mean residue
RA_{2DRMS}	Twice the root mean square of position uncertainty
r_{gd}	Groundwave-to-disturbance ratio
r_i	Range to i^{th} station
R_i	Residue of ith measurement
$R_{Locator}$	Range over ellipsoid defined by Locator
SF_{f1}	f_1 secondary factor value
SF_{f2}	f_2 secondary factor value
SGR	Skywave-to-Groundwave Ratio in dB
SIR	Signal-to-Interference Ratio in dB
SNR_i	Signal-to-noise ratio of the ith measurement
T	Transpose operator
$t_{additional}$	Additional delay due to non-linear propagation effects
$t_{monteath}$	Phase delay calculated by Monteath's method
$Total_{dB}$	Faded groundwave field strength in dB-μV/m
$t_{primary}$	Primary factor phase delay
t_{prop}	Total propagation time between master clock and Locator
$t_{prop,N}$	Total propagation delay between master clock and Locator, via station N
t_{total}	Total phase delay
$t_{S_{Locator}}$	Slave secondary factor delay at Locator
$t_{M_{Locator}}$	Master secondary factor delay at Locator
$t_{M_{slave}}$	Master secondary factor delay at slave station
$t_{total_{i-1,i}}$	Total phase delay between i^{th}-1 and i^{th} stations in chain
$t_{stationdelay_i}$	Station delay at the ith station
t_{SPO_i}	Station phase offset at the ith station
$t_{total_{N_s,Locator}}$	Total phase delay between the last station in chain and the Locator
t_{V_p}	Phase delay assuming constant propagation velocity, V_p

V_{dBm}	Voltage in dBm
V_p	Mk4 Locator assumed propagation velocity of groundwave signals
V_{peak}	Peak voltage
v_x	Magnitude of disturbance vector in x direction
v_y	Magnitude of disturbance vector in y direction
W	Weight matrix
$WHDOP$	Weighted horizontal dilution of precision
w_i	i[th] weighting factor
x	Latitude expressed in radians north of south pole.
x_a	Frequency factor in calculating atmospheric noise
X_k	Coefficient to remove discontinuities at Greenwich meridian
y	Longitude expressed in radians east of Greenwich meridian
z	F_{am} value from atmospheric noise maps
α	Coefficient to ensure single value at poles
α_{geo}	Geographical latitude
β	Coefficient to ensure single value at poles
β_0	Free space propagation constant
β_{geo}	Geographical longitude
δb	Measurement vector
ΔB	Change in the clock bias
Δd	Difference in distance between groundwave and skywave signals
Δf	Difference between the interferer and receiver centre frequencies
Δt	Time difference between groundwave and skywave signals
δx	Change in position vector
Δx	Change in the x direction
$\Delta X, \Delta Y, \Delta Z$	Shifts in origin
Δy	Change in the y direction
η	Surface impedance
η_0	Intrinsic impedance of free space
η_{air}	Refractive index of air
θ	Phase of disturbance vector relative to groundwave vector
ξ	Phase retardation
σ	Surface conductivity

σ_ϕ	Standard deviation of the variable ϕ
σ_d	Standard deviation of the range uncertainty
σ_p	Standard deviation in position uncertainty
σ_x	Standard deviation of range uncertainty in x direction
$\sigma_{x,i}$	Standard deviation of ith range uncertainty in x direction
σ_y	Standard deviation of range uncertainty in y direction
$\sigma_{y,i}$	Standard deviation of ith range uncertainty in y direction
σ_θ	Standard deviation of the variable θ
φ	Bearing of station from receiver
ψ	Earth curvature and terrain height factor
ω_{LO}	Local oscillator (tuned) frequency
ω_s	Signal frequency
Φ	Geomagnetic latitude

Table of Contents

CHAPTER 4
GROUNDWAVE FIELD STRENGTH

CHAPTER 5
SKYWAVE FIELD STRENGTH

CHAPTER 9
REPEATABLE ACCURACY

CHAPTER 12
CONCLUSIONS

APPENDICES

Chapter 1

Introduction

The Datatrak[1] Automatic Vehicle Location System (AVLS) has been in operation since 1989. It began as a commercial venture between Securicor and Wimpey, who required a secure, reliable method of tracking vehicles in real-time in the UK. Securicor is a commercial organisation that specialises in high security transport. For example, part of their service is the transportation of millions of pounds worth of cash every day in the UK [1]. Clearly, a system that can track these vehicles if they were stolen would be of great benefit. So, in order to maintain the security and reliability of the AVLS, the system was built from scratch and maintained by the operating company, formally known as "Datatrak". In May 2000, the AVLS was taken over by Siemens, and the operating company became Siemens Datatrak Ltd.

The AVLS comprises the three major parts as shown in Fig. 1.1: the timing and navigation system, the communications system, and the display system.
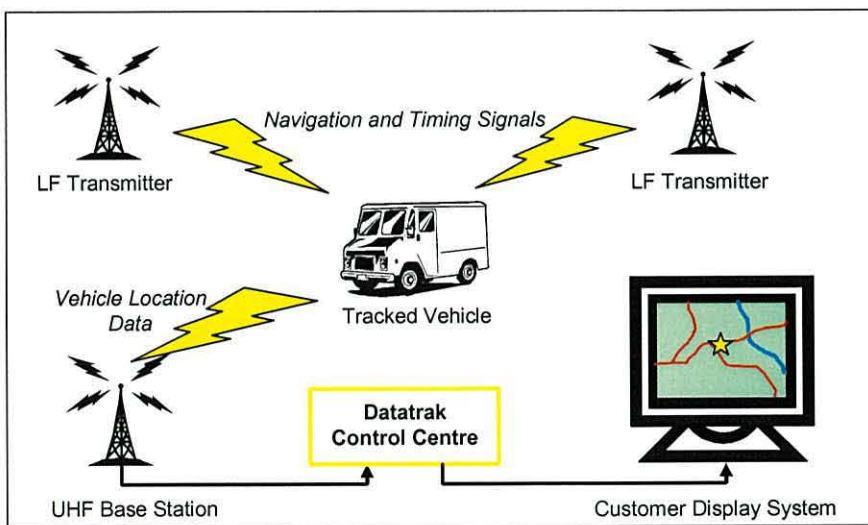
Fig. 1.1 - Overview of Datatrak Automatic Vehicle Location System

---

[1] In this thesis, "Datatrak" can refer to the system, or the name of the operating company.

The navigation system is the section that determines the locations of the vehicles. It also provides the timing and synchronisation needs of the system. To ensure reliability, especially in city centres, low frequency (LF) technology is used. The navigation system was designed by former engineers of another LF navigation system, Decca Navigator, who used their expertise and experience to best effect in the design. Unsurprisingly, many of the techniques used in the Datatrak system are derived from the Decca and related systems. The result was a 13-station UK network that covers 95 % of all road traffic, even in the urban canyons of city centres. The system has since expanded to several other countries.

Once the location of the vehicle has been calculated, position information is relayed back to the Datatrak Control Centre via multiple ultra high frequency (UHF) base stations. The system's reliability is ensured by the high number of these base stations. The control centre then forwards the information to the correct customer.

Vehicles' positions are displayed on maps, together with other information generated on-board the vehicle (e.g. status, messages). Datatrak provides a two-way communications system via the UHF sub-system, which means that the customer may also send information to the vehicle.

Planning a brand-new Datatrak network is not a trivial task. Two separate radio systems must be designed: the LF timing and navigation system, and the UHF communications system. Great care is required to ensure maximum coverage in the area of interest.

In this thesis, we shall concentrate on the planning of the LF timing and navigation system. At Datatrak, there is a pool of experienced engineers who have designed and developed the Datatrak networks currently in operation. However, their planning process is costly in terms of both time and money, since the design techniques are mostly manual.

The University of Wales, Bangor, has many years of experience in developing computer propagation modelling tools. The Bangor techniques can be used to help Datatrak engineers plan new networks, and improve existing ones.

In this thesis, we propose a computer-based Datatrak coverage model which allows the company to plot the coverage of their timing signal, and analyse the coverage and performance of their navigation system. The results should prove to be of great value to Datatrak engineers, as they seek to reduce the cost of planning new networks.

In the Datatrak system, the performance of the system will be determined by signal availability and accuracy of the positions. Datatrak make no claims on the integrity and continuity of the system. So, in this thesis, these performance factors will not be considered.

1.1   Overview of Thesis

Chapter 2 introduces the world of vehicle tracking systems. There are a variety of methods for determining the positions of vehicles, communicating the information back to the customer, and displaying that information. We will identify the technology in use by other vehicle tracking systems, and demonstrate the advantages and disadvantages of their use in this particular application. We will show that Datatrak is unique in terms of technology used, and its system ownership and maintenance arrangements.

In Chapter 3, we will investigate the main subject of this thesis in more detail: the timing and navigation section of the Datatrak system. The techniques used in determining the position of vehicles will be discussed, together with the methods currently used by Datatrak to plan their networks manually. These current methods do not take into account all factors that determine the coverage and performance of the system. This chapter will set out the objectives and scope describes of the more accurate and comprehensive modelling tool that will be developed throughout the rest of the thesis. For the following five chapters, we concentrate on the coverage of the timing and data signal, then move on to the performance and coverage of the location service.

In Chapter 4, we investigate the wanted groundwave signal from the Datatrak stations. Being an LF system, Datatrak enjoys the stability of groundwave propagation, as

documented by the International Telecommunication Union (ITU). This information is used to predict the strength of Datatrak groundwave signals. The techniques used are based on those developed and verified by Poppe [2] for modelling the coverage of radiobeacon Differential GPS (DGPS) systems, which have been applied world-wide.

Skywave is a mode of propagation that can cause disruption to a Datatrak signal. Chapter 5 describes how the skywave produced by Datatrak's own transmitters can cause fading at relatively close ranges from a station. Since skywaves are only significant at night, the model must differentiate between day and night operation. ITU methods of calculating skywave field strengths will be employed. As the fluctuating skywave interacts with the groundwave, it can cause deep fading, resulting in unreliable receiver operation. Using Poppe's own-skywave fading analysis, the fading statistics of the Datatrak signal are modelled. The end result is a night-time coverage plot of each Datatrak station. Later, in Chapter 9, positioning errors caused by skywave fluctuations are analysed.

Another major factor determining Datatrak coverage is radio noise. In Chapter 6, we analyse atmospheric, receiver, and vehicle-generated noise. The atmospheric noise analysis is based on ITU data; the Datatrak model utilises an electronic version of this, to maximise flexibility. The levels of the other noise sources are based on Datatrak's operational experience and measurements. For the first time ever, the new model lets the signal-to-noise ratio of Datatrak signals be calculated and used to determine coverage.

Chapters 7 and 8 look at the very complex subject of interference. In Chapter 7, we analyse the Datatrak receiver to determine its susceptibility to interference. Two forms of interference are identified, and the filtering and overloading characteristics of the receiver are analysed. Chapter 8 then builds the results of these analyses into the coverage model. Using a comprehensive ITU list of stations it identifies potential interferers and quantifies their effects, so allowing signal-to-interference ratios to be calculated. For the first time, we can determine the coverage of a Datatrak signal taking interference into account.

In Chapter 9, we examine the performance of the navigation system. We develop a method of calculating the uncertainty in each station's navigation signal due to own-skywave, radio noise, and interference. Then, by analysing how the Datatrak receiver calculates its position using many navigation signals, the overall uncertainty in the position fix can be calculated. This has never previously been done for the Datatrak system.

Chapter 10 returns to the subject of groundwave signals. Since the LF signals are used to determine the position of Datatrak receivers, any variation from the assumed path characteristics can cause the resulting position to be incorrect. In particular, ground conductivity and terrain height can have significant effects on the measured range to a station. Monteath's method, described in this Chapter, allows not only the field strength but also the signal delays of Datatrak paths to be calculated, using a complex model of the earth. In this way, the model can predict the effects of these delays on measured ranges. Also, the more accurate field strength values calculated using Monteath's method are used to improve the accuracy of coverage predictions.

Chapter 11 estimates the effects of the signal delays predicted by Monteath's method on the accuracy of the measured positions, by simulating the algorithms used in the Datatrak receiver. It also analyses the Datatrak "confidence factor", an important measure of the alignment of the multiple pseudo-ranges in the position solution. These features allow the model to be used to identify those areas of the network that are particularly susceptible to ground conductivity and terrain effects.

Chapter 12 draws together the conclusions from this research and proposes future work.

1.2   Contributions to knowledge

The candidate claims to have made the following contributions to knowledge:

- Identified areas in the current Datatrak planning strategy where computer-based propagation modelling can be of benefit.

- Identified and verified appropriate methods for calculating the groundwave field strength of Datatrak signals. Employing these methods to create the first coverage plot of a Datatrak signal based on field strength.

- Updated and added data to the Bangor Ground Conductivity Database.

- Identified and verified the appropriate methods for calculating the night-time skywave field strength and fading statistics of Datatrak signals. Employing the results to create the first night-time coverage plot of a Datatrak signal, based on field strength.

- Created, using ITU data, a highly-versatile atmospheric-noise mapping tool able to calculating atmospheric noise intensity anywhere in the world, at any time.

- Collected noise data from Datatrak measurements, and combined it with atmospheric noise data, to create the first coverage plot of a Datatrak signal based on signal-to-noise ratio.

- Created the first comprehensive model of an Mk4 Datatrak Locator to determine how it deals with interference, taking into account both the frequency response and the blocking susceptibility of the Locator.

- Created a comprehensive model that uses the Locator frequency response to accurately calculate the degree of rejection the Locator will offer to each potential interferer, including its sidebands.

- Developed a coverage model to identify areas where the Locator will fail due to blocking.

- Produced an algorithm to identify, among the large number of potential interferers, those whose interference could reduce coverage.

- Created the first coverage plot of a Datatrak signal based on skywave, noise, *and* interference.

- Proposed and implemented a method for predicting the resulting degree of uncertainty in measured ranges based on the ratio of groundwave to skywave-plus-noise-and-interference.

- Developed a model of the algorithms in the Locator that allows the uncertainty in the resulting positions to be calculated.

- Created the first plot of repeatable accuracy of a Datatrak network. Also, produced the first Weighted Horizontal Dilution of Precision (WHDOP) plot of the UK network.

- Proposed the use of Monteath's method for calculating the field strength and signal delay of Datatrak signals over inhomogeneous, irregular, terrain.

- Identified suitable databases for use by Monteath's method.

- Identified a suitable interval distance for use by Monteath's method when analysing Datatrak signals.

- Created the first field strength plot of a Datatrak signal using results from Monteath's method, and employing the results to produce high-resolution repeatable accuracy plots.

- Developed a model of the network, using Monteath's method, to calculate correctly the time delay between the master clock and the Locator.

- Measured the delay at Datatrak stations, and used the results in this model.

- Identified the significance of non-uniform signal propagation velocity close to transmitters, and used Monteath's method to account for it.

- Developed a model of the Locator that allows the position to be calculated using the 'measured' ranges as calculated by the network model.

- Created the first position error (absolute accuracy) plot of a Datatrak network.

- Created the first confidence factor plot of a Datatrak network.

- Identified the limits of the databases used by Monteath's method, and their effect on the accuracy of the above results.

Chapter 2

Vehicle Tracking Technologies

2.1   Introduction

An Automatic Vehicle Location System (AVLS) is an arrangement that allows organisations to track their vehicles so as to maximise the effectiveness with which they manage their fleet. By knowing the positions of their vehicles, they can plan the most efficient methods of moving them around.

Many vehicle-tracking systems are designed with vehicle security in mind. An organisation that carries high-value goods, such as cash being moved to and from banks, requires a robust tracking system in case of theft. If a vehicle is stolen, it may take just a few minutes to locate it and allow the police to investigate. The benefits include lower insurance premiums and minimum disruption in the event of vehicle theft.

In this chapter, various location and communication technologies for vehicle tracking are discussed. This thesis will concentrate on the Datatrak AVLS. The technology employed by Datatrak was designed to provide exceptionally-high security and reliability. The way in which this was achieved will be discussed in detail in Section 2.4.

2.2   Vehicle Tracking Technologies

All vehicle-tracking solutions require three major components: a method of locating a vehicle; a method of sending that information back to the customer's control centre; and a method of displaying the information. For example, the Quartix system [3] employs a satellite location system, cellular networks and the internet for communications, and a standard web browser to display the vehicles' locations.

2.2.1 Location systems

System	Accuracy	Availability	Jamming resistance	Coverage	Cost to user
GPS	<36m	Good	Bad	World-wide	Low
LF	<100m	Good	Good	Regional	Medium
Cellular	50m – many km	Medium	Medium	Regional	Medium
Galileo	Better than GPS *	Good *	Medium *	World-wide *	Low *

* Predicted

Table 2.1 – Navigation systems used for vehicle tracking

Table 2.1 summarises the principal navigation systems used to locate vehicles within vehicle tracking systems.

2.2.1.1 Global Positioning System (GPS)

The Global Positioning System (GPS) is currently the most widely-used navigation and positioning system world-wide. It is a Global Navigation Satellite System (GNSS) that employs 24 satellites in medium earth orbits (MEO) at an altitude of 20,200km, with orbital periods of 11h56m (Fig. 2.1) [4].

Each satellite transmits a unique pseudo-random noise (PRN) code; a GPS receiver distinguishes between them, and de-correlates their signals, by generating the same codes. It measures the times of arrival of the signals from each satellite. The satellites also transmit details of their orbital parameters, enabling the receiver to establish their positions in space at the moments of signal transmission. A receiver employs these time of arrival measurements and satellites' orbital positions to establish its location, in three dimensions.

Low-cost receivers designed for urban use are available, some optimised for vehicle tracking. In city centres, these receivers are designed to reacquire rapidly signals temporarily blocked by buildings.

Before May 2000, the satellite clocks and ephemeris were deliberately dithered in order to restrict the accuracy of the system available to civilian users. This "Selective Availability (SA)" technique produced a nominal position accuracy of 100 m, 95% of the time. However, following a US Presidential Decision, SA was reduced to zero [4]. The position accuracy is now better than 36 m, 95 % of the time [5].
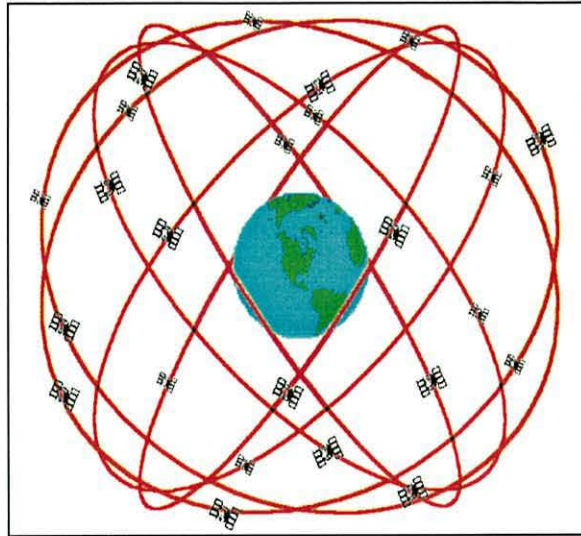
Fig. 2.1 – The Global Positioning System (After: Dana [6])

However, the signals from GPS satellites are very weak (less than -155 dBm, but higher than the specified minimum of -163 dBm [4]) which leaves them vulnerable to interference. The recent Volpe Report stated: "As GPS further penetrates into the civil infrastructure, it becomes a tempting target that could be exploited by individuals, groups or countries hostile to the United States. The potential for denying GPS service by jamming exists. The potential for inducing a GPS receiver to produce misleading information exists". Also, "The GPS service is susceptible to unintentional disruptions from ionospheric effects, blockage from buildings, and interference from narrow and wideband sources" [7].

There have been numerous reports of unintentional jamming of GPS, including by defective UHF television aerial amplifiers and faulty test equipment [8, 9]. In the latter case, the GPS service was denied out to 180 nm from the 0.8 mW 'jammer'.

The Volpe Report also states that spoofing is possible. Spoofing is emulating satellite signals, and transmitting deliberately erroneous information to nearby GPS receivers. This will cause the resulting position fix to be inaccurate, possibly by many kilometres. The ease with which GPS can be jammed greatly reduces its suitability for tracking the high-security vehicles at which Datatrak is aimed.

The current GPS modernisation programme will help mitigate problems with intentional and unintentional blocking by adding additional civilian-accessible signals at two frequencies. Other military-use signals will also be added, but will not be available for public use [10, 11]. However, the new satellites are not due to be operational until at least 2010 and their funding is still uncertain [12].

2.2.1.2 Low Frequency Systems

Many navigation systems have traditionally employed Low Frequency (LF) or Very Low Frequency (VLF) signals [4, 13, 14, 15, 16, 17]. Datatrak, the subject of this thesis, is an LF system. Decca Navigator (LF) [17] and Omega (VLF) [13, 14], formerly provided regional and world-wide coverage for marine and land navigation, using terrestrial transmitters. The Loran-C (LF) system [4, 15, 16] is used by marine and aviation navigators, and also for vehicle tracking, both in stand-alone form [18] and combined with GPS [19].

LF systems employ *groundwave* signals, which have very stable propagation velocities. LF receivers determine their range from the transmitters either by measuring the difference in the arrival times of signals from pairs of stations (early Datatrak, Decca Navigator, Omega, and early Loran-C receivers), or by measuring the times of arrival relative to an internal synchronised clock (later Datatrak and Loran-C receivers). Earlier receivers required their output to be converted into latitude and longitude by manual plotting on maps. More recently, advances in computing power have allowed the receivers to make these conversions on-board.

LF systems have the advantage of being very difficult to jam. The received power from an LF transmitter can be 100 dB greater than that of GPS signals. In order to jam an LF signal, not only is a high transmitter power required, but also a substantial antenna structure, which cannot be covert. A principal limitation of LF systems is that *skywave*-propagated signals interfere with the groundwave signals at night, causing deep fading and phase changes (see Chapters 5 and 9).

2.2.1.3 Cellular Networks

Using cellular telephones for navigation is a relatively new technique. The US E-911 standard requires the location of users who make emergency calls to be determined

within 300m, 95% of the time [20]. Also, location-based services allow companies to target potential customers whose locations are known.

Cellular networks identify the cell that covers each user's location. By measuring field strength, range from the base station can be estimated. The accuracy of the system ranges from 50m to several kilometres [21]. The advantage of this method is that the user need be in range of only a single cell and no modification to the handset is required. A more accurate technique, "Enhanced-Observed Time Difference" compares times of arrival of the mobile's transmissions at a number of base stations. Typical position accuracy is 50-150m [21]. But the mobile telephone must be in range of at least three base stations, which is often not the case, and must be modified to make use of the technique.

2.2.1.4 Galileo

Galileo is a proposed GNSS system, currently being developed. It is funded by the European Union (EU) and European Space Agency (ESA) and is planned to be operated under a Public-Private Partnership (PPP) scheme from 2008. Galileo signal formats have yet to be finalised, but the latest plan suggests that the system will share some carrier frequencies with GPS [22, 23]. A total of 10 navigation signals will be available to users in the frequency range of 1164–1592 MHz. Some signals will incorporate a data channel to transmit orbital parameters and system integrity messages. Position accuracy is said to be better than GPS [24].

Galileo will offer two potential vehicle-tracking services. The Open Service (OS) will be "free of charge", "with no authorisation required". The use of multiple frequencies will minimise jamming. However, the service is provided with "no service guarantee or liability" [24]. The Commercial Service (CS) is for higher performance applications, with access via a signal decryption key. There will be a system guarantee and liability, of a form yet to be decided. This may prove a selling point when Galileo-based tracking systems eventually appear [24].

2.2.2 Communication Techniques

Once a vehicle's location is known, it must be transmitted back to the customer. Commonly, communications are two-way and support additional messages, including

System	Coverage	Availability	Cost to user
VHF/UHF Radio Links	Regional	Good	Low
Cellular communications	Extensive	Medium - Good	Medium
Satellite communications	World-wide	Good	High

Table 2.2 - Communication methods used by vehicle tracking systems.

vehicle status messages from the vehicle and despatching messages to the vehicle. Table 2.2 shows examples of communication systems used by vehicle tracking solutions.

2.2.2.1 VHF/UHF Radio Links

A common technique is the use of conventional mobile radio systems in the VHF or UHF bands. These require substantial investment in terrestrial base stations (although normally shared with other services) since propagation is essentially line-of-sight aided by multipath reflections from buildings and hills. Once operational, the running costs of such a system can be relatively low.

2.2.2.2 Cellular communications

Global System for Mobile Communication (GSM), General Packet Radio Service (GPRS), and Simple Message Service (SMS) cellular communications are becoming the most commonly-used forms of vehicle communication in tracking systems. The technology is tried and tested, and the cost of the communications infrastructure is shared across many users. Coverage is excellent in populated areas, and along major roadways and motorways. One UK cellular operator has over 7,500 base stations [25].

Each vehicle being tracked requires a GSM/GPRS modem, with a unique Subscriber Identity Module (SIM) card. Vehicle tracking service providers usually buy GSM/GPRS bandwidth in bulk in order to reduce costs.

However, cellular coverage may be poor or non-existent in mountainous areas and regions of low population density. So, reliability can be lower than that of operating a VHF/UHF system.

2.2.2.3 Satellite communications

Wide-area communications for international vehicle tracking require satellite communications. The Inmarsat-C geostationary satellites provide global data communications coverage, apart from Polar Regions [26]. GlobalStar uses 48 satellites in low earth orbit (LEO), at an altitude of 1414 kilometres, to give global coverage [25]. EutelTRACS and OmniTRACS are fleet management systems developed by Qualcomm, and employing the EutelSat series of geostationary satellites. It provides not only a secure two-way communications system, but also a proprietary position system with a claimed accuracy of 100 m [28, 29, 30].

A satellite communications channel, however, requires expensive outlay and high running costs. For this reason, its use is usually restricted to applications that require tracking in areas where the other services discussed are not available.

2.2.3 Display Systems

Most commonly, vehicle positions are displayed on a map, together with status messages received from the vehicle. The interface between the system and the customer is generally a proprietary one. However, the Internet is a fast and low-cost method of conveying the information received from the vehicles to the customer, requiring no specialised software or hardware. For this reason, it is rapidly becoming the standard for providing a secure, but flexible interface to a vehicle tracking system. Fig. 2.2 shows an example screenshot of the ViaWeb system provided by Qualcomm,

Fig. 2.2 - Screenshot of Qualcomm ViaWeb internet vehicle tracking service (after [29]).

System	Location	Communication	Display
Orange Fleet Link	GPS/Cellular	Cellular (Voice and Data)	Integrates with existing business systems
Quartix	GPS	Cellular / Internet	Standard e-mail clients and web browsers
StarView	GPS	Cellular/Satellite (Inmarsat-C)	Proprietary software and standard web browsers
Datatrak	LF	UHF	Proprietary map display and communications package

Table 2.3 – Technologies used by some vehicle tracking systems (after [3, 25, 31]).

showing an event mapping solution [29].

Most systems provide a method of tracking vehicles' positions over time on a map, so enabling the customer to assess the efficiency of the routes taken and examine possible improvements. A customer can usually see, at any time, where their vehicles are, as required for fleet management systems. The user interface generally has some form of communications package included so that customers can view status messages from the vehicles, and send messages back in reply. There is usually some form of alert function where the driver of the vehicle can signal an alarm (e.g. vehicle being stolen) in the control centre. The appropriate authorities can be informed by the control centre operatives, who will guide them to the vehicle in trouble.

2.3   Examples of Vehicle Tracking Systems

Table 2.3 shows the combinations of location system, communications and display method employed by a number of vehicle tracking systems. Most, with the exception of Datatrak, and StarView which employs satellite communications, use GPS location, cellular communications, and proprietary map displays.. The reason for choosing this combination is that off-the-shelf components are readily available to provide positioning by GPS and cellular communications. This greatly reduces development and maintenance time and cost, and allows the companies to concentrate more on the user interface and the special features of the service they provide to the customer. However, using this conventional approach means that companies must accept that the availability of the service is mostly determined by third parties, and that they themselves can do very little should the service fail.
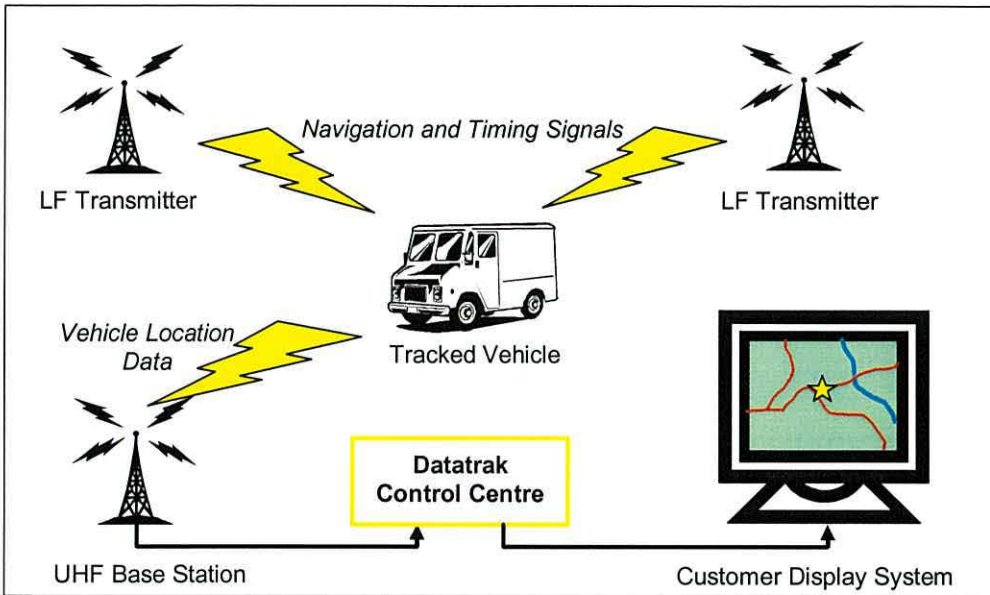
Fig. 2.3 - Overview of the Datatrak Automatic Vehicle Location System.

2.4   The Datatrak vehicle tracking system

Datatrak was originally designed for monitoring high-value cash-in-transit vehicles in a highly-secure and ultra-reliable way; it still fulfils this primary function. A later additional application is tracking stolen vehicles, both private and fleet ones. Datatrak has some 30,000 users in the UK. The technology and the UK system are wholly owned by Siemens VDO Automotive Ltd. Having all parts of the system under the direct control of one company is the foundation of its high security and reliability.

The Datatrak timing and navigation network (Fig. 2.3) employs the low frequency (LF) technology that is the subject of the research presented in this thesis. In some applications and countries, the GPS also is used, especially in remote areas. Vehicles' positions are reported via on-board transmitters operating in the 440-470 MHz UHF band with a transmitter power of 10W. The communication system is two-way [32]. Datatrak have developed a range of display systems to serve a wide variety of applications.

The LF system employs a network of transmitters operating at two frequencies, specific to the network. The frequencies of all networks lie between 130 and 180 kHz. In summary, the 13 stations that serve England, Wales, and Scotland (Fig. 2.4)

Fig. 2.4 – Locations of the UK Datatrak LF stations

transmit precisely-synchronised carrier-wave signals in a time-multiplexed sequence. The vehicle-borne navigation units receive these signals and measure their phases. From these measurements, plus knowledge of the speed at which radio waves propagate, they establish their ranges from the stations and hence their positions. The accuracy is of the order of 100 m. Details of the transmissions and an explanation of the operation of the receivers will be given in Section 3.4.

Each vehicle communicates its position fixes back to base in the form of short data bursts in precise time-slots. It synchronises these transmissions by reference to the timing of the signals it receives from the LF network. In some countries, these communications are supplemented by GSM or GPRS two-way data transfer. The data network is exceptionally efficient in its use of bandwidth and equipment; the 30,000 UK vehicles are supported on just 8 radio channels, with position updates being passed at preset intervals of between 13 s and 28 minutes depending on the application [32].

The network of 108 UHF base stations passes data packets via a highly-secure data network to a secure control centre, where they are decoded. Each customer is supplied with position and status data from his own vehicles only. These are processed using a standard software suite that supports two-way communications. Vehicle information

is displayed by means of maps or data tables. Alternatively, the Datatrak information is fed directly into the customer's own command and control system and integrated there with other data [33].

Datatrak networks have been installed in the UK, the Netherlands, Belgium, Luxembourg, Argentina, South Africa, and Malta. Altogether, they serve a total of some 45,000 vehicles.

The system has been designed to maximise security and availability, key parameters for tracking high-value loads or cash-in-transit security vans. It was this requirement that led to the choice of an LF tracking system, because of the high resistance to jamming afforded by the strong signals, and the exceptionally-narrow bandwidths of the phase-tracking receivers. Also, the transmitter network is highly redundant, the receivers operating in an all-in-view mode. The communications system is under Datatrak's own control and employs Datatrak's proprietary coding. The base station network is also highly redundant, each vehicle transmission normally being received by several base stations; this minimises jamming vulnerability and maximises data availability.

2.5   Conclusions

In this chapter, we have reviewed the principal methods for locating vehicles and communicating their positions in vehicle tracking systems. We have seen that most systems employ GPS tracking and cellular communications. Datatrak, with its low-frequency tracking and proprietary communications, is exceptional. These features are employed to maximise its availability and minimise its vulnerability to jamming.

In the next chapter, we will examine in more detail the Datatrak LF timing and navigation system, the subject of this thesis.

Chapter 3

Datatrak LF Timing and Navigation System

3.1   Introduction

In this chapter, we will look at the Datatrak timing and navigation system. In particular, we will concentrate on the positioning technique it uses for tracking vehicles. Over the years, Datatrak have implemented more than one technique as the computing power of the receiver increased. So, we will look briefly at the history of Datatrak, and see how the system has developed and expanded over the years. The design of a new Datatrak network is a complex and time-consuming process, since many factors combine to determine the coverage and performance of the system. Traditionally, new systems have been designed using manual techniques and the experience of Datatrak engineers. In recent years, however, computer modelling has made it possible to predict with considerable confidence the coverage and performance of a number of LF systems. We propose developing a computer model of this kind for the Datatrak system, to support the process of designing new networks. That computer model will be the focus of this thesis.

3.2   A Brief History of Datatrak

The development of the Datatrak LF hyperbolic navigation system was begun in 1985 as a joint venture, codenamed 'Project 430', between Securicor plc and Wimpey plc. In January 1987, a three-station system covering the London area was demonstrated, with data transmitted from a vehicle to a base station via an early cellular telephone modem. In May 1987, the system - now named *Datatrak* - was demonstrated on the BBC *Tomorrow's World* programme. It employed VHF communications. In 1988, the first commercial unit containing both a vehicle LF receiver and a data transmitter – termed a *Locator* – was produced. Communications were now in the 440 - 470 MHz UHF band. Since then, the UK system has expanded to cover 95 % of the road traffic in Great Britain. By 1998, Datatrak networks had been commissioned in 6 other countries.
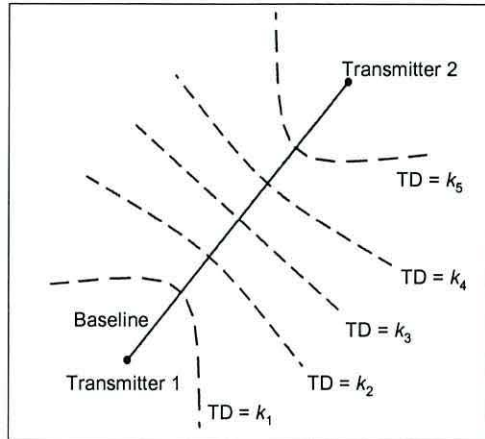
**Fig. 3.1 - Lines of equal time difference (TD) in hyperbolic navigation.
k_n are constants**

3.3   Location Techniques

3.3.1   Time-Difference Method (Hyperbolic method)

In the days gone by, when receivers did not possess the processing power of today's receivers, a simple location method was required. The method usually chosen was to measure the time differences (TDs) between the synchronised signals received from pairs of transmitters at precisely-known locations [13, 14, 15, 16]. The receiver did not need an accurate reference clock in order to measure these differences since no absolute time measurements were involved. Fig. 3.1 shows the loci of equal TD between pairs of stations used in this way. The loci are hyperbolic curves with the stations at their foci, hence the name of this method.
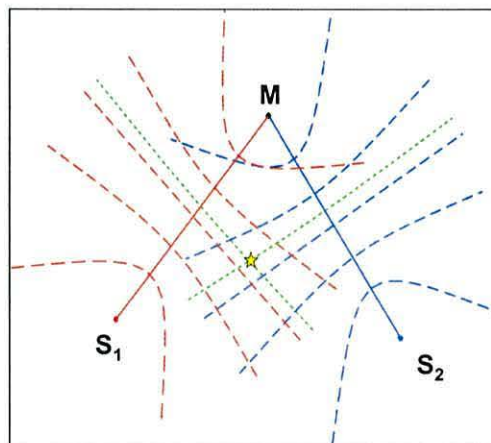
**Fig. 3.2 - Determining location of receiver using hyperbolic mode of operation. Red
lines: measured lines of position (LOPs) from master and S_1 stations. Blue lines:
measured LOPs from master and S_2 stations. Yellow star: Receiver, at intersection
of green pair of LOPs.**

To generate a position fix using a hyperbolic system requires at least three transmitters. In Fig. 3.2, the transmitter marked 'M' is the master transmitter. Slave transmitters S1 and S2 are synchronised, or slaved, to it. The M-S1 pair generates the set of hyperbolic patterns shown in red, the M-S2 pair those in blue. The receiver is at the intersection of the M-S1 and M-S2 measured lines-of-position (LOP), shown in green.

3.3.2 Phase Comparison Technique

In the Datatrak system, as in Decca Navigator on which it was based, receivers measure time differences by measuring the phase differences between the signals received from the stations. However, phase differences are ambiguous, with identical values being received at intervals of integer numbers of cycles of phase difference. Datatrak signals, with their frequencies of approximately 150 kHz, have wavelengths of approximately 2 km. Along the baseline that joins two stations, moving half a wavelength (approximately 1 km) from a point of zero phase difference advances one phase, and retards the other, by half a cycle, so that the phase difference is again zero. The region between lines of zero phase difference is known as a *lane*. In a hyperbolic
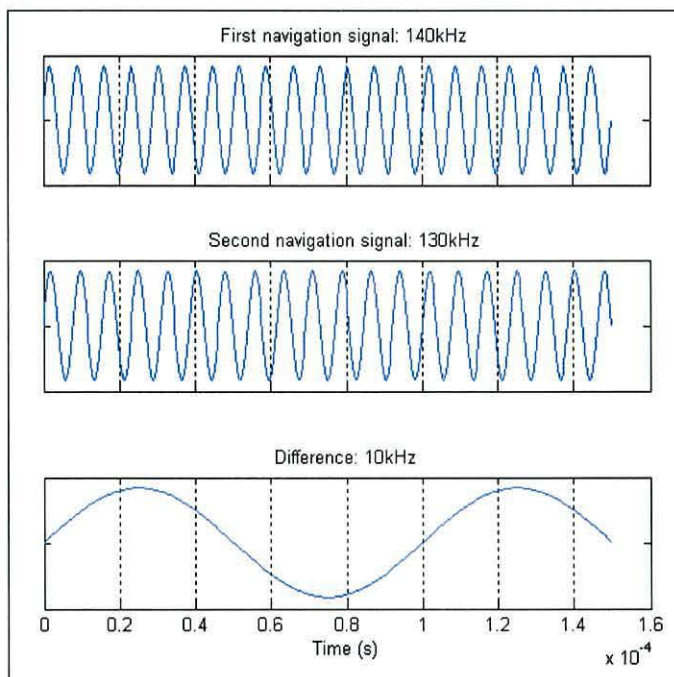
Fig. 3.3 - Principle of frequency difference method as used in phase comparison technique to identify lane number of LOP
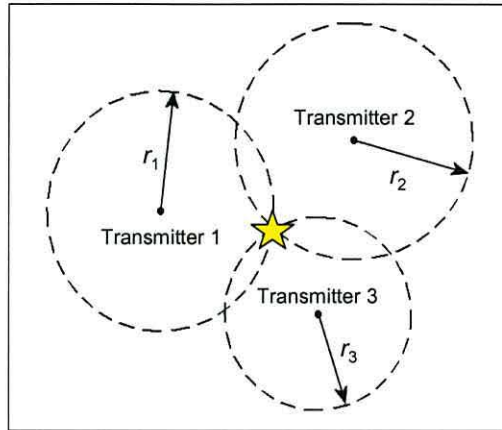
Fig. 3.4 - Circular navigation patterns from three transmitters. The Locator is at the common intersection point of the circles, marked by the yellow star.

system, the lanes become wider away from the baseline.

A means is required to resolve the lane ambiguity. To achieve *lane identification,* the stations transmit at a second frequency. Phase differences measured at the two frequencies are differenced; the result is phase differences at a frequency equal to the difference between the two frequencies (Fig. 3.3). This much lower frequency has much wider lanes. The phase difference measurements in these wider lanes allow the receiver to identify the original, finer, lanes. The ambiguities in the wider lanes are a long way apart and their ambiguities can usually be resolved by other means (see Section 3.4.2). As the receiver moves, it keeps track of the lane number of each station pair.

3.3.3 Time-of-Arrival Method (Circular)

In this method, the receiver measures its range from each transmitter by determining the time the signal from the transmitter has taken to reach it. In principle, the receiver carries an accurate clock, perfectly synchronised to a clock at the transmitter. It measures the time-of-arrival (TOA) of the signal against this clock. It now knows the time taken by the signal to reach it from the transmitter and so, knowing velocity of propagation, it can compute its range from the station. The resulting LOP is a circle centred at the transmitter; this mode of operation is termed *circular.* If three transmitters are used, then the receiver is at the intersection of the three circles (Fig. 3.4). In practice, circular mode operation normally employs an atomic clock to minimise clock error.
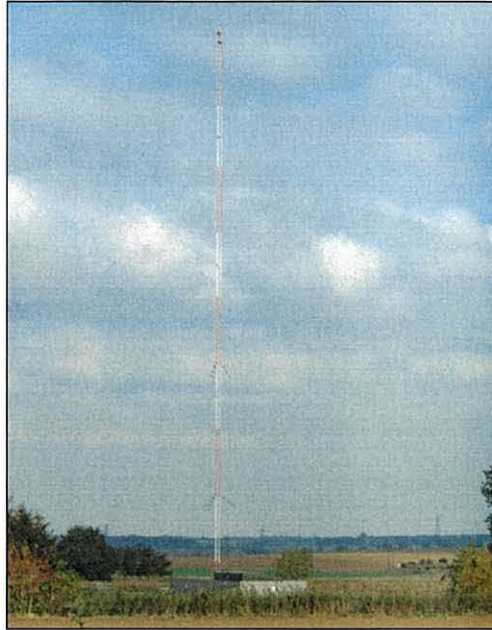
Fig. 3.5 - Datatrak antenna mast and transmitter housing. Photo taken at Huntingdon.

3.3.4 Pseudoranging Operation

A third technique is employed in GPS [4, 13]. The receiver measures the TOA of each satellite's signals against a low-cost clock. The clock error, or clock *bias*, introduces an equal error into each satellite's TOA. The ranges from the satellites calculated using these TOAs, are termed *pseudoranges*; they contain equal clock bias terms. A GPS receiver makes at least four such measurements and, using a least-squares technique, identifies the latitude, longitude, height and the clock bias that "best-fit" the set of pseudoranges. The method requires substantial computational power in the receiver. It can be applied in a two-dimensional phase comparison receiver (see Section 3.3.2 above) with three stations, and with two frequencies to resolve the lane ambiguities, as in Section 3.3.2.

3.4 Datatrak Technology

3.4.1 Transmitters

Each Datatrak LF transmitter radiates powers within the range 20 – 400 W on a pair of frequencies between 130 and 160 kHz. The radiated power is a function of the antenna height and signal frequency, and is chosen according to the requirements of
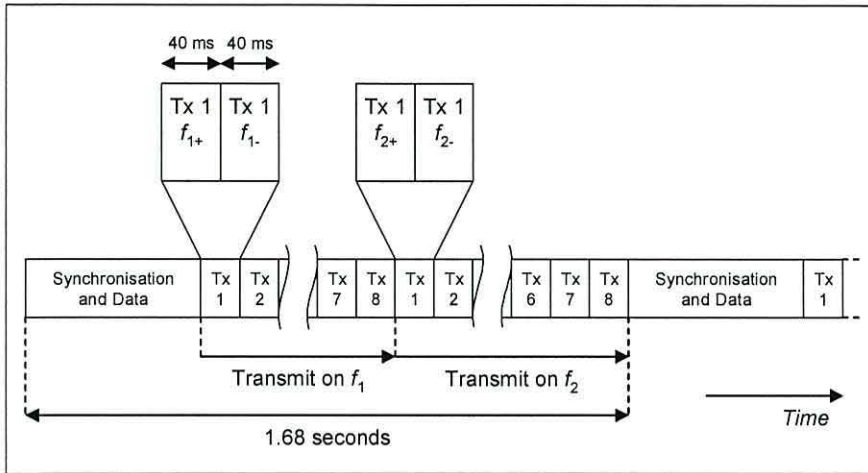
Fig. 3.6 - Datatrak transmission timing sequence

the network. The antennae are guyed lattice-mast monopoles, 50 m in height in the UK (Fig. 3.5), and mostly 100 m elsewhere.

All transmitters in a network operate at the same two frequencies, designated f_1 and f_2, with f_2 about 10 % lower than f_1. They transmit in turn in a repeating time-multiplexed sequence (Fig. 3.6), each sequence lasting 1.68 s, and each transmission slot is 80 ms. Within this 80 ms, the carrier is frequency modulated: at +40 Hz for the first 40 ms, and at -40 Hz for the second. This modulation actually produces two navigation signals from each carrier. These are designated f_{1+}, f_{1-}, f_{2+}, f_{2-}; the sign denoting the direction of modulation.

The section of the sequence marked "Synchronisation and Data" in the figure is a 340 ms-long data transmission of 26 bits which conveys station almanac and receiver parameter information to the receivers and also synchronises them to the network timing. A further 60 ms of the 1.68 s cycle is given over to 'guard slots', which allow for station and receiver settling between the f_1 and f_2 transmission sections and between the 1.68 s cycles (not shown in Fig. 3.6).

The phases of the signals radiated by all the stations of a network are synchronised to those radiated by a master station which takes its timing from a master clock. Stations that are too far from the master station to reliably synchronise to it may do so via an intermediate station. Each station synchronises to the master by operating as a *phase mirror;* that is, the phase of the signal it radiates is controlled to match that of the

signals it receives. More details of this important feature of the network will be given Chapter 11.

3.4.2 Locators

We have learned that a Datatrak combined LF receiver and UHF transceiver is called a Locator. The Locators being produced currently (Fig. 3.7) are the fourth generation to have been developed; they are designated "Mk4" and will be the Locators considered in this thesis. The first three generations of Locator operated in the hyperbolic, phase comparison, mode. The UK frequencies result in baseline lane widths of approximately 1 km. The difference between the two frequencies gives coarse lanes of approximately 10 km width (see Section 3.3.2). A further stage of lane identification is then provided by the 40 Hz phase modulations: the frequencies $[f_{1+} - f_{1-}]$ and $[f_{2+} - f_{2-}]$ give lanes approximately 1,900 km wide. In this *super-coarse* pattern, ambiguities are of little concern. However, super-coarse phase measurements must be made very accurately indeed if they are to be used to identify lanes in the coarse pattern with confidence.

Since the signals from a given transmitter on a given frequency is only available in a series of bursts, the Locator employs an internal crystal clock against which to measure signal phases. It is assumed that this clock is stable over the short time period between transmission slots. The phase difference technique can then be employed, by subtracting one of these measured phase values from another.
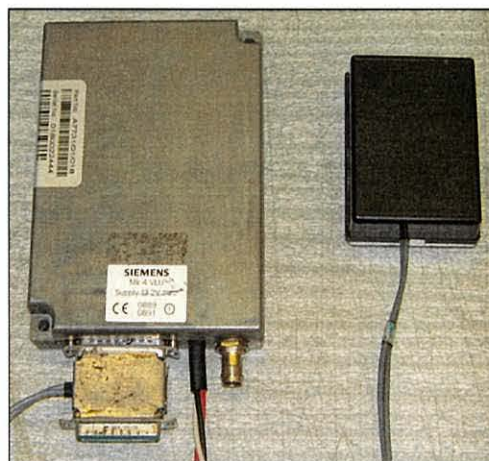
Fig. 3.7 - Datatrak Mk4 Locator and H-field Antenna.

As the processing power of the successive generations of Locator increased, more advanced station selection algorithms were developed. A problem with hyperbolic mode operation is expansion of the lanes with distance from the baselines. Uncertainties in the phase measurement due to noise lead to increased uncertainties in the position fix and the repeatable accuracy worsens (Chapter 9). For this reason, the mode of operation of the Mk4 Locators was changed to pseudorange. This mode also accommodated the reception of many stations, the least-squares computation of position being weighted in accordance with the signal-to-noise ratio of each station's signals.

Datatrak Locators of the earlier generations also employed whip antennas, which supported both LF reception and UHF transmission. Current Locators use loop antennas for reception. This change from E-field to H-field reception gives higher signal-to-noise ratios in urban canyons and makes covert installations easier [34].

The very latest Mk4 Locators also include a GPS module so that it can use the LF and satellite technology together to produce even more robust, accurate, position fixes. A move to use GSM networks for communications is also being planned as a reliable back-up to the UHF communications network.

The technical specification of the Mk4 Locator is shown in Appendix A.

3.5   LF Network Planning

In this thesis, we will concentrate on the LF navigation system, showing how to predict the coverage and performance of a currently operating, or planned, network. This will depend on the factors summarised in Fig. 3.8.

Since the system operates at LF, the main form of propagation used to make measurement is *groundwave*. The signal leaves the transmitter and propagates along the surface of the earth. The field strength and phase of this signal depend on the nature of the surface over which it propagates. Ground conductivity, terrain height, and signal frequency play major parts in determining groundwave behaviour.
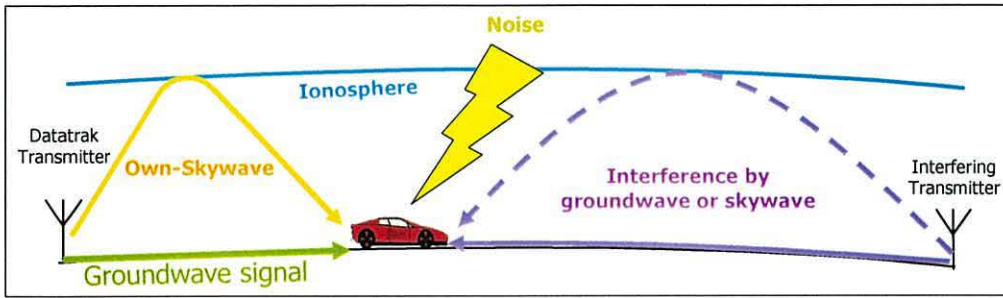
Fig. 3.8 - Wanted groundwave signals, and unwanted signals, received by Datatrak Locator.

However, the groundwave is very stable in time, hence its suitability for navigational purposes.

The absolute accuracy of a position fix also depends on the nature of the propagation paths between the stations and the Locator (see Section 10.1). Any variation of propagation velocity along a path from that expected by the Locator produce errors in the pseudorange and the position calculated (Chapter 11). It will also affect the *confidence factor,* which characterises the agreement between pseudoranges. When the confidence factor falls below a preset criterion, and the Locator will deem the position to be suspect and suppress it.

In order for the Locator to work correctly, the groundwave field strength must be high enough. ITU data allows groundwave field strength to be predicted for a given type of surface and frequency. Using this data, and knowing the characteristics of the receiver, we can compute the maximum working range of the receiver from a transmitter. Later in the thesis, a more sophisticated technique will be introduced that takes into account the effect of hills and mountains on the signal.

At night, LF signals are refracted back to earth as *skywaves* which are added to the groundwave signals at the receiver antenna, causing "own-skywave" signal fading and variations in the phase measurements.

Radio noise can be caused by natural means (e.g. lightning), generated by the vehicle which the Locator is in installed or neighbouring vehicles, or generated in the Locator itself. So, the *signal-to-noise ratio* of the received signal must be adequate.

	Prediction Method
Groundwave Field Strength	
Ground Conductivity	ITU-R P.832 (CCIR)
Groundwave Propagation	ITU-R P.368 (CCIR)
Coverage Method	Range based
Skywave Field Strength	
Method of Calculation	Not Considered
Own Skywave Interference	Not Considered
Atmospheric Noise	Not Considered
Vehicle Noise	Taken to be 27dB-μV/m
Interferers	
Information	Various/Experience
By Groundwave	Yes
By Skywave	No
Repeatable Accuracy	Fixed phase uncertainty
Absolute Accuracy	None
Confidence Factor	None

Table 3.1 - Network prediction methods previously used by Siemens Datatrak.

Finally, interference from other radio services in the same frequency band as Datatrak will be received by the Locator, via both groundwave and skywave. Some interfering energy will penetrate the internal filters causing the signal-to-noise ratio to fall. Also, a nearby powerful transmitter may overload the Locator, causing it to fail.

3.5.1 Datatrak's current prediction methods

Table 3.1 shows the methods currently used by Datatrak engineers to predict the various parameters required to determine the coverage and performance of a planned network. They are rather crude, and some, such as the prediction of interference, are based purely on the experience of engineers in the field. Groundwave coverage is calculated using a simple 'range' method. Fig. 3.9 shows an example of a planned network in Austria. Using ITU maps [35], the ground conductivity in the area is estimated, and the appropriate field strength curves in [36] then gives the range at which the field strength will have fallen to the minimum required by the Locator. This range is then plotted on a map; see, for example, the red and blue circles in Fig. 3.9.

Skywave is largely ignored, except that a safe range limit is imposed in the Locators in selecting stations that contribute to the position solution. The dominant noise source is assumed to be vehicle noise. The repeatable accuracy prediction assumes that all phase measurements have the same, constant, phase uncertainty. The position error at any location then depends solely on the geometrical dilution of precision
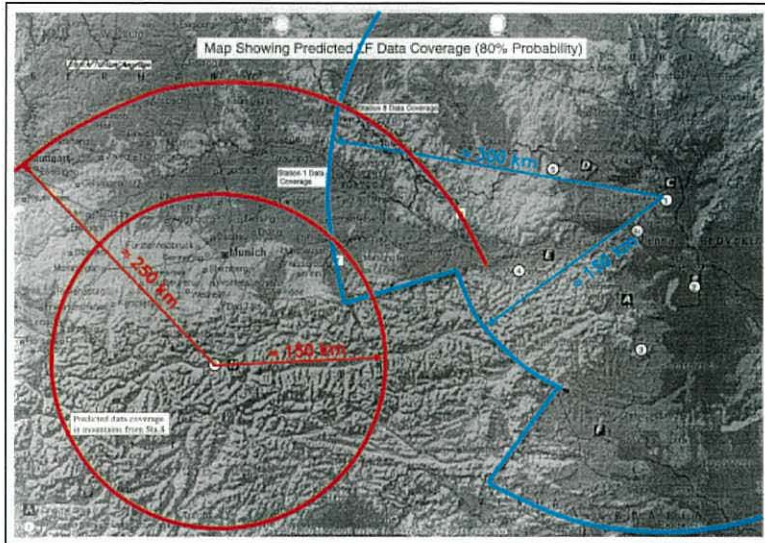
Fig. 3.9 - Range-based coverage plots for planned Austrian network

there. There is currently no means of predicting either absolute accuracy or confidence factor.

3.5.2 Scientific methods

The Radionavigation Group at University of Wales, Bangor, has successfully developed coverage prediction software for Loran-C and Radiobeacon DGPS [2, 37, 38]. Like Datatrak, these systems employ LF groundwave signals. Also, many of the coverage parameters such as noise, skywave and interference are similar.

These coverage models use arrays to hold information. The elements of an array represent computation points that coverage the area of interest. They hold values of groundwave field strength, skywave field strength, noise field strength, etc. (See Section 4.7).

More recent developments have allowed both the field strengths and the phase variations of Loran-C signals to be predicted over paths of non-uniform ground conductivity and variable terrain height [39, 40].

3.5.3 A better way for Datatrak

The basis of this thesis is the proposal to explore the feasibility of developing a coverage and performance computer model for the Datatrak system. It will be

expected to predict all the parameters detailed in Table 3.1. Designing such a model will require a deep understanding of the Datatrak system. It will then be necessary to identify and adapt existing techniques and, where necessary, develop new ones. The objective will be a computer model of the Datatrak system that will form a design tool to be used anywhere in the world.

A specification for the model, proposed by Datatrak, is shown in Appendix B. The Specification is structured in such a way that it follows the natural development of the model. The model will be focussed on the Mk4 Locator with an H-field antenna, which is the future Locator for Datatrak. Also, the existing UK system will be the first network to be modelled, allowing measurements to be taken to support the model.

It is hoped that the model will greatly increase the efficiency and accuracy of Datatrak's planning strategy. It should allow engineers to assess contingencies, such as the results of failures of individual stations. The model will also provide information which Datatrak have not previously been able to predict. This will include predicting the absolute accuracy of the network taking into account the changes of propagation velocity along the signal path. The calculation of such effects is extremely complex, and for a company to create such a models in a time-critical commercial environment is very difficult.

3.6 Conclusion

In this chapter, we have looked at the Datatrak LF navigation and timing system in more detail. Three methods of determining the position of a vehicle have been considered. The hyperbolic and pseudoranging techniques have been used in the Datatrak system. The pseudorange method has let Datatrak Locators produce position fixes with higher repeatable accuracy over a larger area than the hyperbolic method. The Datatrak system of time-multiplex transmissions allows all the transmitters to operate at the same frequency, allowing for simpler receiver design.

Designing a new network is a very hard, time consuming, process. Many of the parameters that determine the coverage of the signals in a network have previously

either been calculated by hand, or using a rule-of-thumb approach based on experience, or simply ignored.

However, computer models that predict many of the parameters required have now been developed for other navigation and communication systems. Some of the techniques can be adapted for Datatrak use. This thesis will describe how the Datatrak requirements will be analysed and a scientifically-based Datatrak coverage and performance model built using a mixture of modified existing techniques, and new ones developed specifically for the purpose. The aim will be to create a computer tool that can be used anywhere in the world, which will improve the accuracy and efficiency of the network planning process.

The next chapter will examine the wanted signal: the groundwave signal from Datatrak transmitters.

Chapter 4

Groundwave Field Strength

4.1   Introduction

The groundwave signal is central to the Datatrak LF system. Its field strength is one of the major factors that dictates the coverage and performance of the timing and navigation system. The attenuation of the groundwave signal as it propagates away from the transmitter depends on the conductivity of the ground over which it passes, the terrain, and range from the transmitter.

In this thesis, two very different methods of predicting groundwave field strength will be demonstrated. This chapter will start with the less computationally-demanding method. The more advanced method, which takes into account terrain height and also calculates the phase delay of the groundwave signal, will be investigated in Chapter 10. However, for the first half of the project, which did not concern itself with signal phase, this simpler and quicker method gives sufficient accuracy.

4.2   What is a groundwave?

Groundwave is the main mode of propagation of radio waves at frequencies up to about 2MHz. Because its propagation velocities are very stable in time, it has been used to measure distances in many radionavigation systems [41].

In free space, radio signals travel in straight paths. However, at lower frequencies, they follow the earth's surface. In addition to dispersion, groundwave signals are attenuated at a rate that depends on the conductivity of the surface over which they travel. A higher conductivity surface, such as sea-water, results in a lower rate of signal attenuation. Low-conductivity ground absorbs more energy from the radio wave, and so cause the field strength to decrease more rapidly. The signal frequency also affects the degree of attenuation: higher the frequency, the higher the attenuation, for a given path [36, 42].

Conductivity (mS/m)	Ground Type	Penetration Depth (m)
5000	Sea water	0.58
30	Very good ground	7.5
10	Wet ground, good dry soil	13
3	Fresh water, cultivated ground	24
1	Medium dry, average ground Mountainous areas	41
0.3	Dry ground, permafrost, snow covered mountains	75
0.1	Extremely poor, very dry ground	130
0.01	Glacial ice	411

Table 4.1 - ITU Standard Ground Conductivity values (milliSiemens per metre) and penetration depths of Datatrak signals

4.3 Predicting Groundwave Field Strength

The ITU publish charts for the 8 standard ground conductivity values listed in Table 4.1. The highest conductivity is that of sea water at 5000 milliSiemens per metre (mS/m), and the lowest that of glacial ice, at 0.01 mS/m. The charts (e.g. Fig. 4.1) allow field strength to be determined as a function of range from the transmitter at a given frequency and ground conductivity [36].

Poppe, who used the ITU curves in her model for the radiobeacon DGPS service, represented each curve as a fifth-order polynomial which she expanded into equations
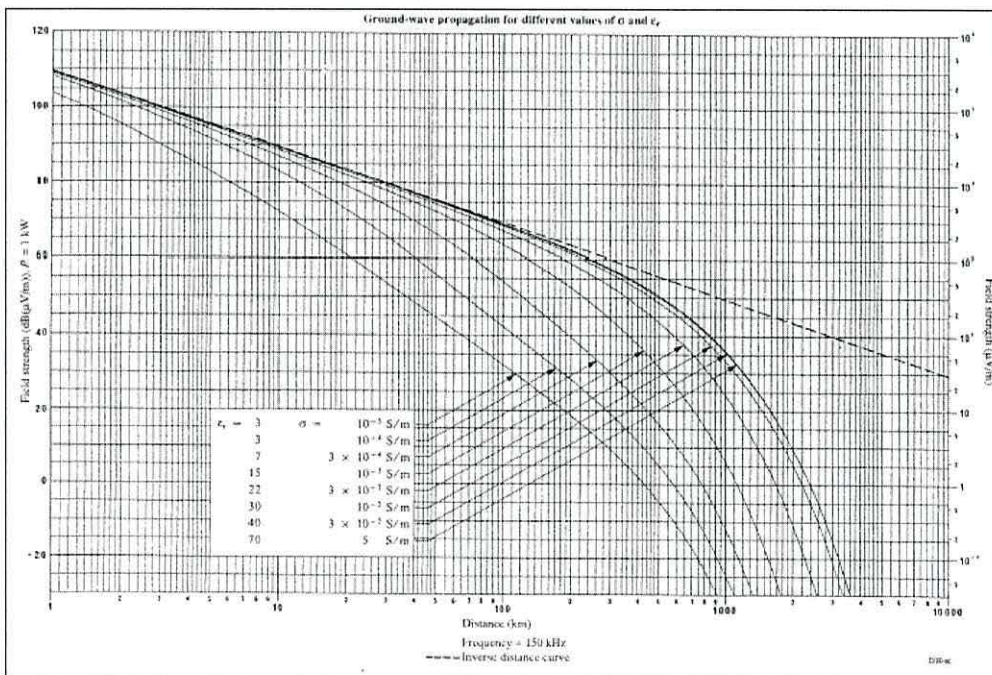
Fig. 4.1 - Groundwave propagation chart for 150 kHz signal (after [36])

Conductivity (mS/m)	c_0	c_1	c_2	c_3	c_4	c_5
5000	110.1811	-32.5492	32.7954	-30.9858	12.3267	-1.7835
30	110.1811	-32.5492	32.7954	-30.9858	12.3267	-1.7835
10	110.1530	-30.7353	27.9819	-26.8291	10.9284	-1.6334
3	110.0982	-27.5777	20.4989	-21.4460	9.4992	-1.5580
1	110.0511	-23.5378	10.2601	-13.1707	6.6296	-1.2665
0.3	109.1080	-31.4541	34.3023	-36.5951	14.6218	-2.1928
0.1	108.0217	-28.8112	28.2534	-38.7146	17.1743	-2.6607
0.01	104.0515	-30.4546	11.5239	-22.1582	11.6544	-2.0461

Table 4.2 - Polynomial coefficients used in the model to represent ITU 150 kHz curves

such as that shown in Equation (4.1), in order to minimise computation time [2]:

$$Gnd_{dB} = c_0 + ld\left(c_1 + ld\left(c_2 + ld\left(c_3 + ld\left(c_4 + ldc_5\right)\right)\right)\right), \qquad (4.1)$$

where Gnd_{dB} is the groundwave field strength for a 1 kW transmission, C_n is the nth polynomial coefficient for the given ground conductivity, and ld is $\log_{10}$(range in km).

We will use this technique for the Datatrak system, replacing Poppe's 300 kHz coefficients with new ones calculated for Datatrak frequencies (130-180 kHz). ITU publish curves for 120 kHz, 150 kHz and 180 kHz. We could use all three sets of curves, and interpolate between them for the Datatrak frequency in use. But the 120 kHz and 180 kHz values differ from the 150 kHz values by less than 2 dB, a figure comparable to the accuracy with which one can read the values from the printed charts and the errors in the polynomial representation. The increase in computation time and complexity of using three charts and interpolating would thus bring no significant accuracy benefit. The 150 kHz curves will be used at all Datatrak frequencies.

The coefficients for the Datatrak use are shown in Table 4.2. The equivalent polynomial curves are shown in Fig. 4.2, the stars indicating the data points read from the ITU charts to which the polynomials have been fitted. The polynomials generally fit the data to better than ±1 dB, which is acceptable given the accuracy of the printed ITU charts. Note that there is no significant difference in attenuation between sea-water and 30 mS/m ground, as there is no difference between the two curves in the ITU document.
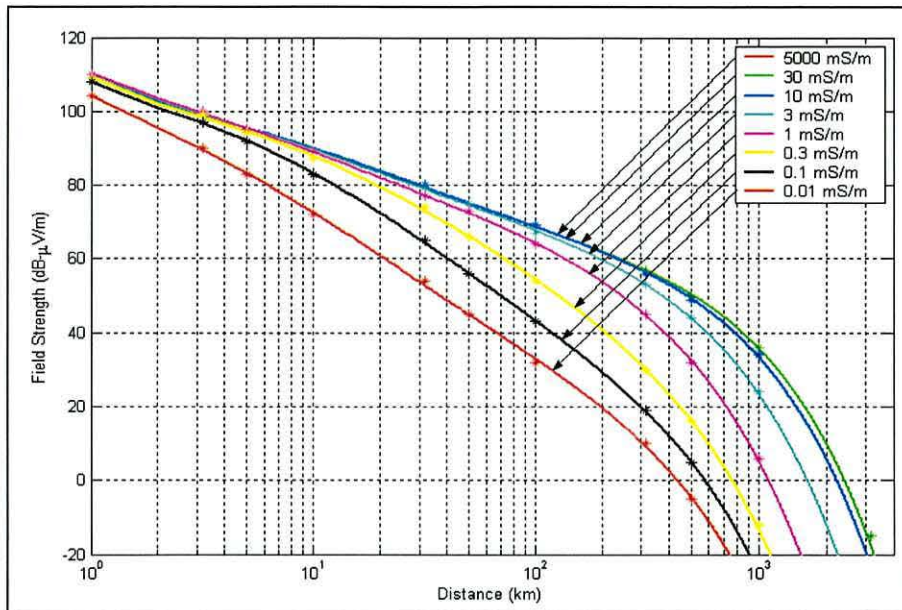
Fig. 4.2 - Groundwave propagation curves for Datatrak signals from Table 4.2.
Stars: data points to which curves are fitted.

4.4   Ground conductivity database

Before the curves can be used to help predict the coverage of a Datatrak system, the ground conductivity distribution must be known throughout the area of potential coverage. The ITU "World Atlas of Ground Conductivities" contains ground conductivity maps of many individual countries [35]. These maps are mostly quantised into the 8 ITU standard ground conductivities (Table 4.1).

The contents of the maps in [35] for European countries have been assembled into a single database at a resolution of 0.1° of latitude and longitude (approximately 11 x 7 km in the UK). Non-standard ground conductivities used in the maps of a few countries, which include the UK, have been rounded to the nearest ITU quantised value [35]. Part of the database is illustrated in Fig. 4.3. Most of Europe and North Africa has ground conductivities of between 1 and 30 mS/m. Norway is an exception, with remarkably low ground conductivity that drops to 0.01 mS/m in some parts of its mountain ranges.

Datatrak also operate networks in South America and South Africa, outside the existing ground conductivity database. So, these large areas were digitised from the ITU maps as part of this work. Also, the values for all European countries were
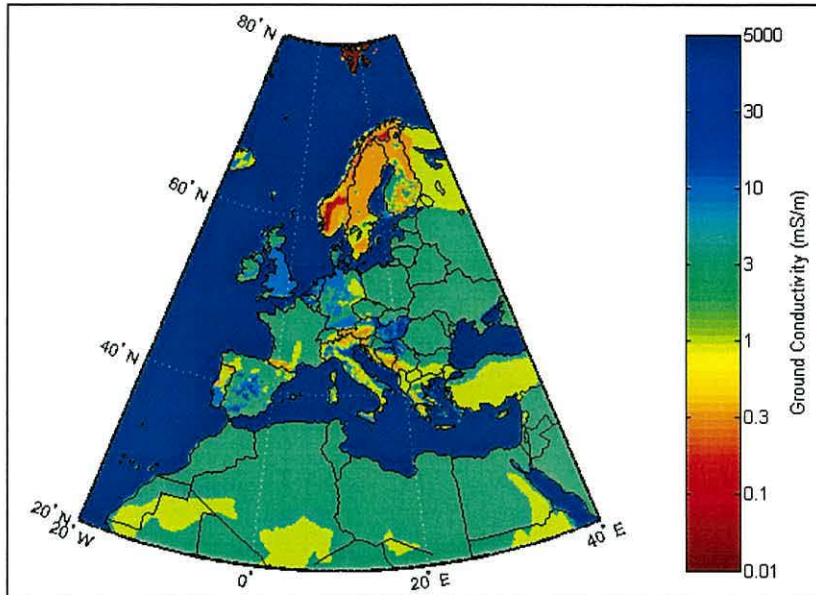
Fig. 4.3 - Ground conductivity in Europe and North Africa

carefully checked against the latest ITU maps and updated where necessary. Importantly given that a Datatrak network is being planned for the country, north-east Austria is now shown to have lower conductivity land than previously. Data was also added for Hungary. Thus, the map could be used for planning a new system proposed for Austria (Section 3.5).

4.5   Millington's method

Most propagation paths from transmitters to receivers are inhomogeneous; that is, they have sections of different ground conductivities. The ITU recommend the use of Millington's method for estimating the signal attenuation over such paths [36]. Fig. 4.4 shows a path with three sections of lengths d_1, d_2 and d_3, the signal travelling from land (green conductivity curve) to sea (blue curve) and back to land (green curve). The figure illustrates the Millington process. The attenuation over the first section is determined using the green curve, the appropriate one for its conductivity. Then, the additional attenuation contributed by the second section is determined from the part of the blue curve corresponding to its spread of ranges from the transmitter. Finally, the additional attenuation contributed by third section is determined using the green curve again. We finish up with an overall attenuation value for the path. The transmitter and receiver are then interchanged, and the process carried out in the opposite direction, resulting in a second attenuation value. Millington's method is
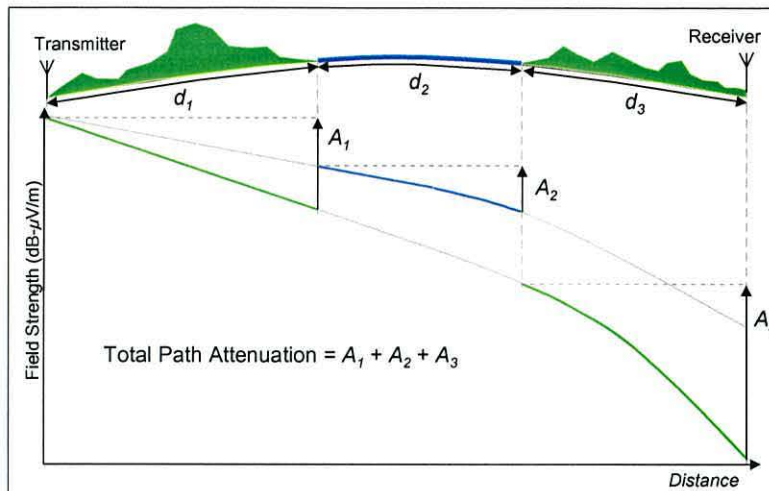
Fig. 4.4 - Graphical representation of Millington's method, applied in one direction
based on the principle that the best estimate of the actual attenuation is the average of
these two estimates.

If the radiated powers of the transmitters are then known, the field strength at the
receiver can be calculated from the attenuation using Equation (4.2):

$$E_{ground} = C - A_{dB} + 10\log\left(\frac{P_{Watts}}{1000}\right), \qquad (4.2)$$

where E_{ground} is the field strength in dB-μV/m, C is the field strength at 1 km with a
1 kW transmission. For a Datatrak frequency of 150 kHz, C is 110.0 dB-μV/m [36].
A_{dB} is the attenuation in dB, as calculated using Millington's method, and P_{Watts} is the
radiated power, in Watts.

4.5.1 Temporal Variation in Ground Conductivity

We need to consider whether snowfall, or the freezing of seawater or ground in
winter, significantly affect ground conductivity at Datatrak frequencies. Following the
approach of Poppe [2], Table 4.1 shows the penetration depths (or "skin depths") of
the Datatrak signal into ground of various conductivities; this is the depth at which the
field strength has fallen to the surface value divided by e, or 37% of the surface value,
an attenuation of 1 neper [13]. Consider sea-water (5000 mS/m) covered with, say,
2 m of ice (0.01 mS/m), as could happen during winter. The penetration depth through
ice is more than 400 m, so very little energy will be lost in the ice. Most of the energy

will be dispersed in the sea-water below, with its skin depth of less than a metre. So, the effective surface conductivity remains close to the summer value and the groundwave attenuation calculated using Millington's method will remain valid all year. The same reasoning can be applied to snow covered or frozen ground. Little energy will be lost in the few metres or so of snow and frozen ground, and most of the energy will be dissipated in the soil below. The implication of this is that the calculated groundwave attenuation applies all year round.

4.6 Transmitter Radiated Powers

Before the field strengths can be calculated, the radiated powers of the transmitters must be known. Datatrak believed that all UK transmitters were radiating 40 W on f_1 and 20 W on f_2 [43, 44]. The difference in power is due to two factors: f_2 is a lower frequency than f_1, so the antenna efficiency is less; and, the antenna tuning is optimised at f_1, with a capacitor switched in to resonate the system at f_2, but with less-than optimal impedance matching.

Given the importance of using correct values of radiated power in the model, it was decided to measure the values at a number of sample stations. The calibrated field strength measuring equipment and measurement technique described in Appendix C was employed close to the Southport, Stratford-upon-Avon and Huntingdon transmitters. The locations of the measuring sites were established using a GPS receiver. These sites were carefully chosen to be clear of trees, which can attenuate local signals, and of power lines which can cause local disturbances of signal level and may radiate interference. The sites were also at least one-half wavelength (at least 1.1 km for Datatrak) from the station to avoid induction-field effects [42].

The following equation is used to compute radiated power from the field strength measured at a known range from the transmitter:

$$P_r = \left(\frac{d \times E}{300}\right)^2, \tag{4.3}$$

where P_r is the radiated power in kW, d is the range from the transmitter in km, E is the measured field strength in mV/m.

Station	Measured Radiated Power (Watts)	
	f_1	f_2
Huntingdon	36	23
Stratford	85	43
Southport	40	22

Table 4.3 - Measured radiated powers of three Datatrak transmitters

This equation assumes a short monopole antenna over a perfectly conducting flat plane [45]. UK Datatrak antennas are 50m high, very short compared to even the shorter f_1 wavelength of approximately 2 km. The measurements were made at ranges of between 1.1 km and 6.2 km. Figs. 4.1 and 4.3 shows that over these very short ranges, ground conductivities of the values found in the UK have negligible effect.

The results of the experiment are shown in Table 4.3. The results for Huntingdon and Southport agree with Datatrak's figures to within 0.6 dB. But Stratford's radiated powers are more than 3 dB higher. According to Datatrak engineers, this may be due to the higher soil conductivity at Stratford's raising the efficiency of the antenna-earth system. All other transmitters, apart from Huntingdon, are on coastal sites, which generally have lower soil conductivities, and lower radiated powers. Southport is an example. In the model, the radiated powers measured will be used for those transmitters investigated and the Datatrak figures of 40W on f_1 and 20W on f_2 for the others.

4.7   Implementing the model

We now have all the information to calculate the field strengths of the Datatrak signals around each transmitter, using Millington's method to calculate the attenuations of the signal paths. To make optimum use of processing time, it was decided to generate once-and-for-all arrays of attenuation values covering the regions surrounding each Datatrak transmitter (Fig. 4.5), following the technique developed by Poppe [2]. Each element of the array is a 'calculation point' at which the signal attenuation from the transmitter is calculated using Millington's method and stored there. Storing attenuation rather than field strength, allows field strength values to be computed for any value of radiated power, using Equation (4.2).
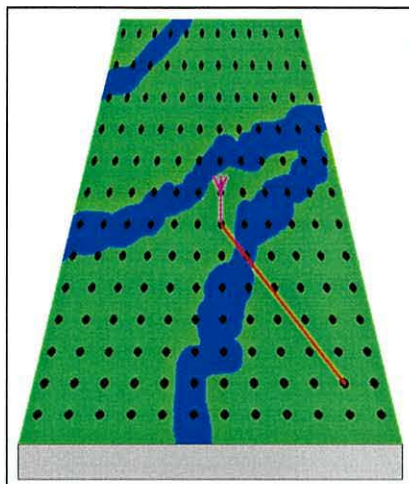
Fig. 4.5 - Array method employed in software model. Black dots are calculation points. Red line is propagation path from transmitter to calculation point.

Let us first calculate the "timing and data signal" range of the UK Datatrak stations, since this can be done for each station in isolation; later computations concerned with position measurements will involve combinations of stations. Datatrak state that the Locator requires a 15 dB minimum signal-to-noise ratio (SNR) to acquire and use these signals and that the Locator's own noise floor is at the equivalent of 5 dB-μV/m field strength [46, 47]. (We will question this latter figure in Section 6.7, but let us accept them at face value for now.) Thus, a minimum field strength of 20 dB-μV/m is required.

The model must employ computation arrays extensive enough to accommodate the transmitter with the highest radiated power of all Datatrak stations: this is a transmitter in Austria that radiates 380W [44]. The greatest range at which the signal from a transmitter of this power will have fallen to 20 dB-μV/m would be over an all-seawater path. ITU curves show that the range would then be 1450 km. To accommodate this range, a transmitter in the UK would require an array of 2900 x 2900 km, or 26° of latitude by 45° of longitude. If we retain the point spacing of the attenuation arrays, 0.1° latitude x 0.1° longitude, which is the resolution of the ground conductivity database, the array will require 133,400 elements.

Again, the implementation developed by Poppe is used to generate the arrays. She showed that her technique was accurate and she made measurements to validate the results. So, since the task of calculating the Datatrak groundwave field strengths is the

same as for her DGPS system, the original 'C' code developed by Poppe was analysed carefully, and used in the Datatrak prediction model, with some minor bug fixes.

The software was much improved with the inclusion of a graphical user interface, written in Microsoft's Visual C++ environment, which plotted the results on the screen as part of the coverage prediction process. Unlike previous Bangor models, including Poppe's, the Datatrak prediction model did not require third party software to view the results. The purpose of such a design was to make the model much easier and faster to use. For example, the user is able to use the mouse to point and click on the plot to print the field strength of the signal at that point. Also, there is a very useful zoom function that allows the user to magnify areas of interest.

Each Datatrak signal attenuation array took approximately 3 minutes to compute on a Pentium III computer running at 650 MHz with 256 MB of memory. Arrays for all 13 stations of the UK network were completed in less than an hour. Recall that each station has one attenuation array to represent the two centre frequencies, as described in Section 4.3.

4.8　Predicted field strengths

Fig. 4.6 shows an example plot exactly as produced by the Datatrak prediction model: it is the field strength array of the f_1 signal from the Stratford transmitter. The colours that represent the field strengths have been quantised for clarity.

The outer boundary is the 20 dB-μV/m contour, the coverage boundary for the timing signal. This coverage boundary is, of course, much more complex than the simple range circles currently employed by Datatrak, since it takes ground conductivity into account. Coverage range is greatest over sea-water, especially along the Bristol Channel. Signal attenuation over Devon and Cornwall is very clear, as is the more dramatic attenuation over the very low-conductivity ground of Norway. Throughout the UK, except in the Orkney and Shetland Islands and the northern Hebrides, the field strength is at least 30 dB-μV/m, well above the minimum level that Locators need to work correctly.
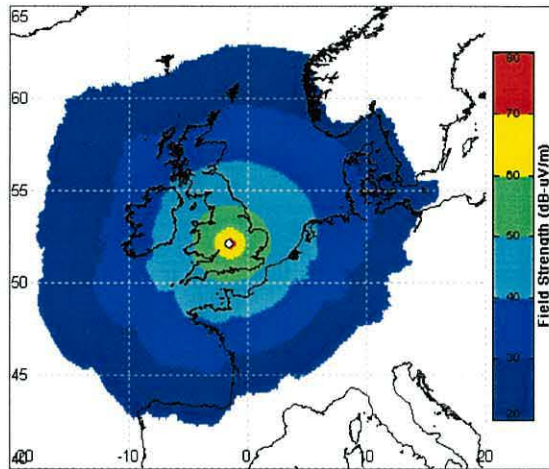
Fig. 4.6 - Predicted groundwave field strength of f_1 signal from Stratford Datatrak station

4.9   Verification

Let us consider what confidence we can place in this model, verifying it by measurements. The model is based on data collected by the ITU over many years, and the purpose of verification is certainly not to attempt verify their data or methods. That has been done elsewhere; the objective here is to confirm that the model is implementing them correctly.

Again, the field strength measurement equipment was used to measure the field strengths of Datatrak signals. The same measurement techinque as before was used, with the spectrum analyser operarated in its time-domain mode. Since, the stations transmit in pre-defined sequence, the pulse from each can easily be identified. Of course, one must careful to ensure that the antenna is pointing in the correct direction for each station, using the technique described in Appendix C.

Station	Range (km)	Radiated Power (Watts)		Predicted Field Strength (dB-μV/m)		Measured Field Strength (dB-μV/m)		Difference (dB)	
		f_1	f_2	f_1	f_2	f_1	f_2	f_1	f_2
Huntingdon	157	36	23	49.7	47.7	50.3	47.8	0.6	0.1
Stratford	117	85	43	56.3	53.5	55.8	54.3	-0.5	0.8
Lowestoft	259	40	20	44.8	41.8	45.3	43.8	0.5	2.0
Skegness	162	40	20	49.8	46.8	49.3	46.8	-0.5	0.0
Southport	77	40	22	56.9	54.3	56.8	54.8	-0.1	0.5
Cowbridge	207	40	20	46.9	43.9	45.8	45.8	-1.1	1.9

Table 4.4 - Measured and predicted groundwave field strengths in Stoke-on-Trent

Table 4.4 shows field strength measurements of the f_1 and f_2 signals made at Stoke-on-Trent (53.1174°N, 2.1814°W), together with the predicted field strengths there. It demonstrates that most of the predicted values were well within ± 1 dB of the measured value over a wide range of distances and paths from transmitters. Thus, it would appear that the model is working correctly and the radiated power values being used are sufficiently accurate. The two exceptions were the f_2 signals from Lowestoft and Cowbridge, which were both some 2dB stronger than predicted. These are two of the three weakest signals and it is suspected that the noise floor of the measuring equipment, which was only a few dB below the signal level, was contributing to these errors. But even with this uncertainty, an agreement within 2 dB is very satisfactory, given the unknowns in the ground conductivity and transmitter radiated power data.

4.10 Conclusion

The field strength of a Datatrak signal is highly dependent on the conductivity of the ground over which it propagates. Higher conductivity surfaces attenuate the signal less rapidly than lower conductivity surfaces. ITU ground conductivity maps have been digitised and stored for use in the Datatrak model. We have seen that the use of ITU field strength data at a single frequency, 150 kHz, is justified given the nature of the source data and its implementation in the model. We have chosen to implement Millington's method, as recommended by the ITU, to cope with inhomogeneous paths. The radiated powers of sample Datatrak transmitters have been checked.

Using techniques developed previously by Poppe, arrays of signal attenuation values were generated for Datatrak transmitters. Storing attenuation values allows the radiated power of the signal to be modified without needing to regenerate the arrays.

The model has been used to predict and plot groundwave field strength maps of all UK Datatrak stations. The results have then been verified by measurements at a test site. Agreement is generally within ±1dB. This gives confidence in the groundwave field strength values that will be used later for predicting coverage.

In the next chapter, we will continue to look at the signal transmitted from Datatrak stations, but this time concentrate on the signal component that takes the skywave route to the receiver.

Chapter 5

Skywave Field Strength and Fading

5.1   Introduction

In the last chapter, we discussed the only signals we wish the Datatrak Locator to receive: the groundwave signals from the Datatrak transmitters. Among the other interfering signals that will inevitably be received, are the skywave signals from Datatrak transmitters. These are components radiated from the transmitting antenna at vertical angles above horizontal and refracted back to earth by the ionosphere. Station-by-station, this unwanted component interferes with the corresponding wanted groundwave component, causing fading and phase distortion. This chapter looks at the methods of predicting the magnitudes of skywave signals, and quantifying their consequences.

5.2   What is Skywave?

Datatrak transmitters use short monopole antennae to launch their signals. These have the vertical polar diagram shown in Fig. 5.1. Clearly, a good deal of energy is radiated at angles high enough to generate skywaves. Skywave refraction is principally from the E-layer of the ionosphere at an altitude of approximately 100 km during the night [13, 15, 42]. At University of Wales, Bangor, the ITU method of calculating skywave field strength has been used with great success and has been shown to predict skywave intensities accurately [2]. Let us consider whether, and how, this approach might be used in the Datatrak propagation model.
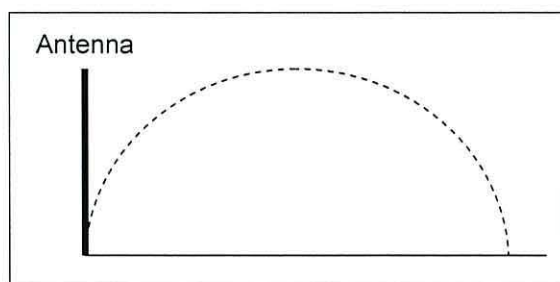
Fig. 5.1 - Vertical polar diagram of a short monopole antenna (after [48])

5.3   Calculating skywave field strength

The ITU method calculates the "annual median night-time skywave field strength" [2, 49] The current version, which we will employ in the model, is based on Equation (5.1):

$$E_{1kW} = G_{ant} + G_s + C_{sky} - 20\log(p) - L_a, \tag{5.1}$$

where E_{1kW} is the annual median night-time field strength in dB-µV/m from a 1 kW transmission, G_{ant} is the antenna gain factor in dB (Section 5.3.1), G_s is the sea gain factor in dB (Section 5.3.2), C_{sky} is a constant equal to 110.2, p is the slant propagation distance (Section 5.3.3), and L_a is a loss factor to account for ionospheric absorption of signal (Section 5.3.4). We will now examine each of these terms.

5.3.1 Antenna Gain Factor

Fig. 5.2 is a curve, produced by the ITU, which relates the vertical gain of the antenna to the range at which skywave signals return to the earth's surface [49]. It takes into account the vertical polar diagram of the monopole antenna (Fig. 5.1) and the reflection co-efficient of the ionosphere. Poppe fitted the third-order polynomial shown in Fig. 5.2 to this curve. Her analysis applies not only to the 300 kHz radiobeacons she was studying, but also to Datatrak signals, because the polar diagrams of the antennas are the same. The low-angle radiation that returns to earth at the greatest distances, is shown as unattenuated; that is, for any ranges greater than 10000 km, the factor is 0 dB. At ever-shorter distances, the signals have left the transmitting antenna at ever-higher vertical angles, and so experienced ever-greater attenuation due to the antenna's vertical polar diagram. Datatrak transmitters are
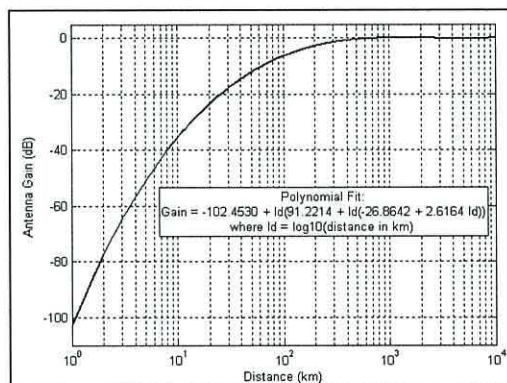
Fig. 5.2 - Antenna gain factor as a function of range from transmitter (after [49])

The polynomial shown on the figure reads:

$$G_{basic\_sea} = -0.0170 + 1.533d - 2.486d^2 + 4.089d^3 - 1.903d^4 + 0.264d^5$$
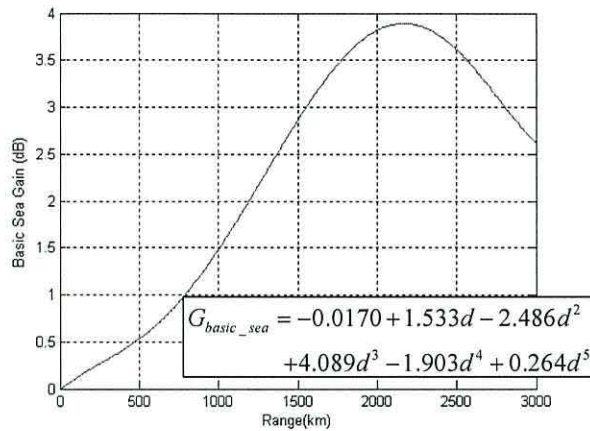
Fig. 5.3 - Basic sea gain as a function of range from transmitter

omni-directional in the horizontal plane so there is no variation in gain with azimuth.

5.3.2 Sea gain factor

The ITU have observed that, for a given range, skywave field strengths are greater when either the transmitter or the receiver, or both, is located close to seawater. In the land-based Datatrak system, the effect of *sea gain* is limited. However, some stations are close to coastlines and sea gains must be taken into account. An example is signals from Cowbridge in South Wales travelling south across the Bristol Channel to Devon and Cornwall.

Fig. 5.3 shows the *basic sea gain*, the gain when signals leave the transmitter or reach the receiver directly by the sea [49]. Poppe showed that the curve can be adequately described by a fifth-order polynomial [2]. Land between the terminals of the path and the sea reduces the sea gain. In estimating the sea gain at each end of a link, the model examines the ground conductivity database and so estimates the ratio of seawater to land near the transmitter and receiver. This ratio is then used to adjust the basic sea gain value.

5.3.3 Slant propagation distance

The slant propagation distance, p, is the distance covered by the skywave signal, from transmitter to receiver, via the ionosphere (Fig. 5.4). Its value is given by:

$$p = \sqrt{d^2 + 40000} \text{ km,} \tag{5.2}$$
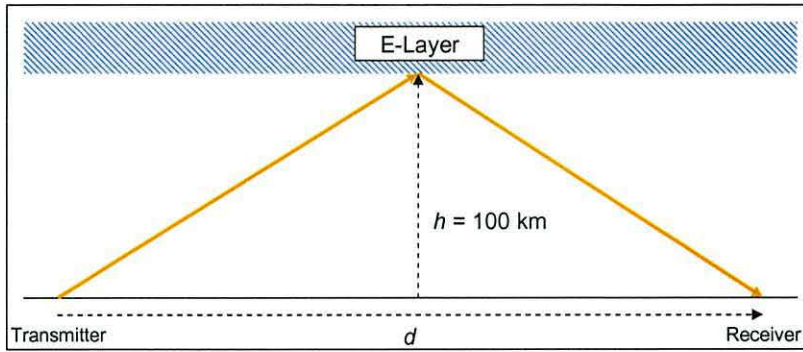
Fig. 5.4 - Calculation of the slant propagation distance, *p*, from *d*, the great circle distance between transmitter and receiver.

where *d* is the great circle distance from transmitter to receiver in km. As *d* increases, *p* asymptotes to *d*. The model applies Equation (5.2) over all path lengths, as recommended by the ITU [49].

5.3.4 Loss factor incorporating effects of ionospheric absorption, L_a

This loss factor incorporates the effects of losses due to power absorption in the ionosphere during the diffraction process, losses in the ground between hops of multi-hop paths, and losses in the ground near both the transmitter and receiver. It is expressed by Equation (5.3):

$$L_a = k_{geo} \sqrt{\frac{p}{1000}} \text{ dB'} \tag{5.3}$$

where *p* is the slant propagation distance (Section 5.4.3). The term k_{geo} is given by:

$$k_{geo} = 2\pi + 4.95 \tan^2 \Phi, \tag{5.4}$$

where Φ is the geomagnetic latitude of the mid-point of the path.

Equation (5.4) shows that the skywave field strength depends on the geomagnetic latitude; that is, the latitude relative to earth's geomagnetic axis. The geomagnetic latitude of the mid-point of the propagation path, which is used in this equation, can be calculated from the geographical coordinates using Equation (5.5). The geomagnetic North Pole is currently at approximately 78.5°N, 69°W [49].

$$\Phi = \arcsin\left[\sin\alpha_{geo}\sin 78.5° + \cos\alpha_{geo}\cos 78.5°\cos\left(69° + \beta_{geo}\right)\right], \tag{5.5}$$

where α_{geo} is the geographical latitude, and β_{geo} is the geographical longitude. If the magnitude of the geomagnetic latitude Φ exceeds 60°, then ITU recommend using the value 60° [49].

5.4   Developing the model

Using Equation (5.1), the model computes the median skywave field strength at each array computation point (Section 4.7). The result is a skywave attenuation array, analogous to the groundwave attenuation array of Chapter 4. As before, each point is visited in turn in the computation. Since both groundwave and skywave attenuation arrays require access to the conductivity database, it is convenient to generate the values at any point simultaneously. Skywave *field strength* arrays are produced from attenuation arrays by adding a transmitter radiated power factor:

$$E_{sky} = E_{1kW} + 10 \log\left(\frac{P_{Watts}}{1000}\right),$$ (5.6)

where E_{sky} is the median skywave field strength and P_{Watts} is the transmitter radiated power in Watts.

Much of the code developed by Poppe could be re-used in the Datatrak model. However, the ITU has updated the method of calculating the median skywave field strength since Poppe's code was written, so the code was changed accordingly. Also, minor bugs were identified and fixed.

Only a single array is produced to represent the signals on the two frequencies from each Datatrak transmitter. All factors, except sea gain, are either completely frequency-independent, or depend simply on the frequency *band* in which the signal resides (e.g. LF or medium frequency, MF). The effect on the results of ignoring the small frequency-dependent differences in sea gain is estimated to be less than 0.5 dB.

5.5   Prediction Model Results

Fig. 5.5 shows the f_1 skywave signal field strength plot of the Stratford transmitter produced by the model. The transmitter is at the centre of the rings of colour, which represent the annual median night-time values, quantised for clarity.
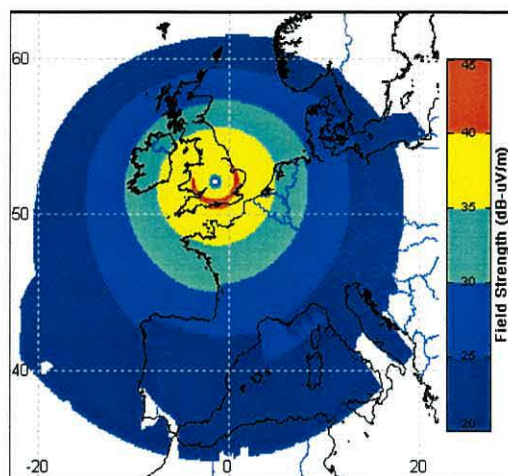
Fig. 5.5 - Annual median night-time skywave field strength of the Stratford transmitter

At the station itself, there is no skywave signal, since an ideal monopole antenna does not radiate vertically upwards (Fig. 5.1). The field strength increases rapidly with range, reaching a maximum of approximately 40 dB-uV/m at 170 km. Thereafter, it decreases slowly with range. The result is a classic skywave, roughly 'doughnut'-shaped, plot with the transmitter in the middle. The influence of geomagnetic latitude can be seen in the half-moon shape of the red boundary. The higher field strength at lower geomagnetic latitudes for the same range can be seen clearly.

The most striking part of the plot is to the south where sea gain effect can clearly be seen. For example, around Southern Italy, the field strength without sea gain would be just less than 20 dB-μV/m; sea gain brings it over the 20 dB-μV/m boundary value.

5.6   Temporal variation of skywave

The skywave field strength calculated according to the ITU method set out above is the night-time *annual median* value. Skywave intensity is stochastic in time. By measurements, the ITU has shown that it does not exceed 6.5dB above this median, 90% of the time. Some authors, including the ITU, use a Rayleigh curve to describe the statistical temporal distribution of skywave intensity with respect to the median [2, 37]. Poppe, however, concluded that it was more accurately represented by a Gaussian distribution. She reasoned that the Central Limit Theorem [2, 50] states that the probability distribution of a random variable (e.g. a skywave signal) tends to Gaussian as the number of variables approaches infinity. This is relevant because the

received skywave signal at a given point is the sum of many skywave components propagated via different paths. They all share the same distribution, but have different amplitudes. Hence, the resulting distribution would be expected to be close to Gaussian. The most-recent (2003) revision of the ITU document now agrees with Poppe. It shows that the 99%-ile field strength measured by ITU agrees within 0.3 dB with that predicted using Poppe's method [51].

5.7 Skywave Fading

If the amplitude of the skywave component of a signal reaching the receiver is comparable to that of the groundwave component there, significant fading will occur. Fig. 5.6 shows the skywave and groundwave field strengths from a Datatrak transmitter, as functions of range. Over seawater (conductivity of 5000 mS/m), the strength of the annual median skywave signal (red curve) becomes equal to the groundwave at approximately 1800km from the transmitter. Over very low conductivity ground, the two are equal just 70km from the transmitter. It is thus clear that the Datatrak system is susceptible to own-skywave interference over a wide spread of ranges. This is the main reason why Datatrak place a limit on the useful range of their transmitters (Section 9.4.1).

However, Datatrak is a system based on time-multiplexed transmissions. We must find whether the skywave signal from one transmitter could interfere with that from another, due to the time delay in the skywave propagation. Here, we follow a similar
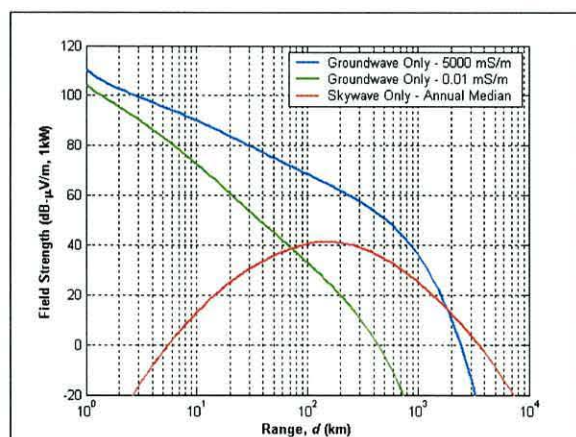
Fig. 5.6 - Field strengths of a Datatrak signal components.
Blue: Groundwave over seawater.
Green: Groundwave over low-conductivity ground.
Red: Annual median skywave.

reasoning to that of Poppe as she examined the effect of time delays on signal phases and hence fading.

The depth of fading that will result from the skywave component's interacting with the groundwave will depend, in part, on the phase difference between the two. The difference in the propagation delays they experience, Δt, is given approximately by:

$$\Delta t = \frac{\Delta d}{c}, \qquad (5.7)$$

where Δd is the difference in signal path lengths and c is the propagation velocity. Here, Δd is given by:

$$\Delta d = p - d$$

$$\Delta d = \sqrt{d^2 + 4h^2} - d \qquad (5.8)$$

where d is the great circle groundwave path between transmitter and receiver, p is the slant propagation distance, and h is the effective height of the ionosphere (Fig. 5.4).

Fig. 5.7 shows Δt as a function of range from the transmitter, when h is assumed to be 100 km [45].

Let us define a "fading zone" as the band of ranges where the median skywave field strength is potentially comparable with the groundwave field strength. Within that
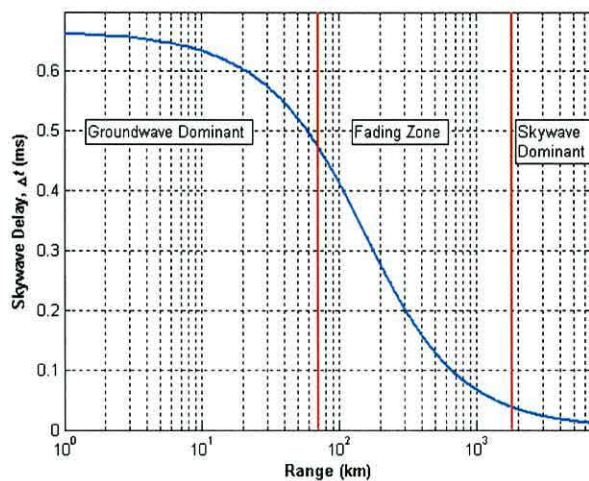
Fig. 5.7 – Skywave-groundwave propagation delay difference with respect range from transmitter.

zone, Δt ranges from 0.04 ms to 0.48 ms. The period of a Datatrak signal carrier is typically 0.007 ms. Thus, Δt is always of the order of many cycles of the carrier. It is reasonable to assume that the phase difference between the skywave and groundwave components is random, with a uniform distribution across 0-2π radians.

On the other hand, Δt is always negligibly short compared to the lengths of the transmissions of the individual Datatrak stations, 40 ms. Thus, there is no danger of the skywave components of one transmission being delayed sufficiently to interfere with the groundwave components of the next. Therefore, we are concerned solely with the skywave-groundwave interactions of each individual transmitter.

Working on radiobeacon signals in the 300 kHz band, Poppe determine the depth of fading of a groundwave signal that would be caused by a skywave component as a function of the skywave-to-groundwave ratio of strengths (SGR) [2].

The analysis describes the two signals as vectors (Fig. 5.8). The groundwave signal, (green) has a constant field strength and phase. The skywave component (red) field has Gaussian-distributed strengths. Its phase is uniformly random, with respect to that of the groundwave. The Locator receives the resultant (vector sum) of the two components (blue). We will first adapt Poppe's analysis of skywave fading for Datatrak frequencies, and later (Chapter 9) consider the effect on Datatrak operation of the phase variations caused by the skywave components.
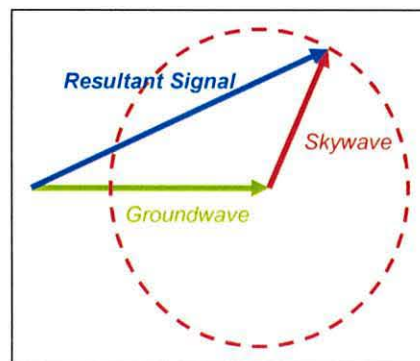
Fig. 5.8 - Vector representation of skywave (red) interacting with the groundwave signal (green). The signal received is the resultant (blue).

5.8   Modelling Own-Skywave Fading

The result of Poppe's analysis is summarised by Equation (5.9) which shows the field strength of the "total" night-time signal – the vector sum of the two components - that can be guaranteed for at least 95% of the time:

$$Total_{dB} = \begin{cases} Gnd_{dB} & SGR < -30 \\ Gnd_{dB} + F_3(SGR) & -30 \le SGR < -5 \\ Gnd_{dB} + F_4(SGR) & -5 \le SGR < 15 \\ Gnd_{dB} + SGR - 8.45 & 15 \le SGR \end{cases} \qquad (5.9)$$

where Gnd_{dB} is the groundwave field strength in dB-μV/m, and SGR is the ratio between the median skywave field strength and the groundwave field strength in dB. The factors $F_3(SGR)$ and $F_4(SGR)$ are given by Equations (5.10) and (5.11), respectively:

$$F_3(SGR) = -11.0087 - 0.8536SGR - 0.0224SGR^2 - 0.0002SGR^3 \qquad (5.10)$$

$$\begin{aligned} F_4(SGR) = &-8.4614 + 0.2005SGR + 0.0811SGR^2 \\ &-0.0014SGR^3 - 3.5 \times 10^{-5}SGR^4 \end{aligned} \qquad (5.11)$$

These are polynomials that define the total field strength of the received signal with fading due to the presence of the skywave signal. They have been derived from data produced by Poppe's fading analysis, and their use in the model saves computation time [2].

We will now use these equations in our Datatrak model to compute the 95%-ile night-time signal field strength at each array point from the groundwave field strength and annual median night-time skywave field strengths there. Fig. 5.9 shows the result of this analysis, with the yellow (seawater) and pink (low-conductivity ground) curves representing the night-time field strength that can be guaranteed 95% of the time. As expected, near the transmitter the groundwave signal dominates; it is much stronger than the skywave component. Further away, the two signals become comparable in field strength, and fading occurs; the total signal field strength is less than that of the groundwave component. Beyond this fading zone, the skywave component
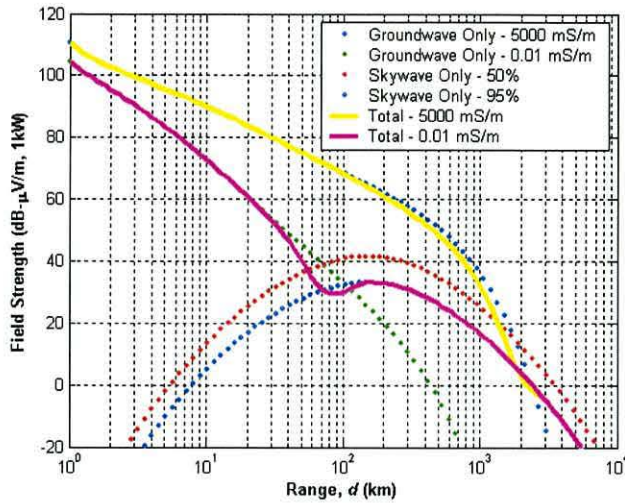
Fig. 5.9 - Received signal field strength.
Yellow: seawater. Pink: low-conductivity ground.

dominates; the curves asymptote to and follow the 95%-ile skywave distribution curve.

5.9   Night-time field strength results

An example of a night-time field strength plot produced by the Datatrak model is shown in Fig. 5.10 (RHS). This is the field strength that can be guaranteed 95% of the time at night. Also shown for comparison (LHS) is the daytime field strength plot (i.e. groundwave only). This plot, like its predecessors, is for the Stratford transmitter located at the white dot. The outer boundaries are where the field strengths have fallen to 20 dB-μV/m.
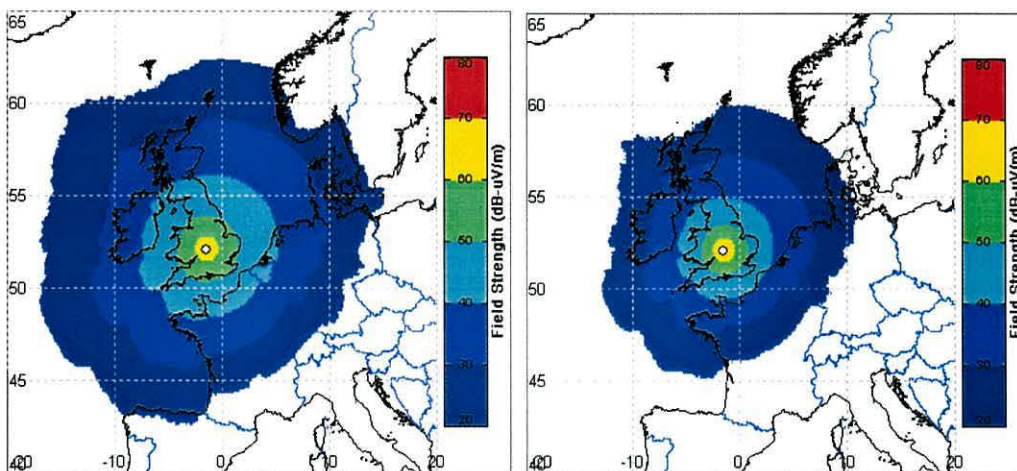
Fig. 5.10 - Left: Daytime (groundwave only) field strength. Right: Night-time (groundwave and skywave) field strength that can be guaranteed 95% of the time.

Comparing the two plots, one sees clearly the effect of skywave fading. For example, in Northern Scotland during daytime, the signal is always greater than 30 dB-μV/m. At night it is much less, falling below 20 dB-μV/m for at least 5% of the time. Because of this effect, the Cumbria transmitter is used rather than Stratford to supply the data and timing signal for Northern Scotland.

5.10 Verification

Poppe made extensive measurements of the field strength of a distant radiobeacon DGPS signal and obtained fading records from which she compared the statistical distribution of the measured field strengths with that predicted in the model. The discrepancy between prediction and measurement was rarely greater than 1 dB.

The field strength values of Datatrak signals recorded over a 24-hour period at the Stoke-on-Trent site (Section 4.9) were analysed to verify the fading model for Datatrak. In Chapter 4, we saw that high quality field strength equipment was used there to measure the daytime field strength. Combining these with the Locator-recorded *daytime*, groundwave only, field strengths, a calibration factor for f_1 and f_2 signals is determined for each station. These calibration factors are added to the relevant transmitter all-day readings from the Locator.

The results of the night-time measurements are shown in Table 5.1. Due to the calibration method, the same six transmitters were used in the experiment as in Chapter 4. The predicted and measured values (last two columns in Table 5.1) agree very well, most within ± 2 dB, over a wide variety of ranges from the transmitters. The one significant discrepancy concerns the Lowestoft transmitter for which the

Transmitter	Range (km)	Predicted Field Strength (dB-μV/m: 95%-ile)		Measured Field Strength (dB-μV/m: 95%-ile)		Difference (dB)	
		f_1	f_2	f_1	f_2	f_1	f_2
Huntingdon	157	46.8	44.9	49.2	46.6	2.4	1.7
Stratford	117	54.4	51.7	55.0	53.1	0.6	1.4
Lowestoft	259	40.5	37.5	43.0	41.1	2.5	3.6
Skegness	162	46.9	43.9	47.2	43.4	0.3	-0.5
Southport	77	56.2	53.6	56.4	53.8	0.2	0.2
Cowbridge	207	43.2	40.1	43.9	43.4	0.7	3.3

Table 5.1 - Predicted and measured night-time field strengths at Stoke-on-Trent

model underestimates the field strength by some 3 dB. In Table 4.4, the groundwave signal from this transmitter appeared to be underestimated by 2 dB; it would appear that this transmitter is radiating 2-3 dB more than Datatrak have stated. The difference on the f_2 signal measurement from the Cowbridge transmitter can be explained by the uncertainty in the groundwave measurement described in Section 4.9. Overall, the model has predicted the night-time field strength values satisfactorily.

5.11   Conclusions

Like all LF systems, transmitted Datatrak signals can propagate into the sky, and get refracted back to earth as skywaves which interact with the groundwave signal, causing deep fading and phase disturbances.

In this chapter, we have introduced an ITU method of calculating the skywave field strength, and applied the technique to Datatrak. Much of the implementation was completed by Poppe for her analysis of skywave at radiobeacon DGPS frequencies. However, it has been updated to take into account the latest updated ITU recommendation, adapted for Datatrak conditions, and errors in Poppe's code have been corrected.

By examining the time delay between the groundwave and skywave signals, it has been clearly shown that skywave signals from a Datatrak station cannot affect the groundwave signals from other stations, despite the time-multiplexed system employed by Datatrak.

It has also been shown that the received skywave signal will contain a random phase element due to the delay being several times the period of the carrier frequency. This is important, since it allows us to use Poppe's analysis of own-skywave fading for Datatrak.

The result is a field strength prediction model that calculate field strengths during the night, taking own-skywave fading into account. The results have been verified against

measurements at a known location. The measured results showed that, overall, the model agreed with reality to within ±2 dB.

In this chapter, we have discussed the effect of skywave on the amplitude of the groundwave signal. However, since Datatrak measures the phase of a signal to calculate its range from a transmitter, the effect of skywave on the variation of groundwave phase is important. In Chapter 9, we will investigate the effect in detail.

Chapter 6

Radio Noise

6.1   Introduction

In the previous two chapters, the signals radiated by Datatrak transmitters have been investigated and a model produced to predict their field strengths. However, Datatrak Locators also receive unwanted radio noise. This can be atmospheric noise, locally-generated electrical interference, or noise generated in the Locator itself. In this chapter, these three sources of noise will be investigated. Then, comparing the predicted Datatrak field strengths with these predicted noise levels, the model will estimate the signal-to-noise ratio (SNR) at each array point.

6.2   Atmospheric noise

In the Datatrak frequency band, the dominant naturally-occurring noise is atmospheric noise – produced by lightning activity around the world. This electrical activity is generally greatest around the equator, the noise generated there propagating to the medium and higher latitudes as groundwave or skywave signals [45, 52].

By its nature, atmospheric noise is random, and its instantaneous value is unpredictable. However, the ITU have collected data over many years that allow radio noise intensity to be predicted in the medium and longer terms [52]. The magnitude, and the statistical parameters, of atmospheric noise vary with location, time-of-day, and season of the year. The ITU publishes 24 world-wide charts (e.g. Fig. 6.1), one for each of the 4 seasons and 6 four-hour time blocks (e.g. 0000-0400, 0400-0800, etc.). They show the contours of the average noise at 1 MHz, expressed in dB above thermal noise. Fig. 6.1 shows the map for summer days from 1600-2000 hours local time. Compare the much higher noise values around the equator with the lower values at medium and high latitudes.
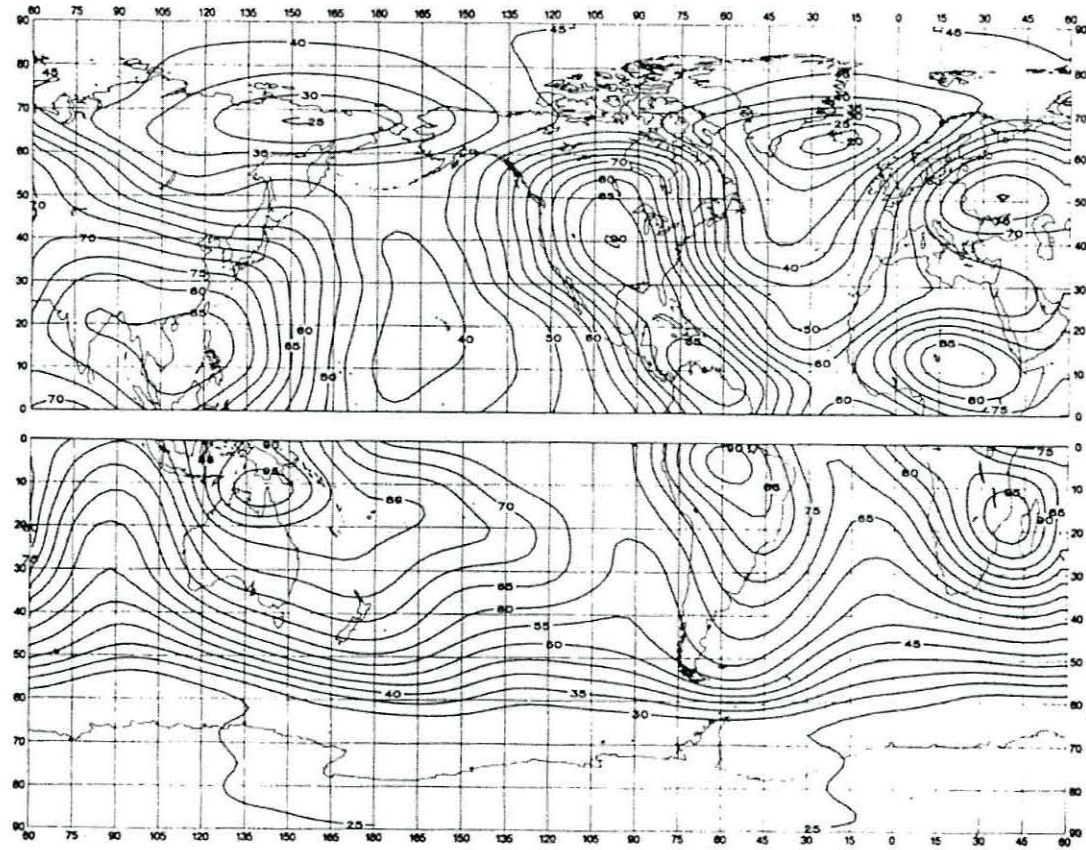
FIGURE 31a – *Expected values of atmospheric radio noise, F_{am} (dB above kT_0b at 1 MHz) (Summer; 1600-2000 LT)*

Fig. 6.1 - ITU atmospheric noise map (dB above thermal noise) at 1 MHz for summer days from 1600-2000 local time (after [52])
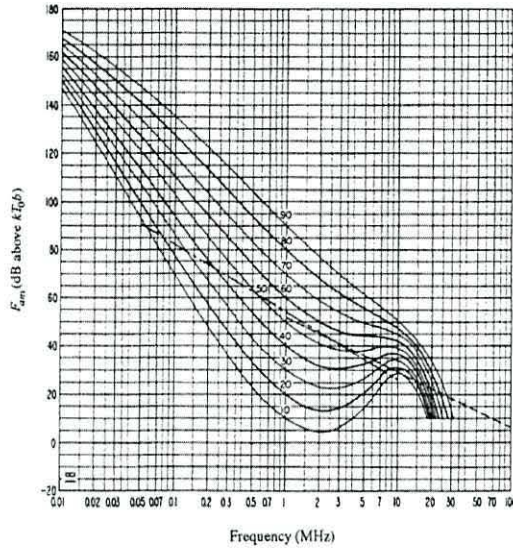
Frequency (MHz)

**Fig. 6.2 - ITU frequency conversion chart for summer days from 1600-2000 hours
local time (after [52])**

Conversion of the 1 MHz noise values to other frequencies is done using the chart that accompanies each map; Fig. 6.2 accompanies Fig. 6.1. It shows that the noise level at the typical Datatrak frequency of 150 kHz is 40-50 dB higher than the 1 MHz values shown on the map.

At a given geographical point and frequency, the median noise strength, $E_{atmospheric}$ (dB-μV/m) is calculated as follows:

$$E_{atmospheric} = F_{am} + 20 \log f_{MHz} + 10 \log b_{receiver} - 95.5, \qquad (6.1)$$

where F_{am} is the noise strength read from Fig. 6.2 given the mapped value at the location from Fig. 6.1, f_{MHz} is the frequency in MHz, and $b_{receiver}$ is the noise bandwidth of the receiver in Hz.

Fig. 6.3 shows the statistical parameters of the noise, which is assumed to be two-sided Gaussian [52]. The figure gives the upper and lower decile values. For example, at the Datatrak frequency of 150 kHz, and the previous time and season, the noise value is less than 13 dB above F_{am} (and therefore $E_{atmospheric}$ too) for 90 % of the time. For predicting Datatrak coverage, other noise value probabilities may be required. It was decided generally to follow common practice and employ the noise value not exceeded 95 % of the time [2, 37, 38].

Frequency (MHz)
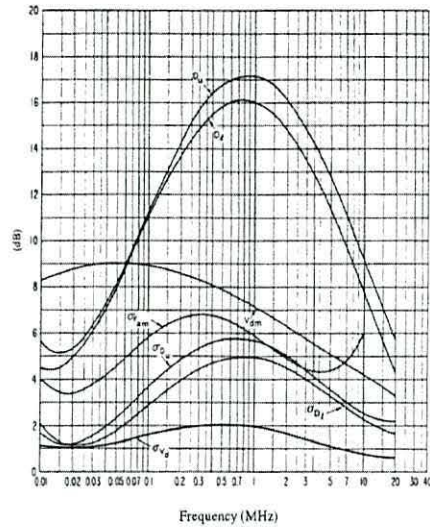
Fig. 6.3 - ITU statistical parameters chart for summer days from 1600-2000 hours local time (after [52])

6.3   Modelling Atmospheric Noise

Previous atmospheric noise models developed at Bangor using the ITU technique required the noise data to be digitised manually and entered into a data table to be accessed by the software. Datatrak is a system that has been deployed in several places around the world, with a view of expanding to other areas (e.g. Austria). Even for a relatively small working area, digitising atmospheric noise data is very time-consuming; it would be impractical for a model intended for use anywhere in the world, especially if different percentiles or situations were required.

Fortunately, Spaulding and Stewart have developed a method of representing all the noise map data in the form of a fitted two-dimensional Fourier sine series [53]. The method calculates F_{am} for use in Equation (6.1). The coefficients they computed have been released by the ITU [52]. We can use this method to automate the process of calculating the atmospheric noise at any given location, season or time-of-day. The result will be a very flexible atmospheric noise model, requiring little effort from the user.

The method is described by the following Equation:

$$F_{am}(x, y) = \sum_{k=1}^{29} \left(\sum_{j=1}^{15} b_{j,k} \sin jy + X_k \right) \sin kx + \alpha + \beta x , \qquad (6.2)$$

where $F_{am}(x,y)$ is the 1 MHz median noise in dB above thermal noise, x is the latitude expressed (curiously) in radians north of the South pole $(0 \rightarrow \pi)$, y is longitude in degrees east of Greenwich $\times \pi / 360$ (ie $0 \rightarrow \pi$), X_k is a coefficient used to ensure that the same value is returned when y is at either 0 or π (i.e. along the Greenwich meridian), α and β are coefficients that ensure a single value at the poles, and $b_{j,k}$ is the jth and k^{th} coefficient (24 sets of 435 coefficients in total) of the fitted Fourier sine series provided by the ITU.

The frequency variation of F_{am} is given by the polynomial:

$$F_{am}\left(x,z\right) = K_1\left(z\right) + K_2\left(z\right)x_a + K_3\left(z\right)x_a^2 + \ldots + K_7\left(z\right)x_a^6, \qquad (6.3)$$

where $F_{am}(x,z)$ is the median noise in dB above thermal noise at the required frequency, z is the 1 MHz F_{am} value from the map [Equation (6.2)], x_a is defined by Equation (6.4) and K_i by Equation (6.5). Thus:

$$x_a = \frac{8 \times 2^{\log_{10} f_{MHz}} - 11}{4}, \qquad (6.4)$$

where f_{MHz} is the required frequency in MHz (e.g. at 1 MHz, $x_a = -0.75$). Also:

$$K_i\left(z\right) = B_{i,1} + B_{i,2}z, \qquad (6.5)$$

where $B_{i,n}$ is the ith and n^{th} polynomial coefficient given by the ITU.

At this stage, the median value of the atmospheric noise at any frequency between 10 kHz and 20 MHz can be calculated by applying the value of $F_{am}(x,z)$ to Equation (6.1). However, the statistics of the noise is required as well, and each parameter is represented by a fitted fifth-order polynomial computed by Spaulding and Stewart, to represent the data in Fig. 6.3. Again, the coefficients have been published by the ITU.
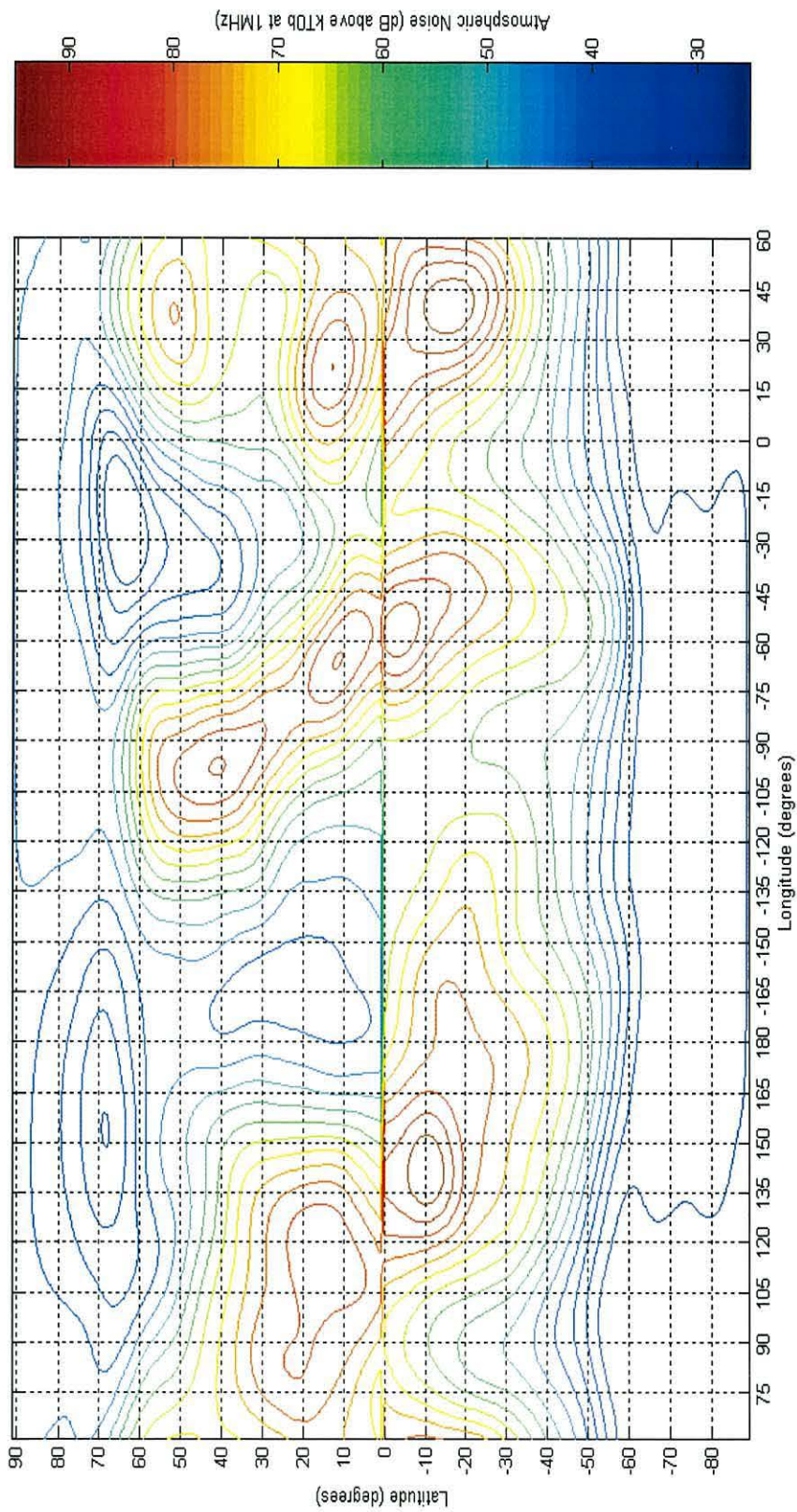
Fig. 6.4 – Atmospheric noise map generated by the model

The ITU also provide interface software, written in FORTRAN by Spaulding and Stewart, which allows the user to enter a geographical position, and retrieve the noise values and statistics at a frequency specified by the user. This software was converted to C-code using a conversion utility, and the noise calculation subroutines extracted from it; the algorithm was left unchanged to minimise the possibility of introducing errors. The C-code version was then checked against manual calculations to ensure that the conversion process had been successful (see examples in Appendix D).

Using this software, the Datatrak model can now generate atmospheric noise maps for anywhere in the world, at any frequency between 10 kHz and 20 MHz, for any season and any time of day. This level of flexibility is unprecedented in this type of coverage and performance prediction model.

An example atmospheric noise map generated by the software is shown in Fig. 6.4. This is for summer days from 1600-2000 hours local time at 1 MHz. The differences between this figure and the published map in Fig. 6.1 are negligible.

The statistics determined using Spaulding and Stewart's method are used to calculate the field strength at any percentile. We have used the values D_u and D_ℓ (Fig. 6.3) to determine the standard deviations above and below the median, respectively. These values can then be used to calculate the atmospheric noise field strength at any percentile required.

As a result of this work, we now have for the first time, the ability to generate atmospheric noise maps for any Datatrak system world-wide. Fig. 6.5 shows the annual median atmospheric noise generated in this way for a centre frequency of 150 kHz and receiver bandwidth of 160 Hz (a value determined by the method explained in Chapter 7). The map represents the noise level in dB-μV/m not exceeded 95 % of the time. As would be expected, the highest noise levels are around the equator and the lowest around the poles. Also, because these are annual median values, they are approximately symmetrical about the equator, whereas the conventional seasonal maps generally are not. Hot spots are observed over the land-masses.
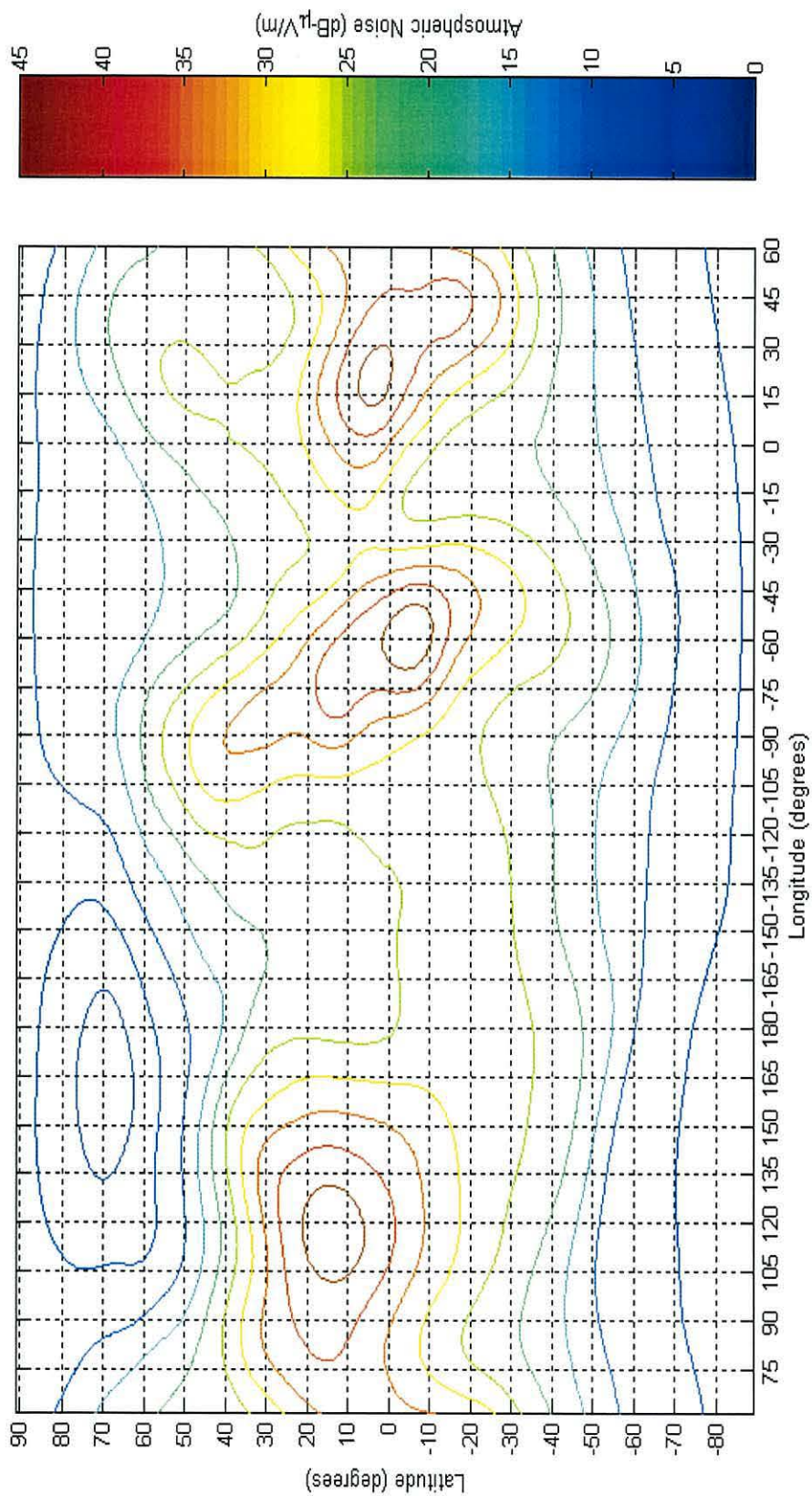
Fig. 6.5 – Annual atmospheric noise field strength not exceeded 95 % of the time

The model will use a single layer to represent a single atmospheric noise value for both frequencies, f_1 and f_2. In the UK, this use of a single value will introduce an error of around 2 dB only. This was judged to be negligible, given the accuracy with which the groundwave and skywave field strengths are known.

The user may select whatever type of atmospheric noise (annual median, worst case, individual time block, etc.) the Datatrak model is to use. For the remainder of this thesis, the annual atmospheric noise field strength, not exceeded 95 % of the time, will be employed in all examples.

6.4　Vehicle Noise

Vehicle noise is radio noise generated by the electrical systems of the vehicle in which the receiver is installed, or by other vehicles (and possibly buildings) in its vicinity. The level of the "own-vehicle" noise depends greatly on the design of the vehicle and the quality of the Datatrak equipment installation, notably the degree to which noise-generating systems have been suppressed. The level of noise from other vehicles varies a good deal and must be treated statistically.

Getting hold of vehicle noise to use in the model proved difficult. Simply measuring the noise of a single vehicle would bias the results to its specific installation and test area. Making a large number of measurements was considered beyond the scope of the present study. Instead, Datatrak engineers were asked to specify a value for use in the model on the basis of their very wide experience of installations and operational situations. They suggested a typical value of 20 dB-μV/m, but requested that the model employ a more conservative, near-worst-case, value: 27 dB-μV/m [54]. This was made the default value; if a different one is required, it may be entered manually.

6.5　Locator Noise Floor

The "noise floor" of the Locator is the noise generated by the Locator itself. Electronic noise is generated by all electronic components. The noise floor of the Mk4 H-field Datatrak Locator had been estimated by Datatrak to be equivalent to a field strength of 5 dB-μV/m [46, 47]. This value will be used initially as the receiver noise in the model.

6.6   Using Radio Noise in the Model

Using the predicted Datatrak signal field strength (daytime or night-time) with the predicted radio noise, the model can predict *signal-to-noise ratio* (SNR) at each array point. We will see later that this factor will determine the repeatable accuracy of the measured position. Let us first, however, introduce the minimum SNR required by the Locator, 15 dB [46], as a coverage-limiting factor, in addition to the minimum field strength of 20 dB-µV/m employed previously.

Fig. 6.6 shows the result when the SNR is determined by the annual atmospheric noise, not exceeded 95 % of the time, is used. The SNR boundary is dominant; it always occurs at field strength above 20 dB-µV/m. Notice, however, that it occurs at higher groundwave field strength in the south-east of the UK than in the north-west, because of the stronger atmospheric noise in the south-east (Fig. 6.6).

Fig. 6.7 shows the Stratford results, but with the boundary set by a vehicle noise level of 27 dB-µV/m. Now, the boundary corresponds to the contour at which the field strength has fallen to 15 dB above the 27 dB-µV/m vehicle noise value; that is, 42 dB-µV/m. The results confirm the general observation of Datatrak engineers that it is normally vehicle noise that limits coverage. A notable exception is in the Gauteng region of network in South Africa (around Johannesburg), where severe electrical storms occur in the area during certain times of the year, causing very high levels of atmospheric noise.
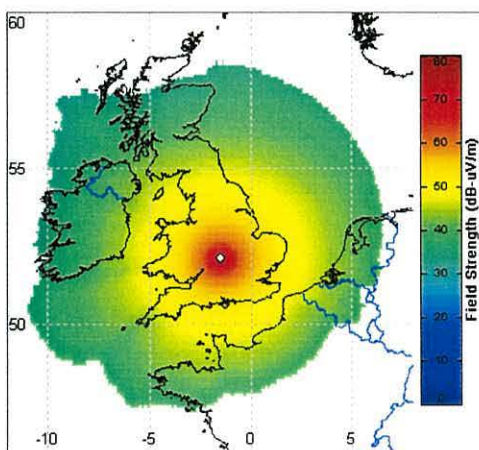
Fig. 6.6 - Daytime field strength plots of Stratford signal with atmospheric noise only. Outer boundary: 15 dB SNR.
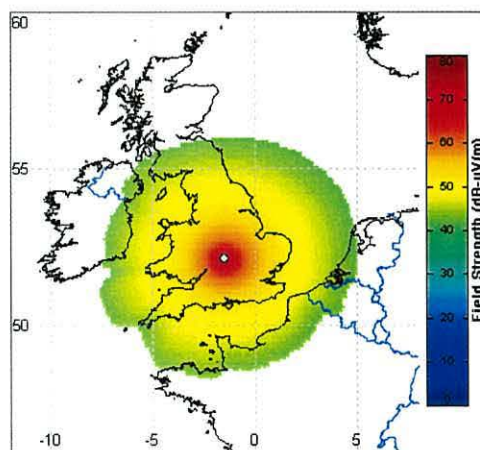
Fig. 6.7 - Daytime field strength plots of Stratford signal with vehicle noise only. Outer boundary: 15 dB SNR.

Since the receiver noise is equivalent to only 5 dB-μV/m, it is invariably much weaker than vehicle noise. In combining the three noise sources (atmospheric, vehicle and noise floor), the root-sum-squared value is taken. Usually, one source dominates, and is the case in the UK. Fig. 6.7 represents the coverage plot taking into account all noise sources, since vehicle noise dominates above the other two noise sources.

6.7 Verification

As part of the set of measurements conducted in Stoke-on-Trent using a calibrated Mk4 Locator, noise field strength values were measured. The antenna was mounted on a brick wall, clear of buildings, and overhead cables. The antenna was a considerable distance away from the nearest road and vehicles, and therefore essentially immune to vehicle noise. So, it would be expected to have measured atmospheric and Locator noise, but not vehicle noise.

Fig. 6.8 shows the noise field strength measurement. They exhibit only small temporal variations; the f_1 values are all close to 29 dB-μV/m, and f_2 to 27 dB-μV/m. These records show none of the variations between night and day that characterise atmospheric noise. The average atmospheric noise field strength predicted for this site is just 2 dB-μV/m and the value predicted not to be exceeded 95 % of the time during the experiment is 20 dB-μV/m. These are well below the values measured. The conclusion has to be that the noise is Locator floor.
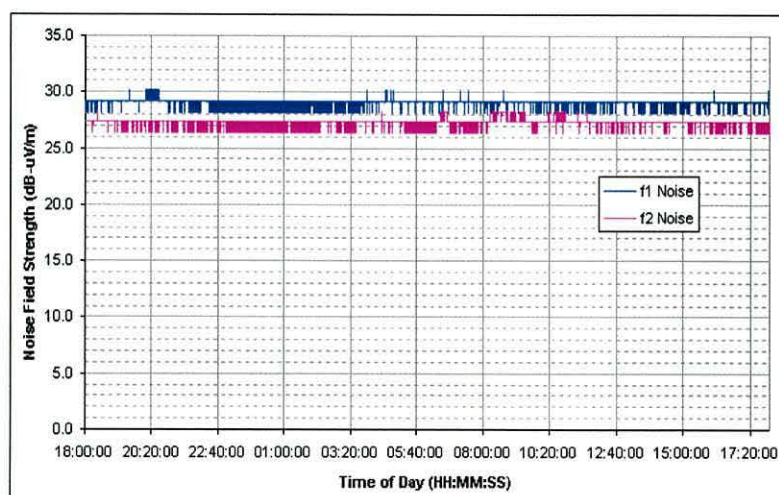
Fig. 6.8 - Noise measurement from Stoke-on-Trent.
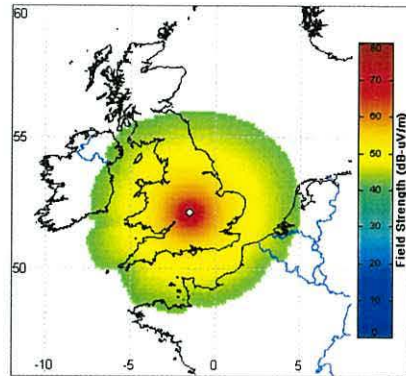
Fig. 6.9 - Daytime field strength plots of Stratford signal with Locator noise floor of 28 dB-μV/m. Outer boundary: 15 dB SNR.

Clearly, there is a huge discrepancy, some 22-24 dB, between the Locator noise floor quoted by Datatrak engineers, and the values recorded in the measurements above. When this was investigated, it was discovered that the noise floor Datatrak had quoted had been that of an E-field Locator system. Unfortunately, the voltage out of the physically-small (no more than 15 mm x 55 mm) H-field antenna for a given field strength is small. Relatively high amplification is required and it is the noise of this amplifier that is being observed. In order to represent this in the model, the Locator noise floor value has been increased to 28 dB-μV/m, the average of the slightly different f_1 and f_2 values.

The process of verification has taken an unexpected turn! It was intended to allow the temporal fluctuations of atmospheric noise to be observed in the absence of vehicle noise. Instead, it has revealed that, when an H-field antenna is used, the dominant noise in almost all situations is that of the Locator antenna amplifier. This noise greatly exceeds any likely atmospheric noise, at least in temperate countries. The only area which atmospheric noise may dominate is in South Africa where severe thunderstorms can generate high noise levels (Fig. 6.1). The Locator noise also exceeds even the conservatively-high value of vehicle noise. We conclude that the signal-to-noise ratio in all but exceptional situations is the signal-to-Locator noise ratio. A revised coverage plot for the Stratford station is shown in Fig. 6.9.

6.8   Conclusions

Noise is a major factor in determining the coverage of a signal. For the Datatrak system, radio noise can be created by lightning activity (atmospheric noise), the

electrical system of the vehicle and surrounding vehicles, and by the Locator and the antenna system itself.

First of all, atmospheric noise was considered. In past models of LF navigation systems, the atmospheric noise data was digitised and manipulated manually. However, here we have built in ITU atmospheric noise maps for anywhere in the world, at any frequency, for any season, and for any time-of-day now available in electronic form. Although, it required some modification, this sophisticated algorithm now forms part of the Datatrak model.

Next, noise generated by the vehicle being tracked, or vehicles and buildings in its vicinity, was considered. In this case, the experience of Datatrak engineers was used to define a near-worst-case value for this type of noise in the model.

Finally, the noise generated by the Locator itself, or the Locator noise floor, was considered. Again, Datatrak engineers were asked for a value, and this was used in the prediction model.

For the first time, we have a model able to combine predicted Datatrak signal field strengths together with predicted noise levels to predict signal-to-noise ratios. Using it, we have shown that coverage is determined by SNR rather than by minimum field strength. This result is of great interest to Datatrak since the plots produced clearly illustrate the coverage of the trigger and data signal.

However, the Locator noise floor was a good deal stronger than we had been led to believe, and is the dominant noise source. It thus obscures atmospheric noise and both prevents it from being measured and renders its calculation largely unnecessary, at least with the present generation of H-field antennas. However, the model now contains all three kinds of noise and so is able to predict the SNR of any Datatrak signal. With future, quieter antennas, atmospheric noise may again become significant in the absence of vehicle noise.

Chapter 7

Interference: Modelling the Locator

7.1   Introduction

Two sources of interference to the Datatrak signals have been investigated so far: skywave from Datatrak transmitters, and radio noise. We now consider interference from other radio signals. To tackle this, the model needs access to a representation of the response of the Locator to unwanted signals across a wide frequency range. The model will then simulate the interference environment at each array point and examine the effect of the interference on the SNR and, hence, the coverage and accuracy performance of the system. Among other benefits, this will help in making the optimal choice of operating frequencies. Interference is a very complex topic and we will deal with it in two stages. This chapter will explore the interference rejection of the Mk4 Locator and how it might be built into the model. The next chapter will analyse the performance of the Locator when exposed to the large and varied range of interferers with which it must deal.

The job of the filters in the Locator is to isolate the wanted Datatrak signal from within the soup of signals being received. We will define interference from strong signals that are insufficiently rejected because of inadequate filtering as *pass-band interference*. This will appear as noise on the wanted signal, and we will see that it can play a major role in determining the SNR. Even stronger signals, however, can overload the input stages of the Locator, causing distortion, or even the complete loss, of Datatrak signals; we call this *blocking interference*.

Datatrak did not have an overall frequency response of their Locator that could be employed in the model. So we will analyse the Locator in detail and produce a response from which we can compute the attenuation of any interferer and hence its effect on the performance of the Locator.
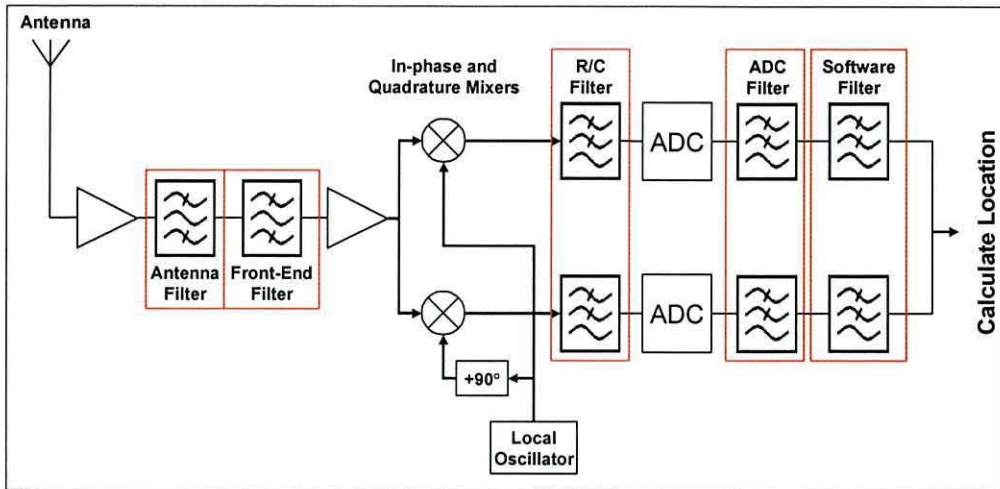
Fig. 7.1 - Block diagram of the signal path in an Mk4 Locator. Filters are highlighted in red.

7.2   Pass-band interference

Fig. 7.1 shows the block diagram of a Mk4 Locator, with all filters highlighted in red [55]. The signal from the H-field antenna passes through a broad-band amplifier and is filtered by an *Antenna filter* and then a *Front-end filter*. It is further amplified and fed to a quadrature mixer, in which a local oscillator at signal frequency converts it to baseband; the Datatrak signal appears at ±40 Hz. Each of the quadrature components of the signal (one only used for navigation, both used for data reception) is low-pass-filtered by a single-pole *R/C filter* with a cut-off frequency of 4.08 kHz [56]. The signals are then over-sampled at 256 kHz, and digitally filtered by an *ADC filter*, a low-pass anti-aliasing filter [57]. Finally, the sample rate is reduced to 2 kHz by decimation, and the signal is passed through a second digital low-pass *Software filter* before reaching the processor.

7.2.1 Frequency Limits of Interference

We need to consider interference over a wide range of frequencies. The upper limit is set by harmonics of the square-wave local oscillator (LO). Because the local oscillator produces a square wave input to the mixer, the receiver responds to signals at odd multiples of its fundamental frequency. When receiving the highest Datatrak frequency of 180 kHz, interference could be received at frequencies around $3 \times 180 = 540$ kHz, $5 \times 180 = 900$ kHz, etc. Datatrak advise that no interference problems have been observed at frequencies above the third harmonic in any of their
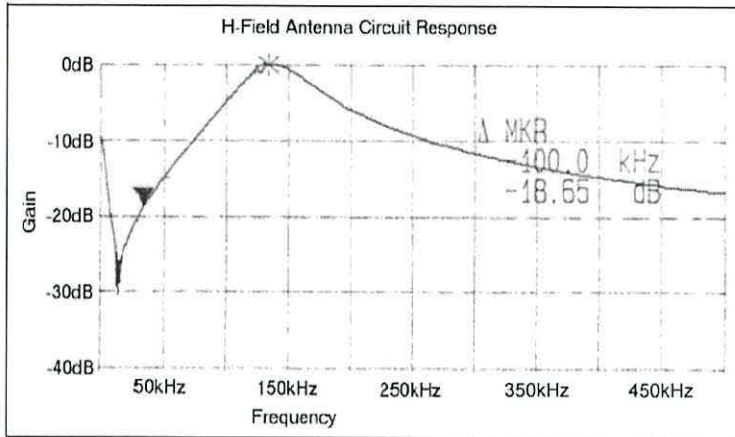
Fig. 7.2 - Antenna filter frequency response (after [58])

networks. So, we will set the upper limit of our range to 540 kHz, plus a 10 kHz allowance for the lower sideband of any interferer, that is, to 550 kHz. No interference has been detected below 50 kHz either, so that will be the lower limit.

7.2.2 Antenna and Front-end Filters

The *Antenna filter* is actually the frequency response of the H-field resonant circuit. This is shown in Fig. 7.2, as measured by Datatrak [58]. The attenuation above 500 kHz, which was not measured, is conservatively assumed to remain at the 500 kHz value of 16 dB at least as far as 550 kHz, the top of our range of interest.

Fig. 7.3 shows the frequency response of the *Front-end filter* [59] and Fig. 7.4 that of the combination of the Antenna and Front-end filters. It is the same in all Locators,
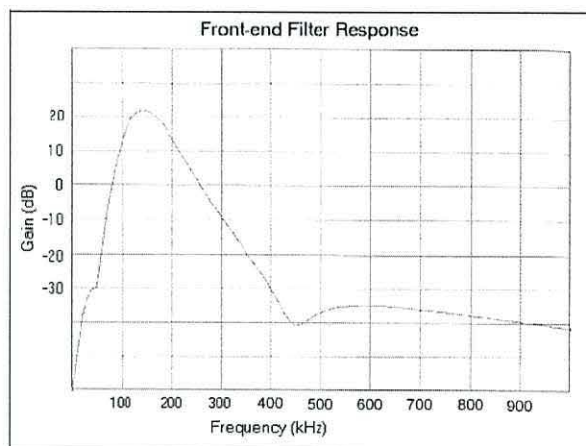
Fig. 7.3 - Frequency response of front-end filter (after [59])
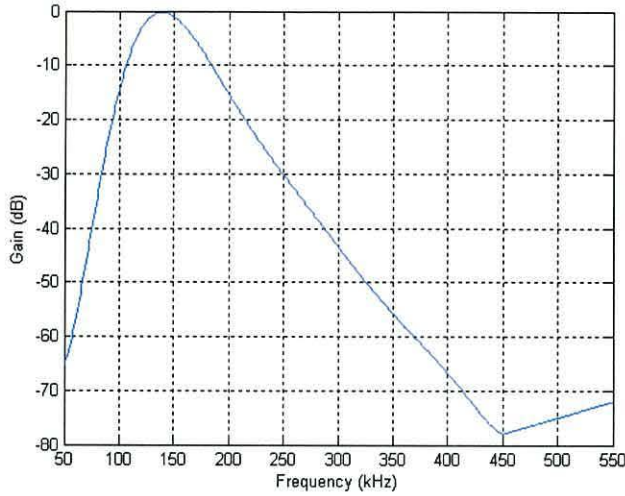
Fig. 7.4 - Combined frequency response of pre-mixer filters

independent of the choice of Datatrak frequencies. To minimise calculation time in the model, we will seek to represent the response of this combined filter (and all later filters) by polynomials. Here the sub-range from 50-450 kHz is represented by an 8th-order polynomial, and that from 450-550 kHz by a straight line, i.e.:

If $50 \leq f < 450$ kHz,
$$
\begin{aligned}
G_{static} = {} & 133.217 - 12.457f + 2.7893 \times 10^{-2} f^2 \\
& + 2.8819 \times 10^{-3} f^3 - 5.5874 \times 10^{-8} f^4 \\
& + 1.1182 \times 10^{-10} f^5 - 1.2232 \times 10^{-13} f^7 \\
& + 5.6439 \times 10^{-17} f^8
\end{aligned}
\tag{7.1}
$$

If $450 \leq f \leq 550$ kHz,
$$
G_{static} = \left[(f - 450) \times \frac{3}{50} \right] - 78
$$

where G_{static} is the gain. This is the response shown in Fig. 7.4. Note the very high levels of attenuation outside the frequency range 100-200 kHz.

7.2.3 Mixer

The local oscillator (LO), operating nominally at f_1 or f_2, mixes down to 40 Hz the Datatrak signals at f_{1+}, f_{1-}, f_{2+} and f_{2-} [60, 61]. Because the mixer is double-balanced, the signal and LO components, and all intermodulation products, should be cancelled out. The output spectrum will, however, include components at the following frequencies [62, 63, 64]:

$$m\omega_{LO} \pm \omega_s \qquad \text{where } m = 1, 3, 5, 7 \text{ etc.} \qquad (7.2)$$

where ω_{LO} is the local oscillator frequency, and ω_s the signal frequency. The amplitude of any third harmonic products will be 1/3 that of the fundamental (i.e. -9.5 dB) [62]. As stated earlier, higher-order products are ignored.

7.2.4 Post-mixer filters

The effects of the post-mixer filters on the frequency response of the Locator will appear relative to the Datatrak frequency in use (or its harmonics) in the response of the Locator. For example, when receiving a Datatrak frequency of 140.04 kHz, the LO will be at 140 kHz; an interferer at, say, 142 kHz will be mixed down to 2 kHz and will suffer the attenuation of the post-mixer filters corresponding to 2 kHz. Thus, their attenuation at 2 kHz will contribute to the Locator's response at 142 kHz.

The R/C filter is a single-pole, low-pass, filter, with a cut-off frequency of 4.08 kHz, designed to reduce the amplitude of the signal components that can cause *aliasing* in the ADC [56]. Its gain is given by:

$$\text{If } f < f_0, \qquad G_{RC} = 0 \text{ dB}$$
$$\text{If } f \geq f_0, \qquad G_{RC} = 20 \log\left(\frac{f_0}{f}\right) \text{ dB} \qquad (7.3)$$

where G_{RC} is the gain of the RC network, f_0 is its cut-off frequency, and f is the signal frequency [65]. We model it, accordingly, as shown in Fig. 7.5.
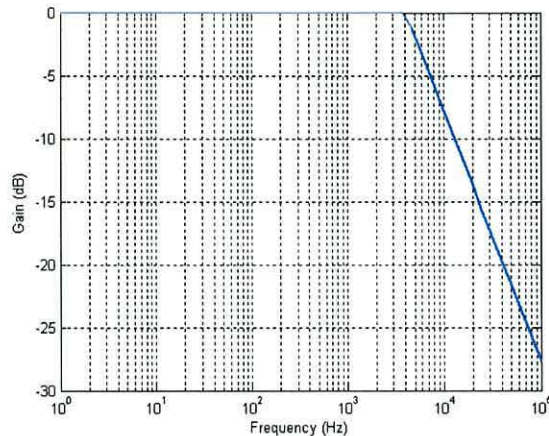
Fig. 7.5 - Modelled frequency response of R/C filter

ADC Filter Response.
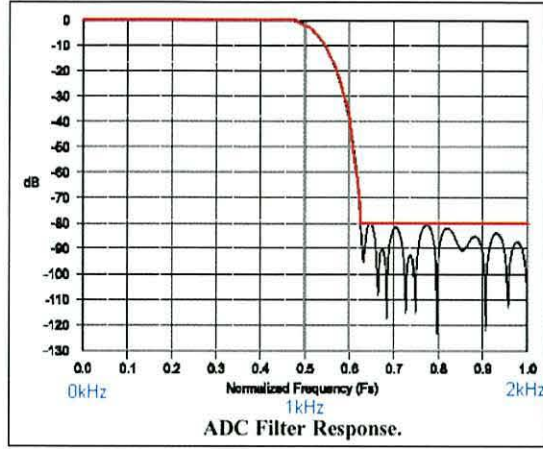
Fig. 7.6 - ADC anti-aliasing filter frequency response normalised to wanted sampling frequency, F_s. Red line: modelled approximation (after [57]).

The signal is now sampled by the ADC. Given the limited performance of the filters ahead of the ADC, aliasing of the higher frequency components will occur. The ADC chip is designed for audio applications with variable sampling rates. Since the anti-aliasing filter needs to change with the required sampling rate, it has been incorporated into the chip as the anti-aliasing *ADC filter* (Fig. 7.6). The actual signal is then over-sampled, and passed through this filter, before the sampling rate is reduced to that required by the process of decimation [57].

In the Locator, the actual sampling rate required, F_s, is 2 kHz. So, the ADC filter cut-off frequency is 1 kHz. This is sufficient to digitise the wanted 40 Hz baseband signal. The over-sampling rate of the ADC is set to 256 kHz. (The R/C filter described above is designed to reduce aliasing at this over-sampling frequency).

For simplicity, we model the ADC filter as the three parts shown by the red line in Fig. 7.6: a pass-band that is flat; a roll-off represented by a 4th-order polynomial; and a stop-band, with a single conservative value of 80 dB. Thus:

$$\text{If } f_{ADC} < 920 \text{ Hz}, \quad G_{AA} = 0 \text{ dB}$$
$$\text{If } 920 \le f_{ADC} \le 1260, \quad G_{AA} = -6187.96 + 25.17 f_{ADC} - 3.8424 \times 10^{-2} f_{ADC}^2$$
$$+2.6141 \times 10^{-5} f_{ADC}^3 - 6.7034 \times 10^{-9} f_{ADC}^4 \tag{7.4}$$
$$\text{If } f_{ADC} > 1260 \text{ Hz}, \quad G_{AA} = -80 \text{ dB}$$

where G_{AA} is the gain of the anti-aliasing filter, and f_{ADC} is defined by Equation (7.5).
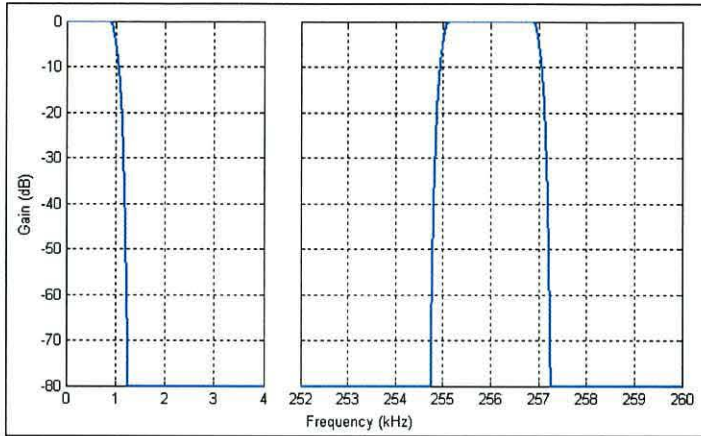
Fig. 7.7 – Modelled ADC filter frequency response. Filter passband repeats every 256 kHz due to aliasing effects at oversampling rate.

Since the ADC is of the delta-sigma variety, any frequency components at integer multiples of 256 kHz away from the tuned frequency will also penetrate the anti-aliasing filter due to aliasing at the over-sampling rate [57]. The model needs to take these effects into account by repeating the shape of the filter every 256 kHz:

$$f_{ADC} = |f_{\Delta t}| \bmod 256 \text{ kHz}$$
$$\text{If } f_{ADC} > 128 \text{ kHz}, f_{ADC} = 256 \text{ kHz} - f_{ADC}$$

(7.5)

where f_{ADC} is the difference between the baseband interferer frequency and the nearest integer multiple of the over-sampling frequency, and $f_{\Delta t}$ is the difference between the interferer frequency and the tuned frequency. Fig. 7.7 shows the modelled frequency response of the anti-alias filter. Notice how the filter is mirrored around the multiples of 256 kHz.
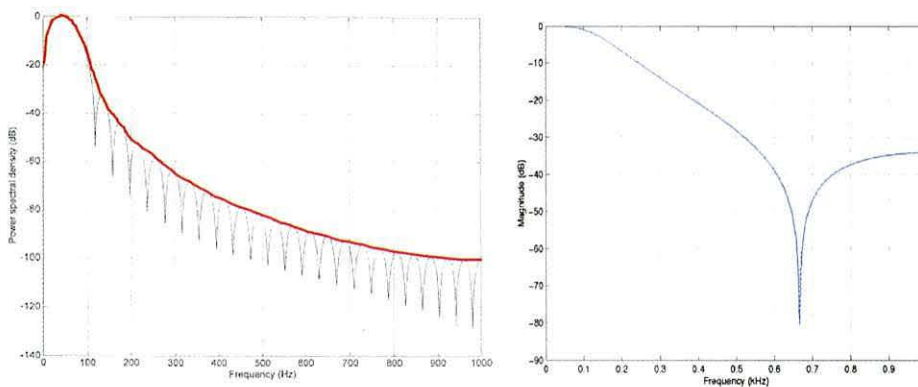
Fig. 7.8 - Frequency responses of software filters. Left: navigation signals. Right: trigger/data signals.

There are two forms of *Software filter* (Fig. 7.8): the *navigation filter*, and the *trigger/data filter* [66, 67]. The navigation filter has a peak at 40 Hz. We again opt to simplify its complex response, albeit conservatively, this time to the 8th-order polynomial curve shown in red; above 920 Hz, a fixed value of -100 dB is used, as follows:

If $f_{AA} \leq 920$ Hz,

$$G_{NF} = -19.267 + 1.0806 f_{AA} - 1.8838 \times 10^{-3} f_{AA}^2 + 1.1626 \times 10^{-4} f_{AA}^3$$
$$- 3.8011 \times 10^{-7} f_{AA}^4 + 7.1786 \times 10^{-10} f_{AA}^5 - 7.8571 \times 10^{-13} f_{AA}^6$$
$$+ 4.6276 \times 10^{-16} f_{AA}^7 - 1.1346 \times 10^{-19} f_{AA}^8$$

$$(7.6)$$

If $f_{AA} > 920$ Hz, $G_{NF} = -100$ dB

where G_{NF} is the gain of the navigation filter, and f_{AA} is defined by Equation (7.8).

The trigger/data filter is much simpler. It is a non-causal filter designed to have the negligible phase distortion required for the reception of the Quadrature Phase Shift Keying (QPSK) data signal. It is modelled in three parts, each represented by a polynomial curve:

If $f_{AA} \leq 110$ Hz, $G_{DF} = 0$ dB

If 110 Hz $< f_{AA} \leq 670$ Hz,

$$G_{DF} = 113.23 - 2.9169 f_{AA} + 3.0927 \times 10^{-2} f_{AA}^2 - 1.7598 \times 10^{-4} f_{AA}^3$$
$$+ 5.6860 \times 10^{-7} f_{AA}^4 - 1.0489 \times 10^{-9} f_{AA}^5 + 1.0286 \times 10^{-12} f_{AA}^6$$
$$- 4.1579 \times 10^{-16} f_{AA}^7$$

$$(7.7)$$

If $f > 670$ Hz,

$$G_{DF} = -3.19 \times 10^8 + 3.4328 \times 10^6 f_{AA} - 1.6384 \times 10^4 f_{AA}^2$$
$$+ 45.522 f_{AA}^3 - 8.1141 \times 10^{-2} f_{AA}^4 + 9.6222 \times 10^{-5} f_{AA}^5$$
$$- 7.5915 \times 10^{-8} f_{AA}^6 + 3.8425 \times 10^{-11} f_{AA}^7 - 1.1323 \times 10^{-14} f_{AA}^8$$
$$+ 1.4799 \times 10^{-18} f_{AA}^9$$

where G_{DF} is the gain of the trigger/data filter, and f_{AA} is defined by Equation (7.8).
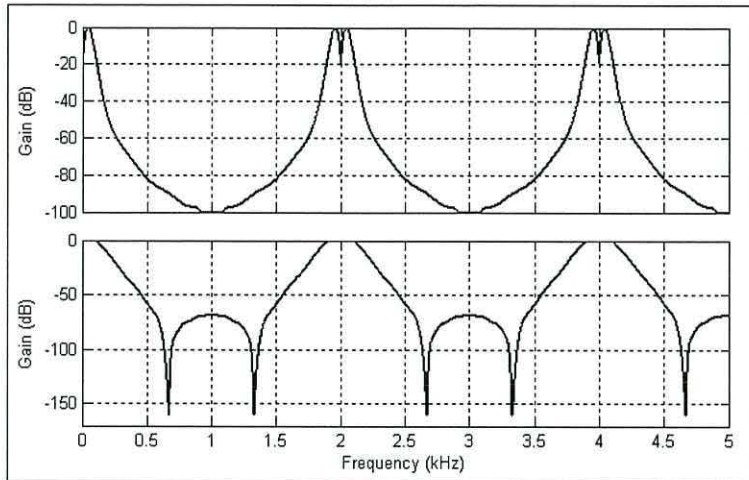
**Fig. 7.9 - Modelled versions of the navigation software filter (top) and the
trigger/data software filter (bottom)**

These filters work on signals sampled at 2 kHz. Now consider a signal 1.5 kHz from
the tuned frequency. The anti-aliasing ADC filter will have attenuated this signal by
80 dB. However, aliasing will still occur, and the signal will appear at 500 Hz. Here it
will be subjected to the same attenuation in the software filters as a signal that is
genuinely at 500 Hz. In effect, the software filter is 'wrapped' around integer
multiples of the sampling frequency. The effect is the same effect as that discussed
above concerning the over-sampling rate in the ADC. So,

$$f_{AA} = |f_{\Delta t}| \bmod 2 \text{ kHz}$$
$$\text{If } f_{AA} > 1 \text{ kHz}, f_{AA} = 2 \text{ kHz} - f_{AA} \tag{7.8}$$

where f_{AA} is the difference between the baseband interferer frequency and the nearest
integer multiple of the sampling frequency, and $f_{\Delta t}$ is the difference between the
interferer frequency and the tuned frequency.

So, the frequency responses of the two software filters are shown in Fig. 7.9. Notice
how the peaks are repeated every 2 kHz, generating a 'comb' effect.

7.2.5 Overall Response

Now that each of the filters in the Mk4 Locator has been modelled, the overall
frequency response of the Locator can be determined by summing their attenuation
values at any signal frequency. We have seen that images of a signal will appear when
it mixes with odd-multiples of the LO frequency in the mixer. In this case, the image
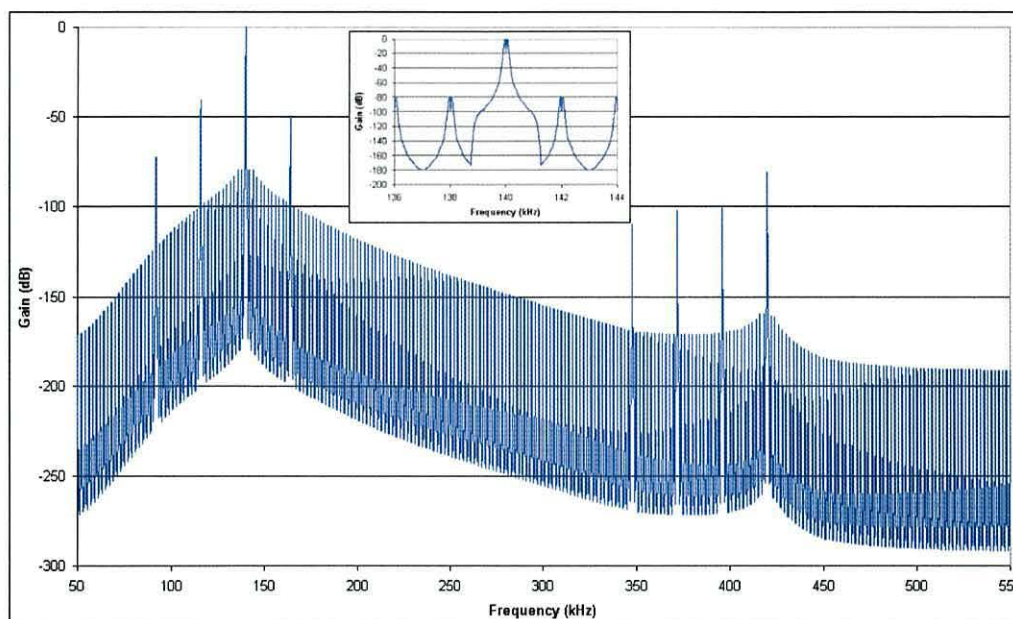
Fig. 7.10 - Overall frequency response of an Mk4 Locator whilst using the navigation software filter. Inset: Frequency response around the tuned frequency.

with the highest amplitude is used, i.e. the signal path of least resistance. Let us now tune the Locator to 140 kHz. The result, in Fig. 7.10, is both novel and interesting.

By definition, the receiver provides zero attenuation at the signal frequencies, ± 40 Hz from the tuned frequency (see inset of Fig. 7.10). The attenuation then increases rapidly as the frequency moves away from the tuned frequency, reaching -100 dB at 1000 Hz difference. The comb effect, with its approximately 100 dB variation, is due to the aliasing in the digital filters. The peaks standing above the main response are due to the local oscillator harmonic products that fall into the pass-band of the anti-aliasing filter. For example, the lowest-frequency peak (at 92 kHz) is due to the signal mixing with the third harmonic of the LO, i.e. $(3 \times 140) + 92 = 512$ kHz. The resulting frequency is an integer multiple of the over-sampling frequency of the ADC (2×256 kHz), and so falls into the pass-band of the anti-aliasing filter. Because this is a third-harmonic effect, there is an attenuation of 9.5 dB compared to fundamental effects; nevertheless, it is a significant peak, from which only the front-end filters protect the receiver.

The other peaks can be explained in a similar manner:

116 kHz: $140 + 116 = 256$ kHz
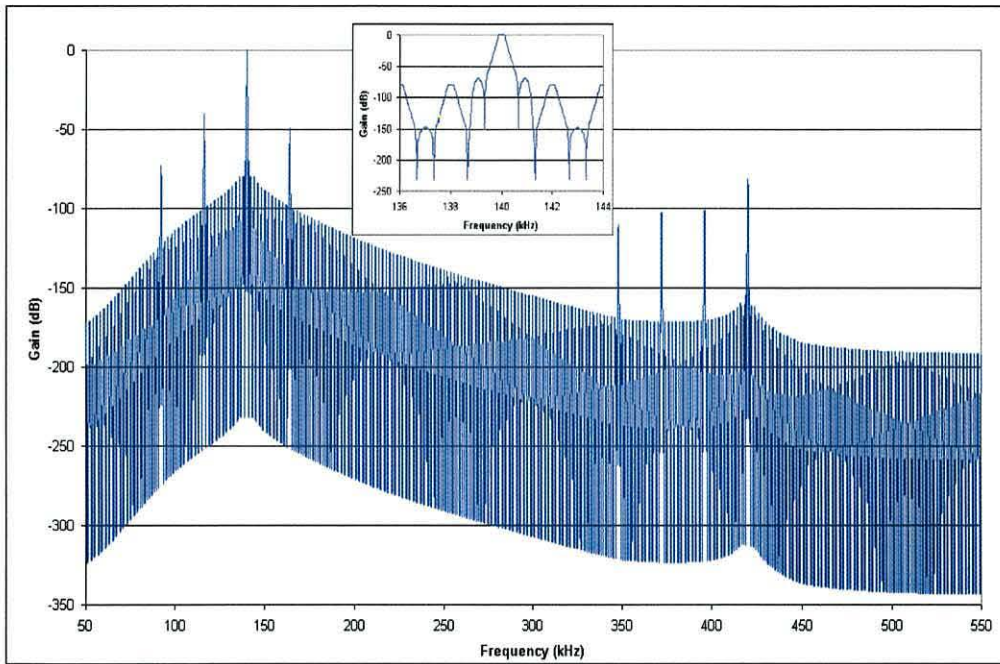
Fig. 7.11 - Overall frequency response of an Mk4 Locator whilst using the trigger/data software filter. Inset: Frequency response around the tuned frequency.

$$164 \text{ kHz:} \qquad (3 \times 140) - 164 = 256 \text{ kHz}$$

$$348 \text{ kHz:} \qquad (3 \times 140) + 348 = 3 \times 256 \text{ kHz}$$

$$372 \text{ kHz:} \qquad 140 + 372 = 2 \times 256 \text{ kHz}$$

$$396 \text{ kHz:} \qquad 140 - 396 = (-1) \times 256 \text{ kHz}$$

$$420 \text{ kHz:} \qquad (3 \times 140) - 420 = 0 \text{ kHz (i.e. baseband)}$$

Fig. 7.11 shows the frequency response of the Locator with the trigger/data software filter selected. The overall response has a greater variation in gain than when the Locator was using the navigation filter. The inset shows that the passband is centred on the tuned frequency, as expected.

It is interesting to note that the Locator specifications (Appendix A) state that the spurious response rejection is greater than 70 dB. Fig. 7.10 and 7.11 certainly shows that this is the case, bar a couple of narrow spikes.

We now have the information we need to arrange for the model to calculate the degree to which the receiver will attenuate the signals of any potential interferer.

7.3 Blocking interference

Blocking interference occurs when a receiver is overloaded by very high field strength signals, usually from a nearby transmitter. Almost no information was available from Datatrak on the overload characteristics of the Mk4 Locator, so it was analysed to identify which stages within it might become overloaded, and at what field strengths. This information will then be incorporated into the model.

Overloading occurs in active components. Fig. 7.12 identifies likely candidates: the antenna amplifier, front-end amplifier, mixer and ADC.

Datatrak engineers stated that they believed that the lowest field strength at which overloading occurred was 85 dB-μV/m, at which level the mixer would go into saturation. At those frequencies at which the antenna and front-end filters protect the mixer adequately, the antenna amplifier would then overload at 105 dB-μV/m [68]. Fig. 7.13 summarises this information: the curve near the Datatrak frequency of 140 kHz mirrors the frequency response of the two pre-mixer filters.

If this curve is correct, the most-likely UK interferer, the 400 kW BBC Radio 4 transmitter on 198 kHz at Droitwich, England, (Fig. 7.14) should cause blocking wherever its field strength exceeds 100 dB-μV/m. That would be everywhere within a radius of 60 km [36]. In practice, Locators are known to operate correctly much closer
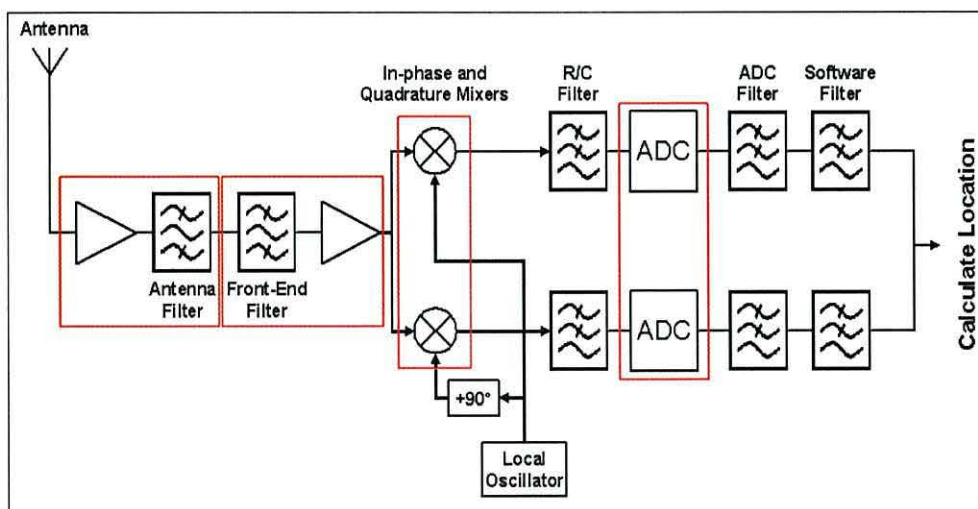
Fig. 7.12 - Active stages in the Locator in which overloading is possible
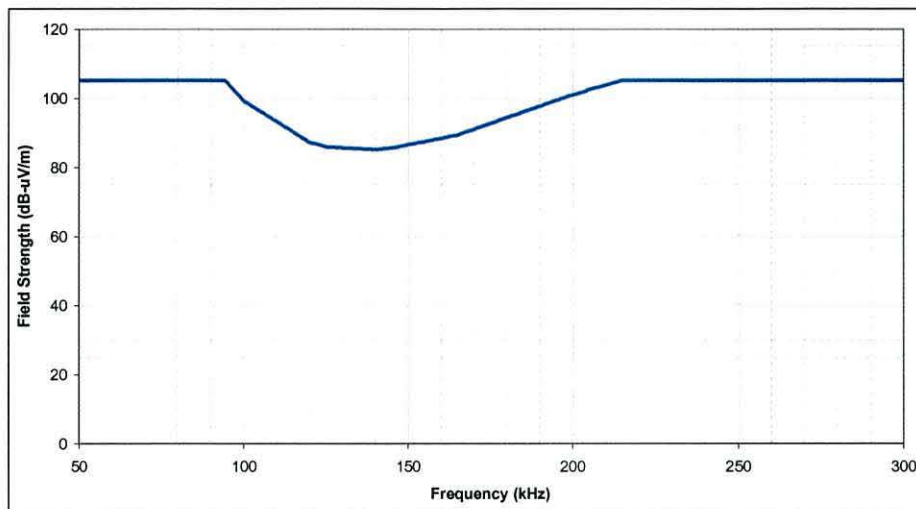
**Fig. 7.13 - Locator blocking field strength as a function of interferer frequency –
initial information**

to Droitwich than this. Clearly, Fig 7.13 cannot correctly describe the Locator's
blocking characteristic.

It was decided to take measurements close to Droitwich with a Locator of the type
being modelled. Using the calibrated loop antenna and spectrum analyser described in
Appendix C, the radiated power of the station was confirmed as being within 1 dB of
its nominal 400 kW. The Locator's performance became worse until approximately
1 km from the station when valid positions stopped being reported (Fig. 7.15). At this
range, the mixer output waveform could be seen on an oscilloscope to be saturated.
The field strength at this range was 136 dB-μV/m. The pre-mixer filters would have

**Fig. 7.14 - Location of the 400 kW BBC Radio 4 transmitter at
Droitwich**
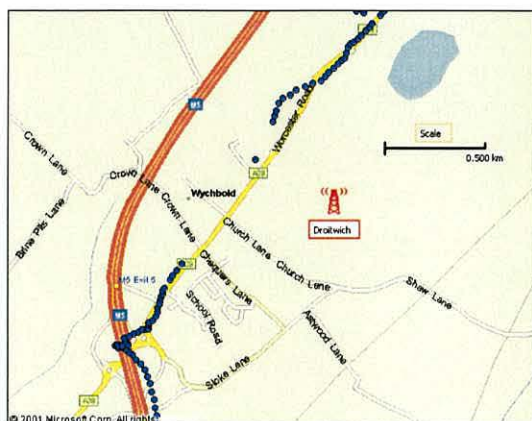
Fig. 7.15 - Locator reported positions around Droitwich. Actual route taken is along the A38.

attenuated the Droitwich signal by 15 dB. Thus, we conclude that the upper limit of correct operation, as far as the mixer is concerned, is at field strength of 121 dB-μV/m. This would be the field strength limit at those frequencies at which there is no filter protection.

Further measurements closer to Droitwich suggested that the antenna circuit overloaded at about 141 dB μV/m. This would allow Locators to approach to within approximately 400m range of the station. This reading confirmed Datatrak's claim that there is an approximately 20 dB difference between the lowest mixer-blocking field strength and the field strength at which the antenna circuitry becomes overloaded [68]. However, the blocking values measured are some 36 dB above those quoted by Datatrak! These measured results have been translated into the amended blocking
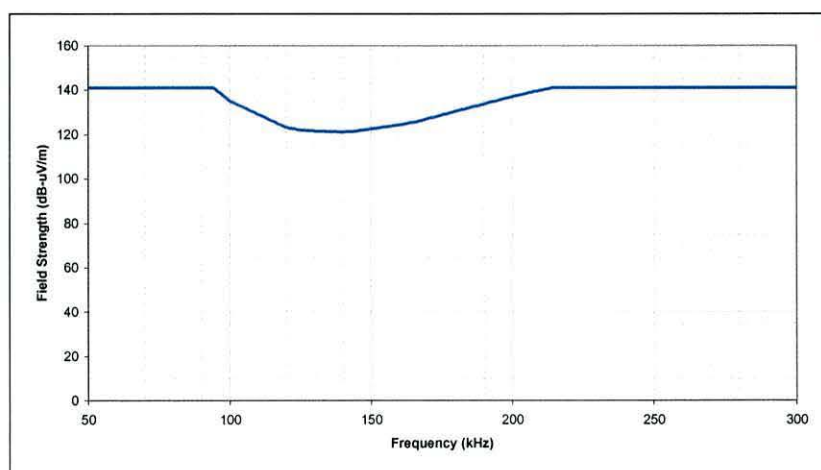
Fig. 7.16 - Revised Locator blocking field strength as a function of interferer frequency.

characteristic shown in Fig. 7.16.

The blocking field strength of 121 dB-μV/m is reached at just over 1 km range from a UK Datatrak station that transmits the nominal radiated power of 40 W. However, a Datatrak transmitter can only overload the Locator during its own transmission slot in the time-multiplexed sequence. The other stations' signals will be unaffected by the blocking signal, and so the Locator continues to work.

The characteristic in Fig. 7.16 was confirmed by laboratory measurements, with a field test used to calibrate the relationship between signal levels in the Locator and Datatrak field strengths. See Appendix E for more details on the calibration method.

The laboratory measurement used a sine-wave signal at the UK Datatrak f_{1+} frequency of 146.495 kHz, injected into the antenna input; in Fig. 7.12, this is the point between the antenna and front-end filters. Signal voltages were then measured and recorded at the pre-mixer amplifier outputs and the mixer. The equivalent field strength was then computed by adding the calibration factor, 93.5 dB, to the measured voltage at the output of the pre-mixer amplifier.

Fig. 7.17 shows the amplitudes of the mixer's input and output signals as a function of the signal field strength. It clearly shows that the input voltage is rising linearly with the field strength. However, the output voltage has begun to overload at field strength
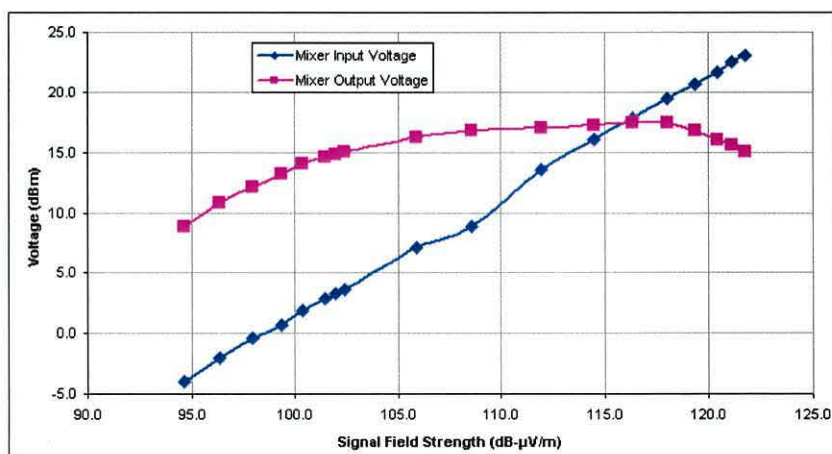
Fig. 7.17 - Mixer input and output voltage as a function of UK Datatrak f_{1+} signal field strength.

of around 105 dB-μV/m. This is some 20 dB above the value quoted by Datatrak. However, despite the apparent overload, the Locator is still capable of giving correct measurements, as shown by the experiments at Droitwich. Finally, at a field strength of 120 dB-μV/m (some 35 dB above the figure quoted by Datatrak), the output voltage begins to *drop*, indicating that severe distortion is taking place. It is at this field strength that the Locator finally gives up, and stops working reliably. Thus, we conclude that Fig. 7.16 appears to correctly represents the blocking characteristics of the Mk4 Locator.

The blocking characteristics of the Locator (Fig. 7.16) can now be implemented in the model, and at any interferer frequency, the blocking field strength of the Locator can be determined.

7.4   Conclusions

In this Chapter, we have investigated how the Locator deals with interference from other radio sources. Two types of interference were defined: passband interference and blocking. The Locator's responses to each were investigated.

To model passband interference requires knowledge of the frequency response of the Locator. This was not available from Datatrak, so it was constructed from analysis of the individual frequency-dependant components of the Locator. The result is a novel, highly sophisticated frequency response description of a Mk4 Locator using an H-field antenna.

The blocking characteristics of the Locator were also largely unknown. An initial estimate was produced from information provided by Datatrak. Through a process of field and laboratory measurements, the blocking field strength was revised to more realistic values.

In the next chapter, we will use the Locator models developed in this chapter to determine how interference from other radio sources will affect the Locator.

Chapter 8

Interference: Analysing Transmissions

8.1   Introduction

In the previous chapter, two forms of interference to the Locator, pass-band and blocking, were analysed. In this chapter we will employ the results of that analysis to determine the attenuation of each interfering signal by the receiver and so, eventually, its effect on the Datatrak signal-to-interference ratio (SIR). Later in the chapter we will identify those areas in which Locators will be unusable because of blocking interference.

8.2   Finding potential interference sources

In order to determine whether any station has the potential to cause interference to Datatrak reception and, if so, to what degree, the model needs to know its: location, frequency, radiated power and the nature and bandwidth of any modulation. Normally, the best source of such information is the ITU, who's attempt to keep an up-to-date record of frequency allocations world-wide in their *Master International Frequency Register* [69]. Fortnightly updates are published in the *Bureau des Radiocommunications International Frequency Information Circular (Terrestrial Services)* (BR IFIC), also known as the *International Frequency List* (IFL). This list contains comprehensive data on stations. However, we will see that unfortunately it lists frequency *allocations*, rather than frequencies known to be in use. As a result, many of its entries are allocations that have apparently not been taken up in practice.

An alternative source of information, based on observations of actual transmissions, is the Klingenfuss *2001 Super Frequency List* [70]. This commercially-available list was compiled from measurement made by many contributors. However, the information on each transmitter is limited to its frequency, name and operating country. Also, only 11 stations are listed across the whole of the VLF and LF frequency bands. Other observation-based lists are available on the Internet, mostly published by radio hobbyists [71], [72], and [73]. None was found to be as comprehensive as the IFL. So,

the other lists are of value in helping confirm whether potential interferers to Datatrak listed in the IFL actually exist. It was decided to employ the IFL, as by far the most comprehensive list, available in electronically-readable format, with the authority of the ITU, and then consult other lists to obtain further information on stations that emerge from the analysis as likely interferers.

8.2.1 Limitations of the IFL

One concern about the IFL is that it lists the *transmitter power* of each station, which may or may not be the same as its *radiated power*. Transmitter power is the power fed to the antenna system; radiated power is the signal power launched from the antenna. At LF and VLF, where antennas are generally short compared to the wavelength, and so may be inefficient, the difference between the two powers can very be great [69]. In the absence of firm data on radiated power levels, it was decided to adopt the conservative assumption that, in those cases where the radiated power is not stated, antenna efficiency is 100%; that is, radiated power is the same as transmitter power. Again, once likely interferers to Datatrak have been identified, further information on their radiated powers can be sought.

There is also a concern that the IFL is not up-to-date. For example, the frequency allocations for the British Decca Navigator stations are still listed, more than three years after the transmitters were switched off [74]. But it is the best source of data we have!

We now need a means to transfer data from the IFL into the Datatrak model, so that at any time the model can use the latest information. The IFL files are designed to be read using Microsoft Access. Working under the candidate's direction, final-year undergraduate student D.R. Hughes created Access software that converts the IFL into a text file suitable for use in the Datatrak model [75]. This software also allows the user to edit each updated version of the list as it is issued, correcting errors and omissions discovered.

8.3 Power Spectra of Interferers

To assess interference, we need to know not only the allocated frequency of each transmission, but also the distribution of energy across its spectrum, since side-band energy can interfere with Datatrak transmissions. This information is not listed directly in the IFL, but it can be deduced from the information provided there on the *emission class* of each transmission.

The emission class is shown as either a 3-character, or 5-character, alphanumeric code, defined in the ITU Radio Regulations. It describes the modulation, content, and (in some cases) purpose, of the transmission [76]. For example, an *A1A* emission is "amplitude modulated, double side-band ... with a single channel containing quantized or digital information without the use of a modulating sub-carrier... [and is a] telegraphy [signal] for aural reception"; that is, usually a Morse code transmission [76].

8.3.1 Modulation Types

Within the frequency range of interest, 50-550 kHz, some 45 different emission classes can be identified. However, noting that only the first three characters of the class descriptor affect the power spectrum lets us reduce this number to 33. When we then analyse these 33 codes, we find that many describe transmissions with very similar spectral shapes, each of can be approximated by one of the six spectral shapes illustrated in Fig. 8.1:

- Double sideband (DSB) amplitude modulation (AM)
- Pulsed (e.g. Loran-C)
- Single sideband (SSB) with carrier
- Wide-band frequency modulation (FM)
- SSB suppressed carrier (SSB-SC)
- Carrier only (no sidebands)

Each of these spectra has been normalised to a total power of 1 W within the published bandwidth; it is assumed that there is no power outside that bandwidth. For example, the wideband FM transmission is approximated by a uniform power spectrum with a *power spectral density* (PSD) of $1/b$ W/Hz. The power spectral
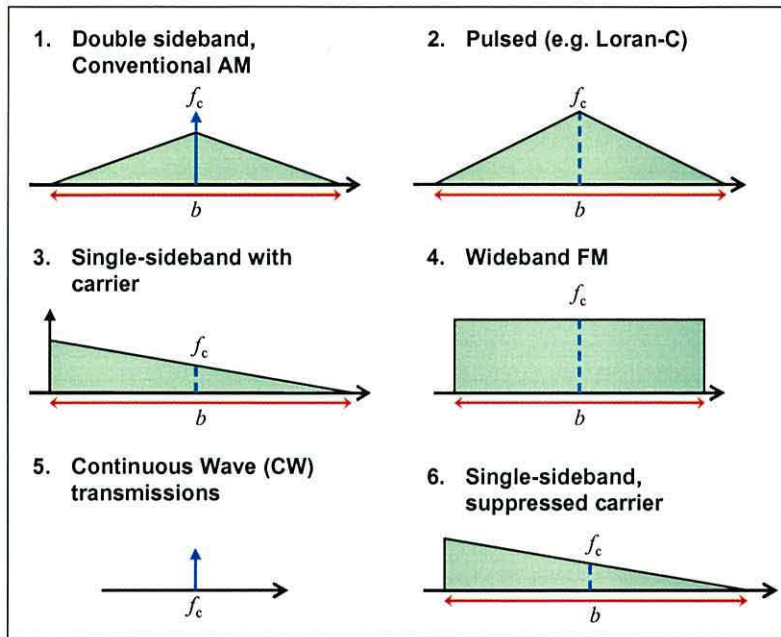
Fig. 8.1 - Simplified power spectra used in the interference analysis; f_c and b are the centre frequency and bandwidth published in the IFL.

densities (PSDs) of the triangular-shaped power spectra are a little more complicated; the normalised PSD at a frequency, f, *within the bandwidth of the interferer* is:

$$PSD(f) = \frac{2}{b} - \frac{4}{b^2}|(f_c - f)| \quad \text{W/Hz} \tag{8.1}$$

where f_c is the published centre frequency of the interferer.

Those transmissions that have both carriers and sidebands are best represented by considering the sidebands and carrier as separate components. We then need to estimate the allocation of power between them. This depends on the type of modulation and also the *power measurement method* employed by the ITU [77], which is one of three possibilities:

- **Peak Envelope Power (PEP)**: "the average power supplied to the antenna by a transmitter during one radio frequency cycle at the crest of the modulation envelope taken under normal operating conditions."

- **Mean Power:** "the average power supplied to the antenna by a transmitter during an interval of time sufficiently long compared with the lowest

frequency encountered in the modulation taken under normal operating conditions."

- **Carrier power:** "the average power supplied to the antenna by a transmitter during one radio frequency cycle taken under the condition of no modulation."

In the IFL, a specific power measurement method is specified for each emission class; for example, all "A2A" transmissions are measured using the mean power method. We will choose, however, to use mean power in all calculations in the model, since it can represent all modulation types, and should give fair, realistic, results. One can convert to mean power from the other power measurement methods using techniques set out in the ITU documents [78, 79, 80].

As an example, consider an "A3E" transmission. This emission class defines a double-sideband (DSB) broadcast AM signal, transmitting audio (e.g., voice and music) [76]. Clearly, this is an example of Spectrum 1 in Fig. 8.1, the DSB AM power spectrum. It is centred on the transmission centre frequency, f_c, and has the bandwidth, b, given in the IFL. The powers of all A3E transmissions are listed using the PEP method. We calculate the ratio of mean power to PEP using the method set out in [81], and then go on to compute the carrier power, making the necessary assumption that the interferer is transmitting "smoothly read text" [81]:

$$\frac{\text{Carrier Power}}{\text{Mean Power}} = \frac{\left[\dfrac{\text{Carrier Power}}{\text{PEP}}\right]}{\left[\dfrac{\text{Mean Power}}{\text{PEP}}\right]} = \frac{0.25}{0.262} = 0.95 \qquad (8.2)$$

Thus, 95% of the power is in the carrier and the remaining 5% is in the sidebands. Document [81] is based on measured values collected in ITU experiments, and realistically represents AM double sideband transmission, as shown in Fig. 8.2.

The normalised power distributions of other emission classes have been dealt with in a similar manner, full details being given in Appendix F.
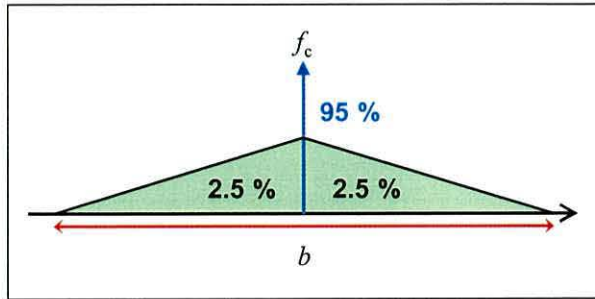
Fig. 8.2 - Power spectrum for an "A3E" emission class transmission. Here 95 % of the total power is in the carrier, and 5 % is distributed across the sidebands, as shown.

8.4   Calculating levels of interference

We can now describe the power spectrum of any interferer using the centre frequency, bandwidth and emission class data from its IFL entry. Now we wish to employ the frequency response of the Mk4 Locator derived in Chapter 7 to determine the degree of rejection provided by the filters in the Locator. This *frequency-dependent rejection* (FDR) is the ratio of the power of the signal after passing through the Locator's filters to the power of the signal in space. We will compute this separately for the carrier and sidebands, then sum the results. The total interferer *carrier* power will be the carrier power, attenuated according to the response of the Locator at the carrier frequency, f_c. Similarly, the total *sideband* power will be the sideband power attenuated by the FDR of the Locator when tuned to f_1 or f_2. Since the total power is normalised to 1 W, the FDR for the whole signal can then be written as:

$$FDR_{dB} = 10\log_{10}\left(P_{carrier} \times 10^{\frac{H(f_c)}{10}} + P_{sideband} \times 10^{\frac{FDR_{side}}{10}} \right) \text{ dB} \qquad (8.3)$$

where FDR_{dB} is the total frequency-dependent rejection the Locator will apply to the interferer, $P_{carrier}$ is the normalised power in the carrier (see Section 8.3.1 above), P_{side} is the normalised power in the sidebands (see Section 8.3.1 above), $H(f_c)$ is the response in dB of the Locator at the frequency f_c of the interferer (see Chapter 7), and FDR_{side} is the frequency-dependent rejection in dB of the sidebands by the Locator.

The only parameter in Equation (8.3) not known is FDR_{side}, the frequency-dependent rejection of the sidebands. This could be simplified by computing the amount of energy in the sidebands falling into the Locator passband. However, almost half of the

interferer list contains transmissions whose bandwidth is less than or equal to 500 Hz (comparable to the Locator bandwidth of 160 Hz); so variations in the Locator frequency response could be significant. For that reason, we follow the ITU-recommended, more sophisticated, method of calculating FDR [82]. The aim is to be able to calculate the FDR of an interferer sideband only, and apply the result to Equation (8.3). From [82], FDR_{side} is defined by:

$$FDR_{side} = 10\log_{10}\left[\frac{\int_0^\infty p(f)\,df}{\int_0^\infty p(f)\left|H(f+\Delta f)\right|^2 df}\right] \text{dB} \qquad (8.4)$$

where $p(f)$ is the power spectrum of the interfering signal at the equivalent intermediate frequency (IF), $H(f)$ is the frequency response of the receiver at frequency f (as defined in Chapter 7), and Δf is defined by Equation (8.5):

$$\Delta f = f_c - f_r \qquad (8.5)$$

where f_c is the "interferer tuned" (i.e. centre) frequency, and f_r is the "receiver-tuned" frequency (i.e. f_1 or f_2 in Datatrak's case).

Let us simplify Equation (8.4) to:

$$FDR_{side} = 10\log_{10}\left[\frac{\int_0^\infty P(f)\,df}{\int_0^\infty P(f)\left|H(f)\right|^2 df}\right] \text{dB} \qquad (8.6)$$

where $P(f)$ is the power spectrum of the interfering signal sideband in W/Hz.

We can further simplify this by normalising the interferer power. The numerator is simply the total power of the interfering signal in space at the receiver's location. Thus:

$$FDR_{side} = 10 \log_{10} \left[\frac{1}{\int_0^\infty P_n(f) |H(f)|^2 \, df} \right] \text{ dB} \qquad (8.7)$$

where $P_n(f)$ is the normalised interferer power spectrum as defined in Section 8.3.1.

To be included in the model, we have to convert this integral to a sum. We have chosen a rectangle method, which provides a good approximation of the integral and is computationally fast [83]. A step size of 10 Hz was selected. This value is sufficient small to allow the rejection within the sharpest point of the Locator frequency response (the pass-band of the navigation software filter) to be accurately represented. Also, since all interfering energy is assumed to lie inside the interferer bandwidth, there is no need to integrate at frequencies outside the interferer's power spectrum. So, the implementation of Equation (8.7) for use in the model is:

$$FDR_{side} = 10 \log_{10} \left[\frac{1}{\sum_{n=0}^{n=\frac{b}{10}} P_n \left(f_c - \frac{b}{2} + 10n \right) \left| H \left(f_c - \frac{b}{2} + 10n \right) \right|^2} \right] \text{ dB} \qquad (8.8)$$

At this stage, the normalised power spectrum of an interferer is known, based on its emission class, centre frequency, and bandwidth, as declared in the IFL. This can now be used in Equation (8.8), together with the Locator's frequency response, to calculate the degree to which the Mk4 Locator will reject the interferer sidebands.

To illustrate this operation, consider the simple example shown in Fig. 8.3. The interferer has a triangular power spectrum of 10 kHz bandwidth. The receiver is assumed to have a perfectly-square pass-band filter, 10 kHz wide, and centred on 140 kHz. The chart shows the amount of rejection the receiver will provide as a function of the *interferer centre frequency*.

If the interferer's centre frequency is exactly the same as the receiver centre frequency, all the interferer's energy passes straight through the filter, and the
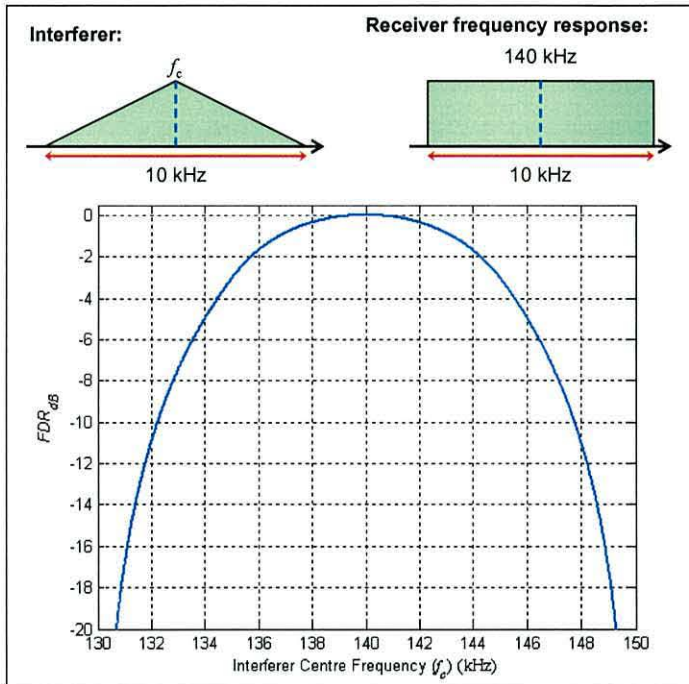
Fig. 8.3 - Example interferer and receiver with the calculated FDR as a function of interferer centre frequency

rejection would be zero (0 dB). However, as the interferer moves away from the receiver centre frequency, the amount of rejection increases. When the interferer centre frequency is 135 kHz, for instance, only half the energy is passed into the receiver, and the rejection is then 3 dB. By 133.55 kHz, 6 dB, or three quarters of the power, is rejected by the receiver; this is very close to 133.54 kHz obtained by theory (see Appendix G). This simple test confirms that the algorithm for use in the model works correctly.

So, FDR_{dB} can now be calculated for signals that contain carriers and sidebands using Equation (8.3). Fig. 8.4 shows an example of interference rejection using the Locator's frequency response. The interferer in this case has an emission class of "A3E", and a bandwidth of 10 kHz. Its power is distributed as shown in Fig. 8.2. So, if the interferer's centre frequency is at, say, 160 kHz, the amount of interferer power penetrating the receiver filters will be approximately 100 dB less than the power of the signal in space. If the interferer's centre frequency is at the tuned frequency (140 kHz in this case), the rejection would be only 0.2 dB. Note that it would not be exactly 0 dB because some of the energy in the sidebands would be rejected by the
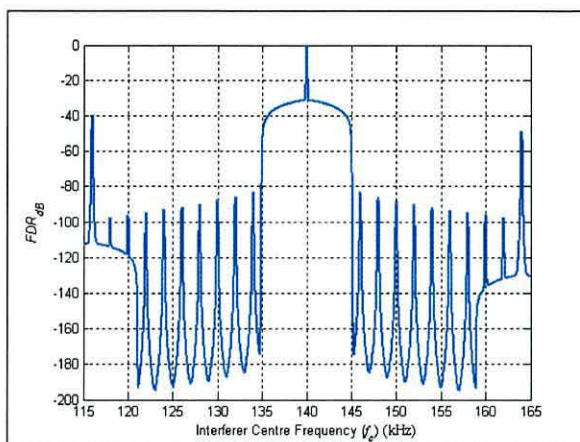
Fig. 8.4 - The signal rejection of an "A3E" transmission in an Mk4 Locator (with navigation software filter) as a function of interferer centre frequency

filters. The rounded shape of the plot near 140 kHz is repeated at 116 kHz and 164 kHz due to the aliasing of mixer products, as was seen in Fig. 7.10.

The amplitude scale of the frequency response created in Chapter 7, and used here, is the amplitude *relative to that of the Datatrak signal*; that is, the amplifiers in the Locator have no effect on the relative amplitudes of the Datatrak signal and the interferer. When calculating the signal-to-interference ratio (SIR), it is only their relative amplitudes that matter. If the receiver had no filtering, the SIR would simply be the ratio between their field strengths. However, because of filtering, the power in the interferer is reduced, and so the *effective interferer field strength* is the signal power in space less the power removed within the receiver. Thus,

$$E_{I_{eff}} = E_I + FDR_{dB} \qquad (8.9)$$

where $E_{I_{eff}}$ is the effective interferer field strength, E_I the field strength of the interferer in space, and FDR_{dB} the rejection calculated using Equation (8.3) (always negative).

Finally, the signal-to-interference ratio (SIR) can be computed by:

$$SIR = E_{Datatrak} - E_{I_{eff}} \qquad (8.10)$$

where *SIR* is the signal-to-interference ratio (SIR), $E_{Datatrak}$ is the Datatrak signal field strength.

So now, for the first time ever, the SIR of a Datatrak signal can be predicted using the IFL list of potential interferers.

8.5   List Reduction

The IFL contains more than 22,000 potential interferers across the frequency range of interest, 50-550 kHz [69]. In principle, we need to calculate the field strength of each at the position of the Locator, taking both ground-wave and skywave propagation into account. Then, for each transmission, we need to determine the rejection provided by the filters in the Locator. This is a daunting task! Datatrak's experience has shown that the overwhelming majority of these transmissions will cause the Locator no problem, because they will either be too distant geographically, or too far separated in frequency from the Datatrak signal. So, we require a simple and quick method of reducing the list from 22,000 entries to just *those transmissions that matter*. Taking that approach should result in a much quicker analysis. We will consider the frequency separation and geographical separation factors separately.

8.5.1   Frequency Separation

Frequency separation can be characterised by a single attribute: FDR. It is possible to place limits on this attribute to determine whether an interfering transmission merits further attention. Consider the dynamic range of the Locator. The lowest possible Datatrak field strength that is of use to the Locator is set by the 15 dB minimum SNR it requires, and its 5 dB-μV/m noise floor. Thus, the minimum signal is 20 dB-μV/m. We use this lower noise floor value as specified by Datatrak (Section 6.5), because there is scope for improvement in the H-field antenna amplifier circuitry; we wish to produce an interferer list which contains too many stations, rather than too few. If an interferer has an effective field strength less than this noise floor field strength it will not be seen by the Locator, because it will be lost in the noise.

The upper end of the dynamic range is set by blocking interference (Section 7.3), of which the lowest value was found to be 121 dB-μV/m. Consider an interferer at a frequency at which the Locator provides 116 dB of rejection (Fig. 8.5). If the field strength of the interferer is high enough to cause pass-band interference, the Locator
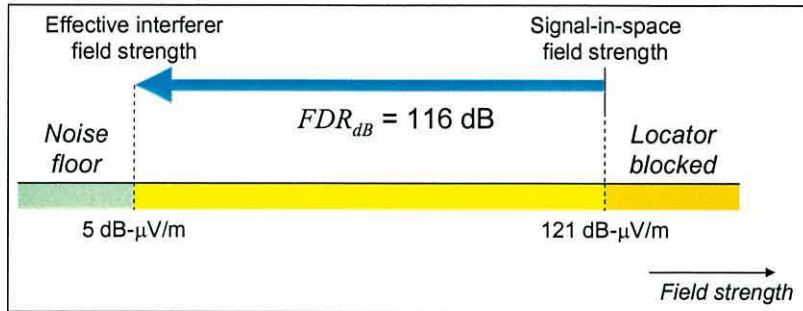
Fig. 8.5 - Effect of FDR on determining how an interferer will interact with the Locator

will overload before the interferer signal is above the Locator noise floor. At any lower field strength and the interferer will be lost in noise floor.

So, an interferer will be included in the reduced list if it satisfies the criterion:

$$|FDR_{dB}| < E_{block}(f_c) - 5 \tag{8.11}$$

where $E_{block}(f_c)$ is the blocking field strength at the interferer's centre frequency, f_c

We now have a simple test. Equation (8.11) will be applied four times to each interferer: at each of the two Datatrak signal centre frequencies, and using each of the two software filters. If, for any such combination, Equation (8.11) is satisfied, the interferer will be included in the reduced interferer list for further investigation. If not, it will be eliminated from the list.

8.5.2 Geographical Separation

The geographical separation of each interferer from the Locator can now be considered; this is more complex. We create a geographical rectangular window that completely encompasses the area of operation of the network. We will attempt to exclude from the list any interferer that cannot cause interference anywhere within this window, via either groundwave or night skywave propagation.

8.5.2.1 Groundwave interference

Let us identify the strongest interferer in the IFL and estimate how far from the edge of the window it would need to be before we could say that it could never cause interference within the box. The most powerful station is one at Ouargla, Algeria that

transmits an ERP of 10 MW, at 198 kHz [69]. Unlike the Datatrak transmitters that use omni-directional antennae, many interferers, including this one, use directional antenna systems to ensure maximum signal strength in a certain direction, or to reduce interference to other transmissions [42]. The *effective radiated power* (ERP) in this favoured direction may be greater than the actual radiated power, and we will take this factor into account [69].

We assume a worst case: that the whole of the groundwave path lies over sea-water. The range at which the field strength of this station would fall to 5 dB-μV/m is 3800 km [36]. Thus, we can ignore groundwave interference from *any* station in the IFL that is located further *from any edge of the network window* than this 3800 km.

So, the first test is to determine if the transmitter is within 3800 km of the edge of the network window. If it is outside this boundary, it will be excluded from the reduced list. Of course, if the interferer is actually within the network window, it will automatically be included in the list.

We now further reduce the number of interferers in the list by eliminating from those located within 3800 km of the window boundary interferers whose field strength at the edge of the window is below 5 dB-μV/m. We again estimate groundwave field strength over a seawater path. Fig. 8.6 shows the shortest path to the edge of the network window based on the transmitter position relative to the window. For all interferers we use the 150 kHz curve, for this reason: the lowest rejection of interferers is always going to be at frequencies near the Datatrak frequency. So, we
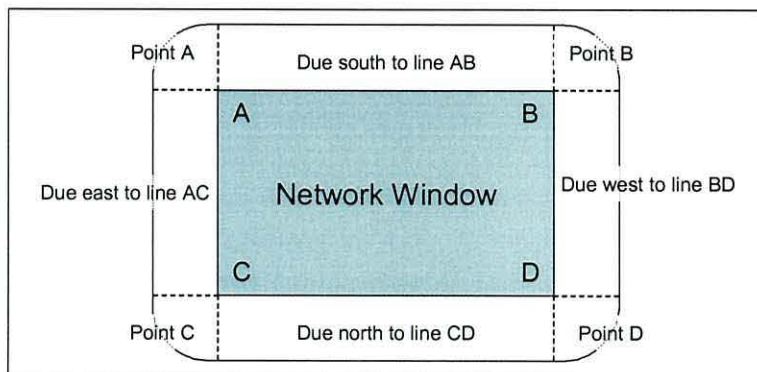
Fig. 8.6 - Method of finding closest point of network window edge to transmitter's location

want the most accurate estimate of strength at those frequencies. For other transmissions, the rejection provided by the Locator will always be high, even for signals mixing to baseband by the third harmonic of the LO (see Fig. 7.10). So, only interferers close in frequency and in range will cause interference and these are accurately represented by the 150 kHz curve. In any case, since the radiated powers in the IFL may be over-estimated by many dB, there is no point in being very accurate (Section 8.2); it is more important to be conservative in excluding interferers.

So, an interferer is included in the reduced list if:

$$E_{Sea}(d) + FDR_{dB} + 10\log_{10}\left(\frac{P_{Watts}}{1000}\right) + A_{gain} > 5 \qquad (8.12)$$

where $E_{sea}(d)$ is the attenuation of a signal at a great-circle range d from a transmitter to the edge of the window, over seawater. Here, FDR_{dB} is calculated as in Equation (8.3), P_{watts} is the radiated power of the interferer, and A_{gain} is the gain of the interferer's antenna system in the direction of the Locator.

A_{gain} is based on data given in the IFL, which lists the antenna gain at steps of $10°$ in azimuth. For daytime interference analysis (groundwave only), the daytime azimuth data is used. For night-time (groundwave and skywave), the night-time data is used. The direction towards the Locator is calculated using the initial Great-Circle course method [84]. Linear interpolation is used for angles between listed data points.

So, to summarise, let d be the shortest distance between edge of the network window and the transmitter:

> If $d \geq 3800$ km: Interferer always excluded from reduced list
>
> If $d < 3800$ km: Interferer included if Equation (8.12) is satisfied
>
> If inside window: Interferer always included in reduced list.

8.5.2.2 Skywave interference

During the night, the skywave signal from a distant interferer can be much stronger than its groundwave signal. All interferers that have been included in the list by virtue of the strengths of their groundwaves will also be potential skywave interferers. In addition, there may be transmissions that are potential interferers via skywave *alone*.
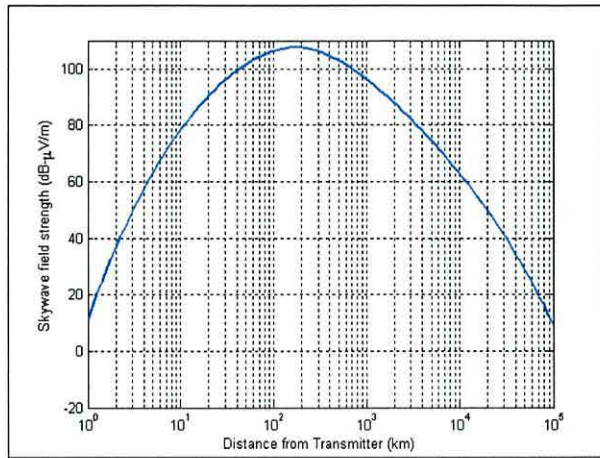
Fig. 8.7 - Skywave field strength, not exceeded 95% of the time, of 10 MW transmitter, as a function of distance, at low geomagnetic latitude

Again considering the highest-powered transmitter in the list (10 MW), let us calculate the strength of its skywave component, using the value not exceeded 95% of the time. Equation (5.3) tells us that the highest field strengths occur at the geomagnetic equator. Fig. 8.7 shows the skywave field strength of the 10 MW signal at this geomagnetic latitude, calculated using the ITU method of Equation (5.1). It exceeds the minimum 5 dB-μV/m for over 100,000 km, more than the circumference of the earth [85]! So, irrespective of its location, this is a potential skywave interferer.

Let us now attempt to reduce the list of interferers by establishing whether their skywaves too can cause a problem within the network window. Peak skywave field strength occurs at about 170 km from transmitters, virtually independent of geomagnetic latitude. If the skywave field strength at this peak is below 5 dB-μV/m, the interferer will never be a problem by skywave and can be excluded. Using the Great Circle path to the nearest point on the edge of the network window, and assuming maximum sea gain, we calculate the annual night-time effective field strength not exceeded 95% of the time at a range of 170 km along this path:

$$E_{max} = E_{sky}(170 \ km) + FDR_{dB} + 10 \log_{10}\left(\frac{P_{Watts}}{1000}\right) + A_{gain} + 8.45 \qquad (8.13)$$

where $E_{sky}(170 \ km)$ is the skywave field strength of a 1 kW transmitter at 170 km range with maximum sea gain [Equation (5.1)], and the other terms are as defined previously. Since skywave only appears during the night, A_{gain} is based on the night-time antenna gain data from the ITU only (which can be different to daytime gain).

For an interferer to be included in the reduced interferer list:

$$E_{max} > 5 \text{ dB-}\mu\text{V/m} \qquad (8.14)$$

Thus, if the interferer is located within 170 km of the edge of the network window and satisfies Equation (8.14), it will be included in the reduced interferer list. The field strengths of interferers at greater ranges are estimated at the edge of the window:

$$E_{edge} = E_{sky}(d) + FDR_{dB} + 10 \log_{10}\left(\frac{P_{Watts}}{1000}\right) + A_{gain} + 8.45. \qquad (8.15)$$

and each interferer is included in the reduced list only if it satisfies:

$$E_{edge} > 5 \text{ dB-}\mu\text{V/m} \qquad (8.16)$$

So, to summarise, let d be the shortest distance between the transmitter and the edge of the network window:

If $d < 170$ km: Interferer included if Equation (8.14) satisfied

If $d \geq 170$ km: Interferer included if Equation (8.16) satisfied

8.5.3 Results of Interference List Reduction

The interferer list reduction process was tested, using the UK network with its frequencies of 146.455 kHz and 133.2275 kHz, the window being bordered by 45°N, 65°N, 10°W and 15°E. It succeeded in reducing the number of interferers from the 22,000 of the IFL to just 160, a reduction of more than 99%.

8.6   Calculating the interference layers

As shown in Section 4.7, the model is based on layers, or arrays. We will now add an interference layer to the Datatrak groundwave and skywave layers. This interference layer will be bounded by the network window, will have the same resolution as other layers, 0.1° × 0.1°, and will contain the effective field strength of the interference at each location.

We need to consider the 8 possible combinations of: day and night propagation; the f_1 and f_2 centre frequencies; and both trigger/data and navigation software filters. So, we will in fact compute eight layers, the appropriate one being used when calculating coverage. Pre-computing the layers saves time, and speeds up the computation of coverage. However, whenever the IFL changes, all 8 layers must be re-computed.

In computing the layers, each interferer in the reduced list is examined in turn. During the list reduction process, the FDRs for both Datatrak centre frequencies with both software filters are stored together with other information on the interferer. They are now used to calculate the effective field strengths. We compute and store groundwave and skywave field strength for each interferer, using $E_{sea}(d)$ and $E_{sky}(d)$, respectively, with d being set to the Great Circle distance from the interferer to the array point. The analysis takes into account the radiated power and antenna gain of the interferer and of the relevant Locator FDR at the interferer's frequency. At each array point, we store the effective field strength of the strongest interferer there.

When the interference analysis is run for the first time, it is not known which transmitters are going to be the main sources of interference. Once these have been identified, an attenuation array can be generated using Millington's method for groundwave signals (as in Chapter 4), or the ITU method for the skywave signals (as in Chapter 5). Re-running the interference analysis will include these arrays for more accurate interference prediction. It can be considered an iterative process; identifying the main sources of interference, and refining the model. Of course, attenuation arrays can be built for every single transmitter in the IFL. But, with over 22,000 potential interferers in the list, this was considered far too time-consuming, and largely unnecessary.

The result is shown in Fig. 8.8: the first-ever plot of interference to the UK Datatrak system. This figure is for daytime propagation, the f_1 frequency (146.455 kHz), and the trigger/data software filter. The colours represent the effective interferer field strength; the clear parts are areas where any such field strength is below the minimum 5 dB-μV/m.
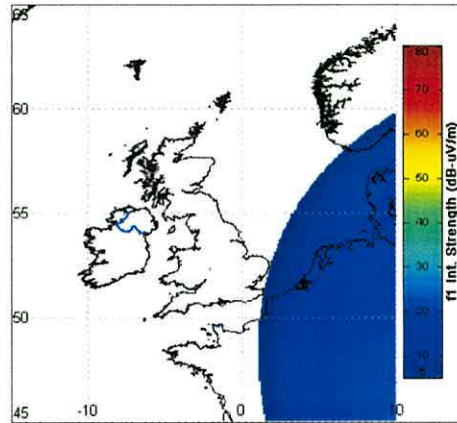
Fig. 8.8 - Interference layer for the Datatrak f_1 signal during the day, using the trigger/data software filter. The colours represent the effective field strength of the strongest interferer.

Happily, we predict that very little significant interference will be received during the day in the UK. This result confirms observations by Datatrak engineers over many years.

8.6.1 Rogue Transmissions

The blue patch of interference to the south-east of the UK is dominated by a Romanian AM broadcast station on 153 kHz, called *"Brasov 1"*. Its carrier frequency is separated from the Datatrak f_1 frequency by 6.545 kHz, so we would expect its lower sideband to be the culprit. Here we have a curiosity: according to the IFL, this station's bandwidth is 20 kHz, i.e. ±10 kHz! This seems very improbable, since the ITU Radio Regulations set the bandwidths (and channel spacing) of broadcast stations in the band from 148.5-255 kHz at 9 kHz across ITU Region 1, which includes Romania, [76]. So, its lower sideband should not be a problem.

It was decided to measure the bandwidth of "Brasov 1" using a spectrum analyser and calibrated loop antenna, by receiving its night skywave signal in Bangor (Appendix C). The spectrum analyser's averaging function was used to smooth out the fluctuating skywave field strength. The result is shown in Fig. 8.9. The Datatrak f_1 and "Brasov 1" signals are clearly to be seen, as is "Allouis" in France on the AM channel above, at 162 kHz. It is clear that the two broadcast signals have similar bandwidths, of 9 kHz, as indeed they must if they are not to interfere with one another. The conclusion is that the bandwidth given for "Brasov 1" in the IFL is incorrect.
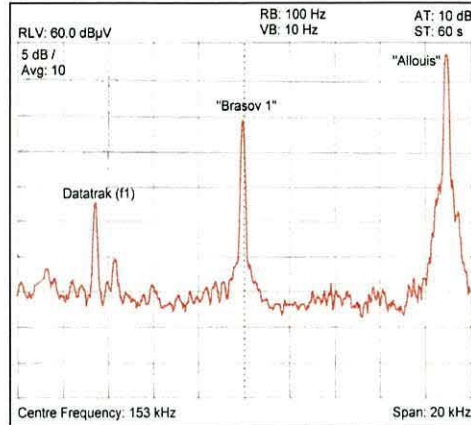
Fig. 8.9 - Spectrum of "Brasov 1" signal received via skywave at Bangor

Replacing the 20 kHz bandwidth by 9 kHz in the list of interferers results in the updated interference layer shown in Fig. 8.10. The large area of blue has now disappeared, leaving just local interference very close to the transmitters at Droitwich, Pinneberg, Brest, "S Assise" and Bad Vilbel.

This experience with "Brasov 1" shows the importance of exploring carefully any cases of potential interference that are revealed by the use of the model. That way, errors in the IFL that actually affect the Datatrak results can be discovered and corrected without wasting time on stations that can have no effect on the Datatrak system. This approach revealed another error. The IFL lists a weather facsimile service on 134.2 kHz, transmitting from Mainflingen, Germany. The model showed that this station might cause interference to the Datatrak f_2 signal on 133.2275 kHz.
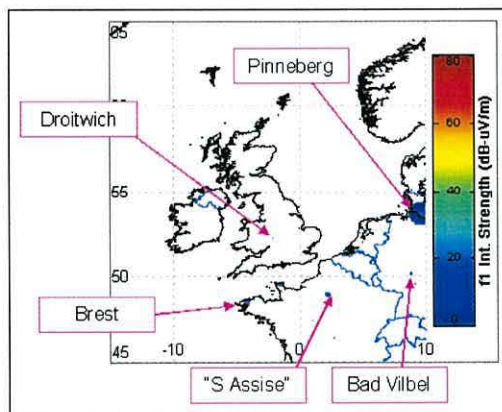
Fig. 8.10 - Revised interference layer following the change to "Brasov 1" bandwidth record. The remaining interference areas have been highlighted with the name of the culprit transmitter.
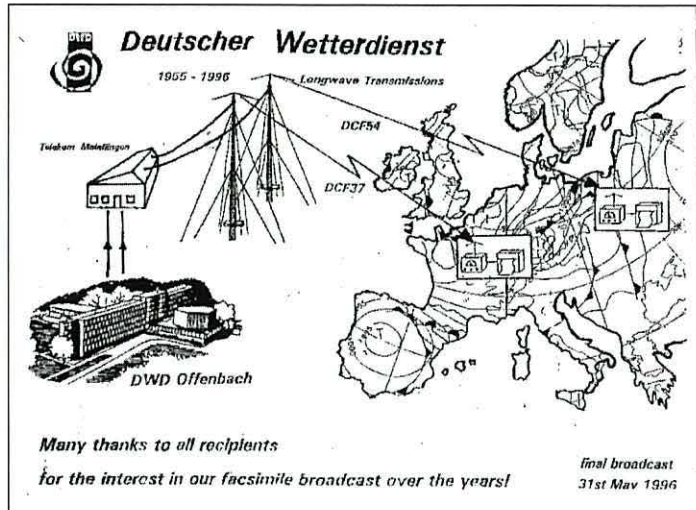
Fig. 8.11 – The last fax transmitted from Mainflingen on 31 May 1996 (after [86])

This Mainflingen signal could not be received in Bangor, where it should have been strong at night. An Internet search revealed that it had been switched off on 31 May 1996, more than 6 years before the publication of the then-current IFL; indeed, the last farewell fax is shown there as evidence (Fig. 8.11) [86]! This transmission was removed from the database in the Datatrak model.

With these corrections made, the interference model now gives results that appear realistic, in that they agree with the observation that there is no significant interference to the UK Datatrak system by day or night. The model forms a powerful tool for exploring the potential for interference of new Datatrak systems and guiding the search for suitable operating frequencies.

8.6.2 Signal-to-interference ratio

Now we know the field strengths of the Datatrak signal and of the interference at each array point, we can compute the signal-to-interference ratio (SIR) there and compare it with a maximum SIR limit. Since pass-band interference appears to the Locator as similar to random noise, with both causing uncertainly in phase measurements, it is reasonable to adopt the same SNR limit of 15 dB as was used for noise in Chapter 6. This has been done for the first time in Fig. 8.12.
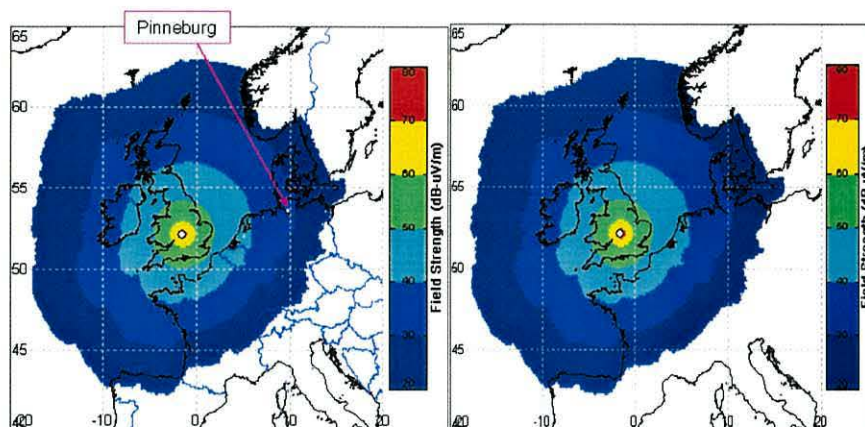
Fig. 8.12 - Field strength plot of the Stratford-upon-Avon transmitter. Left: Boundary limited by 15 dB signal-to-interference ratio, and 5 dB-μV/m Locator noise floor. Right: Boundary limited by 15 dB signal-to-noise ratio, and 5 dB-μV/m Locator noise floor only.

This figure is almost identical to Fig. 4.6 (reproduced in Fig. 8.12 on RHS) in which the SNR is set by the original value Locator noise floor value of 5 dB-μV/m. This is to be expected since (as we have seen) interference is in general weaker than 5 dB-μV/m. However, a hole has now appeared in North Germany surrounding the 1.5 kW interferer at Pinneberg, near Hamburg, on 147.3 kHz. This narrow-band Morse transmission is very effectively filtered in the Locator, leaving a problem area immediately surrounding the station – and well outside the UK Datatrak service area.

8.7   Locator blocking

The other form of interference analysed in Chapter 7 that we wish to build into the model is Locator blocking. It is much easier to establish which interferers will give blocking interference than pass-band interference. Again, we will create a reduced list of potential interferers, which will include as a start all the stations in the reduced list of pass-band interferers.

8.7.1   Reducing the list

Blocking cannot, in practice, be caused by skywaves since even the highest skywave field strength of the strongest, 10 MW, station (Fig. 8.7) is some 20 dB below the lowest blocking field strength. Even taking the stochastic nature of skywave strength into account, we calculate (assuming a Gaussian distribution) that the probability of this 10 MW station's skywaves ever reaching the blocking strength is 0.0000006 %!

The maximum range at which the 10 MW station's groundwave can reach the minimum blocking field strength of 121 dB-μV/m via a sea-water groundwave path is 28 km. So, we can first remove from the reduced list any station further than 28 km from any the window edge. This can still leave many potential interferers, especially to Datatrak networks in land-locked countries such as Austria. We can introduce a minimum blocking range to reduce the number of potential blockers to those that *really matter*. Also, we must consider the resolution of the prediction model, which is 0.1° × 0.1° (approximately 11 km by 7 km in the UK). As we are using the ground propagation curves (which begin at 1 km from the transmitter) to calculate the field strength of a potential blocker, it is convenient to assign a conservative minimum blocking range of 1 km [36].

So, for each interferer in the IFL that lies inside, or within 28 km of, the network window, we check the field strength at 1 km range in the direction of maximum antenna gain. If it is greater than the blocking field strength of the Locator at the interferer's centre frequency, the interferer is included in the blocking list. This process identified 32 potential blockers of the UK Locator, which were added to the reduced blocker list.

8.7.2 Using the reduced blocker list

Armed with the reduced blocker list, the model analyses each interferer in turn. It then uses the groundwave attenuation array for that interferer, or computes the field strength using the seawater propagation curve for 150 kHz, as previously. The model is able to identify those points in the interference layer that lie within 28 km of the transmitter, and check whether the Locator will be blocked at any of them. If it will, then the calculation point will be marked as "blocked" by entering very high field strength (9999 dB-μV/m) into the array there. The coverage model subsequently detects this, and excludes those points from coverage, producing a hole in the coverage plot. An example of this is shown in Fig. 8.13: note the hole within which the Droitwich station overloads the Locator (as observed in Chapter 7).

Note, too, that the loss of coverage due to certain blockers will not appear on these coverage plots. This is because the arrays are produced with a latitude and longitude resolution of 0.1°. In the UK, this corresponds to approximately 11 km × 7 km. If the
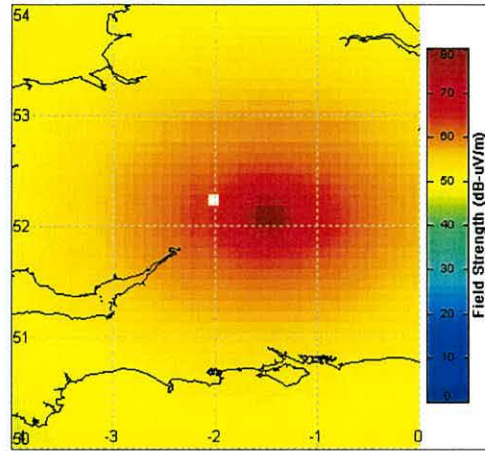
Fig. 8.13 - Field strength of Stratford transmitter around Droitwich interferer. The white 'hole' in the plot is where the Droitwich station overloads the Locator.

blocking radius of an interferer is less than 3.5 km, it might not affect any individual array point. For this reason, a text list showing the locations of blockers is produced during the interference analysis (Fig. 8.14). This can be used to locate all potential blockers.

8.8 Overall signal coverage

We now have all we need to plot the coverage of the Datatrak timing/data signal, by day or night. The field strength of the wanted Datatrak groundwave signal is calculated using Millington's method (Chapter 4). Its night skywave signal and the resulting degree of fading are determined as in Chapter 5. Atmospheric and vehicle noise are known from Chapter 6. And now we have interference, both pass-band and blocking.

For the first time, Fig. 8.15 shows the night-time coverage of the Stratford f_1

```
                    ⋮
4. SAARLOUIS (075000032) GSB-
        Power (Night) : 2000000 W (2000000 W)
        Frequency : 180 kHz
        Lat : 49.2833;  Long : 6.68333
5. DROITWICH (075000056) GSB-
        Power (Night) : 399990 W (399990 W)
        Frequency : 198 kHz
        Lat : 52.3;  Long : -2.1
6. JUNGLINSTER (075000103) GSB-
        Power (Night) : 2000000 W (2000000 W)
        Frequency : 234 kHz
        Lat : 49.6667;  Long : 6.31667
                    ⋮
```

Fig. 8.14 - Blockers list produced during the interference analysis. Details include name, location, and power of each blocker.
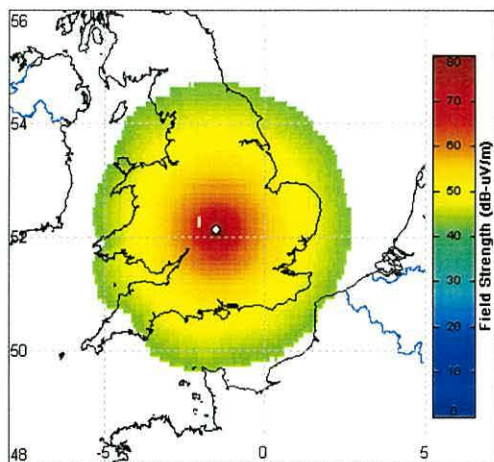
Fig. 8.15 - Night-time coverage of Stratford transmitter f_1 trigger/data signal, radiating 85 W, limited by own-skywave interference, atmospheric noise, vehicle noise, and interference via groundwave and skywave propagation.

timing/data signal, guaranteed for 95 % of the time. It represents the area within which the SNR and SIR are both greater than 15 dB and the field strength (shown as a colour contour) exceeds 20 dB-μV/m. The Locator noise floor is 28 dB-μV/m as determined in Chapter 6.

We see that most of England and Wales lies within the night-time coverage of this transmitter, although the signal falls short of the coverage criteria in Cornwall and other parts of the south-west peninsula. This is due to its failing to meet the SNR criterion because of the lower ground conductivity in the area and therefore an increase in the rate of groundwave attenuation. Notice also the hole to the north-west of the Stratford transmitter in which Droitwich overloads the Locator.

Fig. 8.15 thus takes into account all signals and noise sources that determine timing/data coverage and the model is now complete in respect of this function of the Datatrak system. In the next chapter we will move on to consider the effect of the SNRs and SIRs of the individual stations on the repeatable accuracy of the navigation function.

8.9 Conclusions

The subject of interference is very interesting, but highly complex. The effect of interference on a receiver depends mainly on the design of the receiver itself and the frequencies used by the Datatrak system. With this in mind, the Mk4 Locator and

H-field antenna set-up was analysed with the intention of allowing us to calculate the effect of interference on the Datatrak signal being received. The result was the frequency response and blocking field strength characteristics in the previous chapter.

In this chapter, the Locator's frequency response is used to determine the level of pass-band interference that passes through the its filters and appears as noise on the Datatrak signal. The result is a model that can predict whether the level of interference causes the Locator to become unreliable, and 'out of coverage'.

The blocking model is used to check whether a Locator can be used near an interferer. The model shows on the coverage plot those areas in which the Locator will fail due to overloading. This is backed up by a text report listing the specific transmitters that will block the Locator.

This analysis requires a list of potential interferers. The main list used in the model is the ITU International Frequency List (IFL). It contains the more than 22,000 transmitters throughout the world, within the defined frequency band. A method was developed of reducing the list to just those transmitters that are likely to cause interference. It excluded all interferers too distant geographically, or in frequency, from the Datatrak network to affect it. Both pass-band interference and blocking interference were considered.

The result of the interference analysis is 8 interference arrays, for different times-of-day, Datatrak frequencies and software filters. These arrays cover the area of the Datatrak network. By selecting the appropriate layer, the coverage of a Datatrak signal, limited by SIR, can now be plotted. Once this has been done, stations in the IFL that can potentially cause Datatrak interference stand out. They can then be individually investigated and any errors corrected.

The results confirm that, for the UK network with its well-chosen frequencies, levels of interference are below the noise floor of the Locator. For the first time this model, allows engineers to set up a computer simulation of a Datatrak network and so establish the best frequencies on which to operate it, minimising interference from the many other radio services with which it must share the frequency spectrum.

Also for the first time, we can now predict the coverage of the trigger/data signal, taking into account Datatrak transmitter power, groundwave attenuation due to ground conductivity, own-skywave and its interaction with the groundwave signal, atmospheric and vehicle noise, and interference from other radio services in the Datatrak frequency band.

Chapter 9

Repeatable Accuracy

9.1   Introduction

The coverage model developed so far has dealt primarily with the timing/data signal being received by the Mk4 Locator. Now we consider the effect of the same noise and interference sources on the *navigation* performance of the Locator. The objective is to develop a technique that will let us plot the *repeatable accuracy* of the Datatrak network.

9.2   Defining Repeatable Accuracy

Repeatable accuracy is defined by [16] as: "the accuracy with which a user can return to a position whose coordinates have been measured at a previous time with the same navigation system". Essentially, it defines the variability of the position fix.

In Section 3.4.2, we learned that the Datatrak Locator measures the phases of the signal received from each station at the four frequencies, f_{1+}, f_{1-}, f_{2+} and f_{2-}, against an on-board clock. From these measurements, it establishes its pseudorange from each station and, knowing the stations' locations, computes lines of position, and from these, its own location. Ideally, the Locator would receive simply the stable groundwave signal from each station. In practice, noise and interference from the various sources studied in Chapters 5 to 8, create uncertainty in the phase measurements, and in the resulting pseudoranges. The effect of these uncertainties on the position fix then depends on the *geometry* of the transmitters relative to the Locator.

So, point-by-point throughout the coverage area of a Datatrak system, we will wish to compute the SNR and SIR values, then the pseudorange uncertainties they cause and finally the repeatable accuracy of the position fix.
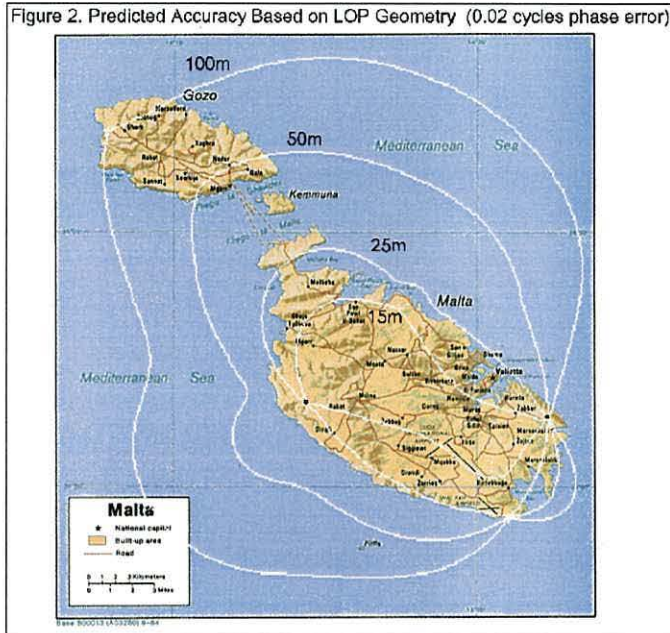
Fig. 9.1 - Predicted repeatable accuracy of the Malta hyperbolic navigation network produced by Datatrak (after [87])

The current state-of-the-art is very basic. The Datatrak company ignore all SNR and SIR spatial and temporal variations, making the simplifying assumption that the phase uncertainty everywhere is 0.02 cycles (about 40 m) [87]. Taking geometry into account, they then compute contours of repeatable accuracy. An example is shown in Fig. 9.1, for the 5-station *hyperbolic* system that serves Malta. No equivalent plot exists for a pseudorange system.

9.3   Phase Uncertainty

The energy received by the Locator is the sum of 6 components: the wanted groundwave signal, its unwanted own skywave, plus Locator noise, atmospheric
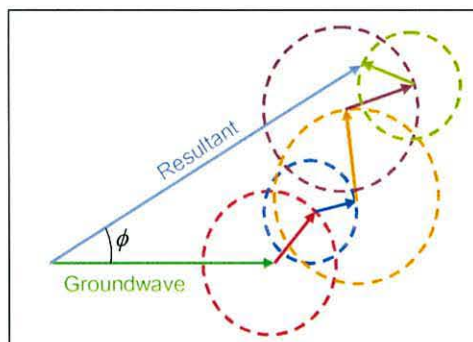
Fig. 9.2 – Instantaneous phase disturbance, ϕ, due to 5 sources of noise or interference, each with uniform phase distribution
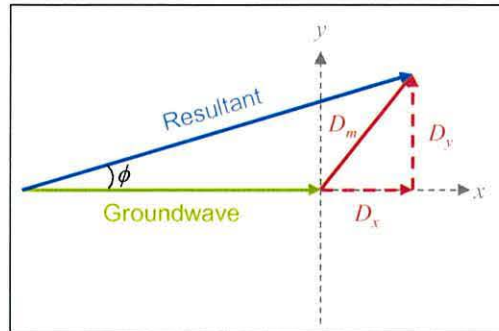
Fig. 9.3 - Phase disturbance as applied in FM signal analysis

noise, vehicle noise and interference. Each component has different field strength and a random phase distribution relative to the wanted groundwave signal. The error, ϕ, in each phase measurement is due to 5 sources of noise or interference, each with a uniform phase distribution, as illustrated in Fig. 9.2.

There will be some variation in the master and receiver clocks. However, as we shall see later, these variations will appear as a clock bias, and is removed as part of the calculating the position. Thus, they will not have any effect on the repeatable accuracy. That leaves 5 sources of disturbance. Although their phase distributions are assumed to be uniform, each of them may have a different amplitude distribution.

If we consider just one of these disturbances, the situation is similar to the classic phase disturbance of frequency-modulated (FM) signals [88, 89]. It was initially thought that analysis of this FM case would yield a useful relationship between the nature of the disturbances, and the phase disturbance in the received signal. In Fig. 9.3, the disturbance signal is generally considered as being independent in the x and y direction with Gaussian distribution and median at (0, 0). Although the resulting interference has a uniform distribution of phase, its amplitude has a *Rayleigh* distribution [88, 90]. But, this does not fit with the known nature of skywave, which has a Gaussian amplitude distribution. Atmospheric noise too has a Gaussian distribution. So, using this analysis will not provide a viable result.

9.3.1 New method

We will instead consider the sum of all the disturbances as a single disturbance vector. The actual nature of this vector may well be extremely complex. However, it can be

simplified since in almost all cases the vector will be dominated by a single source, often the Locator noise floor. The phase distribution of the disturbance is reasonably assumed to be uniform. The amplitude will mostly be determined by the median magnitude of the dominant disturbance. In any case, the amplitude *distribution* of vehicle noise, Locator noise and interference are unknown, only their mean values are known.

Using this simplification, the problem is easier to analyse (Fig 9.4). Then:

$$\tan \phi = \frac{v_y}{g + v_x}$$

$$\tan \phi = \frac{d_m \sin \theta}{g + d_m \cos \theta}$$

$$\tan \phi = \frac{\sin \theta}{r_{gd} + \cos \theta} \qquad (9.1)$$

where ϕ is the resulting instantaneous phase disturbance of the signal, g the magnitude of the groundwave signal, d the magnitude of the disturbance, θ the instantaneous phase of the disturbance relative to the groundwave signal, and r_{gd} the groundwave-to-disturbance ratio (GDR), i.e. $r_{gd} = \frac{g}{d_m}$.

The GDR can be represented in dB, as GDR_{dB}, whence:

$$\phi = \tan^{-1} \left[\frac{\sin \theta}{10^{\left(\frac{GDR_{dB}}{20} \right)} + \cos \theta} \right]. \qquad (9.2)$$

The model can predict GDR_{dB}, since it already computes the field strengths of the
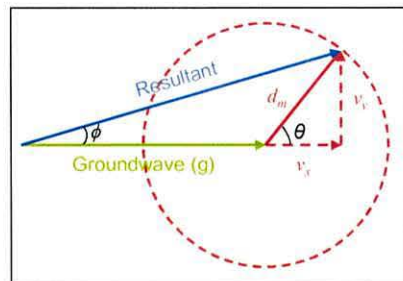
Fig. 9.4 - Method of calculating phase uncertainty of received signal

wanted Datatrak groundwave signal, and of each individual disturbance. Since these disturbances are mutually independent, we can calculate the root-sum-square of their sum, GDR_{dB}, as the sum of the median values of the individual components:

$$GDR_{dB} = E_{ground}$$
$$-10\log_{10}\left(10^{\left(\frac{E_{sky}}{10}\right)} + 10^{\left(\frac{E_{noisefloor}}{10}\right)} + 10^{\left(\frac{E_{atmospheric}}{10}\right)} + 10^{\left(\frac{E_{vehicle}}{10}\right)} + 10^{\left(\frac{E_{Ieff}}{10}\right)}\right) \quad (9.3)$$

where E_{ground} is the groundwave field strength, E_{sky} the median skywave field strength of Datatrak signal [Equation (5.6)], $E_{atmospheric}$ the median atmospheric noise [Equation (6.1)], $E_{vehicle}$ is the strength of the vehicle noise, E_{Ieff} the effective interference field strength [Equation (8.9)], and $E_{noisefloor}$ the Locator noise, all in dB-µV/m.

The statistical distribution of ϕ will also depend on the statistical distribution of θ, the phase difference between the groundwave and the total disturbance. We assume this variable has a uniform phase distribution over the range of $-\pi \rightarrow \pi$ (Fig. 9.5). The variance of θ can be calculated by considering the moments of the probability distribution [50]:

$$E\left[X^n\right] = \int_{-\infty}^{\infty} x^n f_X(x) dx \quad (9.4)$$

where x is the random variable with PDF, $f_X(x)$.

Setting $n = 2$, allows us calculate the variance of X:

$$E\left[\theta^2\right] = \int_{-\pi}^{\pi} \theta^2 f_\theta(\theta) d\theta$$
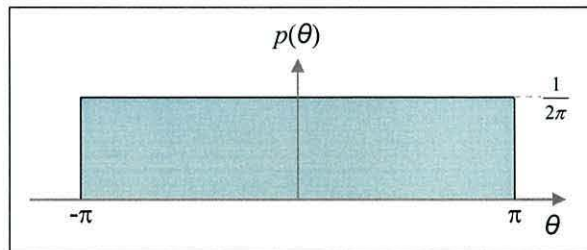
Fig. 9.5 - Probability density function of disturbance phase, θ

$$E\left[\theta^2\right] = \frac{1}{2\pi} \int\limits_{-\pi}^{\pi} \theta^2 d\theta$$

$$E\left[\theta^2\right] = \frac{\pi^2}{3} \tag{9.5}$$

So, the variance of the random variable θ is $\dfrac{\pi^2}{3}$.

However, it is clear from Fig. 9.5, or from Equation (9.4) with $n = 1$, that the mean of θ is 0. Its standard deviation is:

$$\sigma_\theta = \sqrt{E\left[X^2\right]}$$

$$\sigma_\theta = \sqrt{\frac{\pi^2}{3}}$$

$$\sigma_\theta = \frac{\pi}{\sqrt{3}} \tag{9.6}$$

This result is confirmed by Schwartz [89]. If we substitute this value of standard deviation of θ into Equation (9.2), we get:

$$\sigma_\phi = \tan^{-1}\left[\frac{\sin\sigma_\theta}{10^{\left(\frac{GDR_{dB}}{20}\right)} + \cos\sigma_\theta}\right]$$

$$\sigma_\phi = \tan^{-1}\left[\frac{\sin\dfrac{\pi}{\sqrt{3}}}{10^{\left(\frac{GDR_{dB}}{20}\right)} + \cos\dfrac{\pi}{\sqrt{3}}}\right] \tag{9.7}$$

So, the standard deviation of the phase disturbance, in radians, can now be calculated as a function of GDR_{dB} (Fig. 9.6). As the GDR_{dB} increases, the phase error decreases, as would be expected. At very low GDR_{dB} (e.g. below 0 dB), the phase error approaches $\dfrac{\pi}{\sqrt{3}}$ radians. This is as expected, since the disturbance is now the dominant received signal component, and the resultant standard deviation will approach that of the disturbance signal. However, Datatrak is simply not used when
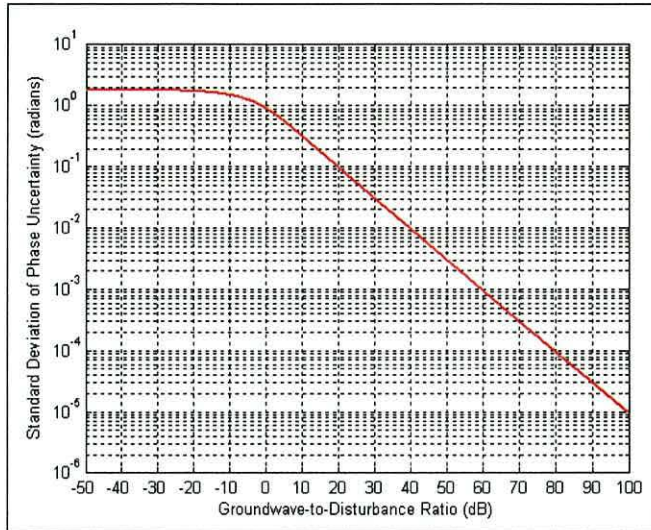
Fig. 9.6 - Resultant phase uncertainty (in radians) as a function of the GDR

the SNR or SIR is below 0 dB, so the maximum phase uncertainty likely to be encountered is around 0.9 radians.

The phase uncertainty can now be converted into a *range uncertainty*, in metres:

$$\sigma_d = \frac{\sigma_\phi \lambda}{2\pi} \qquad (9.8)$$

where λ is the wavelength of the navigation signal, in metres. As an example, Fig. 9.7 shows the standard deviation of the range uncertainty as a function of GDR_{dB} for the UK f_{1+} signal, with its 2047 m wavelength. Again, as GDR_{dB} increases, range uncertainty falls. With the minimum GDR_{dB} of 0 dB, the uncertainty in a measured range is bounded by 30 m. A more typical GDR_{dB} of 30 dB results in 10 m uncertainty.

9.3.2 Phase and Position Filters

However, the phase uncertainty as observed by the *processor* in a Locator is not this simple. Before the pseudoranges are used to calculate the position fix, the phases are filtered in a '*phase filter*'. This is a software function, employing an iterative process in which previous samples are used to predict, and so filter, the current phase value, much as in a Kalman filter. There is also some influence of SNR on the result. The timing constant is over a few cycles of 1.68 seconds, so sudden changes in phase are mostly removed.
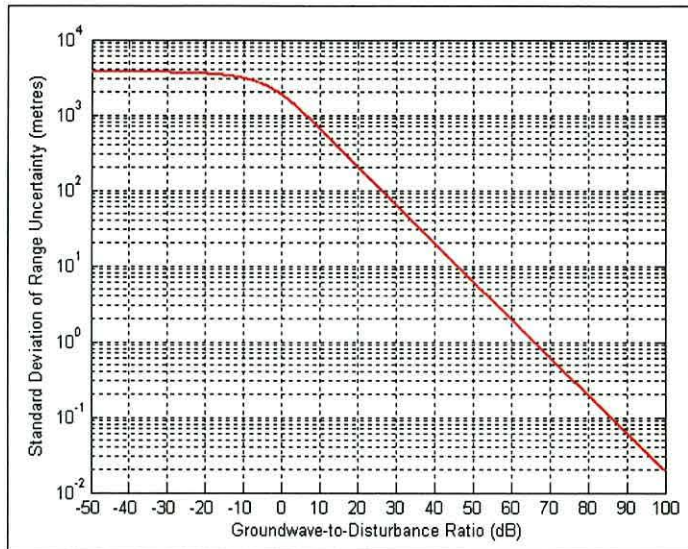
Fig. 9.7 - Uncertainty in measured range of UK f_{1+} signal as a function of GDR

Once a position fix has been calculated, it passes through another filter. Datatrak call this the 'XY filter' because it filters the X and Y coordinates of the position fix. This is an extremely complex software iterative filter with several variables such as the confidence factor (Section 3.5 and Chapter 11), and some user-defined limits, as inputs. Again, the timing constant is over a few cycles of 1.68 seconds.

Datatrak obviously employ these filters to remove short-lived disturbances. Their timing constants are kept deliberately short so that the final position fix remains accurate, even when the vehicle is moving. However, the filters have less effect on own-skywave disturbances, which change more gradually [91]. Unfortunately, simulating the filters in the model in order to predict their effects on the final position fix is almost impossible due to the complexity of the algorithms employed. This situation is made worse by a lack of formal documentation on their operation.

It was decided to take the approach of simplify these filters, in order to include their effect on the repeatable accuracy. We will assume that the two filters in combination will reduce the disturbance in the position fix. The model will first be used to predict the position uncertainty with no filters. Then, the repeatable accuracy will be measured at sample geographical points in the network. The ratio between the predicted and measured repeatable accuracies will be assumed to be due to the effect of the filters. A *filter factor* will thus be calculated which will be applied to all raw

predicted repeatable accuracy values. The result should then be a realistic representation of the Locator's performance. The filter factor will be different between day and night due to the influence of own-skywave interference at night.

To calculate the repeatable accuracy values, we must understand the algorithm used by the Locator to compute its position from a set of pseudorange measurements.

9.4   Locator least-squares algorithm

The Locator position algorithm employs the 'least-squares' method [92], broadly as most GPS receivers do [4, 13]. Starting with an initial position estimate, an iterative computation finds a position which minimises the square of the differences between the measured ranges to the stations and the ranges computed from the current estimated position. It employs the following matrix equation:

$$\delta x = \left(A^{T}WA\right)^{-1} A^{T}W\delta b \tag{9.9}$$

where T is the transpose operator. After each iteration, δx contains the change from the guessed position to the new position and also the change in clock bias:

$$\delta x = \begin{bmatrix} \Delta x \\ \Delta y \\ \Delta B \end{bmatrix} \tag{9.10}$$

where Δx and Δy are the changes in the x and y directions *with respect to the previous iteration*, and ΔB the change in the clock bias.

The ranges from the adjusted position to the stations are then compared with the ranges measured by the receiver, and the differences are stored in δb:

$$\delta b = \begin{bmatrix} O_1 - C_1 \\ \vdots \\ O_n - C_n \end{bmatrix} \tag{9.11}$$

where C_i is the calculated range from the estimated position to the ith station and O_i is the corresponding measured, or observed range.

In calculating the ranges, we need to take into account the bearings of the paths from the stations. This information is stored in a *directional cosines* matrix, *A,* also sometimes called the *geometry,* or *state transition,* or *measurement* matrix [92]. Matrix *A* defines the relationship between the change in δb and the change in the actual position, plus the equivalent in distance of the clock bias, δB:

$$A = \begin{bmatrix} \dfrac{\delta b_1}{\delta x} & \dfrac{\delta b_1}{\delta y} & \dfrac{\delta b_1}{\delta B} \\ \vdots & \vdots & \vdots \\ \dfrac{\delta b_n}{\delta x} & \dfrac{\delta b_n}{\delta y} & \dfrac{\delta b_n}{\delta B} \end{bmatrix} \tag{9.12}$$

where $\dfrac{\delta b_i}{\delta x} = \sin\varphi_i$, $\dfrac{\delta b_i}{\delta y} = \cos\varphi_i$, φ_i being the bearing of the ith station from the receiver.

Matrix *A* is called the *directional cosines* matrix because it contains the cosines (and sines) of the various bearings. The clock bias coefficient is always 1, since clock bias affects the measurements of all stations equally.

A further, important, matrix is employed by Datatrak: the optional *weight* matrix, *W*. This allows each measurement to be weighted, in accordance with a measure of signal quality, so allowing the most accurate measurements to have the greatest influence on the result. *W* is a simple diagonal matrix:

$$W = \begin{pmatrix} w_1 & & 0 \\ & \ddots & \\ 0 & & w_n \end{pmatrix} \tag{9.13}$$

where w_i is the weighting of the ith measurement, in the range 0 (ignore totally) to 1 (use entirely).

9.4.1 Locator-Specific Implementation

The description above gives a fairly general overview of the least-squares method. The Datatrak Locator implements it as follows. First, it employs all four frequencies, f_{1+}, f_{1-}, f_{2+} and f_{2-} from up to 6 different stations; this maximum number being limited

simply by the computational power available in the Locator. Thus, the position solution is based on up to 24 measured ranges [93].

The 6 stations are the nearest 6 to the Locator up to a maximum range: 350 km in the UK [94]. This limit is set by Datatrak in an attempt to minimise the effect of night-time skywave interference on the position fixes. It also acts as a crude lower limit of SNR. Given that skywaves can potentially be relatively strong at ranges much less than 350 km, the choice of range limit is less than ideal. Note that station selection does *not* depend on either measured SNR or station geometry.

Fundamentally, the Locator only requires three stations for a position fix. However, a decision was taken by Datatrak that at least 4 stations should be employed, so as to provide a more *reliable* fix. Additional transmitters above 4 provide redundancy and may improve the accuracy the fix.

Since the same clock is used at all four frequencies, there is only a single clock bias term in the directional cosines matrix, A, in Equation (9.12). The weight matrix, W, is derived from the measured SNRs of the signals [95]:

$$\text{If } SNR_i < 30 \text{ dB,} \qquad w_i = 10^{\left(\frac{SNR_i - 30}{20}\right)}$$
$$\text{If } SNR_i \geq 30 \text{ dB,} \qquad w_i = 1 \qquad\qquad (9.14)$$

where SNR_i is the measured SNR of the ith measurement in dB. So, a measurement with an SNR of 24 dB, for example, will be weighted at 50 %.

The iteration process continues until the change in position calculated by Equation (9.10) falls below 1 m. The total position change across all iterations is summed, and the position estimate updated accordingly and reported.

Since the least-squares method is a weighted *best fit* of the measured ranges, it is very unlikely that the ranges will all align correctly at the calculated point. The Locator combines all the discrepancies to form the *confidence factor*. Thus, this is a measure of how well the calculated point fits the measurements. The Locator uses the confidence factor to determine whether or not each position fix it has generated is valid, as we shall see later.

9.5 Horizontal Dilution of Precision (HDOP)

The Horizontal Dilution of Precision (HDOP) is a dimensionless factor that describes the geometry of the stations, as with many navigation systems. HDOP is the ratio of the position error to the measurement errors [4]. So, a plot of HDOP values can show a network designer which areas will pose a repeatable accuracy problem, based solely on the location of the stations. Essentially, it is an aid to optimally place transmitters. It can be calculated from the results of the least-squares method described above.

When a receiver measures a range from a transmitter, it produces a line-of-position (LOP): a circle, along which the measured range is valid (Fig. 9.8). Any noise on the measured signal will cause the LOP to fluctuate. In Fig. 9.8, the dotted lines represent the bounds of this fluctuation. If a second LOP is introduced, with the same uncertainty, the resulting diamond shape represents the area in which the Locator is likely to be found. The size of this area depends on the *angle-of-cut* between the two LOPs: a small angle of cut results in a large area, and a high HDOP value. If the LOPs have an angle of cut of 90°, the smallest area is produced, resulting in the lowest possible HDOP. Generally, the lowest HDOP is found close to the mid-point among the transmitters of the system.

HDOP can be calculated as [4, 13]:

$$H = \left(A^T A\right)^{-1}$$
$$\text{and } HDOP = \sqrt{H_{11} + H_{22}}$$

(9.15)
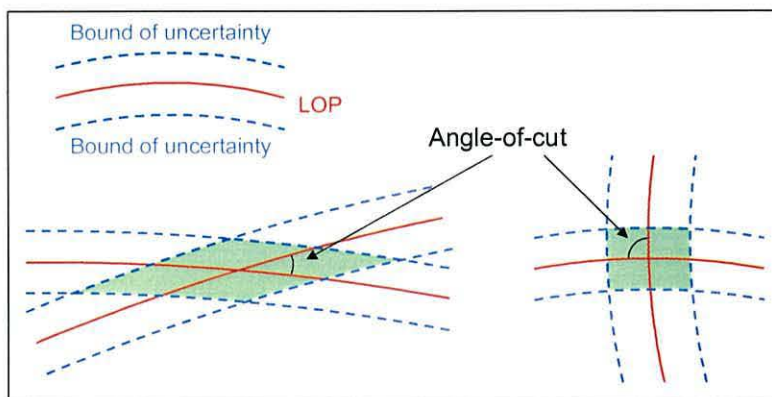
Fig. 9.8 - Top: Uncertainty in line-of-position (LOP). Bottom: Effect of angle-of-cut on position uncertainty.
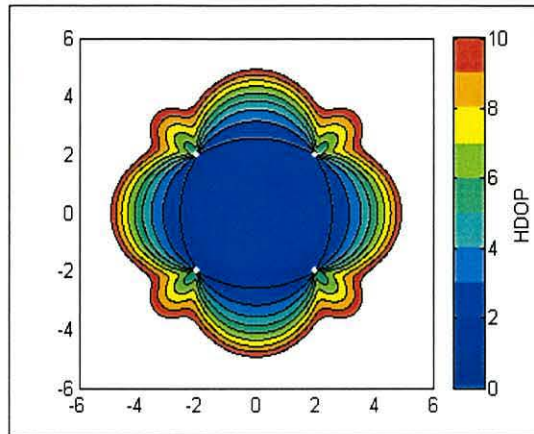
Fig. 9.9 - HDOP plot of network with four stations arranged in a square.

where A is the directional cosines matrix given in Equation (9.12).

The HDOP distribution of a navigation system can be plotted simply from knowledge of the positions of the transmitters relative to the receiver. Fig. 9.9 shows the HDOP contours of a system with four stations in a square configuration. The lowest HDOP is at the centre, where angles-of-cut are close to 90°. As the receiver moves away from the centre, the HDOP increases due to the smaller angles-of-cut. This plot, produced by our Datatrak model, exactly matches Levanon's classic four-station plot in [96].

9.5.1 Weighted HDOP

The Datatrak Locator weights range measurement according SNR. We take this into account by calculating a *weighted HDOP* (WHDOP) [13]:

$$H = \left(A^T W A \right)^{-1}$$
$$\text{and } WHDOP = \sqrt{H_{11} + H_{22}}$$

(9.16)

where W is the weight matrix (Equation (9.13)).

In the example in Fig. 9.10, the south-west transmitter of the four-station network is now weighted at just 10%, the others remaining at 100%. The change from Fig. 9.9 is dramatic; the plot now resembles that of the three-station system, shown on the right-hand side.
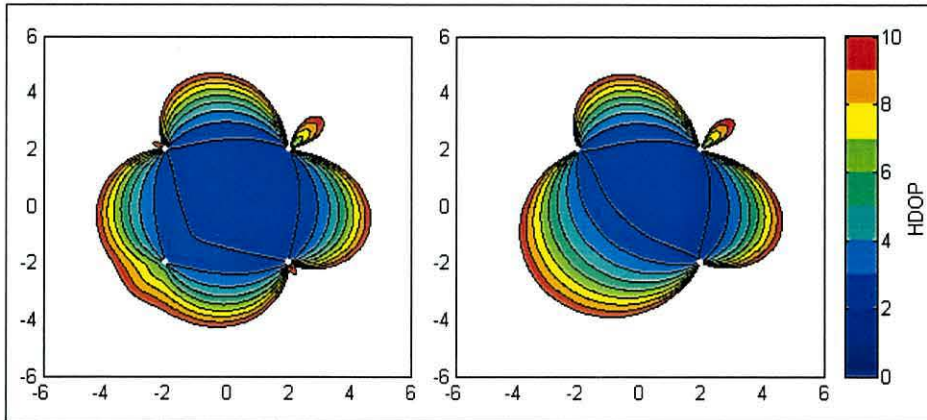
Fig. 9.10 - Left: 4-station WHDOP plot, with signals from the south-west station weighted at 10%; Right: 3-station HDOP plot

We will now calculate WHDOP values point-by-point across the UK Datatrak system. At each point in the array, the Datatrak station selection rules will determine which transmitters contribute to the fix and the WHDOP. Their SNR values will determine their weightings. The result is the first-ever WHDOP plot of the UK Datatrak system, in Fig. 9.11. The colours represent the WHDOP values, and are quantised to 0.5 of a unit. Moving out from the centre of the network, the WHDOP increases, as far as the border defined either a WHDOP of 10, or fewer than 4 stations within 350 km.

Throughout most of England and Southern Scotland, WHDOP is actually below 1. This is because redundancy improves repeatable accuracy, as is normal with over-determined navigation solutions. The lowest possible HDOP (assuming all measurements are weighted 100%) is [96]:
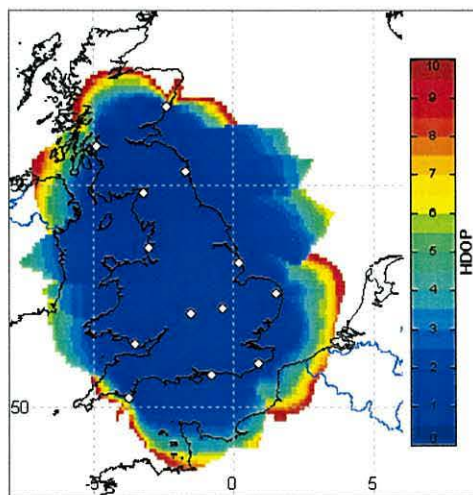
Fig. 9.11 - Weighted HDOP plot of the UK network

$$HDOP_{min} = \frac{2}{\sqrt{N}} \qquad (9.17)$$

where N is the number of measurements used. For Datatrak, with 24 measurements (6 stations transmitting at 4 frequencies), the lowest HDOP is 0.41. In the UK, the WHDOP never quite reaches this lower limit, because of weighting.

9.6   Position Uncertainty

To calculate the uncertainty in the position, consider again Equation (9.9):

$$\delta x = \left(A^T W A\right)^{-1} A^T W \delta b$$

The $\left(A^T W A\right)^{-1}$ term is simply the WHDOP, a geometrical/SNR coefficient as described above. The $A^T W \delta b$ term calculates the influence of each weighted measurement in the x and y directions. If the range measurement uncertainty is σ_d [Equation (9.8)], the weighted uncertainties in the x and y direction are:

$$\begin{aligned}
\sigma_{x,i} &= \sigma_d w_i \sin \varphi_i \\
\sigma_{y,i} &= \sigma_d w_i \cos \varphi_i
\end{aligned} \qquad (9.18)$$

where $\sigma_{x,i}$ is the standard deviation of the uncertainty in the ith measurement in the x direction, $\sigma_{y,i}$ is the equivalent in the y direction, and w_i is the weighting applied to the ith measurement [Equation (9.13)].

We assume that all measurements are independent; this is reasonable, since the Locator makes one measurement at a time, so the instantaneous values of the noise-like disturbances will be different during each measurement. The total standard deviation of the measurements in the x and y directions are:

$$\begin{aligned}
\sigma_x^{\;2} &= \sum_{i=0}^{i=n} \sigma_{x,i}^{\;2} \\
\sigma_y^{\;2} &= \sum_{i=0}^{i=n} \sigma_{y,i}^{\;2}
\end{aligned} \qquad (9.19)$$

where n is the total number of measurements. The position uncertainty (1_{DRMS}), σ_p, is:

$$\sigma_p = WHDOP \times \sqrt{\sigma_x^2 + \sigma_y^2} \qquad (9.20)$$

where WHDOP is calculated by Equation (9.16).

Datatrak normally quote the *2DRMS* repeatable accuracy, RA_{2DRMS}, which contains approximately 95 % of all position fixes:

$$RA_{2DRMS} = 2\sigma_p \qquad (9.21)$$

9.7   Implementation in the model

Once again, an array is used that covers the geographical area of the network. At each calculation point, Equation (9.21) is evaluated using the predicted values of the groundwave field strengths, own-skywaves (if applicable), noise sources, and interference, to determine the value of GDR_{dB}. Fig. 9.12 shows the result of this process: the repeatable accuracy of the UK network during the day (left), and by night (right). The colours represent the magnitude of the repeatable accuracy: dark blue for 0 m, through to dark red for 200 m.

Notice that South-east England and the Midlands have the lowest repeatable accuracy values. This is to be expected, since the stations are closest together here, and many angles-of-cut are near right-angles. Also, comparing the daytime and night-time 200 m boundaries shows clearly the worsening of repeatable accuracy caused by the own-skywave interference that is dominant at night.
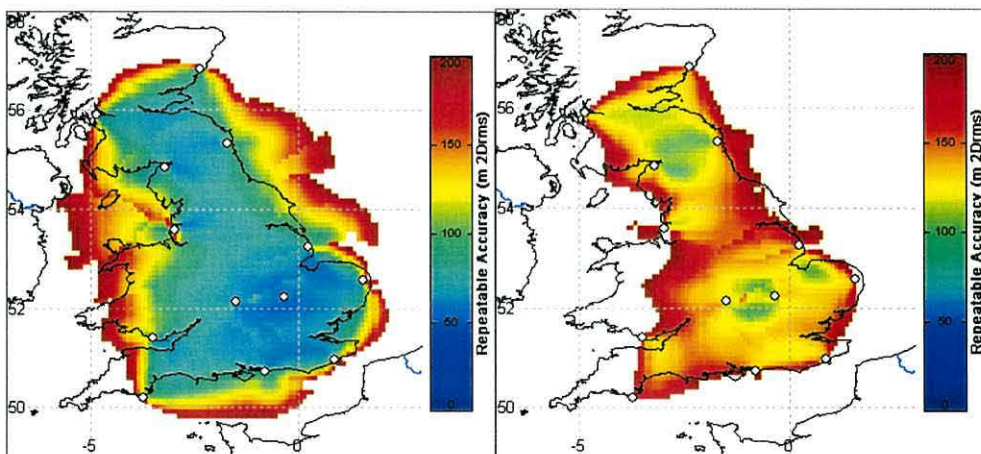
Fig. 9.12 - Daytime (left) and night-time (right) 2$_{DRMS}$ repeatable accuracy plots of UK Datatrak network

However, in Section 9.3.2, we discussed the filters employed in the Locator to improve repeatable accuracy. The results above show the position uncertainty as if no filters are used in the Locator.

9.8   Establishing the filter factors

Now we set up field measurements to establish the filter factors (Section 9.3.2) and ensure that the model reflects reality.

9.8.1 Bangor Tests

Our initial tests were made at the School of Informatics at Bangor, North Wales (53.229 °N, 4.123 °W). A Locator, together with an H-field antenna (Section 3.4.2), was set simply to record position fixes over a time-period. At this site, which by the opinion of Datatrak engineers is outside the service area of the Datatrak system using H-field antennae, the Locator produced very few position fixes. The SNR of the received signals was observed to be low at this site.

We saw in Chapter 5 that the Locator noise floor is at the equivalent of 28 dB-μV/m. This high noise is due to the high-gain amplifiers used in the H-field antenna circuitry. At Bangor, only the Southport signal had an SNR consistently above 20 dB. Other signals' SNR values were as low as 10 dB. This result is supported by predictions made by the model.

As a result, fixes in Bangor generally fail to meet the "confidence factor" (CF) criterion (see also Chapter 11) and the Locator suppresses its output (Section 9.4.1). Also, the low SNR causes considerable uncertainty in the position fix, and so the CF varies considerably.

In contrast, Datatrak Locators employing traditional E-field antennas do work in Bangor. But our model deals with the H-field antenna receiver, now being used in new vehicle installations because of its superior performance in urban canyons (Section 3.5.3).

	Measured Repeatable Accuracy (m 2Drms)	Predicted Repeatable Accuracy (m 2Drms)
Daytime	44.5	80.4
Night-time	82.9	165.5

Table 9.1 - Measured and predicted repeatable accuracy in Stoke-on-Trent

9.8.2 Stoke-on-Trent Tests

The second set of tests was conducted at the Stoke-on-Trent location (Section 4.9). Position fixes were recorded continuously for 24 hours. Here, 94 % of possible position fixes met the CF criterion and so were output. Table 9.1 shows the analysis of a 24-hour set of these results, split into daytime and night-time by reference to sunset and sunrise times [97]. The units are in metres 2_{DRMS}.

9.8.3 Milton Keynes Tests

The third set of tests was conducted in Milton Keynes (52.011 °N, 0.757 °W), where a suitable site with power and appropriate protection from the weather for the receiver was found. The site was chosen because this area has the very best performance offered by the UK Datatrak network. Here, 99.6 % of the position fixes were deemed valid. Table 9.2 analyses the results for 24 hours.

9.8.4 Computation of filter factors

From the measured and predicted values shown in Tables 9.1 and 9.2, on average the measured values are 43 % of the predicted values during the day, and 40 % during the night. Clearly, the Locator was hardly being affected by own-skywave phase disturbances at either Stoke-on-Trent or Milton Keynes. These values will now be used as filter factors and applied to the raw repeatable accuracy values throughout the network to produce realistic modelled repeatable accuracy values.

	Measured Repeatable Accuracy (m 2Drms)	Predicted Repeatable Accuracy (m 2Drms)
Daytime	17.2	55.0
Night-time	31.6	105.8

Table 9.2 - Measured and predicted repeatable accuracy in Milton Keynes

We can now generate revised UK network repeatable accuracy plots, with the additional filtering taken into account. The results are shown in Fig. 9.13. The repeatable accuracy is better than 100 m across most of England and Southern Scotland by both day and night. As expected, night-time repeatable accuracy is markedly poorer than daytime. Since Datatrak specify a 2_{DRMS} accuracy of 100 m, the boundary of the colours in Fig. 9.13 actually represents the *coverage* of the Datatrak system, based on this factor of repeatable accuracy during day and night. Plots such as this are completely novel; they are a major deliverable of this research (see Appendix B).

Fig. 9.13 shows repeatability errors at Bangor of approximately 80 m 2_{DRMS}, relatively high for daytime operation. It does meet Datatrak's requirements of 100 m repeatable accuracy, and therefore in coverage. However, the cause of the problems with the Locator at Bangor was not repeatable accuracy, but poor CF, and we shall investigate this coverage factor in Chapter 11.

It must again be stressed that these plots are for future Locators equipped with H-field antennas, not the E-field models currently deployed in the UK.

The revised predicted repeatable accuracy values at the measurement locations are shown in Table 9.3, together with the measured values. Compared to the original predicted values, the model much more closely represents reality. It is noted that the
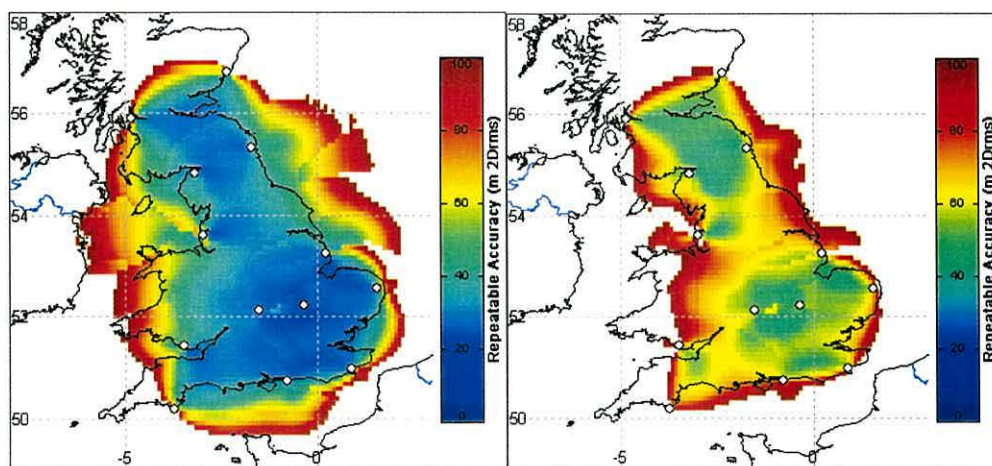
Fig. 9.13 - Revised daytime (left) and night-time (right) 2_{DRMS} repeatable accuracy plots of the UK Datatrak network.

		Predicted Repeatable Accuracy (2Drms)	Measured Repeatable Accuracy (2Drms)
Stoke-on-Trent	Daytime	33.8	44.5
	Night-time	69.5	82.9
Milton Keynes	Daytime	23.1	17.2
	Night-time	44.4	31.6

Table 9.3 - Revised predicted repeatable accuracy results for the measurement locations.

predicted values are higher than the measured ones in Milton Keynes, and lower in Stoke-on-Trent. This is an artefact of the simplification of the filters: the performance of the *phase filter* depends weakly on signal SNR. Since the site at Milton Keynes is generally closer to the transmitters than those at Stoke, the SNRs there are slightly higher. Thus, the filter characteristics are slightly different at the two locations. However, as the receiver approaches one transmitter, it moves away from others. It is assumed that the increase in SNR of the nearest signal will counteract the decrease in the SNRs of the other transmitters, and so the filter factor will remain fairly constant throughout the network.

9.9   Conclusions

Until now, Datatrak have employed a very simple method of predicting the repeatable accuracy of their networks. Only geometrical factors have been taken into account in calculating repeatable accuracy; spatial and temporal variations of SNR and SIR have been ignored. Nor have they taken into account the change from hyperbolic to circular operation.

In this chapter, the effect of disturbances due to the various sources of noise and interference on the phase of the groundwave signal has been investigated. The phase uncertainty is predicted from the field strength predictions in the earlier chapters. Then, the way in which the Locator calculates its position is analysed to show how the fluctuation in range measurements affects position fixes.

The model calculates *weighted* HDOPs of the network, using the positions of the transmitters, the Mk4 Locator algorithms, and the predicted SNR and SIR values. Then, for the first time, it is used to predict the repeatable accuracy of the position

fixes across the network. It does so ignoring the effect of two poorly-defined software low-pass filters in the Locator. Then, by means of field tests, these filters are calibrated and brought into play in the model. The result is a complete model of the UK Locator. It has already proved a valuable tool for Datatrak engineers.

Chapter 10

Monteath's Method: Irregular Terrain and Phase Delay

10.1 Introduction

The previous Chapter discussed the effects of noise and interference on the phases of received signals, and the consequences for repeatable accuracy. Now let us to consider the *absolute accuracy* of the position fix. In [16], absolute accuracy is defined as "the accuracy of a position with respect to the geographic, or geodetic, coordinates of the earth". In practice, absolute accuracy in LF navigation systems is largely determined by the accuracy with which variations in the speed of propagation of radio waves over the earth's surface are taken into account by the Locator. These velocity variations cause variations of phase delay and so errors in the pseudorange measurements and the resulting position fixes. Such errors are generally constant in time and their spatial variations are broad. They may be at least partially corrected by means of calibration measurements (Section 11.3)

The phase delays and the field strengths of Datatrak signals are both affected by variations of terrain height along the signal paths. This chapter shows how a computational technique, Monteath's method, can be used to model not only ground conductivity, as before, but also terrain height, and so predict phase delays and field strengths. It will be employed to create field strength arrays that include terrain effects. These will replace the previous "smooth-earth" Millington's method ones generated earlier. Monteath's method will also be used to generate arrays of phase delay values, which will be employed in the next chapter to help estimate and plot the absolute accuracy and confidence factor of the Datatrak system.

10.2 Phase delays

The process of predicting the phase delays of LF navigation signals started with the Loran-C system. The Millington-Pressey method takes the effects of variations of

ground conductivity on the signal phase along the path into account, by employing essentially the same approach as Millington's method does for field strengths [98]. However, it ignores the effects of mountains except in so far as these are reflected in very low ground conductivity values. This shortcoming needs to be overcome if we are to create a model able to help with the planning of Datatrak systems for mountainous countries such as Austria.

10.3   Monteath's method

The mathematics of signal propagation over irregular, inhomogeneous, terrain is very complex. Hufford proposed an integral-equation method of solving them that proved difficult to implement [99]. Johler and Berry developed a set of equations to tackle the problem; these were first used at 100 kHz [100]. Then Monteath, working for the BBC on coverage planning, devised a *numerical* method for solving Hufford's equations [101, 102]. His technique predicts both the amplitudes and the phase delays of signals propagating over irregular, inhomogeneous, terrain. Williams and Last, working at Bangor on Loran-C propagation, produced computer software to implement Monteath's method [39, 40]. Monteath's method thus appears an excellent candidate for modelling Datatrak propagation.

Monteath's method starts with smooth, perfectly-conducting, flat earth (Fig. 10.1). He calculates the difference, or 'compensation', from this ideal case of propagation over the real irregular, imperfectly-conducting, spherical earth.
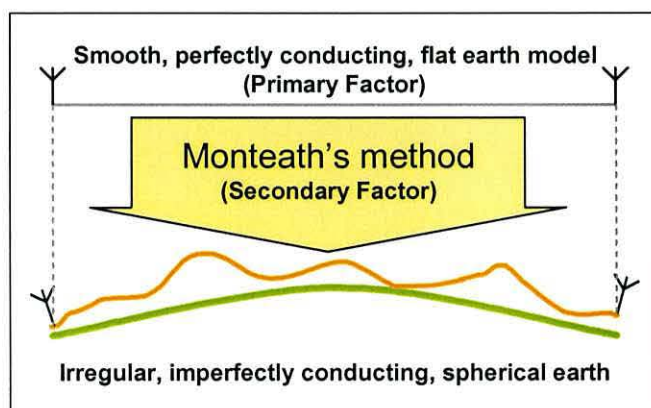
Fig. 10.1 - Monteath's method calculates the secondary factor: the difference between the real irregular, imperfectly-conducting, spherical earth and the ideal smooth, perfectly-conducting, flat earth.

The speed of propagation over an ideal earth is simply the speed of light through air. This is the *primary factor* (PF) [103]. It is straightforward to calculate phase delay and field strength in this case. Monteath's method calculates a *complex attenuation factor,* a *secondary factor* (SF) which, when added to the PF, results in the actual field strengths and phases of the signal over the realistic model of the earth. Note that, in Loran-C practice, SF includes seawater effects alone; ground conductivity and terrain effects then form an Additional Secondary Factor (ASF). So, in Loran-C terms, what Monteath's method calculates is the sum of SF and ASF [15].

The integral equation employed in Monteath's method is [101]:

$$G(R) = 1 - \sqrt{\frac{j\beta_0}{2\pi}} \int_0^R \left(\psi + \frac{\eta}{\eta_0} \right) \exp(-j\xi) \sqrt{\frac{R}{r(R-r)}} G(r)\, dr. \tag{10.1}$$

A detailed description of the terms used in this equation is given in Appendix H. In summary, $G(R)$ is the complex SF. The equation takes into account the terrain height (ψ and ξ), curvature of the earth (ψ, ξ, R and r), ground conductivity $\left(\dfrac{\eta}{\eta_0} \right)$, signal frequency ($\beta_0$ and ξ) and distance along the path (r).

Monteath has devised a discrete version of Equation (10.1) that can be implemented on a computer [101]:

$$G(ND) = 1 - BD^{\frac{1}{2}} \sum_{I=0}^{N} E(ND, ID) C(N, I) G(ID), \tag{10.2}$$

where D is the regular *interval distance*, and N is the total number of iterations (so, $ND = R$, and $ID = r$). Also:

$$E(ND, ID) = \left(\psi + \frac{\eta}{\eta_0} \right) \exp(-j\xi) \tag{10.3}$$

and $C(N,I)$ is a coefficient which takes into account the factor $\sqrt{\dfrac{R}{r(R-r)}}$ in the integrand.
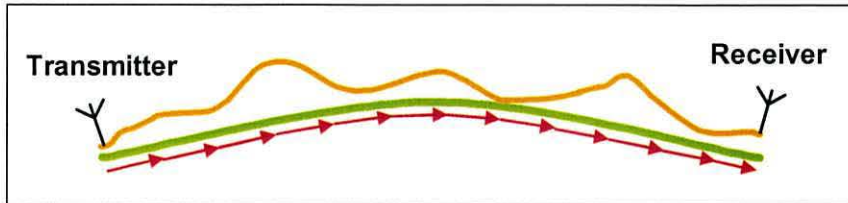
Fig. 10.2 – Profile of path from transmitter to receiver

The complex attenuation factor, $G(R)$, is calculated at each of a series of regularly-spaced points along the signal path from the transmitter to the receiver (Fig. 10.2). Values of ψ, ξ and $\left(\dfrac{\eta}{\eta_0}\right)$ for use in the equation are taken from a *surface profile* of the propagation path, constructed by reference to a terrain database and a ground conductivity database, with a coastline database employed to locate land-sea conductivity transitions precisely (Fig. 10.3). The computation at each point along the path starts from the value calculated at the previous iteration. Thus, field strength and phase delay values are calculated for not only the receiver, but for all computation points along a path.

10.3.1 Using the results

The attenuation, and so the field strength, E_{ground}, at each point along the path is represented by the magnitude of $G(R)$ as follows:

$$E_{ground} = E_{primary}(R)|G(R)| \qquad (10.4)$$

where $E_{primary}$ is the field strength of a 1 kW transmitter at range R metres from over an ideal path [100].
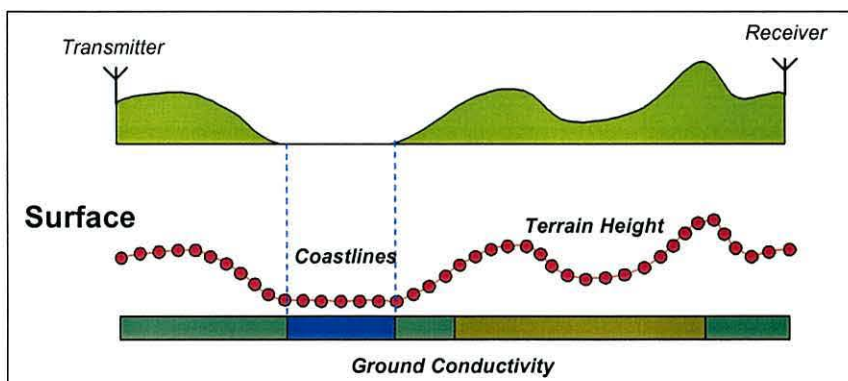
Fig. 10.3 - Surface profile of path between transmitter and receiver

The phase delay is represented by the imaginary part of $G(R)$. Expressed in microseconds, the total phase delay t_{total} is [103]:

$$t_{total} = t_{primary} + \frac{\arg\left[G(R)\right]}{2\pi F},$$
(10.5)

where arg[...] is the argument (or 'phase of') operator, F the signal frequency in MHz, and $t_{primary}$ the primary factor phase delay in μs. Here:

$$t_{primary} = \frac{R}{c\eta_{air}} \times 10^6,$$

where c is the speed of light in free space (299792458×10^8 m/s) [85], and η_{air} the refractive index of air (1.000338) [85]).

10.3.2 Bangor Implementation and Verification

Williams and Last used the 'C' programming language to implement Monteath's method. Their goal was to map the Loran-C ASFs of the North-West Europe Loran-C System (NELS) [39]. They then verified their results against both Monteath's own published data, and Loran-C results computed from their original equations by Johler and Berry at the US National Bureau of Standards [40].

By way of example, Fig. 10.4 shows a test scenario set up by Johler and Berry [40]. The field strength (pink) and SF phase delay (blue) of a 100 kHz signal are computed as it travels to, over, and then away from the Gaussian-shaped hill, the terrain height
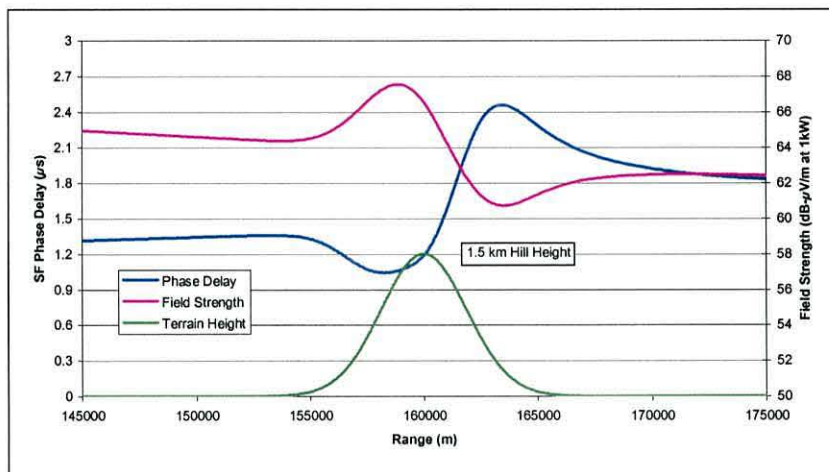
Fig. 10.4 – Field strength (pink) and SF phase delay (blue) of 100 kHz signal crossing hill (green), after Johler and Berry [39]

of which is shown in green. The hill stands 160 km from the transmitter. The ground conductivity along the path is 5 mS/m, that of good soil. On reaching the hill, the field strength ceases to fall; in fact, it increases as the space wave interferes constructively with the surface wave. Beyond the crest of the hill is a shadow zone, followed by an area of diffraction. The phase delay accrued by the start of the hill is 1.1 µs. This value falls on the up-slope where the space wave, which has experienced less delay than the ground wave, contributes more strongly. Beyond the crest of the hill, however, the phase delay increases rapidly because the signal has followed a path of extra time-span, over the hill and down the other side. This extra delay factor falls with increasing distance beyond the hill. The Bangor implementation of Monteath's method gives almost identical results to those shown here which were published by Johler and Berry themselves [39].

10.4   Sources of data

10.4.1 Conductivity and Coastline Databases

The ground conductivity database used in Millington's method (Section 4.4) has a resolution of 0.1° in latitude and longitude, a value more than sufficient to preserve the resolution of the relatively-coarse ITU source data from which it is constructed, and also commensurate with the accuracy of the ground propagation curves employed. However, since Monteath's method is capable of generating results of very high spatial resolution, we must be sure to retain the full resolution of all input data. The only places where an improvement can be effected in the ground conductivity data are coastlines, where profound conductivity changes occur [104]. We can locate these changes most accurately by using an additional coastline database to ensure that they are recorded as being where propagation path crosses the coastline, not simply at the nearest cell boundary in the relatively-coarse conductivity database (Fig. 10.5).

Coastline data is taken from the World Vector Shoreline (WVS) database, available from the British Oceanographic Data Centre (BODC) as a part of their General Bathymetric Chart of the Oceans (GEBCO) digital atlas CD-ROM. Its coastline resolution is 100 m. Williams and Last pioneered the use of coastline data in this application [105]. We will take their Loran-C model and modify it for use with Datatrak. One important change is to extend it to operate world-wide.
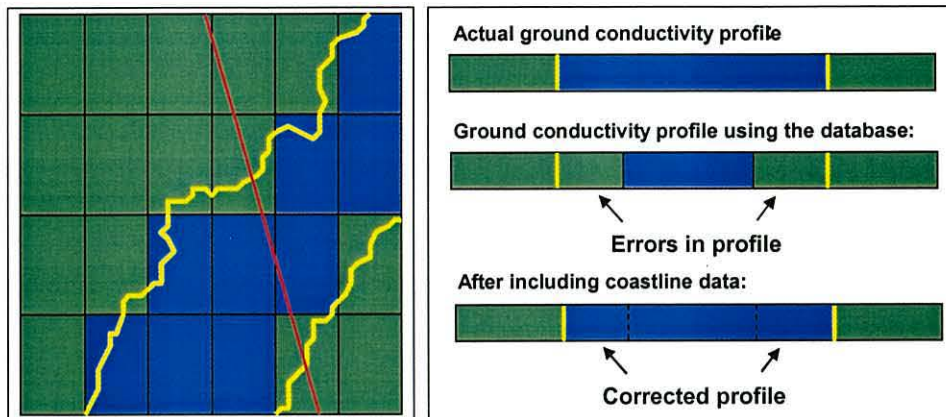
Fig. 10.5 – Use coastline database to identify just where propagation path crosses coast, gives higher ground conductivity resolution

10.4.2 Terrain Database

Williams and Last employed the Digital Terrain Elevation Data (DTED) Level 1 database produced by the US National Imagery and Mapping Agency (NIMA). This provides terrain height values with 90 m resolution. However, this database has not yet been released for commercial applications, and so cannot be used in our Datatrak model. What alternatives are there? Unrestricted-access, high-resolution, databases are available from both NIMA the US Geological Survey (USGS) [106, 107], but they cover the US only. NIMA also publish, free of restriction, the global DTED Level 0 data, with a resolution of approximately 1 km, in a format similar to that of Level 1. Datatrak offered the use of a commercial database produced by ATDI Ltd [108]. Its coverage was global and its resolution 500 m. However, investigation showed it to contain simply interpolated DTED Level 0 data! So, not only did it give no advantage over DTED Level 0, but it was in a format incompatible with the Loran-C Monteath software. A decision was made to use the DTED Level 0 data, provided it is adequate. This approach would allow the higher-resolution Level 1 data to be substituted for the Level 0, should it be released for commercial use in the future.

10.5   Interval Distance

Is the reduced resolution of the Level data adequate? It should be, provided we can live with a reduced computational interval. To clarify, the Monteath equation is solved at intervals along the propagation path. Normally, a fixed *interval distance* (ID) is chosen. The larger the ID, the fewer the computation points and so the shorter the computation time, but also the lower the accuracy and resolution of the results.
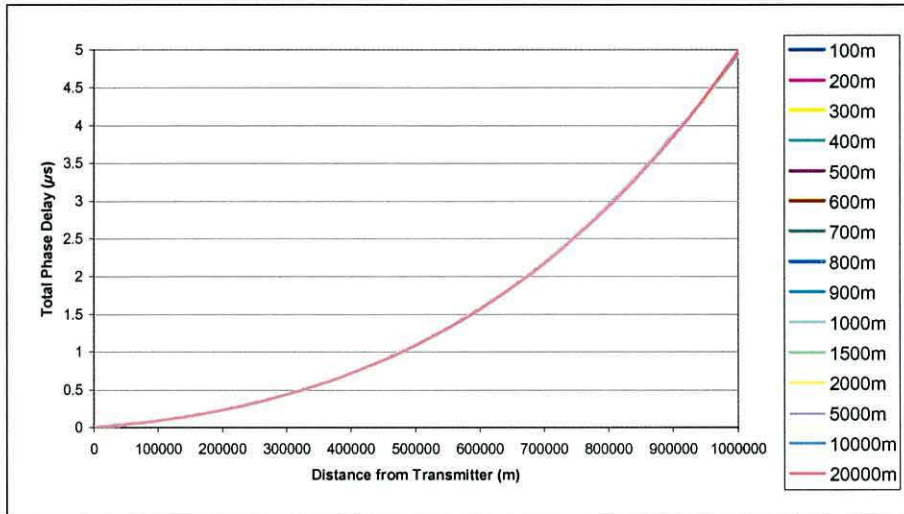
Fig. 10.6 - SF phase delay over seawater calculated using different IDs.

Williams and Last, working at 100 kHz, investigated this trade-off. They showed that, even over a path with exceptionally-fine terrain variations (known with high resolution), the ID had to exceed 630 m before any significant loss of accuracy resulted in the phase delays computed [40].

Let us now explore the choice of ID for use in a Datatrak model. The highest Datatrak frequency is 180 kHz, at which we would expect to need the shortest ID value. The Williams and Last software was now modified for use in the Datatrak prediction model. Most of the modifications were minor (e.g. allow the software to access DTED Level 0 Data, as well as Level 1), since Monteath's method (and its implementation) was designed to work at any frequency and with any ID. Fig. 10.6 shows the Datatrak
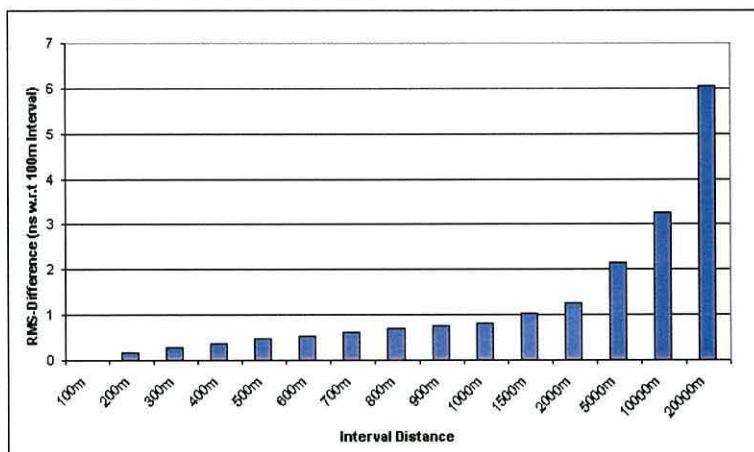
Fig. 10.7 – Difference (in ns), between phase delay computed over 1000 km seawater path using ID value shown, and delay computed using shortest ID (100m)
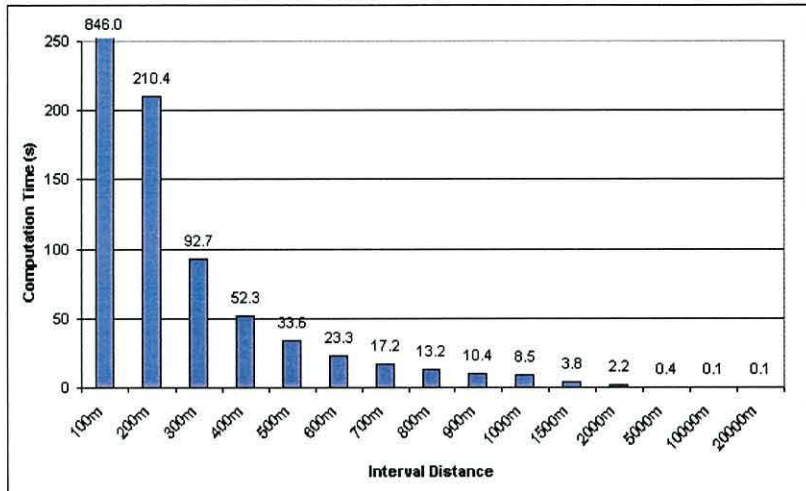
Fig. 10.8 – Computation time taken to generate 1000 km radial with different ID values

Monteath software in operation, predicting the build-up of 180 kHz phase delay with range over a 1000 km-long seawater path. The various colours correspond to ID values from 100 m to 20 km.

Fig. 10.7 plot the increase in error over 1000 km with increasing ID, the reference value at any computation point being the value computed using the shortest ID. Using an ID as large as even 20 km introduces an error of only a few nanoseconds. Fig. 10.8 shows the benefit of increasing the ID value: a dramatic reduction in computation time, from 846 s (100 m ID) to 0.1s (20 km)!

These results were for a sea-water path. In contrast, Fig. 10.9 shows the computed
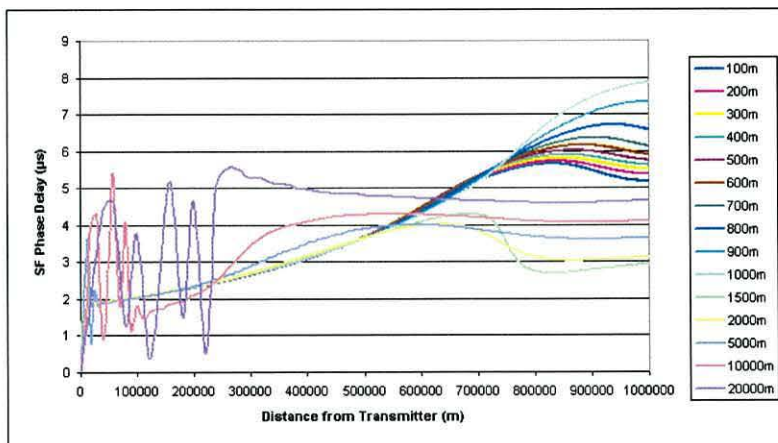
Fig. 10.9 - SF phase delay build-up over ground of exceptionally-low conductivity (0.03 mS/m), calculated using different IDs
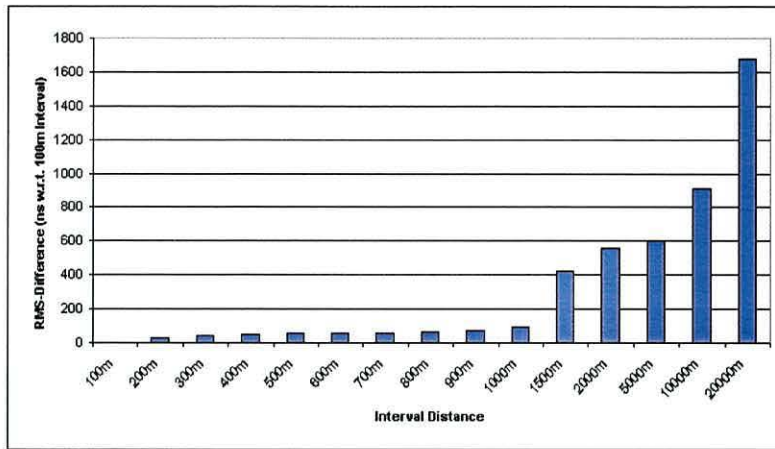
Fig. 10.10 – Difference (in ns), between phase delay computed using ID value shown, and delay computed using 10 m ID over 750 km low-conductivity path.

growth of phase delay over a path crossing ground of exceptionally-low conductivity, such as glacial ice with its conductivity of 0.03 mS/m and dielectric constant of 3. The results change very little as ID increases from 100m to 1 km, at least over ranges up to 750 km (Fig. 10.10). But at greater ranges the curves diverge. ID values much larger than 1 km lead to unstable and implausible results. However, Datatrak signals are normally used within 350 km of the stations, so it would appear that, even over very low-conductivity paths, ID values as large as 1 km are acceptable (Section 9.4.1). These are compatible with the use of DTED Level 0 terrain data.

At ranges greater than 750 km, we see some spatial instability in the results, possibly due to the selection of the ID. For this reason, we will place a usable range limit of 750 km on the method.

Now let us test the technique at the highest Datatrak frequency along a signal path of exceptionally-demanding topography. We employ a test route, devised by Williams and Last, that runs northwards from the Loran-C station at Sylt, Germany (Fig. 10.11). It runs over the sea initially, then over Norwegian mountains with severe variations in terrain height as it crosses deep fjords. The path takes in land with the lowest ground conductivity in the world. Terrain data was taken from the DTED Level 1 database [39, 40]. The ID values tested are integer multiples of the 90 m resolution of this database.

Fig. 10.11 - Test path from Sylt crossing sea and Norwegian mountains

Fig. 10.12 shows the 180 kHz SF phase delays along this path calculated using the Datatrak software, with an ID of 90 m. The terrain height is shown in pink. Now let us examine the errors that arise as we increase the ID value. Fig. 10.13 shows the RMS values of these errors with respect to the 90m ID results. The discrepancies lie in the range 250–300 ns (c75-90 m), virtually independently of ID up to an ID value of 1350m. So, we learn that the ID should be kept below this value.

If DTED Level 0 terrain data is used, with its coarser resolution of approximately 1000 m, there would be no point in choosing an ID value shorter than this resolution. Thus, we would anticipate errors of 250–300 ns over extreme paths such as this one, and perhaps 100 ns (c30 m) over less demanding paths.
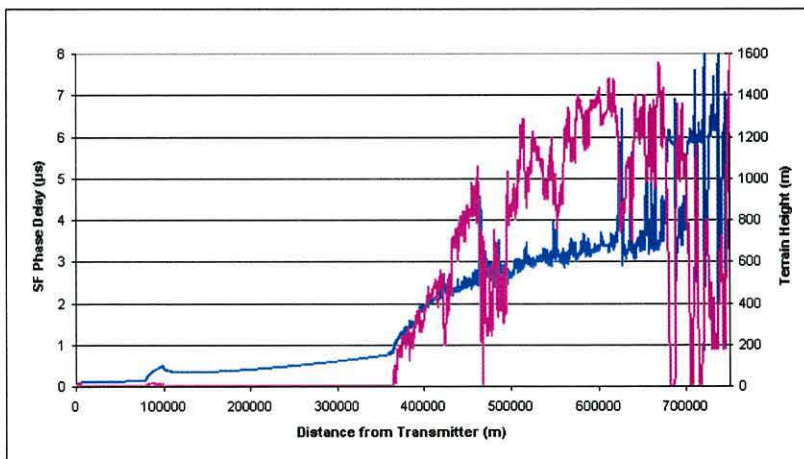
Fig. 10.12 – Terrain height (pink) and SF phase delay (blue) along test path from Sylt
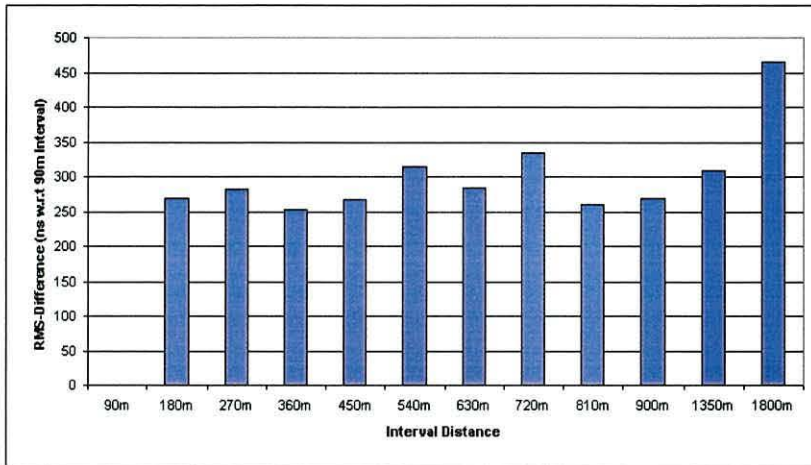
Fig. 10.13 - RMS-Differences of SF phase delay between results using other ID values and those using 90 m ID along test path from Sylt.

We will use an ID value of 1000m, which is compatible with the terrain database resolution and is suitable for all Datatrak frequencies up to the highest.

10.6   Incorporating Monteath's method into the model

When calculating field strengths using Millington's method, the ground conductivity profile of the path between the transmitter and each array point was determined, and then the field strength of the signal at the array point calculated. The model operated point-by-point. Monteath's method, in contrast, calculates results at all computation points along the signal path to the calculation point. Thus, the efficient way of organising the model is to employ calculation points lying on the circumference of a circle, centred on the transmitter, that encompasses the area of interest. Monteath's
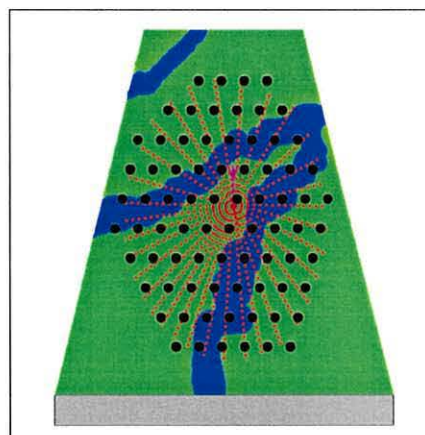
Fig. 10.14 – Monteath's method used to compute values along radials (red) to circumferential points. A gridding process is then used to interpolate values at array points (black dots).

method is then used to generate results at each computation point along the radial from the station to each calculation point (Fig. 10.14). A *gridding* process can then be employed to interpolate the array points from the values at the computation points.

The number of radials required depends on the radius of the circle and the required resolution of the array. With the selected ID of 1000 m, a maximum resolution of approximately 0.01° in latitude and longitude is possible. If, however, we were to employ a resolution of 0.05° of latitude and longitude, this would be fine enough to show the benefits of Monteath over Millington without excessive computation time, and we would be able to operate out to 750 km (maximum range before the long-range instability), requiring approximately 1400 radials. Each radial currently takes 15 s to calculate, so generating an array would require some 6 hours. This is, of course, a once-and-for-all process. For the remainder of the thesis, this resolution and range limit will be used. Clearly, in terms of resolution, the results of Monteath's method will have an advantage over Millington's method, and this should become evident in the results.

10.7 One array or two?

Does each of the Datatrak frequencies, f_1 and f_2, require its own array or could they share one, so saving computation time and storage space? And if they did share, could we adjust the results for the two individual frequencies by means of simple scaling? Although, the relationship between SF and frequency is not a simple linear one, the differences between f_1 and f_2 may be sufficiently small to consider it as being linear. A numerical experiment was designed to explore this idea. Computations were carried out over Sylt/Norwegian mountains path (Fig. 10.11) at the three sets of Datatrak f_1 and f_2 frequencies shown in Table 10.1. These include the North-west Europe network which has the lowest f_2 frequency and the South Africa network which has the highest f_1 frequency. The UK/Argentina network frequencies were used as the basis of comparison.

We first compute SF values along this path using Monteath's method at the UK f_1 frequency. We then calculate UK f_2 values from these SF_{f1} values by scaling them in accordance with the simple frequency ratio:

Network Name	f_1 frequency (kHz)	f_2 frequency (kHz)
South Africa	160.650	143.474
UK/ Argentina	146.455	133.2275
North-west Europe	144.6305	131.7647

Table 10.1 - Pairs of frequencies used in the experiment.

$$SF_{f_2} = \frac{f_1}{f_2} SF_{f_1} \tag{10.6}$$

where SF_{f2} is the SF phase at f_2, and SF_{f1} is the calculated value at f_1, in µs.

Fig. 10.15 shows the SF values along the path computed separately using Monteath's method, at f_1 (dark blue) and f_2 (pink). The green curve then shows the f_2 values calculated from the f_1 values by means of Equation (10.4). Table 10.2 shows the RMS differences between the f_1 and f_2 SF phases, and between f_2 and the estimated f_2, for all three sets of frequencies. It is clear that using a simple ratio to estimate the f_2 SF phase from the f_1 value gives a poor result.

The reason why these single-value compromises do not work well is that the relationship between SF and frequency is not a simple linear one, especially not in complex terrain. The dimensions of some terrain features are comparable with the wavelengths of Datatrak signals. This makes the SF results sensitive to the dimensions of those features.
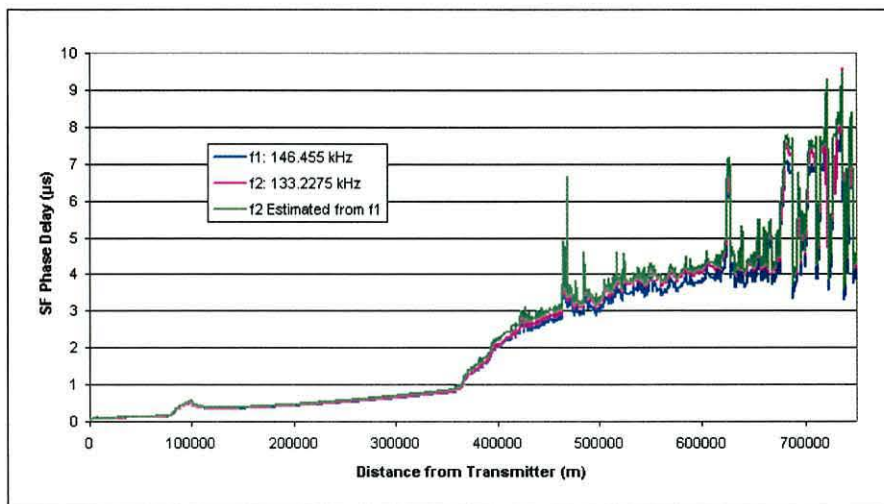
Fig. 10.15 – SF phase delay values estimated along path from Sylt to Norwegian mountains. Dark blue: computed at f_1. Pink: computed at f_2. Green: f_2 values calculated by scaling f_1 values.

Network name	RMS-Difference between actual f_1 and f_2 SF phase delay	RMS-Difference between actual f_2 and estimated f_2 SF phase delay
South Africa	0.24 µs	0.22 µs
UK/Argentina	0.43 µs	0.44 µs
North-west Europe	0.24 µs	0.22 µs

Table 10.2 - Comparison of calculated and estimated radial results using frequency ratio technique.

This experiment has shown that estimating SF phase from a set of results computed at a single frequency does not work sufficiently well. So, it was decided that separate arrays should be generated at the two frequencies. This takes longer - some 12 hours computation time per transmitter - but it only needs to be done once. The arrays for the UK network's 13 transmitters were computed over a single 48-hour period, using several computers running concurrently.

10.8 Using the Monteath Field Strength Arrays

We now have four arrays per transmitter: f_1 and f_2 field strengths, and f_1 and f_2 phase delays. Fig. 10.16 shows, by way of example, the field strengths (normalised to 1 kW) computed at the f_1 and f_2 frequencies using Monteath's method, for the UK network station at Selsey on the south coast of England. The plots have been magnified to show the area around the mountains of North-west Wales. The signal is arriving from the south-east. The overall differences between the two signals are subtle, but clearly visible. For example, to the north-west of the plot, the f_1 signal has a slightly bluer hue to it, indicating a lower field strength. Since f_1 is the higher frequency of the two, this
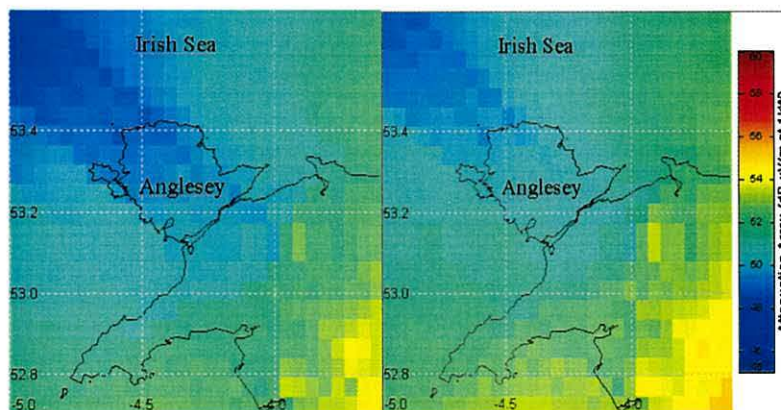
Fig. 10.16 - f_1 (left) and f_2 (right) field strength plots of Selsey signals around North-west Wales
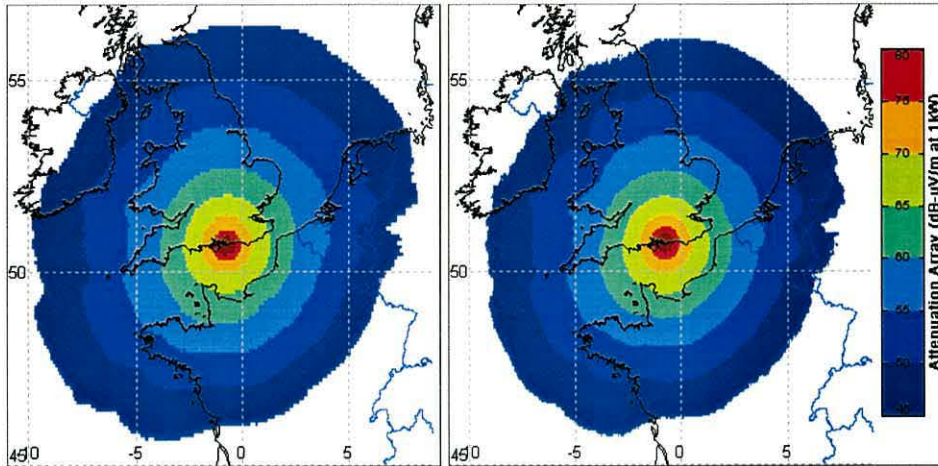
Fig. 10.17 – Comparison of Selsey f_1 field strength predictions made by earlier Millington's method (left) and new Monteath's method (right)

is to be expected. The mountains near the centre of the plots also have an effect: the field strength can be seen to fluctuate as it crosses them, something that is missing, of course, from Millington plots. The field strength of the f_1 signal appears to have been affected slightly more than f_2, as is shown by the darker blue of its plot over Anglesey and the Irish Sea.

Fig. 10.17 directly compares the new Monteath results with the earlier Millington values. As would be expected, the plots are very similar. The differences between them are mainly due to the limited accuracy of the propagation curves used in the Millington's method. Also, because Monteath's method takes terrain into account, the additional attenuations over the mountains of Snowdonia and the hills of the Pennines
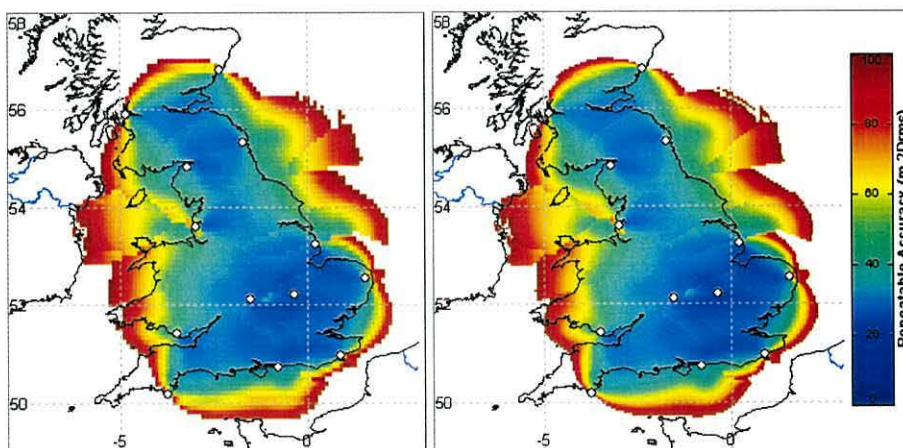
Fig. 10.18 – Comparison of predicted daytime repeatable accuracy using Millington's method (left) and Monteath's method (right)

can be seen. The higher resolution of the Monteath plot also results in more accurate, smoother, contours, which allow the user to magnify areas of interest (as in Fig. 10.16 above).

Now, we can compute daytime *repeatable accuracies* using the Monteath data, rather than Millington (Fig. 10.18). There is very little difference between the two sets of results, although again the higher resolution of Monteath's method gives smoother contours. The expected close agreement between Monteath and Millington over flat terrain is a very satisfactory result. It means we can now take advantage of Monteath's added ability to cope with terrain effects, confident that the results elsewhere have been checked against Millington results, which we have verified.

For the field strength arrays, this is the end of the road. Monteath's method will in future be used predict the field strength of all Datatrak stations. Millington's method will continue to be used, however, for calculating the groundwave field strengths of interferers (as in Chapter 8); given the uncertainties in the IFL data on interferers, the additional accuracy of Monteath is unnecessary and would not justify the considerable increase in computing resources it would require.

10.9 Phase Delay Arrays

The principal reason for moving to Monteath's method was its ability to predict phase delays. Fig. 10.19 shows, for the first time, the Secondary Factor (SF) plot of a
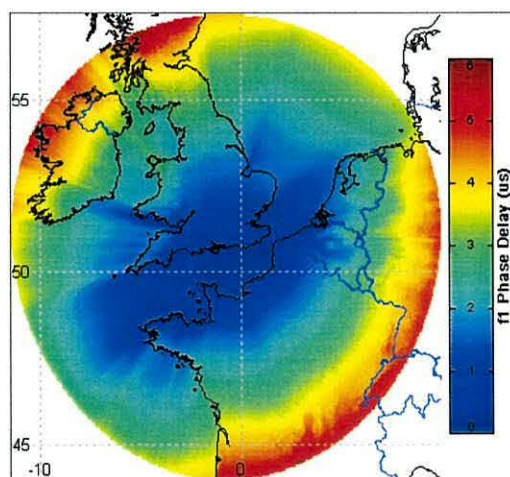
Fig. 10.19 – Secondary Factor (SF) phase delay of f_1 signal from Selsey computed by Monteath's method.
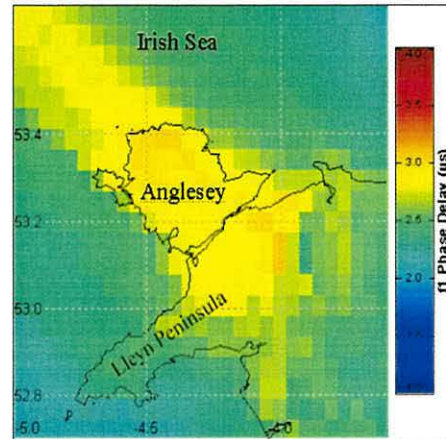
Fig. 10.20 - Detailed SF phase delay of the f_1 signal from Selsey over Anglesey and Gwynedd, North-West Wales.

Datatrak transmission: the f_1 signal from Selsey.

The colours represent delay values. The results are a dramatic illustration of signal propagation. In all directions, phase delay increases with range. But the rate is slow along the sea-paths of the English Channel (though in accordance with Fig. 10.6) and much more rapid over land. It is most rapid over the mountains of Central Scotland and especially of Snowdonia, the 'shadow' of which extends well out into the Irish Sea.

In this mountainous region, the detailed effects of terrain on phase delay modelled by Monteath can be seen in Fig. 10.20. Again, the signal is propagating from the south-east. The Snowdonia mountain range is at the centre of the plot. As the signal passes over the mountains, the SF phase delay increases by 0.5 µs. A similar, but more subtle, effect is seen over North-west Anglesey. As the signal passes over the Irish Sea, some recovery is observed. The effect of the coastline database is clear to see around the Lleyn Peninsula to the south-west, where the slightly higher value of SF phase delay remains within the coastline.

These very detailed and novel maps form the basis for predicting the absolute accuracies and confidence factors, expected to be experienced by Datatrak Locators. They allow engineers to predict potential problem areas that might require additional correction means. The next chapter will provide details of this innovative work.

10.10 Conclusions

In previous chapters, groundwave field strengths were predicted using Millington's method, which assumed that the surface of the earth was smooth. Monteath's method provides an improved, proven, technique for calculating both field strength *and* phase delay that can take into account the additional effects of irregular terrain.

A Monteath algorithm has already been developed, tested, and used to predict Loran-C ASFs. In this chapter, we adapt and test it for use at the higher frequencies used by Datatrak. The choice of Interval Distance (ID) has been explored, with shorter IDs seen to give higher accuracy and resolution, but to require greatly increased computation time. It has been shown that an ID of approximately 1 km gives satisfactory results at even the highest Datatrak frequencies, and that this ID is compatible with the resolution of the DTED Level 0 terrain database that we are obliged to use.

Generating a full set of high-resolution data for each transmitter can take a long time. An investigation into whether the f_2 phase delay could be estimated from the f_1 values showed that simple techniques for doing so were not very accurate and it was decided that complete set of f_1 and f_2 data should be computed.

Field strength and phase delay arrays were then generated using Monteath's method. The field strength results agreed well with Millington's over paths with negligible terrain effects. Monteath revealed clearly the differences between the f_1 and f_2 field strengths.

The vital results, however, will be those on phase delay. This chapter has demonstrated that Monteath's method can provide high-resolution plots that take both ground conductivity and terrain into account. In the next chapter, these results will be used to model Datatrak absolute accuracy and confidence factors.

Chapter 11

Absolute Accuracy and Confidence Factor

11.1   Introduction

The last chapter introduced Monteath's method, which allows the field strengths and phase delays of Datatrak signals to be predicted over a realistic earth model that includes both inhomogeneous ground conductivity and irregular terrain. In this chapter, we will use the predicted signal phase delays generated by Monteath. Differences between actual phase delays, and those the receiver computes using certain built-in assumptions, appear as pseudorange errors which lead to errors in the positions output. We characterise these errors by a measure of *absolute accuracy* (Section 10.1). Locators also compute a *confidence factor* (CF) which is a measure of the discrepancies between the pseudoranges. If the CF exceeds a maximum, no positions are output.

A Datatrak receiver computes its position from a set of pseudoranges, employing the simplifying assumption that all signals travel with a given, fixed, velocity of propagation. Each Datatrak network employs a different velocity value. Datatrak have attempted to cope with discrepancies between the actual delays and those resulting from this assumption, by employing a set of location-dependent adjustments. These are applied in the Locator when it calculates location coordinates; they give an at least partially-corrected solution. The adjustments are based on extensive measurements. However, this has proved a hit-and-miss approach. Gathering data involves driving around the area of interest at sampling points, then analysing the results to see what adjustments are required to provide a better position fix. The adjustment values are not optimal because the absolute measured ranges cannot be measured, only pseudoranges. The area over which each adjustment can be held to apply is also unknown. Clearly, a computer tool which could compute pseudorange adjustments, and their areas of applicability, would be very useful for Datatrak engineers.

Monteath's method gives us a new and powerful basis on which to provide that information. It lets us predict phase delays over all the paths in the Datatrak network: those between stations, and those from the stations to the user. We can then employ the results of our analysis to predict absolute accuracy and confidence factor point-by-point throughout the network. This will enable us to highlight problem areas, and propose solutions.

11.2 Method of Predicting

In order to predict absolute accuracy and CF, the model must simulate the algorithms used by the Locator, as was done when analysing repeatable accuracy (see Chapter 9). The model will be in two parts: a *network model*, which will calculate the phase delays between transmitters and predict the "apparent ranges" the Locator will measure; and a *Locator model*, which will calculate position fixes from these apparent ranges. The measure of absolute accuracy will be the difference between the computed and true positions. The Locator model will also estimate the CF from the discrepancies between the apparent ranges at the computed position. Note the use here of the new term "apparent range" rather than "pseudorange"; a pseudorange includes a clock error component, which the model cannot predict, and which is not needed in this context.

11.3 Network Model

Let us now examine how the timing of the network is organised and see what factors contribute to apparent ranges. All transmissions in the network are synchronised to a
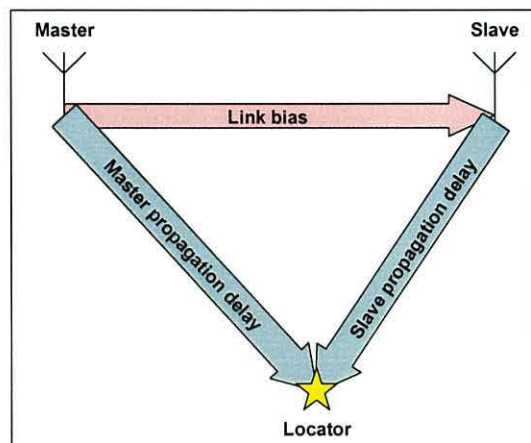
Fig. 11.1 - Definition of master and slave pseudoranges and link bias
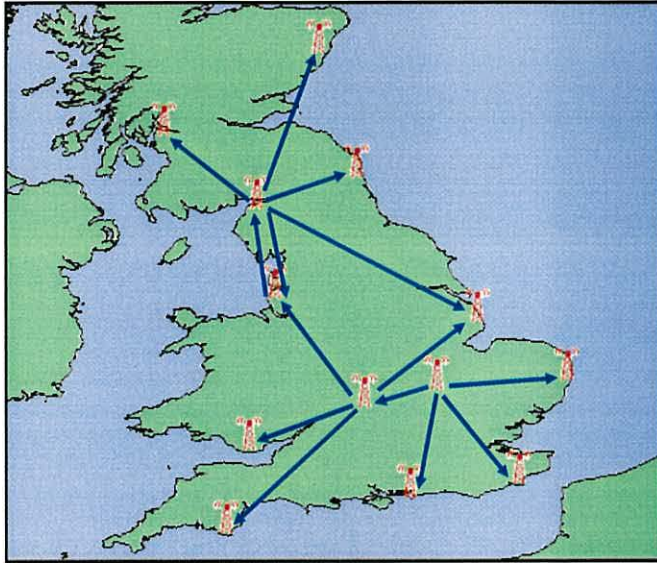
Fig. 11.2 - Master-slave baselines of the UK network. Arrows point towards slave station of each pair.

single rubidium master clock at the station marked 'Master' in Fig. 11.1. The master station transmits its signal in its slot within the time-multiplexed Datatrak transmission sequence. The 'Slave' transmitter receives the Master's signal and adjusts its own transmissions so that they are phase-synchronised to the Master's it receives; that is, it attempts to act as a perfect *phase mirror*.

The propagation delay from Master to Slave is termed the "Link bias". Other stations act as slaves to either the Master, to this Slave, or to other slaves; the configuration of the whole UK network is shown in Fig. 11.2. Here, each arrow linking two stations points from the station that acts as master towards the one that acts as slave. Details of this configuration are sent to the Locator, which holds them in its memory, by means of the timing/data signal. The Locator works on the assumption that all the signals propagate at a constant propagation velocity, V_p. The V_p of the UK network is set to 299,300 kms^{-1}, a value Datatrak believe represents an average across the UK [109].

Now consider the effects of errors in propagation velocity, with respect to this assumed V_p, due to ground conductivity and terrain effects. In Fig. 11.3, these are marked "V_p *error*"; they affect master-slave paths, and also the paths from the stations to the Locator. At the same time, let us include any imperfection in the ability of the Slave to act as a perfect phase mirror: this is termed a *station delay*. Datatrak have
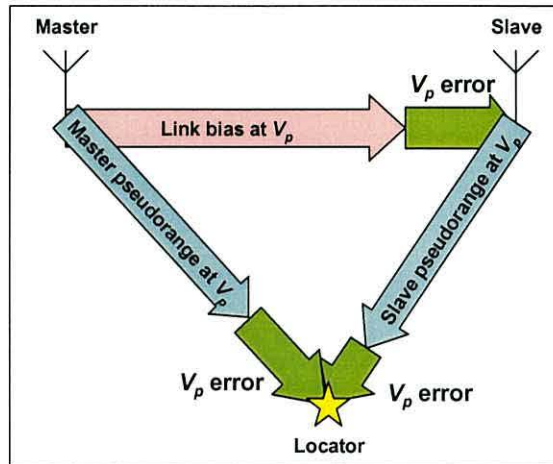
Fig. 11.3 – V_p errors are due to actual velocity of propagation being different from single value assumed.

attempted to counteract the effect of station delay and V_p errors by adding an additional 'delay' to the signal transmitted by each slave: its *station phase offset* (SPO). Fig. 11.4 shows the delays between the Master and the Locator via the Slave. The Locator assumes that the total delay is simply the sum of two of these components: the link bias (pink) and range (light blue), both accrued at velocity V_p. All other terms - the two V_p errors, station delay, and the SPO - are treated as errors, and are unknown to the Locator.

We will now attempt to predict each of these errors using Monteath's method. But first, we must establish values to use in the model to describe the delays at the stations.

11.3.1 Station Delays

Station delays are time delays due to hardware and software uncertainties in measuring the received and transmitted phases at the station, and errors in the
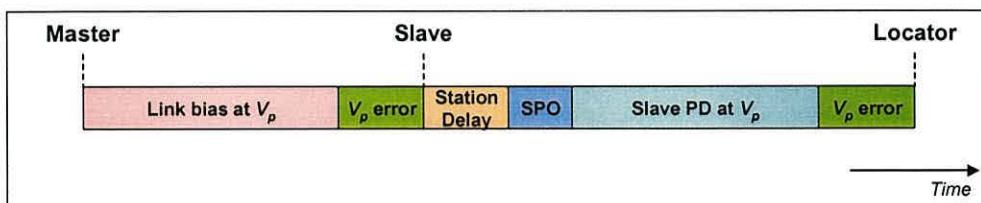
Fig. 11.4 – Total signal delay from Master to Locator via a Slave. Only pink and light blue sections are taken into account by Locator. SPO: station phase offset. PD: propagation delay.
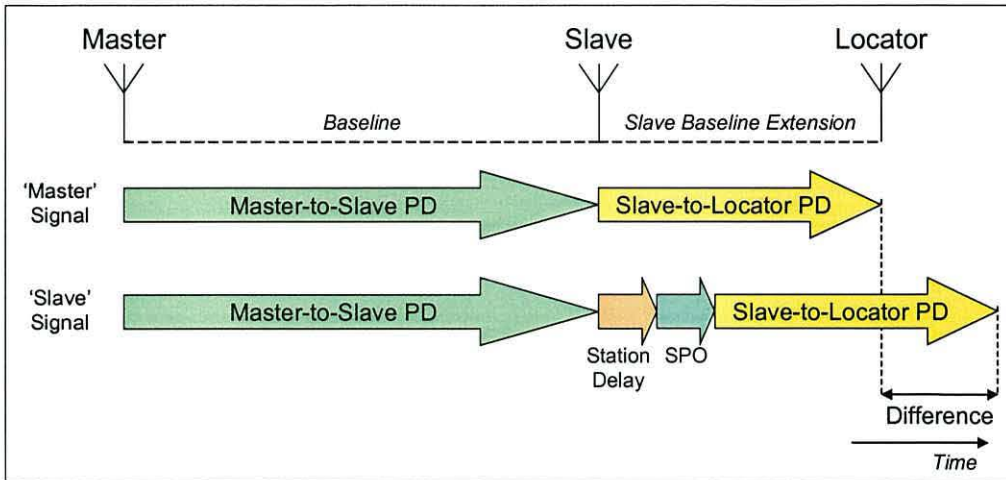
**Fig. 11.5 - Principle of measuring the station delay at the slave station.
PD: propagation delay.**

station's phase offsets. Datatrak do not know the values of station delays; the reason being that they apply adjustments to compensate for this whole group of errors taken together. Since we do need to know the station delays, there appears to be no alternative to going and measuring them.

A traditional method for determining delays at slave stations is to measure the master-slave *phase difference* on the *slave baseline extension* [41]. The slave baseline extension is the extension of the master-slave baseline beyond the slave transmitter. Fig. 11.5 shows the time-line of the master and slave signals received by the Locator placed on the slave baseline extension. Any delay at the slave transmitter will give rise to a corresponding phase difference between the master and slave signals, which can be measured. This technique should reveal the total station delay: the sum of the known SPO and the unknown station delay.

11.3.1.1   *Additional Delay*

This type of measurement assumes that the propagation delay of the Master's signal over the Slave-Locator path is the same as that of the Slave's signal over the same path. Such an assumption has always been made traditionally. But it is not strictly true: Johler and Berry have shown that the velocity of propagation of a signal, even over a homogeneous path, is in fact a function of range [100]. So the velocity of the Master's signal a long way from the Master will be a little different from the velocity
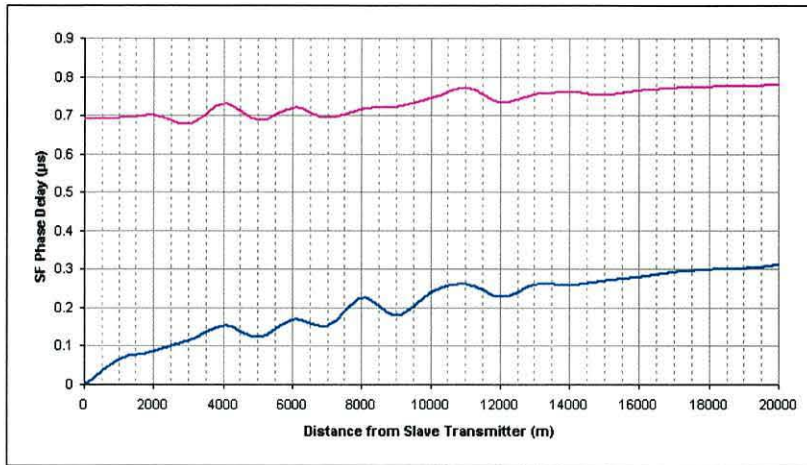
Fig. 11.6 – Secondary factor phase delay values of Master (pink) and Slave (blue) signals along Huntingdon-Stratford slave baseline extension

of the Slave's signal close to the Slave. Happily, we are in a position to compute corrections for this effect using Monteath's method.

Consider the case of the Stratford station, which is a slave to the Huntingdon station (Fig. 11.8). Fig. 11.6 shows the secondary factor phase delays of the master (pink) and slave (blue) along the slave baseline extension, as predicted by Monteath's method. At the slave station (i.e. on the left-hand side of the figure), the master's signal has already accumulated almost 700 ns of SF phase delay. This delay increases by less than 100 ns over the next 20 km along the baseline extension. However, the slave's signal phase delay, starting at zero, increases by more than 300 ns along the same path. If we were to make our phase-difference measurement at that 20 km point, we
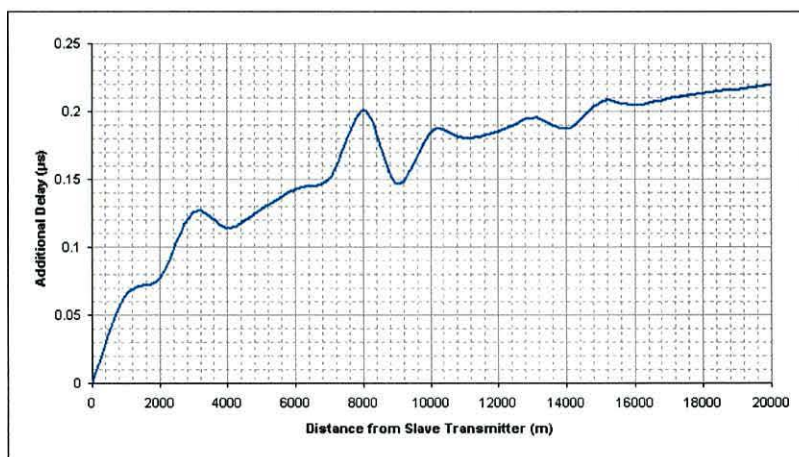
Fig. 11.7 - Additional delay as a function of distance along the Huntingdon-Stratford slave baseline extension
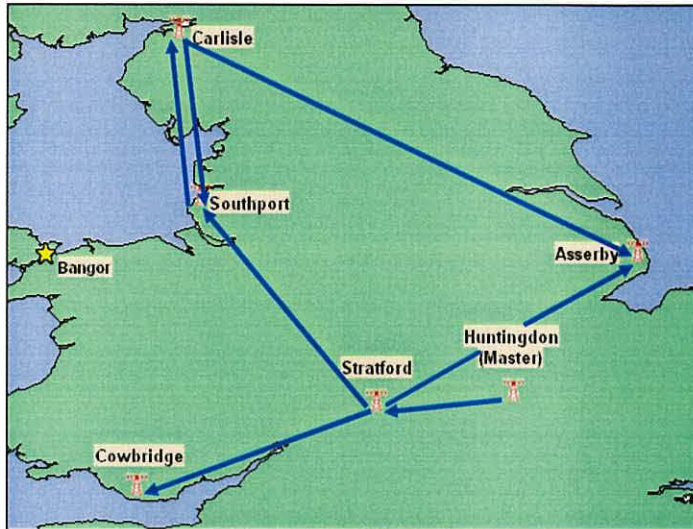
**Fig. 11.8 – Slave stations visited in the station delay measurement campaign.
Arrows point towards slave station of each master-slave pair.**

would need to allow for these additional 200 ns of delay. Fig. 11.7 shows this additional delay of the slave signal as a function of distance along the Huntingdon-Stratford slave baseline extension. In general:

$$t_{additional} = t_{S_{Locator}} - \left(t_{M_{Locator}} - t_{M_{slave}} \right),$$ (11.1)

where $t_{S_{Locator}}$ is the slave SF phase delay at the Locator, $t_{M_{Locator}}$ is the master SF phase delay at the Locator, and $t_{M_{slave}}$ is the master SF phase delay at the slave station. This calculation will be carried out at each location at which measurements are conducted.

11.3.1.2   *Station Delay Measurements*

Ideally, baseline extension measurements would be made at all 12 slaves in the UK Datatrak network; a considerable task. For an initial assessment of the situation, the nearest 5 slave stations to Bangor were investigated. It was hoped that they might give mutually-consistent values, since all stations use the same hardware configuration. If

Slave	Master(s)
Stratford	Huntingdon
Cowbridge	Stratford
Asserby	Stratford Cumbria
Southport	Stratford Cumbria
Cumbria	Southport

Table 11.1 – Slave-Master relationships of stations visited.

	Station Delay (µs)			
	f_{1+}	f_{1-}	f_{2+}	f_{2-}
Stratford	0.12	0.11	0.17	0.14
Cowbridge	0.40	0.39	0.63	0.63
Southport	0.23	0.22	0.18	0.17
Carlisle	0.24	0.20	0.29	0.23
Asserby	0.05	0.03	0.08	0.05
Average	0.20	0.19	0.27	0.25

Table 11.2 - Station delay at the transmitters investigated.

so, the average measured value would be used for all other stations in the model. The five slave stations visited (Fig. 11.8) were: Stratford, Cowbridge, Southport, Asserby, and Cumbria. Table 11.1 shows the slave-master relationships involved. Note that Southport and Asserby each act as a slaves to two masters, using different time slots. This provides us with an opportunity to verify the station delays at each of these slaves using two different signals.

Measurement sites were chosen carefully to minimise the effects of possible local phase disturbances due to power lines or buildings. Also, adopting a minimum range from each slave of 3.5 km ensured that the Locator could not be overloaded, so leading to phase errors. Measurements were conducted at all four frequencies: $f_{1+}, f_{1-},$ f_{2+} and f_{2-}. Further details of these experiments are given in Appendix I.

Table 11.2 shows the station delay values measured, once corrections for additional delay had been applied in accordance with Section 11.3.1.1. The average station delay over the four frequencies turns out to be 0.20–0.25 µs, equivalent to 60–75 m in distance. The model will employ the values measured at each of these 5 stations. The standard deviation of station delay values was 0.17 µs. The variation of values was somewhat larger than expected, but it was decided that it was sufficiently small to allow the average delay to be used in the model for the other 8 stations not visited.

11.3.2 Computing the apparent ranges

To compute apparent ranges, we must take into account all delays between the master station's clock and the Locator, via any slaves. The largest component is the propagation time from station to station and from station to Locator. We will now employ Monteath's method to calculate these values.

As was shown in Chapter 10, Monteath's method computes the difference between the real path and an ideal flat earth path. So, the *total* propagation time, t_{total}:

$$t_{total} = t_{primary} + t_{monteath},$$
(11.2)

where $t_{primary}$ is the propagation time in the ideal case, and $t_{monteath}$ is the additional delay calculated using Monteath's method. Here, $t_{primary}$ can be calculated as the propagation time through the air over the *chord distance* between station and receiver (Fig. 11.9). The chord distance between two points, P_1 and P_2, on the WGS84 ellipsoid used in the model is [15]:

$$d_c = \left[\left(N_1 \cos\phi_1 \sin\lambda_1 - N_2 \cos\phi_2 \sin\lambda_2 \right)^2 \right.$$
$$+ \left(N_1 \cos\phi_1 \cos\lambda_1 - N_2 \cos\phi_2 \cos\lambda_2 \right)^2$$
(11.3)
$$\left. + \left(1-e^2\right)^2 \left(N_1 \sin\phi_1 - N_2 \sin\phi_2 \right)^2 \right]^{\frac{1}{2}}$$

where ϕ_1, λ_1, ϕ_2, λ_2 are the latitude and longitude values of points P_1 and P_2, respectively, and N_1 and N_2 are the curvature radii in the prime vertical at points P_1 and P_2. Here:

$$N_i = \frac{a_{axis}}{\sqrt{\left(1 - e^2 \sin^2\phi_i\right)}},$$

where a_{axis} is the semi-major axis of the ellipsoid (6378137 m for WGS84 [110]), and e is the eccentricity:

$$e^2 = \frac{a_{axis}^2 - b_{axis}^2}{a_{axis}^2},$$

where b_{axis} is the semi-minor axis of the ellipsoid (6356752.314 m for WGS84 [110]).
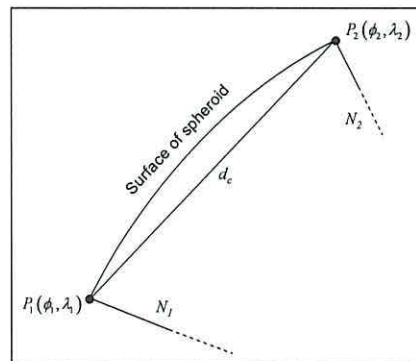
Fig. 11.9 - Calculating chord distance on a spheroid

The primary factor propagation time delay, in μs, is:

$$t_{primary} = \frac{d_c \eta_{air}}{c} \times 10^6 ,$$ (11.4)

where c is the free-space velocity of light (299792458×10^8 m/s [85]) and η_{air} is the refractive index of air (1.000338) [85].

So, the total propagation time of a signal between a Master and the Locator (including the SPOs and station delays of any slaves in the chain) is:

$$t_{prop} = \sum_{i=1}^{N_s} \left(t_{total_{i-1,i}} + t_{stationdelay_i} + t_{SPO_i} \right) + t_{total_{N_s,Locator}} ,$$ (11.5)

where N_s is the total number of slaves in a chain, $t_{total_{i-1,i}}$ the total propagation time between each master and its slave within the chain [Equation (11.2)], $t_{stationdelay_i}$ the station delay at the ith station in the chain, t_{SPO_i} the SPO at the ith station in the chain, and $t_{total_{N_s,Locator}}$ the total propagation time between the last station in the chain and the Locator. When $N_s = 0$ (i.e. receiving the signal directly from the Master), no slaves are in the chain. In this case,

$$t_{prop} = t_{total_{0,Locator}}$$ (11.6)

Whatever the position of the Locator, the summation term remains constant for each station, since the configuration of the network is unchanged regardless of the Locator's position. In order to reduce computation time, it was decided that this term would be computed once only for the whole set of stations, and the results then applied when calculating all apparent ranges. Similarly, the *link bias error* for each station can be pre-calculated. This is the sum of the link V_p error, the station delay, and the sum of the SPOs of all stations between the master and the last slave in the chain. That is:

$$\varepsilon_{linkbias,N_s} = \sum_{i=1}^{N_s} \left(\varepsilon_{V_p,i-1,i} + t_{stationdelay_i} + t_{SPO_i} \right) ,$$ (11.7)

where $\varepsilon_{V_p,i-1,i}$ is the V_p error between a master and slave pair in the chain:

$$\varepsilon_{V_p} = t_{total} - t_{V_p},$$
<div align="right">(11.8)</div>

where t_{V_p} is the propagation time using propagation velocity V_p:

$$t_{V_p} = \frac{R_{Locator}}{V_p}$$
<div align="right">(11.9)</div>

where $R_{Locator}$ is the range over an ellipsoid as calculated by the Locator.

Now a complication! Although the *model* employs the WGS84 ellipsoid, Datatrak use a different ellipsoid for each network, selecting the ellipsoid that provides the best fit across the area of interest [111]. In the UK, they use the Airy Ellipsoid, the basis of the National Grid [112]. So, the value of $R_{Locator}$ depends on the ellipsoid used in the Locator. Whatever the ellipsoid, the Locator itself uses the Andoyer-Lambert formula to compute its ranges from stations [111, 113]. In our model, we will emulate the Locator's calculations. Appendix J shows the ellipsoid coordinate conversion routine used to implement Helmert's formula to ensure that the correct co-ordinates are used.

Since the term $\varepsilon_{linkbias,N_s}$ in Equation (11.7) that represents the constant error resulting from the particular configuration of the network has been pre-calculated, when predicting the apparent range from a given station the model need only calculate the total propagation time from the station to the Locator, and add the link bias error associated with that station. Thus,

$$t_{prop,N} = \varepsilon_{linkbias,N_s} + t_{total_{N_s,Locator}}$$
<div align="right">(11.10)</div>

The result of adopting this approach is a much quicker execution time and a considerable simplification of the prediction model, with no loss in accuracy.

11.4 Locator model

The network model in Section 11.3 can calculate the apparent range of the Locator from any specified Datatrak station, taking the network configuration into account. Now let us examine how the Locator employs that apparent range value.

Chapter 9 showed how the Locator calculates its position using a least-squares method. The algorithm required an estimated initial position. Then, in an iterative

process, it employed measured pseudoranges to refine that estimate until some condition had been met. We will now emulate this Locator process in the model, with apparent ranges taking the role of pseudoranges; in a sense, we will design a Virtual Locator (VL). Then, as ever, we will work through an array of geographical points, employing the VL at each.

The position calculated by the VL is regarded as being static. This is because the groundwave on which the Locator operation is based is temporally stable (Section 4.5.1). Any effect due to the stochastic processes of own-skywave, noise or interference has been dealt with in Chapter 9. Therefore, the absolute accuracy and CF calculated by the VL can be considered as fixed values, for use by day or by night.

The VL uses the position of the calculation point as its initial estimate. It then calculates the position fix using Equation (9.9). The clock bias term, ΔB, will contain the average difference between the calculated and observed pseudoranges. As far as the Locator is concerned, it cannot differentiate between clock bias (which affects all measurements by the same amount) and the average difference between the calculated and observed pseudoranges (which, by definition, affects all measurements by the same amount). So, although we cannot predict the actual clock bias, the clock bias term, ΔB, is still required in the algorithm.

The VL chooses the stations to be used in the position solution in just the same way as does a Locator (Section 9.4.1). However, we must also be careful to specify in which *transmission slots* the signal is radiated by each station chosen, since if a station transmits in more than one slot, each slot will have a different link bias (because they have different masters). Details of slot allocations are given in Appendix K.

In Section 11.3.1.2, we discussed the fact that each of two specific stations in the UK network actually transmit in two separate slots. The two slots each have different masters, and so two different link biases. In Table 11.1, we notice that the dual-slot stations have a common master: the Cumbria station. When a Locator is in Northern England, or Scotland, it will select the slot that has the Cumbria station as its master. Indeed, that means that all stations in Northern England and Scotland have a common master. Any link bias errors of the signal from Huntingdon to Cumbria will

effectively drop-out of the solution, appearing as clock bias, since it affects all measurements by the same amount. This is a clever trick employed by Datatrak to produce better accuracies and CF in the North of England and Scotland!

Using Equation (11.10), the VL now computes apparent ranges, at each of the four frequencies: f_{1+}, f_{1-}, f_{2+} and f_{2-}. So, if six stations have been selected, 24 values will be computed. These will then be converted to apparent ranges in metres:

$$O_i = t_{prop,N_s} \times \frac{c}{\eta_{air}}, \qquad (11.11)$$

where O_i is the ith observed apparent range from station N_s to the Locator's position, and i has a maximum value of $4N_s$ (as each station has 4 signals).

We now compute a position, using the same iterative process as does the Locator. We calculate C_i, the ith calculated range from the initial estimate to the station. So:

$$C_i = R_{Locator}, \qquad (11.12)$$

where $R_{Locator}$ in this case is the range from the Locator initial position to the ith station over the Locator ellipsoid.

The vector δb in Equation (9.11) contains differences between C_i and O_i for all i, as required by the least squares algorithm. The weight matrix is then applied, as described in Section (9.4.1).

The Locator itself stops iterating when, either the change in position between successive iterations is less than 1 m, or the number of iterations has exceeded 9 [114]. In our VL, the iteration process is terminated when either:

$$\sqrt{\Delta x^2 + \Delta y^2} < 1 \text{ m}, \qquad (11.13)$$

where Δx and Δy are defined in Equation (9.10), or the number of iterations has exceeded 9.
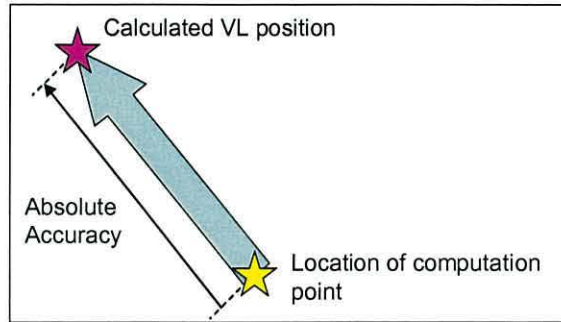
Fig. 11.10 – Calculation of absolute accuracy

The output of the iterative weighted least squares routine is a change in position which, when added to the initial position guess, gives a final position fix that is the best fit to the set of apparent ranges. A clock bias term is also produced, but discarded.

11.5 Absolute accuracy

The output of the VL model described in Section 11.4 is the pair of position coordinates the model estimates would be produced by a Locator at the geographical coordinates of the computation point. The absolute accuracy is thus the distance between this predicted position fix and the actual location of the computation point (Fig. 11.10).

Now, for the first time, we can produce a predicted absolute accuracy plot for a Datatrak network: Fig. 11.11. This plot for the UK network incorporates the V_p value
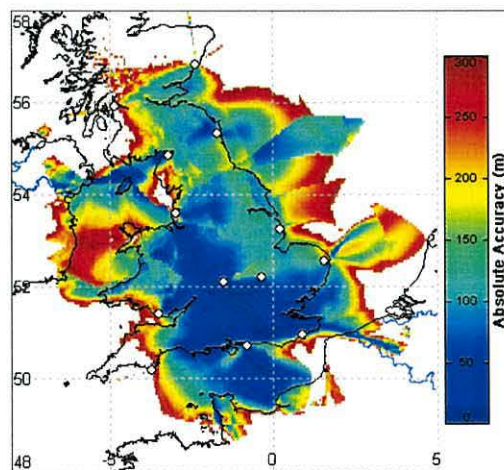
Fig. 11.11 – Predicted absolute accuracy of UK network.

of 299,300 kms^{-1} used in UK Locators. An absolute accuracy limit of 300 m has been chosen to bound the plot; Datatrak themselves do not specify any limiting value.

The absolute accuracy appears to be within 100 m across most of England. The accuracy deteriorates in the further reaches of the network, because of poorer geometry and also because the lower signal strength there affects station weightings in the position solution. Around Bangor, for example, the absolute accuracy is close to 300 m; this is commensurate with the errors experienced at Bangor when trying to obtain a position fixes in the repeatable accuracy experiment. It is interesting to see that there are localised areas in the Scottish Highlands where terrain effects cause the propagation errors to cancel out, the apparent ranges falling back into alignment so that the absolute accuracy falls below 300 m again.

11.6 Confidence factor

Confidence Factor is a measure, computed by a Locator, of the degree of alignment between the measured pseudoranges. Mathematically, it is the residue of the least-squares operation. Fig. 11.12 shows the principle: the yellow lines represent the calculated ranges from the station giving the ith measurement from the calculated position solution. The blue lines represent the corresponding measured pseudoranges. Ideally, each yellow line would have the same length as its blue counterpart. In general, however, there is a residue:

$$R_i = C_i - O_i,$$ (11.14)
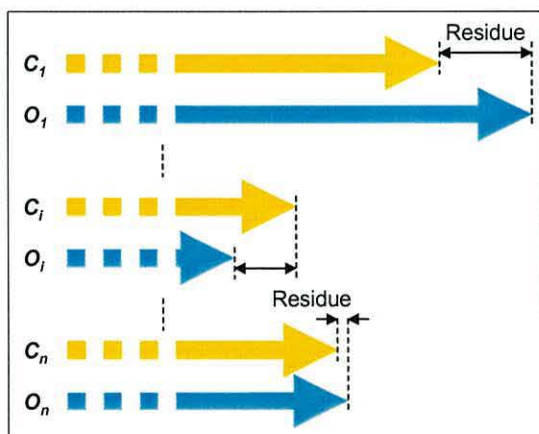
Fig. 11.12 - Definition of residue for calculating confidence factor.

where R_i is the residue in the ith measurement in metres, C_i is the range from the calculated position to the ith measurement station, and O_i is the measured pseudorange.

The CF is the RMS value of all these residues [95]:

$$CF = \sqrt{\frac{1}{n}\sum_{i=1}^{n}(R_i - \overline{R})^2} \ , \qquad (11.15)$$

where $\overline{R}$ is the mean residue, and n is the total number of measurements. The units of CF, like those of all the ranges involved, are metres. A CF of 0 m indicates perfect alignment between the pseudoranges at the calculated position. A higher value indicates less than perfect alignment. The Locator will deem the calculated position to be invalid if the CF value exceeds 95 m. Note that, although the position fix itself is a weighted solution, the residues in the CF calculation are not weighted.

The VL too can predict the confidence factor at each calculation point, by using Equations (11.14) and (11.15). The result for the UK network, again a first, is shown in Fig. 11.13. This plot is limited to a CF of 95 m: thus, it actually shows the coverage of the UK Datatrak system, as far as CF is concerned. The CF value varies in a complex fashion throughout the network. Note that, because of the absence of weighting in the CF calculation, there are sharp boundaries at which individual stations drop out of the calculation due to the station selection criteria. There is an
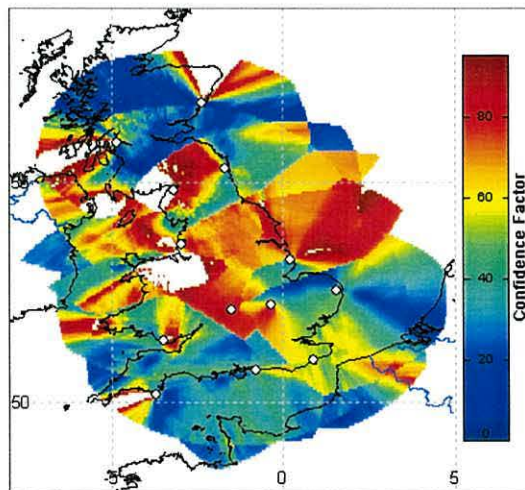
Fig. 11.13 – Predicted confidence factor of UK network

area of poor CF through the Midlands and into North England, which includes the two locations at which repeatable accuracy measurements were made. This plot is supported by the observation that at Bangor the confidence factor was too high for the Locator to operate reliably: the CF predicted for Bangor is 109 m.

11.7 Verification

The absolute accuracy and CF predictions will now be compared with the measurements made at Stoke-on-Trent and Milton Keynes. The mean values of the daytime observations will be employed, to ensure that skywave influence is kept to a minimum.

Table 11.3 shows the measured and predicted absolute values by day at both locations. The measured absolute accuracy at Stoke-on-Trent is approximately half that predicted, whereas at Milton Keynes it is five times greater. At both locations, the predicted confidence factor is some three times the measured value. No location-dependant offsets were in place in the Locator at the time of the experiments, and therefore these discrepancies cannot be attributed to them.

What is the cause of these marked discrepancies? Detailed analysis of the data predicted for, and recorded in, Milton Keynes shows that the discrepancy there between the calculated and observed ranges of the Asserby station (150-190 m over the four frequencies) were much greater than those of the other stations, all of which were less than 75 m. These discrepancies cannot simply be due to delays at Asserby, since these had been measured and the results used in the model. The finger of suspicion, therefore, points towards the Stratford-Asserby and Asserby-Milton Keynes paths V_p errors computed by the model. Could it be that these are not

		Measured	Predicted
Stoke-on-Trent	Absolute accuracy (m)	41	75
	Confidence Factor (m)	32	92
Milton Keynes	Absolute accuracy (m)	74	14
	Confidence Factor (m)	26	76

Table 11.3 - Measured and predicted absolute accuracy and confidence factor.

sufficiently accurate?

The actual delay between the stations of a master-slave pair can, in fact, be measured. The technique is to measure the phase difference between the master and slave signals on the *master* baseline extension (similarly to measuring the slave station delay on the slave baseline extension); details are given in Appendix L. We can then compare the measured delay with that predicted by the model.

The Southport and Cumbria stations (Fig. 11.14), being slaves to one another, allow measurements made separately at each end of the baseline to be checked against one another; good agreement will give a measure of confidence in the procedure. This path includes good farming land, sea-water and the mountains of the Lake District: it contains marked variations of both conductivity and terrain. So it should provide a good test of Monteath's method.

Table 11.4 shows the discrepancies between the modelled and measured delays along this path. The values are expressed in millicycles, (thousandths of a wavelength), the unit employed in Datatrak Locators. To convert them to distance:

$$d = \frac{c}{f} \times \frac{M}{1000} \qquad (11.16)$$
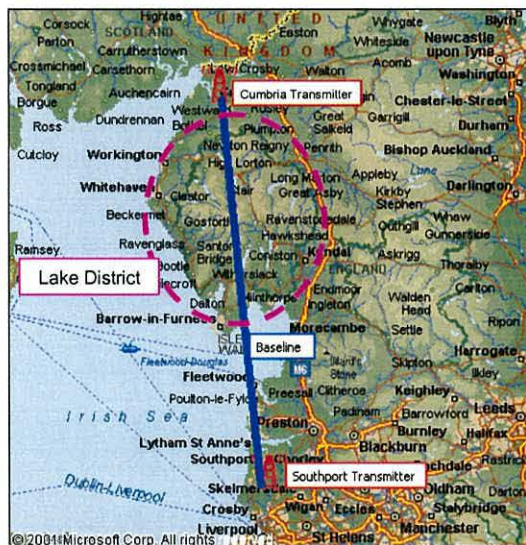
Fig. 11.14 - Terrain map showing Southport-Cumbria baseline, which passes through the Lake District (ringed)

	Master-Slave pair	Delay due to V_p Error along Southport-Cumbria Baseline (millicycles)			
		f_{1+}	f_{1-}	f_{2+}	f_{2-}
Measured	Southport-Carlisle	78.7	77.9	73.4	73.9
	Carlisle-Southport	76.1	76.3	77.0	77.0
	Average	*77.4*	*77.1*	*75.2*	*75.4*
Predicted	Southport-Carlisle	50.3	50.3	47.1	47.1
	Carlisle-Southport	58.5	58.5	54.4	54.4
	Average	*54.4*	*54.4*	*50.8*	*50.8*

Table 11.4 - Measured and predicted delays due to V_p errors along Southport-Cumbria baseline

where M is the number of millicycles, and f is the frequency of the signal.

The average measured V_p error delay along the Southport-Cumbria baseline is 76 millicycles (152 m), with an agreement within ± 3 millicycles (6 m) over all four frequencies and two directions. The average modelled V_p error delay along the same baseline is 52 millicycles (104 m). Thus the model is *underestimating* the delay by 48 m. The Monteath calculation itself had previously been shown to be operating correctly (Section 10.3.2). The conclusion is that these discrepancies derive from errors in the *databases* employed. The ground conductivity database is known to be relatively inaccurate, while the topography and coastline databases are extremely accurate and precise.

11.8 Investigation of the ground conductivity database

The ground conductivity database is mostly derived from the ITU ground conductivity atlas [35]. This document presents ground conductivity maps, mostly for individual countries. Some maps, including the UK's, are very crude, with large geographical areas allocated just a single conductivity value. Also, although many of the maps employ the ITU set of 8 quantised values, others (including the UK's) do not and the nearest quantised values have been entered into the database. This approach has been shown to be adequate for predicting field strengths, but may not be good enough for giving precise phase delay values. Let us investigate the sensitivity of phase delay predictions to ground conductivity along this Southport/Cumbria baseline.

The ITU map shows a single ground conductivity value for the whole of the Lake District of 6 mS/m. This has been quantised to the nearest ITU standard value of

	Master-Slave pair	Delay due to V$_p$ Error along Southport-Carlisle Baseline (millicycles)			
		f_{1+}	f_{1-}	f_{2+}	f_{2-}
Measured	Southport-Carlisle	88.7	88.7	81.7	81.7
	Carlisle-Southport	88.1	88.0	82.9	82.9
	Average	*88.4*	*88.3*	*82.0*	*82.3*
Predicted	Southport-Carlisle	97.0	97.0	99.0	99.0
	Carlisle-Southport	96.0	96.0	98.0	98.0
	Average	*96.5*	*96.5*	*98.5*	*98.5*

Table 11.5 - Measured and predicted V$_p$ error with modified ground conductivity value for the Lake District

10 mS/m in the Bangor ground conductivity database. Had the conductivity shown been below 5.5 mS/m, it would have been quantised to 3 mS/m. We have substituted 3 mS/m for 10 mS/m in the Monteath calculation. The outcome is the results shown in Table 11.5. It shows that the model now *overestimates* the V$_p$ error delay by 26 m: a change of 74 m. This considerable shift results from a change of just one quantisation level over half a path. Clearly, phase delays are highly sensitive to ground conductivity.

A similar measurement conducted on the Stratford-Asserby master baseline extension, has shown that the model is overestimating the delay by approximately 100 m. This would clearly account for Asserby's large contribution to the predicted CF value as shown in Table 11.3. It suggests that the ground conductivity between Stratford and Asserby is nearer to 20 mS/m, than the 10 mS/m value in the database. If we change the SPO at Asserby used in the model to compensate for this error, we obtain the results shown in Table 11.6.

The agreement between predicted and measured values has improved dramatically as

		Measured	Predicted
Stoke-on-Trent	Absolute accuracy (m)	41	28
	Confidence Factor (m)	32	65
Milton Keynes	Absolute accuracy (m)	74	10
	Confidence Factor(m)	26	48

Table 11.6 - Measured and predicted absolute accuracy and confidence factor with SPO modification at Asserby

a result of an adjustment at this one station. We conclude from this investigation that the present ground conductivity database is the limiting factor in setting the accuracy of results predicted by our Datatrak absolute error and CF model. It clearly is not good enough. Creating a more precise database would be very desirable, but lies outside the scope of this project.

The method proposed in this chapter has shown to have huge potential to help Datatrak engineers to improve the accuracy and reliability of the position fixes. It will certainly show which areas require deeper investigation, and should reduce the time required to complete such procedures. However, as with the interferer database (Chapter 8), the model is only as good as the data being supplied to it. We have clearly shown that the conductivity database is preventing the model being used to its full potential when calculating the location-dependant corrections to be entered into the Locator to provide a better absolute accuracy and CF.

11.8.1 Future work

It may be possible to produce a better ground conductivity map, one covering the entire world, from geological maps, or perhaps satellite imagery. This would require a great deal of work. Alternatively, at least for the UK, it would be possible to use Datatrak measurements themselves (as was done above) to estimate the ground conductivities of baselines, and adjust the ground conductivity database accordingly. In the short term, doing this would certainly increase the exactness with which absolute accuracy and confidence factor could be predicted. In contrast, a good deal of work would be needed to produce a comprehensive ground conductivity map of the UK from Datatrak measurements.

11.9 Conclusions

In this chapter, we set out to use Monteath's method to predict the phase delays of paths in the Datatrak system and thus predict and map the absolute accuracies and confidence factors of Datatrak networks.

A network model has been created and used to calculate the "apparent ranges" Locators should receive. The total propagation time of each signal was broken into its

constituent parts and, using SPO values provided by Datatrak, the apparent ranges to the Locator were estimated. A virtual locator was then created which computes position solutions from these apparent ranges using a least squares algorithm, simulating the Datatrak Locator. In this way, the absolute accuracy and confidence factor have been calculated and plotted.

The prediction model works as intended. It is an effective tool for enabling Datatrak engineers to identify areas that require further investigation. Despite the limited quality of the ground conductivity database revealed by the verification measurements, it is a great improvement over the present *ad hoc* method of using numerous measurements to create local adjustments. It has the potential actually to predict these adjustments, thus saving many weeks of development time.

Chapter 12

Conclusions

The primary objective of this research has been to identify methods that will allow the engineers at Siemens Datatrak to predict the coverage and performance of their LF timing and navigation system accurately, and to implement those methods in the form of a suite of computer software.

Prior to this research, the task of predicting the coverage and performance of Datatrak networks were very much based on the extensive experience of Datatrak engineers and the rules of thumb they had developed. The result was a method that was simple but inexact. For example, using data from the ITU, they were able to determine the *range* from a transmitter at which the groundwave field strength would fall to a certain value, and plot a circle around the transmitter accordingly. But they then tended to deem this the 'coverage' of the station. In doing so, they ignored many factors. For example, the effects of skywave signals were not considered at this stage. Also, they had no means whatsoever of predicting signal delay - a crucial element in predicting absolute accuracy and confidence factor.

This research has provided more scientific, accurate methods of predicting the coverage and performance of Datatrak networks. The result is a valuable suite of

Topic	Status
Review of Datatrak methods	Completed
Station radiated power	Completed
Ground conductivity	Completed
Skywave interference	Completed
Atmospheric noise	Completed
Vehicle noise	Completed
Interference	Completed
Station geometry	Completed
Repeatable accuracy	Completed
Terrain effects	Completed
Groundwave phase delay	Completed
Absolute accuracy	Completed
Confidence factor	Completed

Table 12.1 - Status of coverage/performance factors as required in the specification

software tools that allows engineers to enter details of new networks, and run scenarios to see how well they will perform.

Table 12.1 summarises the status of all the coverage and performance factors in project as defined by the specification laid out in the project outline (Appendix B). It shows that we have met all the targets and, in some cases, exceeded them. For example, the specification did not mention Locator noise floor at all, but our investigations found it to be the dominant noise source in the Locator. As far as the project is concerned, we can say that we have successfully completed it.

12.1 Review of Thesis

In Chapter 2, we saw how the Datatrak AVLS fits into the world of vehicle tracking systems. Most of its competitors rely on the GPS for their location sub-systems, and on GSM or other cellular networks for transporting information between vehicle and customer. Datatrak turned out to be unique in that a single company wholly owns both the timing and navigation system (LF) and the communications network (UHF). This, together with highly-redundant networks, gives the system an unparalleled level of security and reliability.

We took a closer look at the LF timing and navigation network in Chapter 3. We saw that all the transmitters in a given network transmit on the same frequency. Receivers differentiate between stations by their transmission positions in a time-multiplexed sequence. Originally, Datatrak receivers operated in the hyperbolic mode, because of the resulting simplicity of receiver design. As receiver processing power increased, the use of pseudo-ranging became feasible. The current Datatrak receiver model, the Mk4 Locator, uses this mode of operation by default; this is the standard receiver studied in this thesis.

We also discussed what factors Datatrak uses to define the coverage of their networks. It became clear that all the techniques used currently could be replaced by computer modelling based on concepts that are more fundamental. With this in mind, we set the outline of the research on which the rest of the thesis is based on.

In Chapter 4, we studied the most important factor of the Datatrak system: the groundwave signal. The attenuation of the groundwave signal depends chiefly on ground conductivity. Using the Bangor Ground Conductivity Database, and further developing the techniques used in previously-developed coverage models for other navigation systems, we were able to predict accurately the groundwave field strengths of Datatrak signals. This enabled Datatrak to predict the true coverage of a signal based on its field strength. Measurements using calibrated field strength measuring equipment verified the results of the model.

The other signal produced by Datatrak transmitters is the unwanted skywave, which became the subject of Chapter 5. Skywave can cause deep fading and produce uncertainty in range measurements. In this chapter, we concentrated on the effect of skywaves on the field strengths of the received signals. The skywave field strength can be calculated using data collected by the ITU, and the method they suggest has been implemented in the software. So, for the first time, the skywave field strength of Datatrak signals could be calculated. Using a technique developed by Poppe, the degree of signal fading with respect to the groundwave signal could be predicted. This allowed us to produce the first coverage plots based on groundwave and own-skywave field strength. These plots, too, were verified using experimental data.

Chapter 6 discussed the subject of radio noise. Three sources of noise were identified: atmospheric noise, vehicle noise and Locator noise. Data for atmospheric noise was obtained from the ITU. A new technique was developed that uses this data in electronic data and produces atmospheric noise maps on-the-fly, for anywhere in the world, with no need for slow manual digitisation and data entry. Using measurements and data concerning the Locator noise floor and vehicle noise, provided by Datatrak, we were able to predict the signal-to-noise ratio of Datatrak signals for the very first time. This let us produce the first Datatrak coverage plots based on both field strength and signal-to-noise ratio.

The difficult task of analysing interference was the subject of Chapters 7 and 8. In the past, Datatrak have used experimental techniques to determine the best frequencies for their networks. This is expensive in terms of cost and time, and the possibility of replacing it by a computer-based interference model was attractive. The model had to

be designed from scratch, on the basis on information provided by Datatrak and measured data. This was a complex task, but the result is a detailed model of the receiver's response to both passband interference and receiver blocking. Chapter 8 examined the use of an ITU database of radio transmissions as the main source of information on potential interferers. A novel technique was developed to analyse interferers. Then, the model developed in Chapter 7 was used to predict the degree of rejection the Locator would offer each transmission, taking into account its groundwave and skywave field strengths, frequency, and the nature of its modulation. In that way we were able to establish where the Locator would be capable of operating. The first coverage plots could now be produced which included the effects of interference from some 22,000 stations. Exclusion zones were defined around strong interfering transmitters that could block Locators.

The subject changed in Chapter 9 to an investigation of the effect of all these unwanted signals on the phase measurements used to calculate the location of the receiver. Noise and interference cause uncertainty in these phase measurements, which translate into uncertainty in the position, or repeatable accuracy. The amount of uncertainty was analysed, using the predictions developed earlier of groundwave field strength and the field strengths of the unwanted signals. A novel solution was devised in which, by simulating the processes employed in the Locator, it was possible to calculate the repeatable accuracy provided point-by-point across the coverage of a Datatrak network.

We returned to the subject of groundwave signals in Chapter 10. In the method introduced in Chapter 4, the groundwave field strength had been calculated by assuming a spherical, smooth, earth. Now Monteath's method was introduced, which allowed hills and mountains to be taken into account. It provides not only field strength but also signal delay predictions. The field strength replaced the earlier the Millington ones, not only adding the effects of topography, but also giving results of finer resolution.

Chapter 11 demonstrates the use of the signal delay results produced by the Monteath computations. Since the position calculated by a Datatrak Locator is determined by the propagation delays experienced by the signals reaching it from the stations, any

errors in these delays will affect the result. Modelling the network, and predicting the signal delay values for each signal, let us estimate the location that would be determined by an Mk4 Locator. This in turn allowed us to map the absolute accuracy and confidence factor throughout the coverage of a network. Verifying the results showed that the performance of the model is limited principally by our imperfect understanding of the ground conductivity of the UK. These novel results will truly benefit Datatrak engineers in their planning of new networks.

12.2 BANgor Datatrak Performance Analysis Software Suite (BANDPASS)

All the tools described in this thesis have been built into a Windows-based software suite called the Bangor Datatrak Performance Analysis Software Suite (BANDPASS). Written in a Microsoft Visual C++ environment, it provides an intuitive interface to the software propagation prediction tools. Some original code was adapted from Poppe's programs. It was checked, debugged, and converted from a form designed for use under MSDOS, to one compatible with Windows. Providing a truly user-friendly interface, required the candidate to learn various aspects of Windows programming and understand the principles of object-orientated programming. The development of the software was enhanced by a process of feedback from Datatrak engineers who took it over as soon as it became available and highlighted functionality issues or desirable additional features. The manual for the software forms Appendix M of this thesis; from it can be seen the comprehensive set of options it provides. Happily, the feedback on the software has been very positive. The system has been used extensively by Datatrak, to test and analyse various scenarios both in planning new networks and in understanding the operation of current ones.

12.3 Further Work

The entire model as described in this thesis is far better than the manual, crude methods of coverage and performance prediction Datatrak used in the past. It is possible to determine factors that Datatrak were not able to predict before.

However, there are areas of the model that could be improved. At the end of Chapter 11, the limit of Monteath's method was discussed. We showed that the

quantisation levels in the ground conductivity database were causing signal delay results to be inaccurate. This was proved by measurements along baseline extensions.

There is little that can be done with the existing database because the nature of the storage means that it cannot hold conductivity values other than the standard ITU ones. To optimise the results from Monteath's method, the number of quantisation levels in the database should be increased, or quantisation abandoned. This would require a completely new database structure. Providing this would be a major task in itself, although given the rather inexact nature of the ground conductivity information from the ITU, the resolution of the database can remain unchanged at 0.1° x 0.1°.

Better still would be to improve fundamentally the ground conductivity data. This might require reference to geological maps, or even satellite imagery. The latter might be a route to creating maps for areas not covered in the ITU source (e.g. France). Novel work such as this would prove useful well beyond Datatrak. For example, it could be used to predict ASFs more accurately in Loran-C systems around the world.

12.4 Conclusions

At the start of this research, Datatrak had no means of accurately determining the groundwave and skywave field strengths of their signals, determining the noise strength, or calculating repeatable accuracy. They also had no means whatsoever to predict the effects of interference on their Locators, to predict signal delay of Datatrak signal (including effects of irregular terrain), or to calculate either absolute accuracy or confidence factor.

Following the decisions set out in Chapter 3, we have taken a scientific approach to analysing the unique Datatrak LF timing and navigation system, and developing existing and novel techniques to determine accurately the factors which Datatrak engineers wish to know when planning new networks.

The result is a suite of modelling tools, which will allow Siemens-Datatrak to plan and enhance Datatrak networks anywhere in the world.

References

[1]   Last, J.D. & Wade, M., *Vehicle Tracking: Is GPS Always Best?*, Vehicle Tracking and Fleet Management Colloquium, Autotech 1997

[2]   Poppe, D.C., *Coverage and Performance Prediction of DGPS Systems Employing Radiobeacon Transmissions*, PhD Thesis, University of Wales, Bangor, 1995

[3]   Quartix Ltd, *Quartix Home Page*, http://www.quartix.net/, July 2003

[4]   Enge, P, Misra, P., *Global Positioning System – Signals, Measurements, and Performance*, Ganga-Jamuna Press, ISBN 0970954409, 2001

[5]   Assistant Secretary Of Defense for Command, Control, Communications, And Intelligence, *Global Positioning System Standard Positioning Service Performance Standard*, United States Department of Defense, October 2001

[6]   P.H. Dana, *Global Positioning System Overview – The Geographer's Craft Project*, http://www.colorado.edu/geography/gcraft/notes/gps/gps_f.html, 1999

[7]   John A. Volpe National Transportation Systems Center, *Vulnerability Assessment of the Transportation Infrastructure Relying on the Global Positioning System*, Office for the Assistant Secretary for Transportation Policy, US Department of Transportation, August 2001

[8]   Clynch, J.R., Parker, A.A., Adler, R.W., Vincent, W.R., McGill, P., Badger, G., *The Hunt for RFI – Unjamming a Coast Harbor*, GPS World, Vol. 14 No. 1, January 2003

[9]   Wagoner, P., *GPS Interference Event*, Heritage Foundation Homeland Security Task Force Report, US Heritage Foundation Homeland Security Task Force, http://gbppr.dyndns.org/PROJ/mil/gps/inter.txt, 4th March 2002

[10]   Fontana, R.D., Cheung, W., Stansell, T., *The Modernized L2 Civil Signal*, GPS World; http://www.navcen.uscg.gov/gps/modernization/default.htm, September 2001

[11]   Federal Aviation Administration, *GPS Modernization* http://gps.faa.gov/gpsbasics/GPSmodernization-text.htm, July 2003

[12]   Divis, D.A., *Washington View*, GPS World, Vol. 14, No. 6, June 2003

[13]   Forssell, B., *Radionavigation Systems*, Prentice Hall, ISBN 0137510586, 1991

[14]   Beck, G.E. (ed.), *Navigation Systems: A Survey of Modern Electronic Aids*, Van Nostrand Reinhold Company, SBN 442006357, 1971

[15]   Laurila, S.H., *Electronic Surveying and Navigation*, John Wiley & Sons, Inc, ISBN 0471518654, 1976

[16]   United States Coast Guard, *Loran-C User Handbook*, COMDTPUB P16562.6; U.S. Department of Transportation; 1992

[17]   The Decca Navigator Company Ltd, *The Decca Navigator - Operating Instructions and Datasheets*, Vol. 1 and 2, Rev. 8, May 1983

[18]   Locus Inc, *Loran Receivers and Related Products*, http://www.locusinc.com/loran.html, Nov 2003

[19]   Reelektronika bv, *Reelektronika Home Page*, http://www.reelektronika.nl/, July 2003

[20]   United States Federal Communications Commission, *Wireless 911 Services*, http://www.fcc.gov/cgb/consumerfacts/wireless911srvc.html, March 2004

[21]   GSM Association, *Location Based Services*, http://www.gsmworld.com/technology/applications/location.shtml, January 2003

[22]   Hein, G., H., Godet, J., Issler, J-L., Martin, J-C., Erhard, P., Lucas-Rodriguez, R., Pratt, T., *Status of Galileo Frequency and Signal Design*, Galileo Signal Task Force, European Commission, http://europa.eu.int/comm/dgs/energy_transport/galileo/documents/technical_en.htm, 25th September 2002

[23]   Hein, G.W. *et al*, *Galileo Frequency and Signal Design*, GPS World, Vol. 14, No. 6, June 2003

[24]   Wilson, Andrew (ed.), *Galileo: The European Programme for Global Navigation Services*, BR-186 (2nd Impression), European Space Agency brochure, March 2003

[25]   Orange plc, *Orange Home Page*, http://www.orange.co.uk/, July 2003

[26]   Inmarsat, *Inmarsat – Coverage Maps*, http://www.inmarsat.org/support_maps.cfm, March 2004

[27]   GlobalStar, *GlobalStar Satellite Phones*, http://www.globalstar.com/, July 2003

[28]   EutelSat S.A., *EutelSat Home Page*, http://www.eutelsat.com/products/2_4_1_3a.html, November 2003

[29]   QUALCOMM Wireless Business Solutions bv, *QUALCOMM Home Page*,
         http://www.qualcomm-europe.com/english/index.shtml, November 2003

[30]   D.L. Clarke, M.E. McCauley, T.J. Sharkey, T.A. Dingus, J.D. Lee,
         *Development of Human Factors Guidelines for Advanced Traveler
         Information Systems and Commercial Vehicle Operations: Comparable
         Systems Analysis*, Report No. FHWA-RD-95-197, Federal Highway
         Association, US Department of Transportation,
         http://www.fhwa.dot.gov/tfhrc/safety/pubs/95197/sec6/sec6.html, December
         1996

[31]   mi-Trek Pty Ltd, *StarView Tracking Systems*,
         http://www.mi-trek.com.au/Pages/Software%20Pages/StarView.html,
         November 2003

[32]   Siemens Datatrak Ltd, *Solutions for a world in motion*, Marketing brochure,
         2001

[33]   Siemens Datatrak Ltd, *CommBase V3.04 Datasheet*, Siemens VDO
         Automotive, May 2003

[34]   Last, J.D., Turhan, B.E., Grafton, M.H., *Land coverage of radiobeacon
         DGNSS*, Proceedings of the Royal Institute of Navigation/International Loran
         Association, ILA28/NAV99 Convention and Technical Symposium, Paper 35,
         London, 1-3 November 1999

[35]   International Telecommunication Union, *World Atlas of Ground
         Conductivities*, Recommendation ITU-R P.832-2, 1999

[36]   International Telecommunication Union, *Ground-wave Propagation Curves
         for Frequencies Between 10kHz and 30MHz*, Recommendation 368-7,1992

[37]   Farnworth, R.G., *Loran-C Coverage Prediction in Western Europe*, PhD
         Thesis, University of Wales, Bangor, 1992

[38]   Grant, A.J., *Availability, Continuity, and Selection of Maritime DGNSS
         Radiobeacons*, PhD. Thesis, University of Wales, Bangor, 2003

[39]   Williams, P and Last, J.D., *Mapping additional secondary factors for the
         North-West European Loran-C chains – Initial Results and Further Work*,
         27th Annual Convention and Technical Symposium; International Loran
         Association, Danvers, Mass. USA; 11-15 Oct, 1998

[40]   Williams, P., *ASF Modelling in Regions of Mountainous Terrain*, University
         of Wales, Bangor, 1999

[41]   Tetley, L., Calcutt, D., *Electronic Aids to Navigation*, Edward Arnold, ISBN
         0713135484, 1986

[42]   Miller, G.M., *Modern Electronic Communication*, 6th Ed., Prentice-Hall, Inc., ISBN 0138598282, 1999

[43]   Discussion with Cousins, N. and Willson, M., Siemens Datatrak Ltd, 9th July 2001

[44]   Cousins, Nigel, *Datatrak LF Chain Information*, Siemens Datatrak Ltd, 24th October 2000

[45]   Watt, A.D., *VLF Radio Engineering*, Pergamon Press Inc., 1967

[46]   Cousins, N., Siemens Datatrak Ltd, Private Communication, 27th February 2001

[47]   Cousins, N., Siemens Datatrak Ltd, Private Communication, 26th March 2001

[48]   Rudge, A.W., Milne, K., Olver, A.D., Knight, P., *The Handbook of Antenna Design*, 2nd Ed., IEE Electromagnetic wave series, Peter Peregrinus Ltd., 1986

[49]   International Telecommunication Union, *Prediction of Sky-wave Field Strength at Frequencies Between About 150kHz and 1700 kHz*, Recommendation ITU-R P.1147-1, 1999

[50]   Haykin, S., *Communication Systems*, 4th Ed., John Wiley & Sons, Inc., ISBN 0471178691, 2001

[51]   International Telecommunication Union, *Prediction of Sky-wave Field Strength at Frequencies Between About 150kHz and 1700 kHz*, Recommendation ITU-R P.1147-2, 2003

[52]   International Telecommunication Union, *Radio Noise*, Recommendation ITU-R P. 372-8, 2003

[53]   Spaulding, A.D., Stewart, F.G. *An Updated Noise Model for Use in IONCAP*, Report 87-212, National Telecommunications and Information Administration, US Department of Commerce, January 1987

[54]   Meeting between University of Wales, Bangor and Siemens Datatrak Ltd, Minutes, 16th February 2001

[55]   Siemens Datatrak Ltd, *Mk4 Locator Functional Specifications*, Document No. S0314, Issue 2, October 2000

[56]   Siemens Datatrak Ltd, *Circuit Diagram for Mk4-2 Motherboard Assembly*, 2001

[57]   Cirrus Logic, *CS4222 20-Bit Stereo Audio Codec with Volume Control Datasheet*, December 2002

[58]   Cousins, N., *H-field Antenna Response*, Private Communication, Siemens Datatrak Ltd, October 2000

[59]   Cousins, N., *Mk4 Front-end Bandpass Filter*, Private Communication, Siemens Datatrak Ltd, October 2000

[60]   Cousins, N., Siemens Datatrak Ltd, Private Communication, 30th March 2001

[61]   RF Micro Devices, *RF2721 Quadrature Demodulator Datasheet*, Revision A2, 2001

[62]   Straw, R.D. (Ed.), *ARRL Handbook for Radio Amateurs*, The ARRL, Inc., 77th Edition, ISBN 0872591832, 2000

[63]   Gosling, W. (Ed.), *Radio Receivers*, Peter Peregrinus Ltd, ISBN 0863410561, 1986

[64]   Roddy, D., Coolen, J., *Electronic Communications*, 4th Edition, Prentice Hall, ISBN 013312083, 1995

[65]   Brimicombe, M.W., *Electronic Systems*, Nelson, ISBN 0174480679, 1985

[66]   Cousins, N., *PSD of single cycle 40 Hz tone busrt with raised cosine*, Private Communication, Siemens Datatrak Ltd, October 2000

[67]   Cousins, N., Siemens Datatrak Ltd, Private Communication, 7th August 2001

[68]   Cousins, N., Siemens Datatrak Ltd, Private Communication, 11th April 2001

[69]   International Telecommunication Union, *International Frequency List*, Bureau des Radiocommunications International Frequency Information Circular (Terrestrial Services), 14th November 2000 and 10th December 2002

[70]   Klingenfuss, *The 2001 Super Frequency List*, Klingenfuss Publications, 2000

[71]   Boel, H., *European Medium Wave Guide*, http://go.to/emwg, 1st May 2001

[72]   Tripod.com, *The UK Radio Frequency Bands*, http://ukspec.tripod.com/spectrum.html, 2001

[73]   Jacobson, T., *LF, Low Frequency, Guide for 30 kHz – 150 kHz*, BeaconWorld, http://www.beaconworld.org.uk/files/lfguide.pdf, 5th August 2002

[74]   Thales Avionics, *Decca Navigator Closure Ends an Era*, Press Release 00/017, http://www.thalesavionics.co.uk/press/pr38.html, 6th April 2000

[75]   Hughes, D.R., *Transmitter Database*, BEng (Hons) Dissertation, University of Wales, Bangor, 2002

[76]   International Telecommunication Union, *Radio Regulations*, Volumes 1 – 4, 1998

[77]   International Telecommunication Union, *Radiocommunication Data Dictionary*, Recommendation ITU-R SM.1413, 2001

[78]   International Telecommunication Union, *Spectra and Bandwidth of Emissions*, Recommendation ITU-R SM.328-10, 1999

[79]   International Telecommunication Union, *Determination of Necessary Bandwidths including Examples for their Calculation and Associated Examples for the Designation of Emissions*, Recommendation ITU-R SM. 1138, 1995

[80]   International Telecommunication Union, *Necessary Bandwidth*, Recommendation ITU-R SM. 853-1, 1997

[81]   International Telecommunication Union, *Determination and Measurement of the Power of Amplitude-Modulated Radio Transmitters*, Recommendation ITU-R SM. 326-7, 1998

[82]   International Telecommunication Union, *Frequency and Distance Separations*, Recommendation ITU-R SM.337-4, 1997

[83]   Janusz, G.J., *Calculus*, William C. Brown Publishers, ISBN 0697153746, 1994

[84]   Bowditch, N., *The American Practical Navigator*, National Imagery and Mapping Agency, 2002

[85]   United States Coast Guard, *Specification of the Transmitted Loran-C Signal*, Document COMDTINST M16562.4A, 1994

[86]   Rensen, M., *HF-FAX*, http://ourworld.compuserve.com/homepages/HFFAX/toc7.htm, 12th October 2001

[87]   Cousins, N., Siemens Datatrak Ltd, Private Communication, 10th January 2001

[88]   Blachman, N.M., *Noise and its effect on Communication*, McGraw-Hill, 1966

[89]   Schwartz, M., *Information Transmission, Modulation, and Noise*, McGraw-Hill, 1959

[90]   International Telecommunication Union, *Probability distributions relevant to radiowave propagation modelling*, Recommendation ITU-R P.1057-1, 2001

[91]   Last, J.D., Wade, A.J., *Differential-Mode Correction of Skywave Errors in Low-Frequency Time-Sequence Position Monitoring Systems*, Radio and Electronic Engineer, Vol. 48, No. 11, IEE, November 1978

[92]   Bishop, J., *Formulas and Algorithms for Incorporating Linearized Least-Squares Pseudoranging into Datatrak Locators*, Siemens Datatrak Ltd, 1998

[93]   Cousins, N., Siemens Datatrak Ltd, Private Communication, 9th October 2001

[94]   Willson, M., Siemens Datatrak Ltd, Private Communication, 22nd August 2001

[95]   Cousins, N., Siemens Datatrak Ltd, Private Communication, 15th May 2001

[96]   Levanon, N., *Lowest GDOP in 2-D Scenarios*, IEE Proc.-Radar, Sonar Navigation, Vol. 147, No. 3, June 2000

[97]   Astronomical Applications Dept., *Interactive Sun or Moon Rise/Set Table,* US Naval Observatory, http://aa.usno.navy.mil/data/docs/RS_OneYear.html, April 2002

[98]   Samaddar, S.N, *The Theory of Loran-C Ground Wave Propagation – A Review*, Navigation: Journal of the Institute of Navigation, Vol. 26, No. 3, pp 173 – 187, Autumn 1979

[99]   Hufford, G.A., *An Integral Equation Approach to the Problem of Wave Propagation Over an Irregular Surface*, Quart. J. Appl. Math., No. 9, 1952

[100]   Johler, J.R., Berry, L.A., *Loran-D Phase Corrections Over Inhomogeneous, Irregular Terrain*, ESSA Technical Report IER 59-ITSA 56, November 1967

[101]   Monteath, G.D., *Computation of Groundwave Attenuation Over Irregular and Inhomogeneous Ground at Low and Medium Frequencies*, No. 1978/7, Research Department, British Broadcasting Corporation, March 1978

[102]   Monteath, G.D., *Application of the Compensation Theorem to Certain Radiation and Propagation Problems*, Proc. IEE, Vol. 98, Part IV, pp 23 –30

[103]   Johler. J.R., Keller, W.J., Walter, L.C., *Phase of the Low Radiofrequency Ground Wave*, National Bureau of Standards Circular 573, 1956

[104]   Millington, G., *Ground Wave Propagation Over An Inhomogeneous Smooth Earth*, Proc. IEE, 98, Pt. III, 53, 1949

[105]   Williams, P, Last, J.D., *Mapping additional secondary factors for the North-West European Loran-C chains*, 26th Annual Convention and Technical Symposium; International Loran Association, Ottawa, Canada; 6-9 Oct, 1997

[106]   US National Imagery and Mapping Agency, *Geospatial Engine*, http://geoengine.nima.mil/, 2002

[107]   US Geological Survey, *Digital Elevation Models (DEMs)*, http://edc.usgs.gov/products/elevation/dem.html, 2002

[108] ATDI Ltd., *Free Cartography*, http://www.atdi.com/down_carto_b.htm, 2002

[109] Cousins, N., Siemens Datatrak Ltd, Private Communication, 18th January 2002

[110] European Organisation for the Safety of Air Navigation (EUROCONTROL) and Institute of Geodesy and Navigation (IfEN), *WGS84 Implementation Manual*, Version 2.4, 12th February 1998

[111] Cousins, N., Siemens Datatrak Ltd, Private Communication, 9th December 2002

[112] Ordnance Survey, *National Grid / ETRF89 Transformation Parameters*, Geodic Information Paper No. 2, National Mapping Agency of Great Britain, 1995

[113] Pierce, J.A., McKenzie, A.A., Woodward, R.H., *Loran – Long Range Navigation*, Office of Scientific Research and Development, National Defense Research Committee, McGraw-Hill Book Company, 1948

[114] Cousins, N., Siemens Datatrak Ltd, Private Communication, 9th November 2002

[115] Emco, *Model 6502 Active Loop Antenna Operation Manual*, 2001

[116] National Semiconductor, *LF147/LF347 Wide Bandwidth Quad JFET Input Operational Amplifiers*, Datasheet No. DS005647, August 2000

[117] European Organisation for the Safety of Air Navigation (EUROCONTROL), *Datum: A Report and Software Package for the Transformation and Projection of Coordinates*, EEC Report No. 237, December 1993

[118] Cousins, N., Siemens Datatrak Ltd, Private Communication, 6th December 2002

Appendices

Appendix A

Technical Specification of Mk4 Locator

The specifications below are an extract from the Mk4 Locator Functional Specification (Siemens Datatrak Document S0314 Issue 2).

A.1 LF Receiver Description

The system requires two LF channels, nominally 300 Hz wide, in the frequency band 120 kHz to 180 kHz, the higher of the two frequencies (designated f_1) being approximately 10 % above the lower frequency (designated f_2).

To permit future roaming capability between independent navigation chains, each LF frequency should be dynamically switchable, by on-board software, over the specified band.

With reference to the LF Receiver Block diagram (Fig. A.1):-

The LF receiver is based on direct conversion architecture, where the local oscillator (LO) is on the same frequency as the incoming LF signals. Two LO signals in quadrature are produced, each feeding a mixer, from which in-phase and quadrature (I & Q) components of the demodulated signal are produced. These signals are passed through simple low pass filters before being sampled by two 20 bit A/D converters at
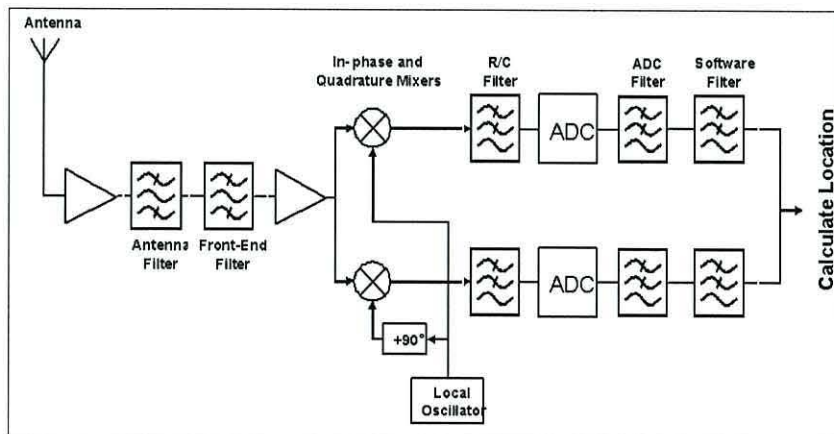
Fig. A.1 - Block diagram of Mk4 Locator.

5 kHz rate (this has change since to 2 kHz). The sampled signals are read by the processor, via LF data capture registers in the ASIC and then by one of the two DMA channels in the 68340 processor. The software then filters the signals and extracts the phase. The front end of the receiver is broadband, enabling the receiver to work over a wide range of frequencies (approx 130 – 160 kHz), though this means that the receiver must have strong signal handling capability, to avoid being overloaded by strong interfering signals. The dynamic range of the receiver is set by the A/D converters, 20 bits giving a dynamic range in excess of 100 dB. There is some filtering in the antenna amplifier and in the receiver front end and just prior to the A/Ds, but the majority of the filtering is done in software. The design allows for a second channel to be implemented, if required, to allow for a dual ferrite rod H-field antenna to be used.

A.2 LF Receiver Performance

Frequency Band:	120 to 180 kHz
Frequency Agility:	Software selectable over a single band 120 to 170 kHz. Hardware changes required outside this band
Dynamic Range:	80 dB (-20 to -100 dBm)
Phase Shift vs. Level:	Less than ± 1.8° over full dynamic range (< 10 millicycles)
Spurious Response Rejection:	< -70 dB
Third Order Intercept Point:	> 65 dB
Blocking:	-20 dBm for less than 1 dB compression interfering signal < 10 kHz from wanted signal
Input Impedance:	50 Ω

A.3 UHF Transmitter Performance

Radio Type Approval Standard:	ETS 300-113
Data Rate:	3,600 baud or 5,000 / 10,000 baud
Modulation Type:	2 or 4 level FSK using Raised Cosine Channel Response
Power Output:	10 W (nominal)

A.4 Environmental

Temperature:	- 20 °C to + 60 °C
Vibration, Bump and Drop:	To BS2011 Part 2
IP Rating:	IP 54

Appendix B

Specifications of the Datatrak Coverage Prediction Software

Project Outline
Datatrak Coverage Prediction Software

The phases described below are aimed at giving the company a useful software tool early in the project and as it is developed it will become applicable to more diverse network configurations in the future. It is envisaged that 1,2 and 3 will be completed quickly and 4 and 5 be the main body of the project.

Main Phases

1. Investigation, theoretical and practical, into how Datatrak currently predict coverage & performance.

2. Develop a software model to predict coverage based primarily on signal level. This model should take into account: radiated power, ground conductivity, atmospheric noise and typical vehicle-generated noise. This model should be further developed to take into account skywave (winter/summer) for the region being modelled, including atmospheric noise and interference. The skywave model should also define the ground/skywave phase cancellation zone. This should give us a tool that will enable us to predict Trigger/Data coverage for 'simple' networks.

3. Further develop this modelling tool to produce a simple accuracy contour map, based on LOP geometry, taking into account signal & noise level constraints, dropping out stations when appropriate. This will give us a tool that we can use with reasonable accuracy for 'simple' networks, enabling us to predict both Trigger and Data coverage, plus positioning accuracy. Validate this model against known performance from existing networks.

4. Develop this software further by introducing phase delays caused by variations in ground conductivity. This software should be able to generate a graphical output indicating phase delay variations for each transmitter station. From this we should be able to define areas of poor LOP alignment. This would be further enhanced by running the predicted phases through the least-squares algorithm, giving us a predicted error and a predicted measure of misalignment (confidence factor). A suitably accurate ground conductivity database that is available for Datatrak use, will be required for this. Validate this against existing networks where Station Offsets have been used (e.g. Northwest Europe).

5. Introduce a terrain database into this model, enabling us to predict Trigger and Data coverage, plus positioning accuracy in 'difficult' networks.

Deliverables

At agreed stages throughout the project, a documented copy of source and executable code should be made available to Datatrak, with guidance written and verbal given by the student, on how to operate the software. The final document deliverables will be as set down in Section 4.

Appendix C

Field Strength Measurements

This appendix details the equipment and the method used to measure signal field strength.

C.1 Equipment and Set-up

The Radionavigation Group has high-accuracy field strength measuring equipment. This consists of an Anritsu MS2667C Spectrum Analyser, and an Emco Model 6502 calibrated loop antenna mounted on a tripod, connected together using standard 50 Ω co-axial cable (Fig. C.1).

Being a calibrated loop antenna, it is possible to convert the voltage reading on the spectrum analyser directly into the signal-in-space field strength. At Datatrak frequencies (150 kHz), adding a calibration factor of 11.8 dB to the voltage reading given in dB-μV (dB relative to 1 μV) on the spectrum analyser given the signal field strength in dB-μV/m [115].

The spectrum analyser essentially has two modes of operation. The default mode is the frequency domain plot, where the spectrum analyser sweeps through a pre-defined frequency range, and plots the power levels as a function of frequency. This is useful for observing any interference in the Datatrak band (Chapter 8).

The MS2667C also has a time-domain mode, where the power level at a specific frequency is plotted as a function of time. This is especially useful for measuring the field strength of a Datatrak signal within the time-multiplexed sequence (e.g. measurements described in Chapter 4).

C.2 Making measurements

As the antenna is of the loop variety, it is directional. This means that in order for the antenna calibration factor to be valid, the position of maximum response must be
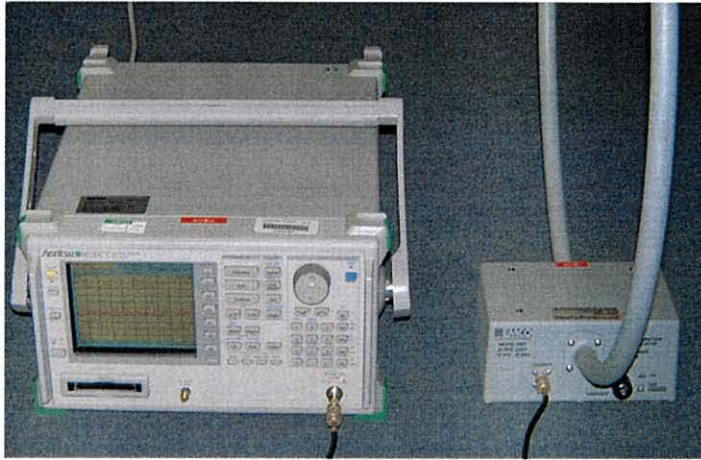
Fig. C.1 - Field strength measuring equipment: Anritsu spectrum analyser and Emco loop antenna.

pointing towards the radio source. To ensure that this is the case, the sharp null in the response is exploited. The antenna is turned until the field strength of the signal being measured reaches a minimum. From this position, the antenna is turned through 90°, and the maximum response is in the direction of the source, thus ensuring the calibration factor is valid.

The overload indicator on the calibrated loop antenna was checked at each site to ensure that it was operating in its linear range. It was found that it could operate at only 125 m from a UK Datatrak station without being overloaded.

Appendix D

Atmospheric Noise Model Manual Checks

D.1 Introduction

Below are a couple of examples to show that the automated atmospheric noise model built into the model works very well against the values manually determined from the ITU recommendation ITU-R P.372-7. The locations were chosen at random.

D.2 Example 1

Below are the model and manual atmospheric noise parameters for winter days between 0800-1200 hours local time. Location is 50°N, 0°E (south coast of England). Assumed receiver bandwidth is 160 Hz:

Parameter	Manual	Automated Model
F_{am} at 1 MHz from map (dB above thermal noise)	28.0	27.9
F_{am} at 150 kHz (dB above thermal noise)	76.0	76.5
D_u at 150 kHz (dB)	13.0	13.1
D_l at 150 kHz (dB)	8.2	8.2

Table D.1 - Atmospheric noise parameters for example 1 determined using manual means and the automated model.

D.3 Example 2

Below are the model and manual atmospheric noise parameters for summer days between 1600-2000 hours local time. Location is 50°S, 150°W (south of Australia). Assumed receiver bandwidth is 160 Hz:

Parameter	Manual	Automated Model
F_{am} at 1 MHz from map (dB above thermal noise)	50.0	51.5
F_{am} at 150 kHz (dB above thermal noise)	92.0	93.0
D_u at 150 kHz (dB)	13.0	13.2
D_l at 150 kHz (dB)	12.9	12.7

Table D.2 - Atmospheric noise parameters for example 2 determined using manual means and the automated model.

D.4 Conclusions

Clearly, the model is working well and giving results very similar to the manually determined values. The discrepancies are well within the accuracy of the data printed by the ITU. Since the technique is common to all seasons and locations, it can be concluded that the model is working correctly.

Appendix E

Calibration of Locator Internal Voltages to Signal Field Strength

E.1 Introduction

In this Appendix, the details of calibrating the signal voltages inside the Locator to the signal field strength are detailed. This was required in order to perform measurements under laboratory conditions, and relate them to the signal in space.

E.2 Method

This calibration was carried out at two sites, at ranges of 1.5 km and 6.2 km from the Southport Datatrak transmitter (Fig. E.1). At both these sites, the Datatrak signal field strengths were measured using the calibrated loop antenna and spectrum analyser operating in the time-domain mode (Appendix C). The Locator was opened up, and the signal level at the output of the pre-mixer amplifier was monitored; at this monitoring point the signal voltage is sufficient to be viewed reliably on the oscilloscope. Also, if the voltages are measured at this point, it removes the need to carefully match the impedances of the function generator at the Locator antenna input.
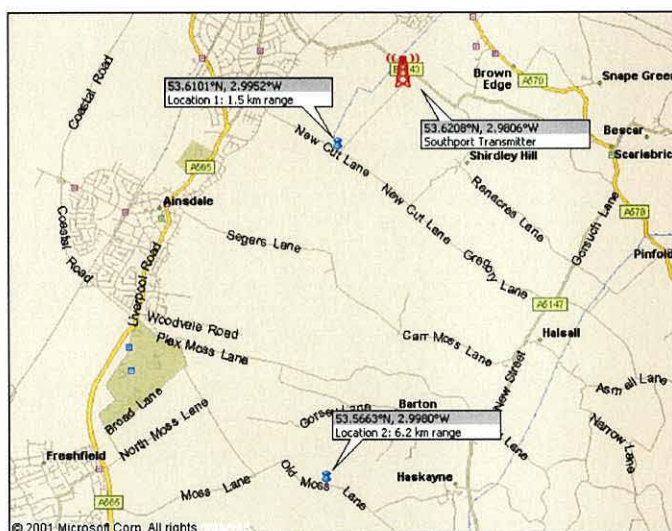
Fig. E.1 - Locations of Southport transmitter and two measurement points

	Range (km)	Field Strength (dB-µV/m)	Voltage at pre-mixer amplifier (dBm)	Calibration Factor (dB)
Location 1	1.5	91.8	-2.0	93.8
Location 2	6.2	78.8	-14.4	93.2

Table E.1 – Measuring the signal field strength to internal voltage calibration factor.

The input impedance of the oscilloscope was 1 MΩ, which is very high compared with the output impedance of the op-amp used by the pre-mixer amplifier (40 Ω maximum) [65, 66]. So, the voltages at this point in the circuit can be measured accurately with an oscilloscope. The peak voltages are converted to the equivalent value in dBm (dB above 1 mW RMS into 50 Ω load) using Equation (E.1):

$$V_{dBm} = 10\log_{10}\left(10V_{peak}^2\right) \tag{E.1}$$

where V_{dBm} is the equivalent voltage in dBm and V_{peak} is the peak voltage in volts.

E.3 Results

Table E.1 shows the field strength of the signal in space, and the voltage at the pre-mixer amplifier in dBm. At both locations, the calibration factor is calculated to be 93.5 dB (the average of the two measured values).

So, in the laboratory, when we add 93.5 dB to the measured value at the pre-mixer amplifier, we are able to calculate the equivalent field strength of the signal in space.

Appendix F

Modelled Emission Classes

F.1 Introduction

In Chapter 8, we saw that the power spectrum can be derived from the emission class of each interferer. In Table F.1, each identified emission class in the $50 - 550$ kHz band have been decoded, and allocated an appropriate spectrum type. The two-digit spectrum type defines the assumed power spectrum (number referring to the appropriate spectrum in Fig. F.1), and the type of power measurement (letter referring to the description in Table F.2). Using this information, together with relevant ITU documents, the distribution of normalised power between the carrier and sidebands can be deduced. These are given in the two right-most columns of Table F.1.

Emission Class	Description	Spectrum Type	Normalised Power	
			Carrier	Sidebands
A1A	AM, Double Sideband, Single channel containing quantised or digital information without the use of a modulating sub-carrier, Telegraphy - for aural reception	5 X	1.0	0.0
A1B	AM, Double Sideband, Single channel containing quantised or digital information without the use of a modulating sub-carrier, Telegraphy - for automatic reception	1 X	1.0	0.0
A2A	AM, Double Sideband, Single channel containing quantised or digital information with the use of a modulating sub-carrier, Telegraphy - for aural reception	1 Y	0.8	0.2
A2B	AM, Double Sideband, Single channel containing quantised or digital information with the use of a modulating sub-carrier, Telegraphy - for	1 Y	0.8	0.2

	automatic reception			
A3A	AM, Double Sideband, Single channel containing analogue information, Telegraphy - for aural reception	1 Y	0.8	0.2
A3C	AM, Double Sideband, Single channel containing analogue information, Facsimile	1 Y	0.667	0.333
A3E	AM, Double Sideband, Single channel containing analogue information, Telephony (including sound broadcasting)	1 Y	0.95^3	0.05^3
A7B	AM, Double Sideband, Two or more channels containing quantised or digital information, Telegraphy - for automatic reception	1 Y	0.667	0.333
A8E	AM, Double Sideband, Two or more channels containing analogue information, Telephony (including sound broadcasting)	1 Y	0.95	0.05
AXX	AM, Double Sideband, Other Signals, Type information not defined	1 Y	0.667^4	0.333^4
B8E	AM, Independent Sidebands, Two or more channels containing analogue information, Telephony (including sound broadcasting)	1 X	0.025^5	0.036^5
F1B	FM, Single channel containing quantised or digital information without the use of a modulating sub-carrier, Telegraphy - for automatic reception	4 Y	0.0	1.0
F1C	FM, Single channel containing quantised or digital information without the use of a modulating sub-carrier,	4 Y	0.0	1.0

---

[3] Assuming "voice"

[4] Assumed to be similar to "A3E" (i.e. sound broadcasting)

[5] Assumed reduced carrier, two voice channels

	Facsimile			
F3C	FM, Single channel containing analogue information, Facsimile	4 Y	0.0	1.0
F7B	FM, Two or more channels containing quantised or digital information, Telegraphy - for automatic reception	4 Y	0.0	1.0
FXX	FM, Other Signals, Type information not defined	4 Y	0.0	1.0
G1D	Phase Modulation, Single channel containing quantised or digital information without the use of a modulating sub-carrier, Data transmission, telemetry, telecommand	4 Y	0.0	1.0
G1W	Phase Modulation, Single channel containing quantised or digital information without the use of a modulating sub-carrier, Combination of information	4 Y	0.0	1.0
GXX	Phase Modulation, Other Signals, Type information not defined	4 Y	0.0	1.0
H2A	AM, Single Sideband, Full Carrier, Single channel containing quantised or digital information with the use of a modulating sub-carrier, Telegraphy - for aural reception	4 Y	0.91[6]	0.09[6]
H2B	AM, Single Sideband, Full Carrier, Single channel containing quantised or digital information with the use of a modulating sub-carrier, Telegraphy - for automatic reception	4 Y	0.91[6]	0.09[6]
H3E	AM, Single Sideband, Full Carrier, Single channel containing analogue information, Telephony	3 Y	0.91[7]	0.09[7]

---

[6] Assuming similar to "H3E"

	(including sound broadcasting)			
J3E	AM, Single Sideband, Suppressed Carrier, Single channel containing analogue information, Telephony (including sound broadcasting)	6 X	0.0^7	0.1^7
J7B	AM, Single Sideband, Suppressed Carrier, Two or more channels containing quantised or digital information, Telegraphy - for automatic reception	6 X	0.0^8	0.5^8
JXX	AM, Single Sideband, Suppressed Carrier, Other Signals, Type information not defined	6 X	0.0	0.5
K2A	Pulses, Modulated in Amplitude, Single channel containing quantised or digital information with the use of a modulating sub-carrier, Telegraphy - for aural reception	2 X	0.0	1.0
N0N	Unmodulated, No Modulating Signal, No information transmitted	5 Z	1.0	0.0
P0N	Sequence of Unmodulated Pulses, No Modulating Signal, No information transmitted	2 X	0.0	1.0
PXX	Sequence of Unmodulated Pulses, Other Signals, Type information not defined	2 X	0.0	1.0
R2B	AM, Single Sideband, Reduced or Variable Level Carrier, Single channel containing quantised or digital information with the use of a modulating sub-carrier, Telegraphy - for automatic reception	3 X	0.025^9	0.354^9

[7] Assuming voice

[8] Assuming two channels

[9] Assumed similar to "R7B"

R3E	AM, Single Sideband, Reduced or Variable Level Carrier, Single channel containing analogue information, Telephony (including sound broadcasting)	3 X	0.025[7]	0.071[7]
R7B	AM, Single Sideband, Reduced or Variable Level Carrier, Two or more channels containing quantised or digital information, Telegraphy - for automatic reception	3 X	0.025[8]	0.071[8]
XXA	Emission not defined by ITU, Other Signals, Telegraphy - for aural reception	2 X	0.667[10]	0.333[10]

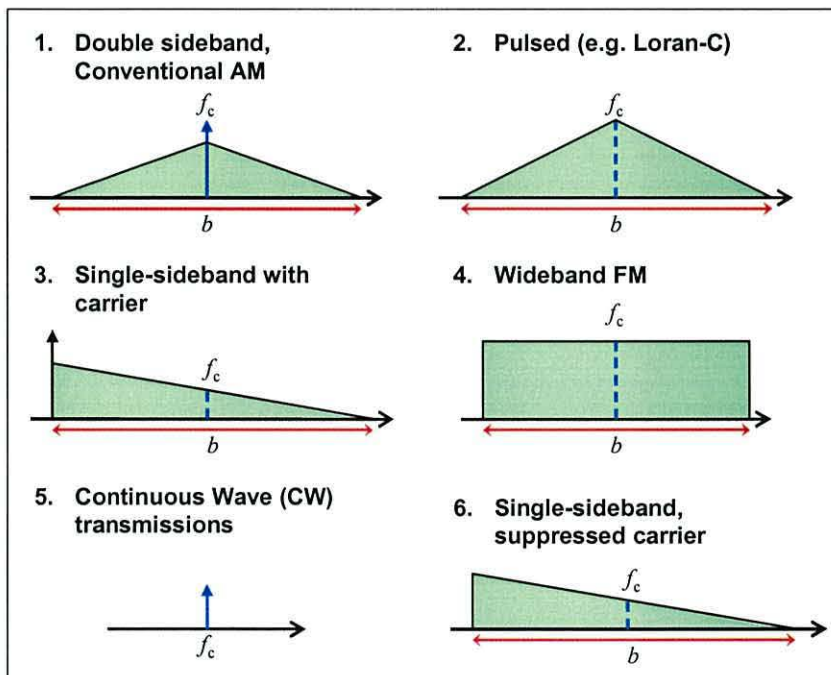**Table F.1 - Emission classes defined in the interferer model**

Fig. F.1 - Simplified power spectra used in the interference analysis; f_c and b are the centre frequency and bandwidth published in the IFL.

---

[10] Assumed to be "AXX" (i.e. typographical error in list)

Power Type	Description
X	**Peak Envelope Power**: the average power supplied to the antenna by a transmitter during one radio frequency cycle at the crest of the modulation envelope taken under normal operating conditions.
Y	**Mean Power**: the average power supplied to the antenna by a transmitter during an interval of time sufficiently long compared with the lowest frequency encountered in the modulation taken under normal operating conditions.
Z	**Carrier power**: the average power supplied to the antenna by a transmitter during one radio frequency cycle taken under the condition of no modulation.

Table F.2 - Power measurement types as defined by the ITU

Appendix G

Example Test of the FDR Algorithm

G.1 Introduction

In Chapter 8, we see that the FDR implementation in the model has been tested against theory. This Appendix shows the manual calculation behind the theory.

The situation is described in Fig. G.1. The interferer has a triangular power spectrum, 10 kHz wide, and a centre frequency, f_c. The receiver is assumed to have a perfectly rectangle frequency response, 10 kHz wide, centred on 140 kHz.

The graph in Fig. G.1 shows the FDR provided by the receiver as the interferer centre frequency is varied. The implementation of the model shows that a 6 dB point occurs when f_c is 133.55 kHz. We shall show the manual calculation to show that this is correct.

If P is the total interferer power within its bandwidth, b, then the peak power spectral
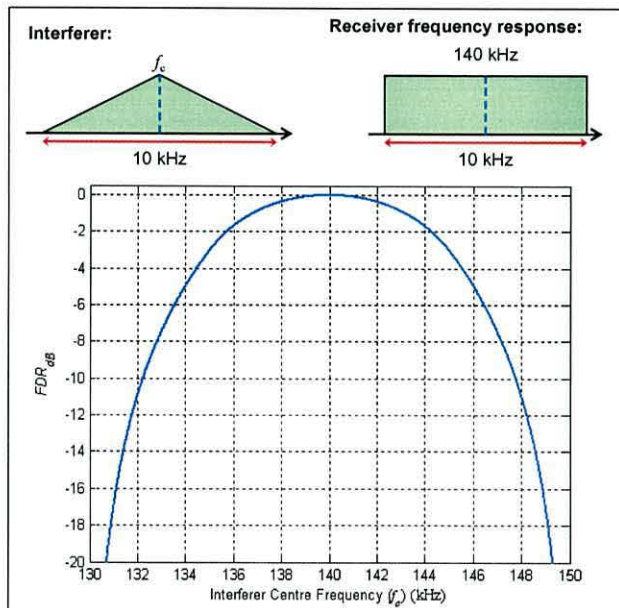

Fig. G.1 - Example interferer and receiver with the calculated FDR as a function of interferer centre frequency.
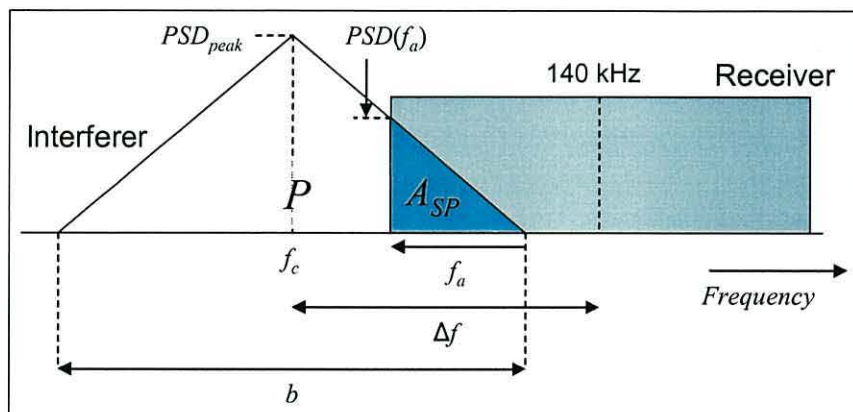
Fig. G.2 - Definition of terms to verify implementation of FDR algorithm

density (i.e. the power spectrum density at f_c) is:

$$PSD_{peak} = \frac{2P}{b} \qquad (G.1)$$

Now, if only quarter of the interferer power is penetrating the receiver (i.e. -6 dB), the situation can be shown as being that in Fig. G.2. The triangular form of the interferer power spectrum only slightly overlaps the filter passband of the receiver. The difference between f_c and the receiver centre frequency is Δf. The area marked A_{SP} represents the total power penetrating the receiver. We need to establish how this varies with Δf.

The gradient of the PSD in that section of the power spectrum can be calculated to be:

$$PSD_{gradient} = \frac{-PSD_{peak}}{\left(\dfrac{b}{2}\right)}$$

$$PSD_{gradient} = -\frac{2PSD_{peak}}{b} \qquad (G.2)$$

If we define f_a as the frequency range that the area A_{SP} covers with the origin at the point where the PSD is 0, the PSD at the *filter edge* can be found using the equation for a straight line:

$$PSD(f_a) = PSD_{gradient} \times (-f_a)$$

$$PSD(f_a) = \frac{-2PSD_{peak}}{b}(-f_a)$$

$$PSD(f_a) = \frac{4Pf_a}{b^2} \tag{G.3}$$

Now, the triangular area A_{SP}, which is the total power penetrating the receiver, can be calculated as follows:

$$A_{SP} = \frac{PSD(f_a) \times |f_a|}{2}$$

$$A_{SP} = \frac{2P}{b^2}f_a^2 \tag{G.4}$$

In our example, we need to know the value of f_a when $A_{SP} = \frac{P}{4}$. So,

$$\frac{P}{4} = \frac{2P}{b^2}f_a^2$$

$$\therefore f_a = \frac{b}{\sqrt{8}} \tag{G.5}$$

which we find that $f_a = 3535.53$ Hz in our example.

By observation, the difference in centre frequencies is:

$$\Delta f = \frac{b_{receiver}}{2} + \frac{b}{2} - |f_a| \tag{G.6}$$

where $b_{receiver}$ is the bandwidth of the receiver filter. In this example, $\Delta f = 6464.47$ Hz, which implies that the centre frequency of the interferer, f_c, when only quarter of the power is penetrating the receiver is $140000 - 6464.47 = 133535.53$ Hz, or 133.54 kHz.

This is very close to the value determined by the model of 133.55 kHz.

Appendix H

Description of Monteath's method

H.1 Integral Equation

This Appendix describes Monteath's method in greater detail. The technique is based on this integral equation:

$$G(R) = 1 - \sqrt{\frac{j\beta_0}{2\pi}} \int_0^R \left(\psi + \frac{\eta}{\eta_0} \right) \exp(-j\xi) \sqrt{\frac{R}{r(R-r)}} G(r) \, dr \qquad \text{(H.1)}$$

where $G(R)$ is the complex attenuation factor at the receiver, j is the imaginary operand, η is the surface impedance in ohms, η_0 is the intrinsic impedance of free space (120 π ohms), β_0 is the free space propagation constant:

$$\beta_0 = \frac{2\pi}{\lambda}$$

where λ is the free-space wavelength in metres. Other variables in Equation (H.1) are defined in Fig. H.1:

$$R = a\Phi \qquad \text{(H.2)}$$

$$r = a\phi \qquad \text{(H.3)}$$

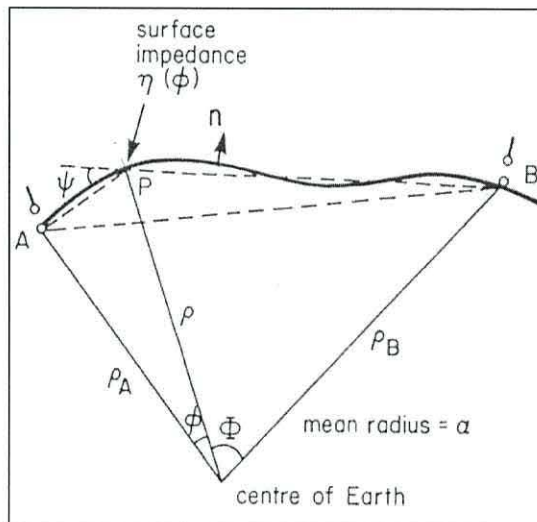$$\xi = \beta_0 \left[(AP) + (PB) - (AB) \right] \qquad \text{(H.4)}$$

Fig. H.1 - Definition of terms in Monteath's method (after Monteath [83])

where a is the mean radius of the earth along the path. The height of the receiver above the earth's radius is given by the terrain elevation database.

The relative surface impedance is given by:

$$\frac{\eta}{\eta_0} \cong \frac{1}{\sqrt{(\varepsilon_r + 1)}} \tag{H.5}$$

where ε_r is the complex permittivity, given by

$$\varepsilon_r = k - j1.8 \times 10^{10} \frac{\sigma}{F} \tag{H.6}$$

where k is the dielectric constant, σ is the conductivity in S/m, F is the frequency in Hz. The parameters k and σ are obtained from the Bangor ground conductivity database, enhanced by the presence of the coastline database.

H.2 Implementation

Monteath describes the implementation of Equation (H.1) so that it can be numerically evaluated on a computer. Equation (H.1) was converted into a sum:

$$G(ND) = 1 - BD^{\frac{1}{2}} \sum_{I=0}^{N} E(ND, ID) C(N, I) G(ID) \tag{H.7}$$

where D is the regular interval distance, and N is the total number of iterations (so, $ND = R$, and $ID = r$). Also,

$$E(ND, ID) = \left(\psi + \frac{\eta}{\eta_0} \right) \exp(-j\xi) \tag{H.8}$$

and $C(N,I)$ is a coefficient which takes into account the factor $\sqrt{\dfrac{R}{r(R-r)}}$ in the integrand. $G(ID)$ is the previous complex attenuation factor, hence the iterative nature of the method.

Monteath recommends that the regular interval distance satisfies Equation (H.9):

$$D < \frac{2a^2\lambda}{9R^2} \qquad (H.9)$$

For a typical Datatrak signal travelling to a range of 750 km, the interval distance should be less than about 32 km to ensure that the phase changes between computation points are not too large.

Appendix I

Details of Baseline Extension Measurements

I.1 Introduction

In this Appendix, details of the baseline extension measurements are given. Using phase difference techniques, information about the slave station and the path between the master and slave can be deduced. This information will prove invaluable to complete the modelling of a Datatrak network, and to verify the model.

I.2 Baseline Extension Measurements

The delay at a Datatrak slave station is an unknown quantity, and must therefore be measured so that the network model described in Chapter 11 is complete. A known method of measuring the station delay is to place a receiver on the baseline extension, and measure the phase *difference* between the synchronised master and slave pair (Fig. I.1).

The principle is based on the fact that the master-Locator and master-slave-Locator signal paths are the same. If the slave had no station delay (i.e. a perfect phase mirror), then the phase difference would be zero. Any delay at the slave station would cause a delay the slave-to-Locator signal, and a difference in phase would be observed.
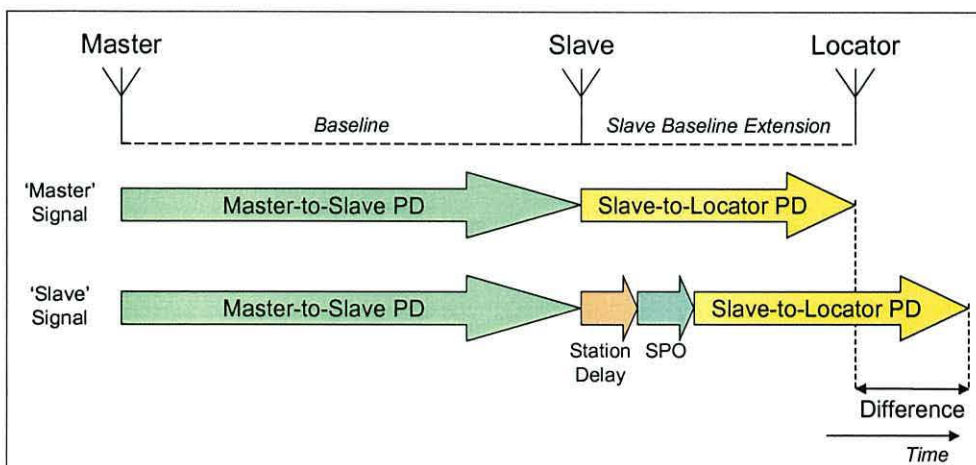

**Fig. I.1 - Principle of measuring the station delay at the slave station.
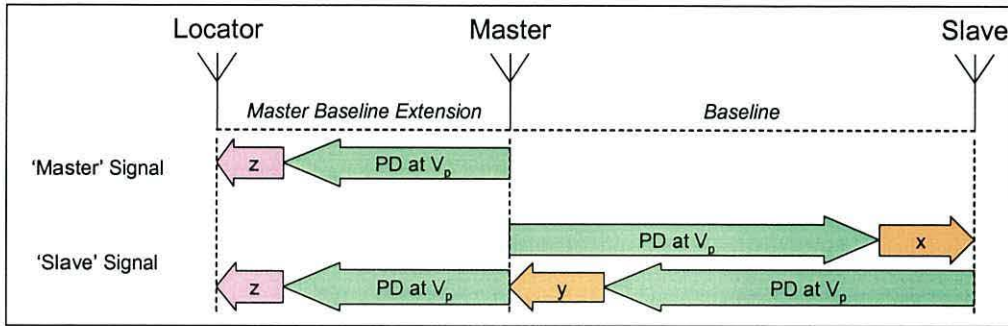PD: propagation delay.**

Fig. I.2 - Principle of measuring the V_p error between the master and slave stations. x, y and z are V_p errors. PD: propagation delay.

It should be noted that the measurements will include the station phase offsets (SPOs), as well as the station delay. The SPO values are known, and therefore the station delay can be calculated.

Similar phase difference measurements along the *master* baseline extension can reveal information about the signal propagation between the two stations. Fig. I.2 shows the principle. Along the baseline extension, the Locator will receive the master signal directly from the station. The Locator assumes a constant propagation velocity, V_p, to determine the range. However, the actual signal propagation velocity will vary with the nature of the ground, and so an error will appear. This is called the V_p error. For the master signal, the V_p error is marked as the 'z' purple arrow.

The slave signal represents the range from the master station to the slave station, and then to the Locator. Along the master baseline extension, the slave signal can be considered in three parts: master-to-slave, slave-to-master, and master-to-Locator. Because the path of the master-to-Locator section is identical to the master signal path, during the phase difference process, the 'z' V_p errors effectively cancel out. The propagation delays at V_p along the baseline are already taken into account by the Locator, and cancel out. The remaining measured phase difference is the sum of the 'x' and 'y' V_p errors which is used to calculate the average V_p error along the baseline.

One must be careful to ensure that the station delay and the SPO of the slave station are removed from the measured phase differences for the results to be correct. The effect of the non-linearity of signal propagation also needs taking into account (see Section 11.3.1.1).

I.3 Measurement Strategy

An Mk4 Locator with an H-field antenna (see Section 3.4.2) is used to record phase the phase difference between the master and slave signals. The magnetic-mount antenna was placed on the roof of the car, clear of other metal objects (e.g. car aerial). This also ensured it did not move during the measurement.

A differential-enabled GPS receiver was used as a location reference, as it is known to have an accuracy of better than 5 m, and sometimes better than 1 m. This level of accuracy will be sufficient as the Locator has a resolution of 1 millicycle (c2 m). We can expect an error of 1-2 millicycles due to Location uncertainty.

It was decided not to visit all Datatrak transmitters to conduct baseline extension measurements. For convenience, the five closest transmitters to Bangor were picked.

I.4 Measurement Location Requirements

When choosing a site to make these measurements, certain rules were observed in order to minimise any measurement errors.

I.4.1 Minimum distance from transmitter

The minimum distance allowed from a transmitter is dependent on two factors. Firstly, the Locator must be outside the transmitter near-field and near-far-field. This distance is based on the signal wavelength, and for the Datatrak system, the minimum is 970 m (for 133.2275 kHz).

Secondly, the field strength of the signal can cause the Locator to overload. This means that the Locator will be operating in a non-linear fashion, and the phase measurements will become meaningless. At Datatrak frequencies, the Locator overloads at a field strength of 121 dB-μV/m. The strongest transmitter is the Stratford station, with an effective radiated power of 85 W at 146.455 kHz. This means that the Locator must be at least 3.5 km away from any Datatrak transmitter in order to be sure that it is not overloading. Note, this does not mean that the Locator will not work within 3.5 km of a Datatrak transmitter. As the system uses a time-

division method of working, it is only the signal from the overloading transmitter that will not be usable.

I.4.2   Maximum distance from transmitter

The maximum distance from the slave is determined by the signal strength of the furthest station's signal. The further away from the transmitter, the lower the field strength, and therefore the signal-to-noise ratio (SNR). A reduction in SNR will cause a higher uncertainty in the phase measurement. Therefore, it is decided to tolerate 10 dB reduction in the furthest transmitter field strength, relative to its value at the closest transmitter. Master stations are typically 150 km away from the slave transmitter. At this range over average soil conductivity (3 mS/m), the field strength drops by 10 dB over a distance of 30 km. So, a 30 km range limit from the closest transmitter is placed on the measurement.

I.4.3   Power lines and buildings

Certain obstacles such as power lines and buildings can cause localised phase disturbances. This is due to the metal structures picking up the radio signal, and reradiating it, causing an area of phase distortion. It is important to be outside such areas, and as a rule-of-thumb, it is accepted that a measurement site should be at a distance of at least three times the height of the power line/building.

Also, any areas that appear to contain high radio frequency noise sources must be avoided, in order to prevent any uncertainty in the phase measurements. The level of noise is monitored to ensure that it does not affect the measurements.

I.4.4   Lateral distance away from baseline extension

Ideally, the measurements would take place on the baseline extension. Unfortunately, this cannot always be arranged. So, a limit on the distance away from the baseline extension must be observed. By analysing the way in which the phase difference increases as the Locator moves away from the baseline extension, a maximum distance from it can be determined. It was decided that a maximum of 10 millicycles of error would be tolerated. Any greater tolerance and the phase delay error might start to influence the station delay measurement. At 3.5 km (the minimum distance), a

lateral displacement of 450 m will produce an error of 10 millicycles at 146.455 kHz. Therefore, the measurements should be within 450 m of the baseline extension.

I.4.5 Time of day

The measurements must be made during the day. This is to minimise the effects of skywave on the measurements, and causing uncertainty in the phase measurements. The allowed time of day is generally dependent on the time of year and latitude. A location near Chester was used as the 'average' location of the measurements. At the time of the measurement (January 2003), the sun rises at 0800 GMT and sets at 1650 GMT. An hour after sunrise and an hour before sunset, the skywave level is negligible [49]. Therefore, the measurements should not commence until after 0900 GMT and finish before 1550 GMT.

I.4.6 Somewhere to park

Perhaps an obvious requirement for measurement, but an area where the car can be park safely is required. On the side of a busy road is not ideal, and can be dangerous. Our safety and that of other road users is a priority.

I.5 Measurement Locations

The locations used during the measurement campaign are detailed in Table I.1. At each site, at least 1 hour of measurements were taken, equal to just over 2000 readings. This number of readings should be enough to remove most of the uncertainty in the measurement due to noise and interference.

I.6 Conclusion

These baseline extension measurements have proved useful in completing the network model and verified the model. The results of the measurements are recorded in Chapter 11.

Name	Location	Latitude (°N)	Longitude (°E)	Range to Closest Transmitter	Purpose
Stratford	Site 1	52.1384	-1.5912	5.9 km	Huntingdon-Stratford Slave Baseline Extension
	Site 2	52.1221	-1.7520	17.1 km	Huntingdon-Stratford Slave Baseline Extension
	Site 3	52.0963	-1.5806	7.6 km	Stratford-Asserby Master Baseline Extension
	Site 4	52.0300	-1.6788	17.6 km	Stratford-Asserby Master Baseline Extension
Cowbridge	Site 1	51.4189	-3.5647	5.4 km	Stratford-Cowbridge Slave Baseline Extension
	Site 2	51.4258	-3.5331	3.1 km	Stratford-Cowbridge Slave Baseline Extension
Southport	Site 1	53.5333	-2.9664	9.7 km	Southport-Carlisle Master/Slave Baseline Extension
	Site 2	53.5160	-2.9580	11.7 km	Southport-Carlisle Master/Slave Baseline Extension
	Site 3	53.6418	-3.0249	3.8 km	Huntingdon-Southport Slave Baseline Extension
Cumbria	Site 1	54.9126	-3.1933	5.6 km	Southport-Carlisle Master/Slave Baseline Extension
	Site 2	54.9527	-3.2005	10.1 km	Southport-Carlisle Master/Slave Baseline Extension
Asserby	Site 1	53.3063	0.2877	5.2 km	Stratford-Asserby Slave Baseline Extension
	Site 2	53.2958	0.2768	3.9 km	Stratford-Asserby Slave Baseline Extension
	Site 3	53.2395	0.3014	5.9 km	Cumbria-Asserby Slave Baseline Extension

Table I.1 - Location sites used during the baseline extension measurement campaign.

Appendix J

Coordinate Conversion between Ellipsoids

J.1 Introduction

The model uses the WGS84 reference ellipsoid for calculating the arc distances between two points. However, the Locator employs different ellipsoids in different networks, to ensure that the arc distance calculation is the most accurate for the given area.

A coordinate conversion routine is required to make sure that all the computation points in the model are translated to the appropriate coordinates in the Locator. Once the Locator was produced its position, the position fix is then converted back to the equivalent in WGS84.

J.2 Helmert's Formula

The coordinate conversion is based on Helmert's formula [110]:

$$
\begin{bmatrix} X \\ Y \\ Z \end{bmatrix}_{New} = \begin{bmatrix} X \\ Y \\ Z \end{bmatrix}_{Original} + \begin{bmatrix} \mu & +\varepsilon_Z & -\varepsilon_Y \\ -\varepsilon_Z & \mu & +\varepsilon_X \\ +\varepsilon_Y & -\varepsilon_X & \mu \end{bmatrix} \begin{bmatrix} X \\ Y \\ Z \end{bmatrix}_{Original} + \begin{bmatrix} \Delta X \\ \Delta Y \\ \Delta Z \end{bmatrix} \tag{J.1}
$$

where $[\ldots]_{New}$ are the Cartesian coordinates of the converted position on the new ellipsoid, $[\ldots]_{Original}$ are the Cartesian coordinates of the original position, μ is a scaling factor, $\varepsilon_{X,Y,Z}$ are rotational factors, and ΔX, ΔY, ΔZ are shifts in origin.

Assuming a height of zero, the elements of $[\ldots]_{Original}$ is given by:

$$
X = v \cos \phi_o \cos \lambda_o \tag{J.2}
$$

$$
Y = v \cos \phi_o \sin \lambda_o \tag{J.3}
$$

$$
Z = v \left(1 - e^2 \right) \sin \phi_o \tag{J.4}
$$

where ϕ_o and λ_o are the latitude and longitude of the point on the original ellipsoid in radians, v is the radius of the curvature in the prime vertical:

$$v = \frac{a_{axis}}{\sqrt{1 - e^2 \sin^2 \phi}} \qquad (\text{J}.5)$$

where a_{axis} is the semi-major axis of the original ellipsoid, e is its eccentricity:

$$e^2 = f_e \left(2 - f_e\right) \qquad (\text{J}.6)$$

where f_e is the flattening of the original ellipsoid:

$$f_e = \frac{a_{axis} - b_{axis}}{a_{axis}} \qquad (\text{J}.7)$$

where b_{axis} is the semi-minor axis of the original ellipsoid.

The scaling, rotational and origin shift terms are available from document [110]. However, Datatrak have already obtained these parameters for use within the Locator to combine GPS coordinates with the LF ones. For example, to convert from the Airy spheroid (as used in the UK) to WGS84, the parameters are: $\Delta X = 364.7$, $\Delta Y = -109.42$, $\Delta Z = 429.00$, $\varepsilon_X = 0$, $\varepsilon_Y = 0$, $\varepsilon_Z = -0.156$, and $\mu = 1.2$ (parts per million).

Once $[...]_{New}$ has been calculated using Equation (J.1), it must be converted to geographical coordinates on the new ellipsoid. The process is iterative if height above the ellipsoid is required [110], but the Locator simply calculates a two-dimensional position, and height is assumed to be 0. This actually has very little effect on the calculated position, as determined in [117]. So,

$$\phi_{new} = \arctan\left(\frac{Z}{\sqrt{X^2 + Y^2}\left(1 - e^2\right)}\right) \qquad (\text{J}.8)$$

$$\lambda_{new} = \arctan\left(\frac{Y}{X}\right) \qquad (\text{J}.9)$$

where ϕ_{new} and λ_{new} are the latitude and longitude of the point on the new ellipsoid in radians, X, Y, Z are the elements of $[...]_{New}$ and e^2 is calculated with Equation (J.6), but with f_e determined by the semi-major and semi-minor axes of the new ellipsoid.

Appendix K

Locator Slot Selection

K.1 Introduction

In Chapter 3, we described the timing sequence of signals from Datatrak transmitters. Nominally, eight stations transmit on f_1 in the first half, before transmitting on f_2 in the second half.

K.2 More stations?

However, a restriction of this method is that only eight stations can be used in a network, otherwise stations would interfere with each other. To overcome this, Datatrak use an 'interlace' method. While eight stations transmit on f_1, another eight can transmit on f_2, and visa versa during the second half of the timing sequence; thus doubling the number of possible transmitters used in the network. Since the Locator only has a single local oscillator (LO), it cannot simultaneously tune to both f_1 and f_2 transmissions. So, it must choose which transmissions it wants to listen to, and retune the LO accordingly during the timing sequence.

K.3 UK Network

This is the situation in the 13-station UK network. A station occupies one or more transmission *slots*, numbered 1 to 16. Stations that have slots numbered 1 to 8 all transmit on f_1 in the first half, then on f_2. Stations that have slots number 9 to 16
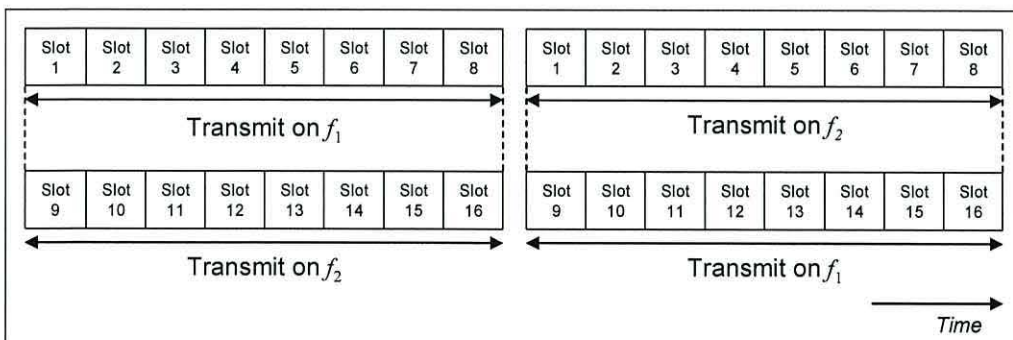

Fig. K.1 - Interlaced timing sequence showing simultaneous transmission of two slots on different frequencies.

Name of Station	Transmission Slot	Master Slot
Huntingdon	1	N/A
Selsey	2	1
Kent	3	1
Stratford-upon-Avon	4	1
Lowestoft	5	1
Asserby	6	4
	16	10
Southport	7	1
	13	10
Cowbridge	8	4
Cumbria	10	7
Greenock	12	10
Alnwich	11	10
Kingsbridge	14	4
Stonehaven	15	10

Table K.1 – Allocated UK station transmission and master slots.

transmit on f_2 first, then on f_1. Fig. K.1 shows the principle as a timing diagram. So, if the Locator chooses to use the station transmitting on slot 7, it cannot use a station transmitting on slot 15 because it is transmitting on the other frequency at the same time.

Table K.1 shows which transmission slots the UK stations are allocated, and which slots their master uses. For example, the signal from Lowestoft transmits only on slot 5 that is synchronised to the signal on slot 1, which is Huntingdon. Most stations only transmit on a single slot and so only have one master. When it comes to calculating the link bias error [Equation (11.7)], the procedure is simple.

However, two stations in the UK transmit on two slots (Asserby and Southport), each with a different master. So, the link bias error will depend on which slot the Locator chooses from these stations. The reason for doing this is to ensure that six stations can be selected without any slot clashes occurring.

The Locator has rules which define which slots it will use in the position fix. They are [118]:

- Select the nearest 6 stations.
- If a station has two slots, pick from slots 1 - 8 first.

- If there is a slot clash (e.g. 7 and 15) and there is an alternative slot available from one of the stations, use that.
- Don't use stations above the distance limit.

The Southport transmitter transmits on slots 7 (master: Huntingdon station) and 13 (master: Cumbria station). In the south where most of the stations transmit on slot numbers 1 to 8, the Locator will use slot 7 from Southport. However, as the Locator moves North, the nearest six stations will contain a station transmitting on slot 15 (Stonehaven in Scotland). This clashes with the first choice of slot 7 from Southport. Since there is an alternative slot available from Southport (slot 13), the Locator will choose that instead.

K.4 Implementation

These rules, along with the information in Table K.1, have been implemented in the model so that it correctly simulates the operation of the Locator. The link bias errors are calculated by following the chain of stations that the slot represents. Using the rules, the model selects the correct slot (and hence the link bias error) from each station, and uses it to calculate the position fix in the Virtual Locator.

Appendix L

Publications

Below is a list of papers co-authored by the candidate during the course of the research detailed in this Thesis. The full text of the papers follows.

L.1 Conference Papers

- Last, J.D., Williams, A.I. & Cousins, N., 'Coverage and performance of the Siemens-Datatrak vehicle location system', NAV02 Conference on GNSS Vulnerability, Royal Institute of Navigation, London, 5-7 Nov, 2002
- Last, J.D., Grant, A., Williams, A. & Ward, 'Enhanced accuracy by regional operation of Europe's new radiobeacon differential system', ION GPS 2002

Coverage and Performance Model for the Siemens Datatrak Vehicle Location System

Professor David Last
Alwyn Williams
University of Wales, Bangor, Gwynedd, United Kingdom

Nigel Cousins
Siemens Datatrak Location and Information Systems Ltd

Abstract

The Siemens Datatrak automatic vehicle location system (AVLS) was originally designed as a high reliability tracking solution for cash-in-transit vehicles in the UK. As GPS has increasingly been employed for the less-demanding, low-cost, location and tracking applications, Datatrak's exceptionally high availability and low vulnerability have made it an attractive solution for applications that demand the highest standards. As a result, its coverage is being expanded into other countries, where it is employed both independently and in co-operation with GPS.

The Datatrak system uses a network of LF transmitters positioned to optimise tracking performance. The mobile units are equipped with exceptionally narrow-band receivers that establish the vehicle's position by making phase comparisons between the signals from these stations. Location measurements and other data are then sent to the control centre via highly-redundant uhf links that employ precise timing controlled by the low-frequency network.

The process of designing the new Datatrak networks now being planned is a complex one, especially as coverage must be optimised whilst minimising the number of transmitter sites. This paper presents a new coverage and performance prediction model developed for this purpose by the authors. The model employs data from International Telecommunications Union sources and from Datatrak's own extensive monitoring records. It predicts, point-by-point through arrays that span the region, the groundwave and skywave field strengths of each of the transmissions, and the levels of atmospheric and vehicle noise. It also considers the complex interference received from the many stations with which the system shares its frequency band, taking into account the high rejection of the narrow-band receiver. At each geographical point, the quality of the navigation signals is determined in this way. Then, by mimicking the operation of the receiver, the model determines the repeatable location accuracy obtained. The paper describes the ideas and techniques used in the model, and demonstrates its use in quantifying the performance of the UK Datatrak system.

Introduction

The Siemens Datatrak automatic vehicle location system (AVLS), which has been in operation in the UK since 1989, provides high-security tracking for cash-in-transit vehicles and other applications [1]. In the past few years, Datatrak has expanded to cover parts of Europe, South Africa, and Argentina. The system comprises three major components: the *navigation network*, the *data network*, and the *display system*.
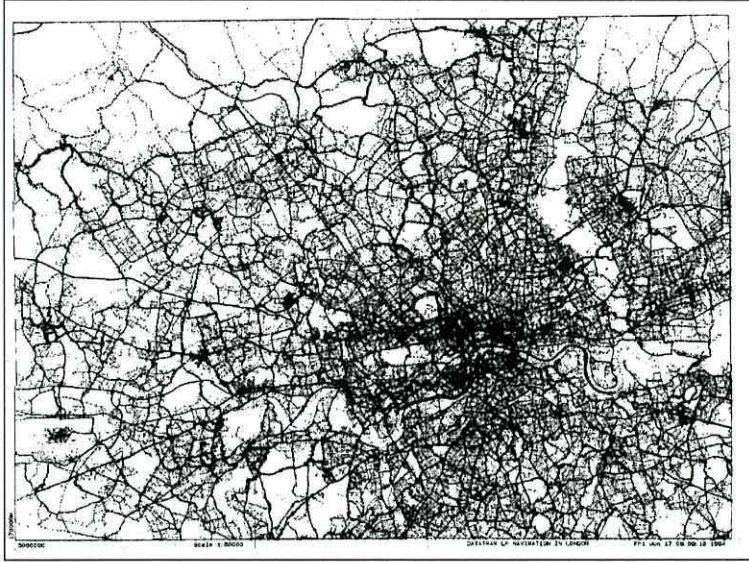
Fig. 1: Position fixes of mobile units in London over 2 months. The figure is built up solely from the individual fixes; there is no map background.

The *navigation network* employs a group of synchronised, low power, low frequency (LF) transmitters that emit phase-modulated signals. These stations spaced approximately 160km apart, radiate on two frequencies (f_1 and f_2) in the 130-180kHz band, in a time-multiplexed sequence. The system originally operated as a hyperbolic navigation system, but has recently changed to pseudo-range operation.

Vehicle-borne units measure their own positions using the LF signals. The *data network* carries this position information, and other data, to a control centre. It employs a large number of UHF base stations [2]. The data network is synchronised to the navigation network, each mobile transmitting in a unique time slot. The network is very robust, with most mobile transmissions being received by more than one base station. Once position data has been received at the control centre, it is forwarded to the *display system* of the customer. There, positions are usually presented on a graphical display, with maps of various scales. Alternatively, vehicles' identities and locations are tabulated. In all cases, the information is accessible in a format the customer requires, often interfacing with a proprietary control system.

System security and performance

Because the system tracks cash-in-transit vehicles, security is paramount. High security and integrity are maintained through the use of the narrow-band LF transmissions and redundancy throughout the system. The relatively high field strengths and low frequencies of the navigation signals minimise the effectiveness of jamming. Redundancy in the data network makes the reception of mobile position data highly probable. All LF transmitters have

duplicate electronics, with automatic switch-over, to safeguard against hardware failure. Planned or unplanned station outages are notified via the LF network to the mobiles, which reconfigure their operation accordingly.

The great benefit of an LF navigation system is that the signals penetrate urban areas much better than do GPS signals. Fig. 1 shows this dramatically; it is a plot of the position readings of every mobile in London area over two months. Features such as Regents Park, Hyde Park and the Thames stand out. Also striking is the absence of rogue positions in the park areas.

Datatrak LF signals

This paper is concerned with the Datatrak LF navigation system, which will now be described in more detail. A Datatrak mobile determines its own position by receiving the signals from a number of ground stations and measuring their phases against an on-board clock. From knowledge of the velocity of propagation, it computes a pseudorange from each station. Cycle ambiguities are resolved first by comparing the phases of the signals at the two Datatrak frequencies, which differ by approximately 10%, and then by use of 40 Hz phase modulation of the transmissions. Pseudoranges from the strongest and nearest stations, together with knowledge of the stations' precise locations, are then employed to compute the mobile's position. Two of the Datatrak stations also distribute system timing information to the receivers.

The strength and quality of the highly stable LF groundwave signals received at a mobile from the transmitters depend, by day, on the radiated powers of the stations and the ground conductivity of the signal path. At night, skywave-propagated components become significant and can cause phase errors and amplitude fading. Noise received is both atmospheric and man-made, principally from vehicles. The Datatrak frequencies are adjacent to signals from many other radio services, which can cause interference. As signal-to-noise ratio falls, the error in the timing measurements increases, and hence the uncertainty in the pseudoranges from which the mobile's position is computed. This causes an increase in position measurement error, the repeatable accuracy being dependent on the geometrical dilution of precision at the location.

Existing Datatrak networks have been designed to maintain high signal-to-noise ratios and minimise skywave errors. But when a new network is being planned, we ask: where should the transmitters be sited; what power needs to be radiated to provide the required coverage; what levels of noise should be anticipated; and what are the likely sources of interference? The answers to these questions determine the resulting repeatable accuracy. This paper describes software that allows the operation of proposed systems to be modelled with confidence, and the network design optimised.

Modelling the System

The model has been developed at the University of Wales. It draws upon experience built up from the development and extensive use of models of two other LF systems: Loran-C [3] and DGNSS radiobeacons [4]. The software uses a system of arrays, or *layers,* that hold information on the groundwave field strength, skywave field strength, noise and interference surrounding each transmitter. Fig. 2 illustrates the concept. Each array consists of a grid of points, spaced by 0.1° in latitude and longitude (approximately 11x7 km at UK latitudes).
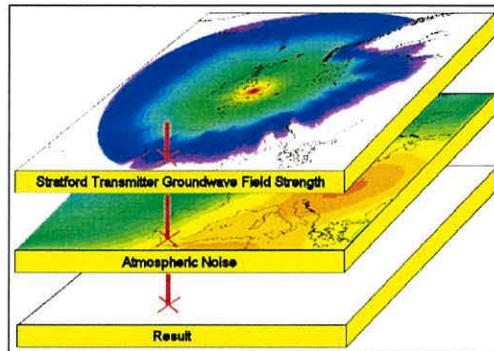
Fig. 2: Layers structure used in the prediction model, showing here the layers
required to calculate the daytime signal-to-atmospheric noise ratio of the signal
from a transmitter near Stratford upon Avon, UK

An array of groundwave field strength values is first computed for each station, using built-in databases of ground conductivity derived from International Telecommunication Union (ITU) data [5]. A skywave array is then created using ITU ionospheric data [6]. A further array maps the spatial variations of atmospheric noise [7], and the model also holds a database of potential interferers [8]. Once the appropriate set of databases has been created, the various parameters are examined at each geographical point in turn. The strengths of the groundwave and skywave components of a station's signal are extracted from the arrays and compared with the strengths of atmospheric noise, vehicle noise, and interference to establish the ratios of groundwave-to-skywave, signal-to-noise (SNR), and signal-to-interference (SIR). From these we compute the pseudorange uncertainty of that station. This process is carried out for all stations that contribute to the position fix. The dilution of precision (DoP) for those stations is then computed and the position error statistics calculated from the pseudorange uncertainties and the DoP. The results are then mapped as accuracy contours. The edge of coverage is that contour at which the repeatable accuracy has fallen to a value of 100m at 95% confidence. We separately compute *timing coverage areas* for the two stations that distribute system timing. The limit here is a minimum SNR or SIR of 15 dB.

Groundwave field strength

Fig. 3 shows how the groundwave field strength of a 1kW, 150 kHz, transmitter varies with distance and ground conductivity. The curves are fifth-order polynomials fitted to the ITU curves for their 8 standard levels of ground conductivity [9]. Millington's method is employed for inhomogeneous paths, as recommended by the ITU. For each Datatrak frequency pair, a set of curves at the mean frequency is used; this is sufficiently accurate. Sets of such curves have been generated for the frequency pairs employed by Datatrak systems in various countries. Conductivity values are taken from the *Bangor Ground Conductivity Database*, with its resolution of 0.1° in latitude and longitude [3].
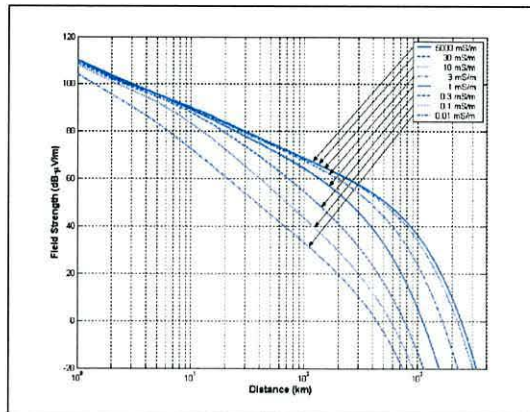
Fig. 3: Variation of groundwave field strength with distance and ground conductivity

The Datatrak transmitter is at the centre of the array of calculation points, and the attenuation of the signal from the transmitter to each point in turn is calculated. Since groundwave propagation is very stable with time, these arrays can be stored for repeated use, the actual field strengths being computed using the transmitter radiated power. The results have been verified by comparison with measurements made at various points in the United Kingdom.

Fig. 4 shows contours of field strength from one of the UK Datatrak transmitters computed by the model. Note the higher field strengths of signals propagating along the Bristol Channel compared with those that have crossed the low-conductivity land of Devon and Cornwall.
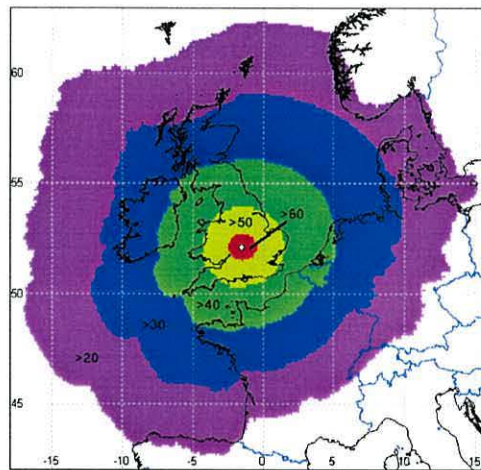

Fig. 4: Contours of groundwave field strength (dBμV/m) of
Datatrak transmitter near Stratford upon Avon, UK. Radiated power is 70W.

Skywave field strength

At night, the skywave component of the Datatrak signal is significant. In contrast with the stable groundwave signal, the field strength of the skywave varies stochastically, the mean level being a function of the time of day, season of the year, and point in the solar cycle. The ITU have published a method, based on extensive measurements, of calculating the field strength not exceeded for various percentages of the time [6]. In Fig. 5, the light blue curve is the skywave field strength not exceeded 50% of the time by a 1kW, 150kHz, transmitter, at geomagnetic latitude of 55° (a value typical for the UK). The value exceeded 95% of the time, in red, was computed by assuming a Gaussian distribution with time [4].

Own-skywave interference

Fig. 5 shows that the field strength of the skywave signal may become comparable to those of groundwave component (dark blue or green) with increasing range from the transmitter. Because the skywave path is many wavelengths longer than the groundwave, the phase difference between the two components is randomly distributed. The received signal is the vector sum of the two components. Thus the *phase* of the resultant is that of the groundwave plus a variable stochastic term, the magnitude of this disturbance being a function of the skywave-to-groundwave ratio (SGR). The *amplitude* of the resultant also varies; when the two components are of comparable size there may be substantial fading. The statistics of these phase disturbances and amplitude variations are built into the model, the analysis being based on that of Poppe [4].

Fig 6 shows the predicted total field strength exceeded 95% of the time over sea-water, conductivity 5000 mS/m, (yellow) and very low conductivity land (purple). Over such land, substantial fading and phase disturbances can occur as close as 50 km from the transmitter. Existing Datatrak networks have typical ground conductivities in the range 1 to 10mS/m, and so these effects only become significant at distances over 200km. Over sea-water, they occur at even greater distances.
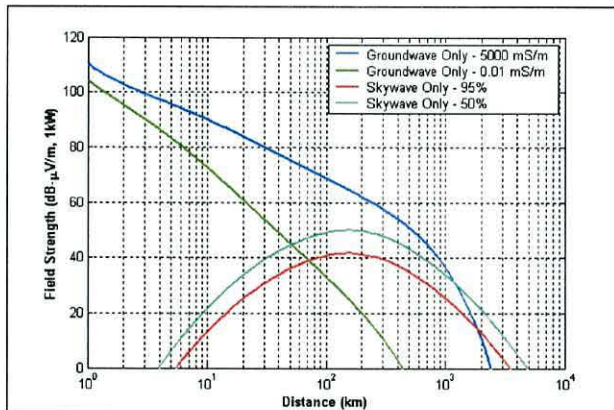

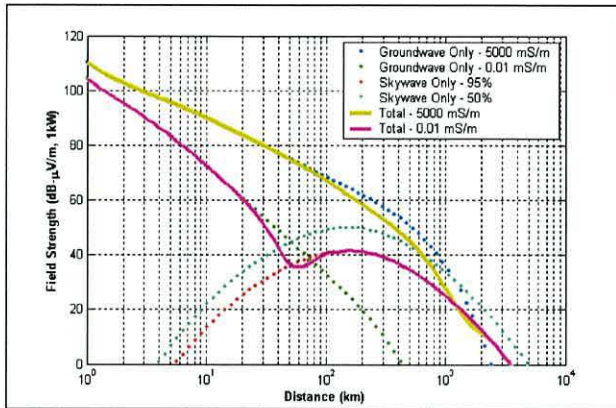*Fig. 5: Skywave and groundwave field strength variations with range*

Fig. 6: Total field strength (groundwave and skywave) exceeded 95% of the time

Radio noise

Three kinds of noise affect the Datatrak system: *atmospheric noise*, local *vehicle noise*, and *receiver noise*. The ITU publish maps and charts showing the diurnal, seasonal and annual variations of atmospheric radio noise, based on extensive measurement programmes [7]. The model employs a computerised version of the ITU data [10] that allows it to compute the atmospheric noise likely to be experienced by a Datatrak receiver anywhere in the world. Fig. 7 maps typical results across northwest Europe: it shows the level in dBµV/m not exceeded 95% of the time throughout the year.

Datatrak have conducted extensive measurements of the levels of *vehicle noise* experienced by their locators, which includes contributions from nearby buildings. The value rarely exceeded in the UK is 27 dBµV/m and this value is used by the model as a default value. The *receiver noise* is characterised by a noise floor, which is built into the model. In most urban situations, *vehicle noise* is dominant.
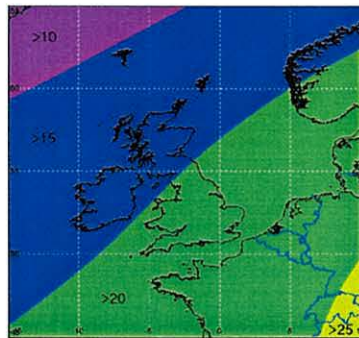

*Fig. 7: Atmospheric noise (dBµV/m) not exceeded 95% of the time throughout the year*

Interference

The Datatrak signals occupy frequencies within a band that contains a wide range of radio services, using various bandwidths and types of modulation. To calculate the SIR of the signal from a Datatrak station at an array point, the model must estimate the strength of the Datatrak signal itself, and the level of energy in its narrow pass-band from each potential interfering station. Current receivers employ a total of 5 filters; we created an overall response curve which allows the model to compute the rejection of any off-frequency signal, in accordance with a method recommended by the ITU [11]. A second interference mechanism is also taken into account: blocking of the front end of the receiver, ahead of most filtering, by a very strong local signal.

The model employs a database of all transmitters worldwide in the frequency range 50-540 kHz, listed in the ITU International Frequency List (IFL) - more than 19,000 transmissions [8]. The spectra of most transmissions are much wider than the Datatrak receiver channel. Thus it is necessary to establish the energy distribution across each transmission so that the power within the receiver bandwidth can be computed [12, 13]. The modulation of each station was determined from its *emission class* in the IFL, and its power spectrum classified according to one of six basic forms (eg Fig. 8).

The model estimates the strengths of both groundwave and skywave components of potential interferers at each array point using the same ITU methods as for the beacon itself. Filter rejection is then taken into account and an *effective interferer field strength,* and hence the SIR, computed.

The model is, of course, only as accurate as the database it uses and the IFL contains many uncertainties: missing beacons, listed beacons no longer on the air, and confusion between transmitter output power, radiated power, and effective radiated power! In establishing interference, the model first rejects the very many interferers that are too distant, too low-powered, or too far from the operating frequency to cause problems. The few remaining stations are then investigated carefully to resolve uncertainties and ensure their database entries are as accurate as possible.
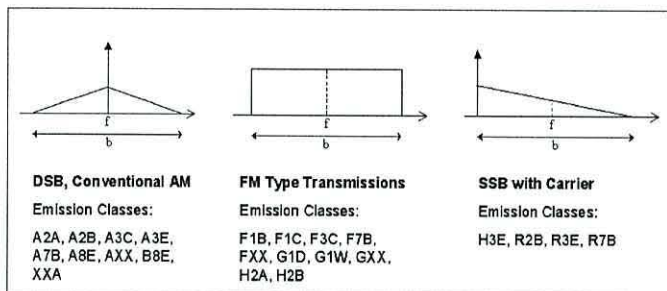
Fig. 8: Three of six types of power spectrum modelled in the software.
Published centre frequency: f, bandwidth: b.

Coverage of the timing signal

All factors that determine the strength of the Datatrak signal, and the noise and interference levels, having been analysed, the coverage of the timing signal can be determined. The receiver requires at least 15dB SNR and SIR. The model establishes conditions at each array point and produces a coverage contour. Fig. 9 shows the results for the Stratford upon Avon station by day, and also by night when skywave effects reduce the wanted signal and can increase the interference. Note that this is the service area of one of two timing stations, and *not* the coverage of the UK Datatrak network.
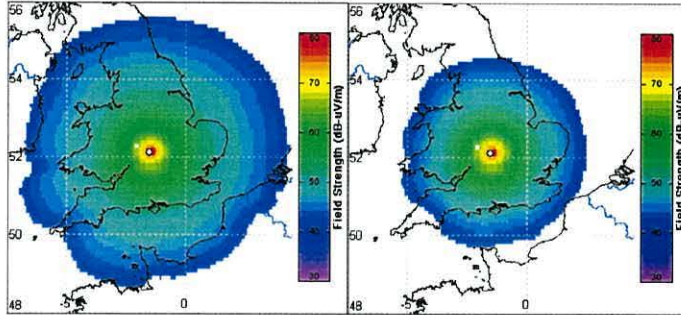

Fig. 9: Daytime (left) and night-time (right) service area of timing transmission from Stratford upon Avon Datatrak station.

Repeatable accuracy

A Datatrak mobile employs the phase of the groundwave signal to determine its range from each station. The ranges (strictly *pseudoranges* since they include clock bias errors) are then used to work out its location, and clock corrections. Uncertainties in these phase measurements causes uncertainties in the pseudoranges and hence in the resulting position fixes. The *repeatable accuracy* of the fix at a given location thus depends on the ratio of the wanted groundwave signal to all disturbing factors; we will refer to this as the groundwave-to-interference ratio, *GIR*. There are three such disturbing factors: the beacon's own skywave; atmospheric noise; and interference from other stations. By day the first of these factors, and the skywave component of the third, may be neglected. Fig. 10 shows the variation of the standard deviation of the range uncertainty with GIR. It is applicable to all three disturbing factors.

The model establishes at an array point, for a given station, the values of all wanted and unwanted factors and so determines the range uncertainty. The process is repeated for all stations. Receivers compute their positions using a weighted least-squares solution, similar to that employed by many GPS receivers. The choice of stations included, and of weighting factors, depends on the proximity of each station and the quality of its signal. The model takes these factors into account, mimicking the receiver. It finally computes the repeatable accuracy of the resulting position fix by estimating the horizontal dilution of precision (HDOP) from knowledge of the stations' locations.
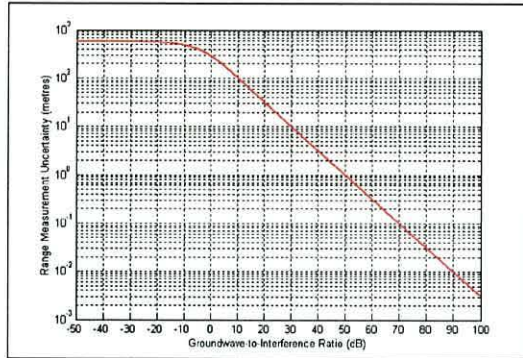
***Fig. 10: Variation of standard deviation of range measurement uncertainty (in metres)
with groundwave-to-interference ratio; UK network, f₁ frequency.***

Fig. 11 shows the daytime predicted repeatable accuracy obtained using selected UK network
transmitters. The outer boundary is the 100m, 95%-confidence, contour. The results in
Fig. 11 are supported by data from the Datatrak system monitors. Further detailed verification
measurements are being made in other areas of the UK.

The model has used extensively in the design of new Datatrak systems. The software is
extremely flexible: a user can change station locations, power levels, and many receiver
parameters, via a Windows interface. Thus, many plots may be produced in the process of
optimising a new system.

Future developments

A phase delay prediction model is being built that will take into account not only ground
conductivity but also topography. This new model will predict phase correction values to be
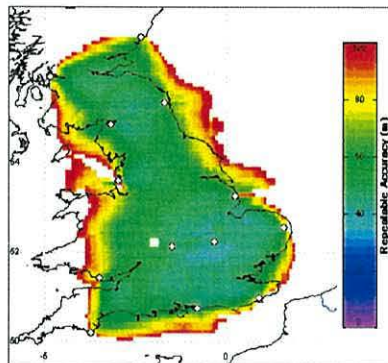employed by receivers, so further enhancing accuracy.

***Fig. 11: Predicted repeatable accuracy of position fixes using selected transmitters of the
UK Datatrak system***

Conclusions

The model described in this paper has been designed to predict the coverage and performance of the Datatrak location system. The wanted groundwave field strength of the signals is determined using published data by the ITU. The levels of various disturbances (own-skywave, radio noise, and interference) are also estimated. From the resulting signal-to-interference ratios, the coverage of the timing signal can be determined. The model can also calculate the pseudorange uncertainties and, by mimicking the signal processing in the receiver and from knowledge of the stations' locations, the repeatable accuracy of mobiles' position fixes can be computed. Siemens Datatrak have already made extensive use of this modelling software to investigate both potential new networks and the possibility of extending existing networks. In the past the uncertainty and risks involved in this activity meant time-consuming desk studies and speculative in-country surveys. This software allows Datatrak to condense much of these activities to a few hours of modelling work.

Acknowledgements

References

1.   Scorer, T. & Last, J.D; *The current status of the Securicor Datatrak system*; J. Roy. Inst. Nav., 48, 2, pp204-214; May 1995

2.   Last, J.D. & Wade, M; *Vehicle tracking – Is GPS always best?*; Vehicle tracking and fleet management colloquium; IMechE Conference 'Autotech 97', Birmingham, 4-6 Nov, 1997

3.   Farnworth, R.G.; *Loran-C coverage prediction in Western Europe*; Ph.D. Thesis; University of Wales, Bangor; January 1992

4.   Poppe, D.C.; *Coverage and performance predication of DGPS systems employing radiobeacon transmissions*; Ph.D. Thesis; University of Wales, Bangor; October 1995

5.   International Telecommunication Union; *World atlas of ground conductivities*; Rec. ITU-R P.832-2; 1999

6.   International Telecommunication Union; *Prediction of sky-wave field strength at frequencies between about 150 and 1700 kHz;* ITU-R P.1147-1; 1999

7.   International Telecommunication Union; *Radio noise*; Rec. ITU-R 372-7; 2001

8.   International Telecommunication Union; *Radiocommunication Bureau International Frequency Information Circular (Terrestrial Services)*; November 2000

9.   International Telecommunication Union; *Ground-wave propagation curves for frequencies between 10 kHz and 30 MHz*; ITU-R 368-7; 1992

10.   http://www.itu.int/ITU-R/software/study-groups/rsg3/databanks/ionosph/index.html

11.   International Telecommunication Union; *Frequency and distance separations*; ITU-R SM.337-4; 1997

12.   International Telecommunication Union; *Spectra and bandwidth of emissions*; ITU-R SM.328-10; 1999

13.   International Telecommunication Union; *Determination and measurement of the power of amplitude-modulated radio transmitters*; ITU-R SM.326-7; 1998

Enhanced accuracy by regional operation of Europe's new radiobeacon differential system

David Last, Alan Grant and Alwyn Williams, *University of Wales, Bangor, UK*
Nick Ward, *Trinity House Lighthouse Service, UK*

BIOGRAPHIES

Professor David Last has a Personal Chair in the University of Wales and is Head of the Radio-Navigation Group at Bangor. He holds the BSc(Eng), PhD and DSc degrees. He is a Fellow and former Senior Vice-President of the Royal Institute of Navigation, a Fellow of the Institution of Electrical Engineers, a Chartered Engineer, and Vice-President of the International Loran Association. He acts as a consultant to companies and to governmental and international organisations. He is an instrument-rated pilot and user of terrestrial and satellite navigation systems.

Alan Grant received the degree of BSc (Hons) from Staffordshire University in 1999 and is studying for a PhD at the University of Wales, Bangor. He is a member of the Royal Institute of Navigation, the Institute of Navigation, the Institution of Electrical Engineers and the Institute of Electrical and Electronic Engineers.

Alwyn Williams received the degree of MEng (Hons) from University of Wales, Bangor in 2000. He is currently studying for a PhD at Bangor. He is a member of the Royal Institute of Navigation, the Institution of Electrical Engineers and the Institute of Electrical and Electronic Engineers.

Dr Nick Ward is Principal Development Engineer for the General Lighthouse Authorities of the UK and Ireland, specialising in radionavigation. He is Chairman of the International Association of Lighthouse Authorities' Radionavigation Committee which co-ordinates the development of Differential GNSS. He is a Fellow of the Royal Institute of Navigation and a Member of the ION.

ABSTRACT

The maritime radiobeacon differential GNSS service in Europe has expanded very rapidly in the last two years. In September 2001, a new frequency plan was brought into effect across the whole of the European Maritime Area (EMA). This resulted in reduced levels of interference and enhanced coverage. There are now 162 maritime differential beacons positioned so that, as far as possible, all critical coastal locations are served by at least two stations.

Along many coastlines, inevitably, three or more beacons can now be received simultaneously. Indeed, by day when coverage is greatest, more than 20 signals are available at some locations. This provides an opportunity to make use of multiple transmissions. With the ending of Selective Availability, spatial dilution of position has come to dominate the accuracy of radiobeacon differential fixes. We have proposed using these multiple sources of pseudorange corrections in a Regional Area Augmentation System (RAAS) to minimise spatial dilution. The approach would be similar to that demonstrated successfully on a larger scale with Loran-C in the Eurofix system.

The paper presents the results of measurements made simultaneously on groups of radiobeacon stations under various receiving conditions. It demonstrates the degree to which RAAS processing of the results enhances position accuracy. In this work, the results from several receivers were combined. The same effect could be achieved with a multi-channel receiver, or by combining the data at a central point and re-broadcasting the result.

Using recently-developed mapping techniques, the paper then analyses the availability of multiple beacon signals across the EMA and maps the areas in which enhanced performance is expected to be available using this new RAAS mode of operation by day and by night.

INTRODUCTION

Differential Global Satellite Navigation Systems (DGNSS) employ the principle that the main sources of error in satellite navigation are consistent over large geographical areas. These errors can be corrected by using reference stations at known locations to measure the satellites' pseudorange errors. They transmit corrections to users' receivers, which adjust their

2723

236

position measurements accordingly. The advantages of DGNSS are improved accuracy and integrity.

One of the oldest radio aids-to-navigation technologies, that of marine radiobeacons, is widely employed to transmit DGNSS corrections for maritime users [1,2]. In Europe and North America, the recent expansion of the numbers of beacons in this system has ensured that, at most locations, at least one DGNSS beacon can generally be received [3]. Frequently there is a choice from several. It is customary to use the nearest beacon that provides a signal meeting the appropriate standards, with the second-nearest acting as an alternate.

This paper questions whether that is the best policy. A user who can receive several beacons simultaneously has access to corrections from a number of geographically-separated reference stations. Working satellite-by-satellite, it should be possible to compute a best set of corrections for the user's actual location. This is analogous to the use of a wide-area augmentation system (WAAS), and very similar to the use of a regional area augmentation system (RAAS), such as Eurofix [4]. We explore in this paper the question of whether corrections computed using a number of radiobeacon stations can be more accurate than those from the alternate beacon - or even corrections from the nearest beacon.

COVERAGES OF BEACONS

The radiobeacon band supports three types of transmission: marine radiobeacons (MB), aeronautical non-directional beacons (NDB) and differential radiobeacons (DGNSS). The area within which the signal of any of these services provides satisfactory coverage is determined by minimum standards laid down by the International Telecommunication Union (ITU), the International Civil Aviation Organisation (ICAO), the International Association of Lighthouse Authorities (IALA) or, in the US, the US Coast Guard [5-9]. Within the European Maritime Area (EMA) of the ITU Region 1 [5], the field strength and signal-to-atmospheric noise ratio of each service must exceed the minima shown in Table 1 [7,8]. The signal-to-interference ratio (SIR) must exceed the appropriate protection ratio in Table 2; these values are derived from the minimum performance standards for receivers [10]. Thus, for a geographical point to be deemed to lie within the coverage of a DGNSS beacon, the beacon's field strength there must be not less than $10\mu V/m$ ($20dB\mu V/m$), or a higher figure specified by the national administration. The SNR must be not less than 7dB. Finally, no interfering signal may exceed the protection ratios shown in Table 2.

In computing the coverage area of a beacon, we estimate the level of its signal point-by-point throughout an array centred on the station. By day, this strength depends on the radiated power of the station, its distance and the nature of the propagation path. At night, signal

components are also received from the beacon via ionospheric propagation. The intensity of these skywave components depends on range, latitude, time of day and season of the year. Skywave will interfere with the groundwave, causing fading. We customarily compute the signal level from the beacon that can be guaranteed for at least 95% of the time at night. This value is weaker than that of the daytime groundwave.

Table 1

	Units	Marine (MB)		Aero (NDB)	DGNSS
Min. Field Strength	µV/m	N of 43°N	50	70	10
		S of 43°N	75		
	dB µV/m	N of 43°N	34	37	20
		S of 43°N	38		
Min. SNR	dB			15	15	7

Minimum field strength and SNR for MB, NDB and DGNSS services in the European Maritime Area of ITU Region 1 [3,8,11].

Table 2

Wanted signal:	Marine (MB)	Aero (NDB)	DGNSS	
Interfering signal:	Any	Any	MB or NDB	DGNSS
Separation (kHz)				
0	15	15	15	15
0.5	-39	15	-25	-22
1	-60	9	-45	-36
1.5	-60	2	-50	-42
2	-60	-5	-55	-47
2.5	-	-12.5	-	-
3	-	-20	-	-

Protection ratios (dB) for minimising interference between interfering and wanted beacons of various types [8,11].

The intensity of the atmospheric noise is also estimated at each array point; it varies in a random fashion, its mean value over an interval being a function of geographical location, time of day, and season of the year. The values of the wanted signal and the atmospheric noise determine whether or not the point lies within the 'interference-free' coverage of the station.

It is customary to compute the daytime and night-time coverages separately. Daytime coverage is determined

by the groundwave signal strength, and night-time coverage by the weaker 95%-ile of the fading signal.

At each point we also estimate the level of any interference from stations on the same frequency as the beacon, or on adjacent frequencies. Interference may be received via either a groundwave or a skywave propagation path, or both. We assess whether the strength of the interference relative to that of the wanted beacon exceeds the protection ratio in Table 2, taking into account both the transmission types of the two stations and their frequency difference. With skywave interference, we use the signal level not exceeded more than 5% of the time. The coverage of the beacon is then that part of the interference-free coverage within which no protection ratio is infringed. These techniques are employed in the widely-used Bangor Coverage Prediction Software for DGNSS Beacons [12-14].

GROWTH OF DGNSS IN EUROPE

By 1998, many European administrations had either closed, or were planning to close, their maritime DF services and were introducing new, or additional, DGNSS beacons. This provided an opportunity for designing a completely new frequency plan for the radiobeacon band in Europe. The object was to reduce the very high levels of skywave-borne interference between beacons that share channels, and so maximise range and performance. Without this reorganisation it was clear that this interference – already at unacceptable levels - would increase significantly, since most of the new DGNSS beacons would be of substantially higher power than the old marine beacons they replaced.

In order to co-ordinate this reorganisation, IALA first requested each administration in the EMA to submit details of its future requirements. The result was a list of 427 beacons in total. It contained a massive increase in the number of DGNSS beacons, from the previous 62 to 154, and an equally dramatic cut in marine beacons, from 226 to just 77. The new band-plan would need to pack these 427 stations into the 64 available channels. But among these stations were also 196 aeronautical NDBs which had to be left on their existing frequencies. So, too, would 26 MBs located in countries whose administrations had not responded to IALA's request. The new band-plan would have to accommodate all these stations.

The tool developed for the unique task of fitting these many stations into these few frequencies in such a way as to minimise mutual interference, was a set of Optimisation Software [15,16]. This employed the groundwave and skywave modelling techniques of the Bangor Coverage Prediction Software to estimate the potential for interference between each beacon and every other beacon. It took into account both groundwave and skywave propagation, and in both directions. The software then employed a novel algorithm to find the allocation of beacons to channels that minimised mutual interference, a task that was mathematically NP (Non-deterministic Polynomial)-Complete.

This process was successful. When tested on the population of the band before re-organisation, it produced a dramatic reduction in the level of interference. Whereas previously certain stations had lost 90% of their coverage to interference, with the reorganised band-plan no station lost more than 6%. The software was accepted by IALA and used to generate the new band-plan, which was first published for comment by administrations, and then implemented. Across Europe, beacons changed to their new frequency allocations on 18 & 19 September 2001.

A CHANGING RADIOBEACON DGNSS SERVICE

Since the reorganisation, a number of administrations have added further DGNSS beacons. The current population of the band is 461 stations: 162 DGNSS beacons, 143 MBs and 146 aeronautical NDBs [17]. The locations of all these stations are shown in Fig. 1.
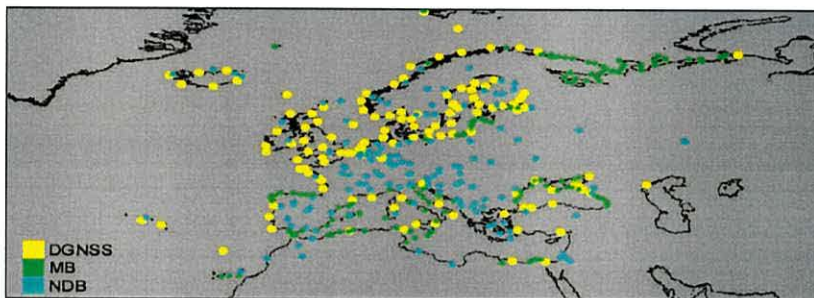

Fig. 1: The 461 beacons of the European Maritime Area radiobeacon frequency band

The development of this large number of new stations has fundamentally changed the nature of the DGNSS service in Europe. In most coastal locations, and over large inland areas, several beacons can now be received simultaneously. This has raised the question for users: which is the best beacon to use. The present authors have developed a further software model that answers this question [18,19]. At all locations across the EMA, it identifies the best beacon, and also the best alternate should that beacon not be available. We have shown that, in general, the best beacon at any location is the nearest beacon that meets international standards: specifically, that has a sufficiently-high signal-to-atmospheric noise ratio, and signal-to-interference ratio, to meet the time-to-alarm requirement. Identifying this beacon is a complex matter that requires analysis point-by-point. The software designed for this process employs a more advanced architecture than that for determining coverage. It is capable of giving access to the groundwave and skywave field strengths of all beacons simultaneously, since this is necessary for identifying the best beacon.

In this paper, however, we question whether using the best beacon guarantees the most accurate position fix. The reason for choosing the *nearest* beacon (provided it meets the time-to-alarm requirements) is that the accuracy of radiobeacon DGNSS fixes is now dominated by spatial dilution of precision of the corrections. The degree of dilution increases with the distance of the receiver from the reference station. This dominance of spatial dilution is in marked contrast to the traditional situation: in the days of selective availability (which was a major factor driving the growth of the radiobeacon DGNSS system) it paid to use the beacon with the highest SNR and SIR, thus minimising the error rate of the messages and so the latency (ie delay) of the corrections. In that way, the effects of the rapidly-changing errors due to SA were minimised by differential operation, and the accuracy of the fixes thus maximised.

But, if we truly wish to minimise spatial dilution of precision could we not do better than using the nearest station - or the next nearest, if the nearest is unavailable? If, as a result of the growth in the numbers of stations, we now have access to multiple sets of correction data, could we not compute the best set of data for the receiver's actual location? After all, that is essentially what happens in a wide-area augmentation system such as WAAS [20] or EGNOS [21]. It is also the basis of Eurofix [4]; as with radiobeacon DGNSS, Eurofix employs a series of independent Local Area Augmentation (LAAS) reference stations, each co-sited with its own transmitter - a Loran station. The Eurofix user receives a number of these stations simultaneously and computes the corrections at his location using these multiple sets of data. In Eurofix, this is called a RAAS – a Regional Area Augmentation System [4].

Let us explore whether we can turn our radiobeacon DGNSS LAAS system into something better? And even

if users would not have sufficient stations everywhere, where could we expect improved accuracy from doing so? We also sought to know whether there are snags, such as clock bias differences between the stations, that would prevent this idea succeeding?

We decided first to identify the areas in which users enjoy the benefits of multiple stations; that could be done using our new-architecture software. Then we would try out the idea using off-air signals. We would attempt to answer the questions: is the concept feasible; is it worthwhile; and, if so, where will it work?

NEW SOFTWARE ARCHITECTURE

The Bangor Coverage Prediction Software was designed to identify the coverage area of a single beacon. By computing the coverage of each member of a group of beacons in turn, it can also generate their combined coverage. But if we are to consider the use of multiple beacons at a point where more than one signal is available, we require simultaneous access to data on all those beacons at that point. Achieving that goal required the development of a new and different software architecture that will now be described briefly.
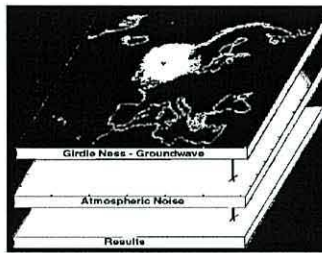

Fig. 2: New software architecture employs a three-dimensional array. This simple example has just three layers. They hold the groundwave strength of a single beacon, the atmospheric noise, and (in the results layer) coverage computed using the first two.

The factors that determine the coverage of a beacon have been identified as the field strengths of: the beacon's groundwave and skywave, atmospheric noise, and the groundwave and skywave components of all potential interferers. The groundwave and skywave field strength distributions of each beacon are first pre-computed at every point in a very large array, spaced by 0.1° of latitude by 0.1° longitude. This array covers an area exceeding that of the European Maritime Area (EMA).

The array structure (Fig. 2) is three-dimensional. The computed groundwave distribution of each beacon is stored in a single level (the top level in this figure). Since there are hundreds of beacons in the EMA, the structure must be capable of accommodating hundreds of such

levels. The skywave distributions are stored in a further such set of levels. The atmospheric noise distribution across the area is contained in a single additional level (the middle one in this figure).
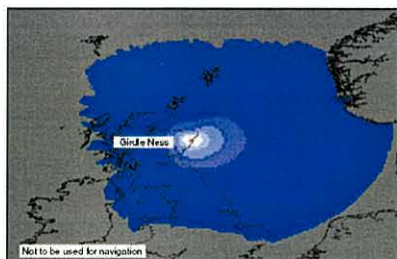

Fig. 3: Groundwave field strength contours of a beacon at Girdle Ness, Scotland. The outer boundary is the limit of daytime interference-free coverage computed using data from top two layers in Fig. 2.

We can choose to extract and plot the data from a single layer - as in Fig. 3, which shows contours of the groundwave field strength of a beacon, taken from the top layer in Fig. 2.

Likewise, by accessing point-by-point the groundwave, skywave, atmospheric noise and interference relevant to a single beacon, we can plot its coverage. For example, the top two layers in the figure contain sufficient data for producing a plot of the simple interference-free groundwave coverage. In Fig. 3, the region within the outer boundary of the contour plot is that coverage. At all points within it, both the field strength (top layer) and signal-to-atmospheric noise ratio (top and second layers) meet the international standards.

This three-dimensional, multi-layer, structure is the tool we need to help us identify the number of beacons that provide coverage simultaneously at any point.

SERVICE FROM MULTIPLE BEACONS

We ran the software analysing at each location in the array, and for each beacon, whether all criteria for coverage were met. That is: whether the field strength exceeded its minimum, including taking fading into account at night; whether the signal-to-atmospheric noise was adequate; and whether all signal-to-interference ratios exceeded their appropriate protection ratios. This latter check involved analysing the groundwave signals from every other beacon, plus at night the skywaves too. In this way, we established beacon-by-beacon whether the array point lay within the beacon's service area. Finally, we totted up how many beacons provided service simultaneously at that point.
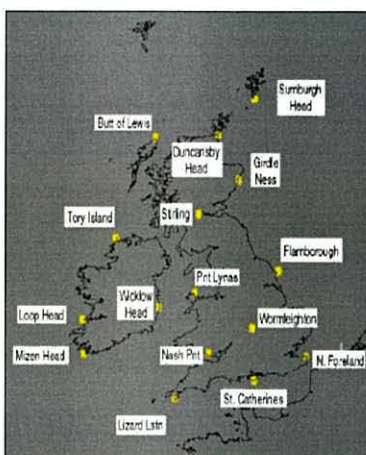

Fig. 4: The 16 DGNSS beacons that serve the British Isles (Duncansby Head and Wicklow Head are planned but not implemented)

This computation was first carried out using just the system of 16 beacons designed by the General Lighthouse Authorities (GLAs) to serve the United Kingdom and Ireland (Fig. 4). Of these beacons, 14 are now on air and two are yet to be installed. The result of the computation is shown in Fig. 5. The number of beacons simultaneously available varies from just one, in regions close to the edge of coverage, to 7. A large proportion of the critical coastal areas, and of the land areas, are served by at least three beacons. Whilst not all beacons are available everywhere all the time, we have shown recently that availability levels of individual beacons generally exceeds 99.5% [22]. Thus, there is a very high probability in practice of these numbers of beacons' signals being available simultaneously.

We now extended the analysis to the whole of the European Maritime Area, with its 162 DGNSS beacons. Fig. 6 shows the result by day when, in many areas, there are large numbers of beacons with overlapping coverage. The greatest concentration - in the North Sea - is 23! By night, of course, many fewer signals that meet the minimum standards are available because of fading of the beacons' signals, and an increase in skywave-borne interference from distant co-channel stations. Nevertheless, there are still many areas with simultaneous coverage from multiple beacons.
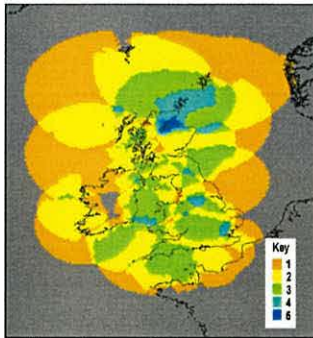
2727

Fig. 5: Number of GLA beacons available simultaneously (worst case, at night), including stations at Wicklow and Duncansby Head that are planned but not implemented

These analyses have shown that over large areas of the EMA at least three signals are available with a quality that will ensure a high availability of correction messages. We will now employ the signals at one such location to explore the degree to which the use of these multiple signals is both possible and advantageous.

TEST RESULTS

Tests were carried out at our laboratories in Bangor, North Wales (N53°13, W004°08). The nearest DGNSS station is Point Lynas, at just 23km range. By day, Bangor lies within the coverage of 7 stations: Point Lynas (primary), Nash Point (alternate), Flamborough Head, Lizard, Tory Island, Stirling and Wormleighton (Fig. 4). At night, only Point Lynas meets all coverage criteria. The strongest of the other beacons just fails to meet the 95% skywave-borne interference criterion. As we will see, this does not prevent these other beacons being used in a regional area augmentation system.
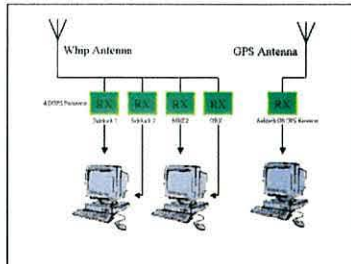

Fig. 7: Experimental set-up for testing RAAS concept

We set up the equipment shown in Fig. 7: four DGNSS radiobeacon receivers (two Cambridge Engineering Sidekick receivers, a CSI MBX2, and a CSI GBX). We also installed an Ashtech G8 GPS receiver. We allocated one beacon receiver to the nearby station of Point Lynas and the others to Wormleighton, Stirling and Loop Head (Fig. 4). Each of these stations is equipped with Trimble 4000MSK Reference Station equipment and transmits Type 9-3 messages at a data rate of 100 bps. We recorded the RTCM data from the beacon receivers, and the full data output stream of the GPS receiver, for 24 hours. The tests were conducted in August 2002.

The RTCM data sets from the four beacon receivers were converted to text format. The results, in the form of pseudo-range corrections (PRCs) and range rates (RRs) were entered into a Microsoft Excel spreadsheet for processing. Since the reference stations are not synchronised in such a way that they broadcast the PRCs of a given satellite simultaneously, we first processed the data so as to enable us to compare PRC values that were as close to simultaneous as possible. The time-skews were less than 10s. Post-SA, PRCs vary very slowly; our measured average range rate was only 0.027m/s; thus, the errors resulting from using PRCs that were not precisely simultaneous should have been less than 0.3m, even with the maximum time-skew.
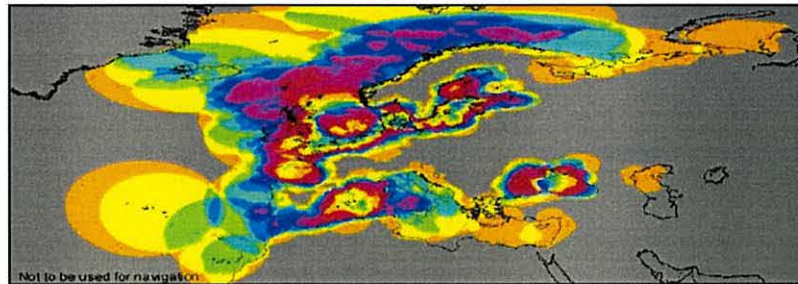

Fig. 6. Numbers of beacons available throughout the EMA under daytime conditions [22].

We were concerned about clock bias differences between the reference stations. A clock bias error results in an equal shift of all PRCs from the station. They are of little significance when radiobeacon DGNSS is used in its conventional way, with all corrections being taken from a single station, since the result is a small error in the time output of the navigation solution, not in the position. In the same way, when we come to combine PRCs from multiple stations, clock bias errors should not matter provided we use the same proportions of each station's PRC for all satellites. But such bias errors could mask the small differences in PRCs between stations that we wish to investigate in this study.

To estimate the magnitudes of any such clock bias components, we first computed for each station the average of all PRCs, for all satellites, over the 24 hours. The reasoning was that, with stations located relatively close together like these, the effects of location on these averages should be very small and differences between averages would be due principally to clock bias discrepancies.

Table 3

Station	PRC average	Distance from Point Lynas (km)	Weighting factor
Wormleighton	-11.08	219	0.45
Stirling	-10.90	336	0.29
Loop Head	-11.14	385	0.26
Point Lynas	-10.92		

Table 3 lists the "PRC average" values of the first set of stations investigated. Happily, each of these four average values lay within 0.13m of the overall mean value (-11.01m). These are negligible differences; we concluded that we could safely proceed with comparing the PRCs between these stations.

We first looked at the discrepancies between the PRCs for a given satellite measured at Point Lynas, and those from each of the other three stations: Stirling, Wormleighton and Loop Head (let us call those the "outstations"). We asked: how much error would there be in the PRCs if a user at Point Lynas employed corrections from each of these outstations? We first computed, satellite-by-satellite the correlation coefficients of each outstation's PRCs with those at Point Lynas. These correlation values ranged from 0.852 for Satellite 10 at Wormleighton, to 0.990 for Satellites 11 and 20 there. We then averaged the correlation coefficients for each station across all satellites. The results are shown in Table 4 in the column headed "Correlation coefficient". The average correlation coefficient was 0.963 at both Wormleighton and Stirling, and a lower 0.940 at more distant Loop Head.

We now calculated a set of PRCs for Point Lynas by interpolating between the PRCs at the three outstations. This RAAS interpolation was weighted by the reciprocals of the ranges from the outstations, so favouring the nearest. Table 3 shows these ranges and the weighting factors: Wormleighton 0.45, Stirling 0.29 and Loop Head 0.26. The "interpolated PRCs" for Point Lynas were then compared, satellite-by-satellite, with the PRCs actually recorded there. The correlation, 0.982 (Table 4), was much better than that at any of the individual outstations; the degree of de-correlation was between 30% and 49% of that at the outstations. It appears, therefore, that RAAS interpolation offers a significant benefit.

Table 4

Station	Correlation coefficient	PRC difference (m)
Wormleighton	0.963	1.05
Stirling	0.963	1.06
Loop Head	0.940	1.40
Interpolated	*0.982*	*0.66*

Computing the correlation coefficients in this way measures the agreement between the variations in the PRCs. We separately assessed the situation by examining the discrepancies between the actual PRC values. We computed the average of the modulus of the errors between each outstation PRC and the corresponding PRC at Point Lynas. The results, averaged across all satellites, are in the columns of Table 4 headed "PRC difference". These average discrepancies vary from 1.05m at Wormleighton to 1.40m at Loop Head. When we then compared the *interpolated* PRCs for Point Lynas with the values *measured* there, the average difference fell to 0.66m; this error is between 47% and 63% of those for the individual outstations. Again, we see a marked improvement.

We conclude that, in this case, a user would obtain PRC values much closer to the correct ones by interpolating the PRCs from these three outstations than by simply using the PRCs from any one of them, even Wormleighton the recommended night-time alternate.

The complete test was now repeated using Wormleighton with Tory Island (358km) and Mizen Head (417km). The two new stations are a little further away than Stirling and Loop Head. There was a larger discrepancy between clock bias values, with maximum differences of approximately 0.5m. But, again, the interpolated PRCs for Point Lynas proved much closer to the PRCs actually measured there than did the PRCs from any individual outstation. In other words, the results confirmed those from the first group of stations.

Finally, using this second group of beacons, we also checked the position results at Bangor over a total of 24h. Table 5 shows the 2-d and 3-d errors with respect to an antenna position established by long-term code-differential GPS measurements. Using corrections from the nearby station, Point Lynas, reduced the 2-d mean error from 5.3m to 2.5m. Corrections from the individual outstations also reduce the error, but by less. But

interpolating their PRCs gave 2.6m, a value within 0.1m of that of Lynas itself. The 3-d results followed the same pattern. We conclude that interpolating the PRCs from these three outstations, even including one as distant as 417km, gives results almost indistinguishable from those provided by the local beacon.

Table 5

Station	Distance from Bangor (km)	Mean error (m)	
		2-d	3-d
No differential		5.3	15.2
Wormleighton	219	2.6	2.7
Tory Island	358	3.4	3.5
Mizen Head	417	4.9	5.0
Lynas	23	2.5	2.5
Lynas interpolated		2.6	2.7

WHERE RAAS PAYS OFF

Our analysis of these test results suggests that it pays to use a RAAS solution, rather than any of the possible alternate beacons, where three beacons contribute to that solution and the receiver lies within the triangle they form. Interpolating between three beacons in this way takes into account the gradients of the PRCs, of course.

But if the receiver were to lie outside the triangle, we would still have knowledge of those gradients and it would be reasonable to apply them, at least in regions close to the triangle. Then, a different way of calculating the PRCs at the receiver would then be required, since the process would be one of extrapolation, not interpolation. This option has not so far been explored.

Similarly, if only two beacons were available, the gradient in one direction would be known. This should also provide a limited benefit. It would be interesting to explore where, and for how far, a two-beacon solution would provide more accurate PRCs than either beacon alone.

But even if extrapolation and the use of two beacons are excluded, we can employ our computer model to identify those areas in which the receiver lies within a triangle of beacons each of which meets the full coverage criteria. In such regions, it should pay to use a RAAS solution. Fig. 8 shows the area in which these fairly conservative criteria are met by day when the British Isles beacons are used. Fig. 9 shows the (much smaller) area at night. The equivalent results for the entire EMA are presented in Figs. 10 and 11.

FURTHER BENEFITS OF RAAS OPERATION

There are fundamental differences between a three-beacon RAAS solution and the traditional single-beacon LAAS approach. We have seen that RAAS should be more accurate than LAAS in many cases. But, with the ending of SA, the key reason for using radiobeacon DGNSS is not its greater accuracy but the enhancement of integrity it provides [18,21]. And, of course, a receiver that can take advantage of multiple beacons will enjoy at least as great an integrity benefit as a traditional single-beacon receiver. Indeed, provided the receiver marks a satellite as unhealthy as soon as it is flagged by any of the reference stations being received, the degree of integrity improvement afforded by differential operation will actually be increased.

Fig. 8: Orange highlights the region in which it pays to use RAAS: ie we are within a triangle of three stations, each of which meets full coverage criteria by day.

Fig. 9: As Fig.8, but at night

Fig. 10: Red highlights the region in which it pays to use RAAS: ie we are within a triangle of three stations, each of which meets full coverage criteria by day.

A further benefit of RAAS operation is that it should extend the area over which high-quality differential reception is available. We have seen that, with the ending of SA, the need for rapid updates of PRCs has gone. In principle, delays of many tens of seconds between PRC updates would lead to little degradation of position accuracy. Thus, we could make use of weaker signals from more distant radiobeacons. The 24-hour test data analysed above actually employed two groups of three beacons outside the area in which their coverage *at night* fully meets the international standards. Yet these beacons clearly provided accuracy benefits. The factor that requires us to continue to employ tight specifications in stating the coverage of radiobeacons post-SA is the time-to-alarm [18]. Indeed, we show in another paper in this session that no easing of standards can be permitted if this specification is to be met [21]. But if the receiver now has access to multiple beacons, the probability of receiving an alarm message will be greatly enhanced, and that is likely to extend substantially the area within which the TTA specification can be met.

In that case, multiple beacon operation – even employing beacons outside the standard coverage limits - is likely to provide both accuracy and integrity benefits.

It remains to explore this aspect of multiple beacon operation fully. We would also wish to investigate the degree to which even better results than those demonstrated above could be achieved by the use of other algorithms than simple weighted interpolation. We envisage exploring at the same time the dependence of accuracy on the geometry of the outstations, including the use of extrapolation to areas outside the region bounded by the outstations.

That done, we will be in a position to set formal criteria to be met if a RAAS solution is to be better than a LAAS one. We will then go on to prepare coverage plots according to those criteria; we anticipate that these will be more extensive than the plots presented above, especially at night.

Fig. 11: As Fig. 10, but at night

CONCLUSIONS

This paper has presented a preliminary exploration of the benefits of receiving multiple beacons from a radiobeacon DGNSS network. It has shown that the feasibility of doing so is now commonplace, especially by day, given the recent substantial increases in the numbers and ranges of European beacon systems. We have demonstrated that PRCs calculated by interpolating the values from three stations at ranges of approximately 200-400 km from the receiver are more accurate than the PRCs from any single such outstation. Thus, when a local station fails, interpolation is a better option than the use of a simple alternate.

We go on to argue that the benefits of a RAAS solution over a conventional LAAS one include not only higher accuracy but also a greater degree of integrity. We propose exploring whether these benefits are available, at least in part, outside the area within which the PRCs of three stations can be interpolated. Indeed, we show good reason to believe that RAAS operation could even extend the use of the radiobeacon service beyond its present boundaries.

ACKNOWLEDGEMENTS

REFERENCES

1. Enge, P.K. and Olsen, K.E., *Medium Frequency Broadcast of Differential GPS Data*, IEEE Transactions on Aerospace and Electronic Systems, Vol.26, No. 4, July 1990, pp. 607-617.
2. Enge, P.K. and Ruane, M.F., *Marine Radiobeacons for the Broadcast of Differential GPS Data*, Record of the IEEE Position, Location and Navigation Symposium, Las Vegas, NV, November 1986.
3. International Association of Lighthouse Authorities, *List of Radionavigation services*, Issue 7 – August 1999.
4. Offermans, G.W.A, Helwig, A.W.S. & Van Willigen, D., *Eurofix system and its developments*, Royal Institute of Navigation NAV98, London, 1998
5. International Maritime Organisation, Resolution A.815 (19), *World-Wide Radionavigation System*, November 1995
6. International Maritime Organisation, Resolution A.860 (20), *Maritime Policy for a Future Global Navigation Satellite System (GNSS)*, November 1997
7. International Association of and Lighthouse Marine Aids to Navigation Authorities (IALA), '*Recommendation on the performance and monitoring of a DGNSS service in the Band 283.5 - 325 kHz'*, Rec.121, June 2001
8. International Association of and Lighthouse Marine Aids to Navigation Authorities (IALA), 'Draft Recommendation on the performance and monitoring of DGNSS services in the frequency band 283.5 – 325KHz', June 2001
9. International Association of and Lighthouse Marine Aids to Navigation Authorities (IALA), '*Draft Revision of IMO Resolution A.815(19)*' Nav 47/.J.., 31ˢᵗ March 2001.
10. United States Department of Defense & Department of Transportation, *Federal Radionavigation Plan* 2001.
11. United States Coast Guard, '*Broadcast Standards for the USCG DGPS Navigation Service*', COMDTINST M16577.1 April 1993.
12. Poppe, D.C., *Coverage and Performance Prediction of DGPS Systems Employing Radiobeacon Transmissions*, Ph.D. Thesis, University of Wales, Bangor, October 1995.
13. Last, J.D. & Poppe, D.C., *A coverage prediction model for radio beacon differential satellite navigation systems*, Navigation (USA) - Journal of the Institute of Navigation, 43, 4, pp451-467, Winter 1996-1997
14. Last, J.D. & Turhan, B.E., *European radiobeacon DGNSS - Making the most of the frequency band*, Journal of the Royal Institute of Navigation, 52, 2, pp176-188, May 1999
15. Last, J.D., Turhan, B.E. & Ward, N., *IALA's new European DGNSS radiobeacon plan*, International Association of Institutes of Navigation/ Institute of Navigation (USA), IAIN/ION 25th Anniversary World Congress, pp.329-335, San Diego, CA, 26-28 June 2000
16. International Association of and Lighthouse Marine Aids to Navigation Authorities (IALA), Frequency Plan *fplan46*, 2002
17. Last, J.D, Grant A.J. & Ward, N., *Radiobeacon DGNSS Station Selection Strategies – Can We Do Better?*, ION National Technical Meeting, Long Beach, CA, USA, 22-24 January 2001
18. Grant, A., Last, J.D. & Ward, N., *Quality criteria for the maritime DGNSS system in a world without SA*, GNSS2001 Conference, Seville, Spain, 8-11 May 2001
19. United States Department of Defense & Department of Transportation, *Federal Radionavigation Plan* 2001
20. http://www.esa.int/export/esaSA/GGGE3A50NDC_navigation_0.html
21. Last, J.D., Grant, A. & Ward, N, *Radiobeacon DGNSS service – predicting availability and continuity*, ION GPS 2002
Last, J.D., Grant, A. & Ward, N., 'Understanding and predicting the availabilities of radiobeacon DGNSS systems' National Technical Meeting 2002, Institute of Navigation (USA), San Diego, CA, 28-30 Jan, 2002

Appendix M

BANDPASS Instruction Manual

The instruction manual for the BANgor Datatrak Performance Analysis Software Suite, the Windows implementation of the Datatrak model described throughout this Thesis, follows. The latest version is v2.0.

BANDPASS

Version 2.0

BANgor Datatrak Performance Analysis Software Suite

Software Instruction Manual

By Alwyn I. Williams

Date: 17th June 2003

CONTENTS

2

3

Introduction

The BANgor Datatrak Performance Analysis Software Suite (BANDPASS) is a collection of applications that analyses the performance and coverage of Siemens-Datatrak Automatic Vehicle Location System networks using prediction techniques developed by the Radionavigation Group at University of Wales, Bangor.

This version of the software uses ground conductivity and propagation data from the International Telecommunication Union (ITU) and the European Broadcasting Union (EBU) to calculate the field strength of transmitters throughout the network area. The ITU also provided the atmospheric noise data to calculate signal-to-atmospheric noise ratio. Vehicle noise can also be included, and is based on measured data collected by Datatrak.

A substantial effort has gone into getting a good interference model into the software. Based on data from the ITU, the software will select which transmitters will affect the network area, and determine how strong the interferer will be. It will then be possible to calculate the signal-to-interference ratio (SIR) for a given area. The MkIV Datatrak Locator filters have been modelled in the software, so the interference rejection analysis is as accurate as possible.

By combining noise, interference and signal field strength to produce a signal-to-trouble ratio (STR), it is possible to determine the coverage of the trigger/data signal. Using theoretical analysis, it is also possible to determine the repeatable accuracy of the system in the network area by using the pseudoranging algorithm employed by the MkIV Locator. By applying limits to the performance plots, the coverage of the Datatrak navigation system can be shown.

New to version 2.0 of BANDPASS is the phase delay prediction algorithm using the Monteath Method. This allows the phase delay from any Datatrak transmitter to be calculated, and using multiple transmitters, the confidence factor and absolute accuracy of a given network can be calculated.

Included in the software suite is a Datatrak transmitter and network administrator. This will allow the user to change transmitter or network parameters, and see their effect on the network performance/coverage. The administrator also creates the signal attenuation arrays required by the performance/coverage application.

BANDPASS is designed to be used in any part of the world.

4

1. Installation Guide

The BANDPASS CD comes with its own installation application that sets up the software suite, and install data if required.

To install the software, please follow the installation guide below.

1.0 Installation Procedure

1. When the CD is placed in the CD-ROM drive, the BANDPASS installer should automatically run. If not, then click on the Start Menu, then 'Run...', and type in "<drive >:\install.exe", where <drive> is the CD-ROM drive letter. Click on 'Ok', and the installer will run.
2. A box showing the contents of the README.TXT file on the CD will be displayed. This might have important information with regards to the software or the installation procedure.
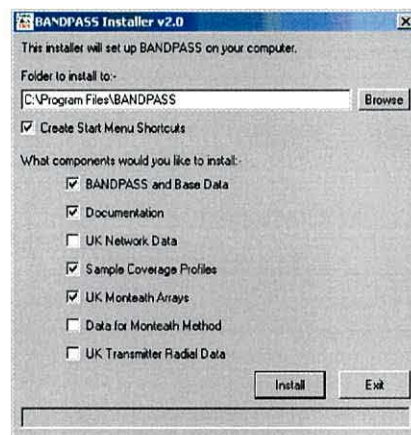3. Click on 'Continue'. This will close the text box, and open the main installation application.

Fig. 1 – BANDPASS Installer Options

4. The installer will provide options on what components of BANDPASS you would like to install, and where. The first piece of information required is the installation folder. This is the folder on your computer where the installer will place the BANDPASS files. A default folder is suggested, but you can change the folder to suit your needs. If the folder structure does not exist, then it will be created.

When the 'Create Start Menu Shortcuts' option is ticked, the installer will create a 'BANDPASS' folder under 'Programs' in the Start Menu, and add shortcuts to the applications. You will then be able to run the software suite from the Start Menu.

5

There are seven components which can be installed. 'BANDPASS and Base Data' is required to actually run the software. This will copy BANDPASS applications and the basic data required for it to function correctly to the installation folder. When ticked, 'Documentation' will copy this instruction manual to the installation folder. The installer will create a shortcut on the Start Menu to the documentation, if required. Ticking 'UK Network Data' will install all the data for the UK network, including the transmitter attenuation arrays, and the interference layers. 'Sample Coverage Profiles' will install a sample of setting profiles to generate different coverage/performance plots.

New to version 2.0, 'UK Monteath Arrays' option allows you to install the arrays produced using the Monteath method for the UK network transmitters. These must be install in order to generate any plots based on phase delays (e.g. absolute accuracy). 'Data for Monteath Method' installs the coastline and terrain databases on your computer. This requires approximately 850 MB of space. Finally, the 'UK Transmitter Radial Data' option allows you to install the radials used to produce the UK Monteath Arrays. This option requires approximately 3.5GB of disk space.

NOTE: If any of the files copied actually exist in the installation folder, then they will be overwritten, without warning.

5. Once all the options are set, click on 'Install'. If all is well, the status bar at the bottom of the installer will display the installation status as the files are copied from the CD to the installation folder on your computer.

6. When the installation is complete, a box will be displayed to confirm that, and then the installer will close. BANDPASS is now installed on your computer.

7. To start the applications, click on the shortcut on the Start Menu.

6

2. ArrayCreate

2.0 Introduction

The purpose of ArrayCreate is to efficiently manage the transmitters in BANDPASS. Its other main purpose is to create the attenuation arrays required by the coverage/performance analysis software (CPSCoverage).

Towards the end of the section, there is a small tutorial on how to create a new network, and add transmitters to it. By the end, you should have a complete set of attenuation arrays for the UK network. These will then be used by CPSCoverage to generate coverage/performance plots.

To run ArrayCreate, double click on its icon.

2.1 Main Window Layout

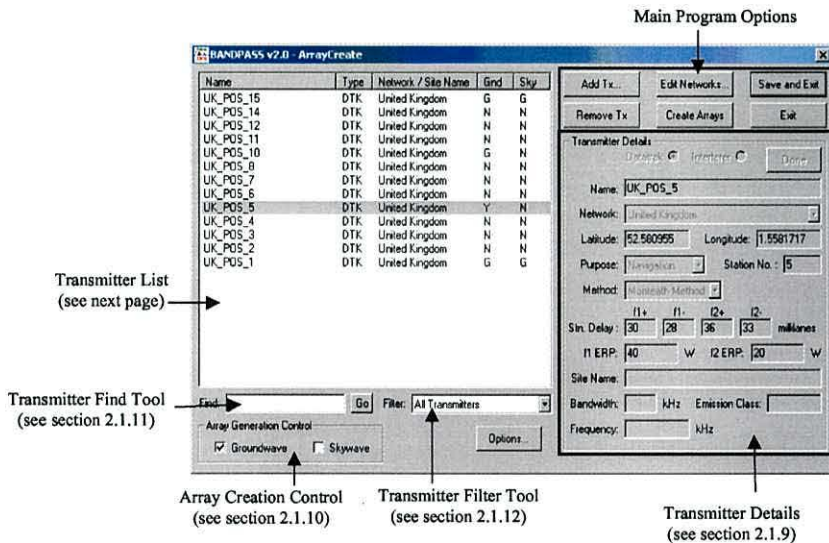Below is a screenshot of the main ArrayCreate application.

Fig. 2 – Main Window Layout

7

2.1.1 Transmitter List

This list shows all the Datatrak and interferer transmitters that are in the BANDPASS system. Description of the fields is given below.

Name	Name of the transmitter. This will also be the filename of the attenuation arrays for the transmitter.
Type	Type of transmitter. This field can have one of two values:- DTK – Datatrak Transmitter or INT – Interferer Transmitter.
Network/Site Name	For a Datatrak transmitter, the network to which the transmitter belongs is displayed in this field. For an interfering transmitter, the site name is displayed.
Gnd	This is the groundwave attenuation array status. It has four possible values:-

- N – An array does not exist, and will not be created during the next creation session.
- Y – An array does not exist, but will be created during the next creation session.
- G – An array has been generated, and will not be rebuilt during the next creation process.
- R – An existing array will be rebuilt during the next creation session.

Sky	Same as *Gnd*, but for skywave attenuation arrays.

Using the transmitter list, you can select transmitters to browse or edit.

Selecting Transmitters

Selecting transmitters from the list simply involves clicking on the transmitter name.

You may select multiple transmitters by dragging a box around the transmitters you wish to select. You can also select multiple transmitters by holding the CTRL button down, and clicking on the transmitters you require.

Browsing

By clicking on a transmitter name, you can view its details in the 'Transmitter Details' section.

If multiple transmitters are selected, then only details of the last transmitter selected will be displayed.

8

Editing

To edit a transmitter, simply double click on the transmitter name. The fields in the 'Transmitter Details' section will allow you to edit the details. Once you have finished, click on 'Done'. To discard the changes, simply click on another transmitter name in the transmitter list.

If the location of the transmitter is changed, then the software will automatically invalidate any attenuation arrays that have been created for the transmitter, and they will have to be generated. The other details may be modified without needing to regenerate the arrays.

2.1.2   Add Tx

This option allows you to add a new transmitter to the list.

By default, the fields required for a Datatrak transmitter will be available. However, by clicking on 'Interferer', you can specify an interfering transmitter instead (which have additional fields).

When you have completed entering the details for your new transmitter, click on 'Done', and the transmitter details will be saved. The transmitter list will be updated to include the new transmitter.

By default, the new transmitter will have its attenuation array status set to 'create', and therefore you will have a 'Y' in both Gnd and Sky fields of the transmitter list. This will make sure that it will be included in the next attenuation array creation session. If necessary, you can stop the array being created by using the 'Array Creation Control' (see section 2.1.9).

2.1.3   Remove Tx

This option allows you to remove the selected transmitters from the list. The software will ask you to confirm the deletion of the transmitter data before doing so.

You can select more than one transmitter from the list, and remove them all in one operation.

If you have removed transmitters by mistake, then you can restore them by clicking on 'Exit' immediately, and restarting the application. However, any changes you have made since the application was started will be lost.

2.1.4   Edit Networks

Before any transmitters can be entered into the system, a network must be set up. Clicking on this option opens a box which allows you to create and edit network data.
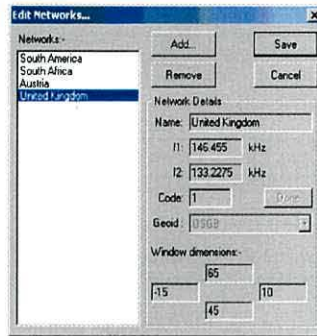
9

Fig. 3 – Edit Networks dialog box

The list of currently available networks is shown on the left-hand side of the dialog box. When one of the networks is selected, its details appear in the 'Network Details' section of the window. Double clicking on the name in the list allows you to edit the details of the network.

Network Details

Name	The name for the network.
f1	The f_1 centre frequency in kHz.
f2	The f_2 centre frequency in kHz.
Code	A generic code for administration purposes (not used in the BANDPASS software).
Geoid	Name of the Geoid used in the Locator when used on the selected network. Name and parameters are defined in *geoid.dat* file in the same directory as ArrayCreate. See appendix for the format of this file.
Window dimensions	These dimensions define the maximum area of interest for the network. All dimensions are in degrees. South and West coordinates are negative (e.g. 15°W should be entered as – 15).

Adding a network

To add a new network, click on 'Add', and fill in the details. Once you have completed the form, click on 'Done' to add the network to the list.

10

Removing a network

To remove a network, select the network from the list, and click on 'Remove'. You will be asked to confirm the removal of the network. If any transmitters exist for the removed network, then an error message will appear as the network name for the transmitters. You will have to manually delete the transmitters, or assign the transmitters to another network.

Save

Clicking on 'Save' will close the network box, and save any changes made.

Cancel

Clicking on 'Cancel' will close the network box, but you will lose any changes made to the network details.

2.1.5 Create Arrays

This option opens up the window which allows you to create the attenuation arrays. The arrays will be created for transmitters that have a 'Y' or 'R' in the 'Gnd' or 'Sky' field of the main transmitter list.

In version 2.0 of BANDPASS, the Create Arrays function has been modified to include the Monteath method. If any transmitter has been marked for array generation AND the generation method is Monteath, then it will take precedence over transmitters using the Millington/Skywave method. Also, the skywave arrays will not be generated for the transmitters using the Monteath algorithm. In order to successfully complete the task, the CreateArrays function must be restarted once the Monteath method has finished.

Depending on whether any transmitters require the Monteath method, ArrayCreate will start the Monteath or the Millingtion/Skywave array creation method.
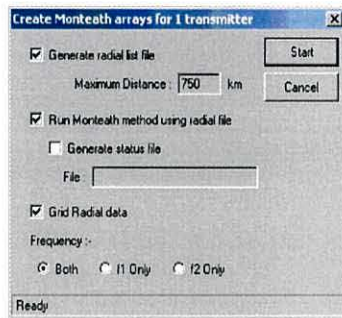
Monteath Array Creation Method

Fig.4 – Monteath method option dialog box

11

If any transmitter requires the Monteath method for its arrays, then the Monteath method option dialog box shown in Fig. 4 will be displayed. This will allow you to select which parts of the overall method you wish to execute. For a complete array, all three main options must be selected as shown in the figure.

Generate radial list file   When selected, the software will automatically produce a radial list file containing the end points of the radials at the maximum distance shown. This distance can be changed in the main ArrayCreate options dialog box. If you have your own radial list file, then uncheck this option so that the software does not overwrite it.

Run Monteath method using radial file   Using the radial list file, the Monteath method is applied to the path between the transmitter and each radial end point. This will require the terrain database (DTED format), coastline database and the ground conductivity database. An optional status file can be generated that captures messages produced by the method. This may be of use when solving any problems.

Grid Radial data   Once the Monteath method has produce all the radials for a transmitter, they must be converted to be used in CPSCoverage. You may disable this option if you only require the radials.

Frequency   The Monteath method is frequency dependant. You may select which frequency the Monteath method uses, or select both.

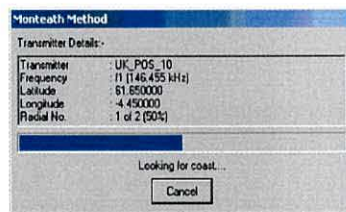*Start*   Start the processes selected above.

Fig. 5 – Monteath method status dialog box

When the Monteath method starts, it will load the required coastline information from the coastline database. The terrain and conductivity databases will be accessed when the information is required. Fig. 5 shows the Monteath method being applied to one transmitter on its f1 frequency. In this example, only two radials were required. You have the ability to cancel the method, but it may take some time because some memory clear up is required.

12

Millington/Skywave Array Creation Method

If all the transmitters require skywave or Millington method arrays, then the usual Millingtion/Skywave Create Arrays dialog box will be displayed, as shown in Fig. 6.
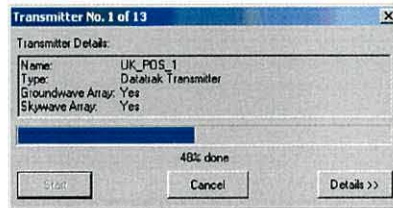

Fig. 6 – Millington/Skywave Create Arrays dialog box

Start

Starts the array creation process.

Cancel/Close

Closes the window. If the array creation process is not finished, then it will be aborted, and any remaining transmitters will not be processed.

Transmitter Details

When the attenuation arrays are being created, this section of the window provides you with details about the transmitter being processed. Details shown are the name and type of the transmitter, together with information on which arrays are being generated.

Details

When you click on this button, the window expands to include more information on the array creation process. It provides information such as which conductivity files are being used by the software to create the current array.

2.1.6   Exit and Save

Quits the application and saves changes you have made to the networks and transmitters.

2.1.7   Exit

Quits the application. Any changes made will be discarded. This option is useful if you have made any errors in the modifications you have made.

13

2.1.8   Options

Clicking on this button will bring up the 'Options' window.
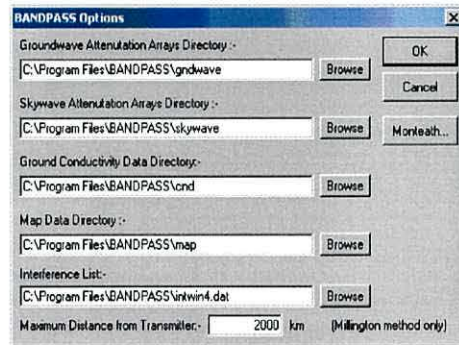

Fig. 7 – ArrayCreate Options dialog box

From here, you can modify the location to store the groundwave and skywave attenuation arrays.

All groundwave/skywave attenuation arrays are stored together regardless of network or transmitter type. However, the groundwave and skywave arrays must be stored in separate directories as their filenames are the same.

You need to specify the location for the ground conductivity files required by the array creation process. Failure to do this will cause the process to fail.

You also need to specify the directory containing the data used by CPSCoverage to produce the map for the plots.

New to version 2.0, you are also required to specify an interference list which is used by the interference analysis in CPSCoverage. This will be a file generated by the Access interference database developed by Dafydd Hughes. Details of the database are given in a separate instruction manual and dissertation.

Clicking on 'Browse' next to any of the options will cause a separate window to appear which will allow you to select the directories/files using the familiar tree structure used in Windows Explorer.

The 'Maximum Distance from Transmitter' option allows you to modify the size of the generated Millington attenuation array. This value is the maximum distance away from the transmitter that the software will produce an attenuation value, and hence, it has a direct effect on the size of the attenuation array, and computation time.
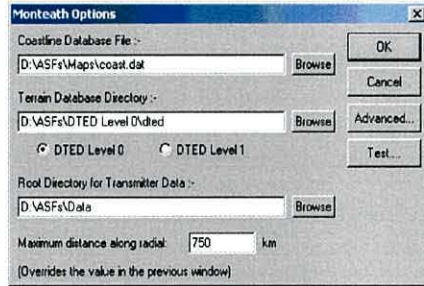
14

Monteath Options

Fig. 8 – Monteath specific main options

Due to its complexity, the Monteath method requires more settings than the Millington method. The main Monteath options dialog box is shown in Fig. 8.

|	
Coastline Database File	This is the file that contains the high resolution coastline database for use in the Monteath method.
Terrain Database Directory	The DTED terrain database is held in a number of subdirectories (e001, e002, etc.). The root of these directories should be placed here. The DTED level must also be selected depending on the resolution of the database. The database supplied on the BANDPASS CDs is DTED Level 0.
Root Directory for Transmitter Data	All generated Monteath data is held in a well-defined directory structure. The directory defined here is the root directory for all transmitter data. For the format of the directory structure, see appendix.
Maximum distance along radial	This is the maximum distance along a radial the Monteath method will be applied to. This also defines the size of the automatically produced radial list file.

15

Monteath Advanced Options
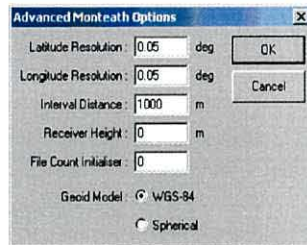
Fig. 9 – Advanced Monteath Options dialog box

The advanced Monteath options (Fig. 9) allow you to fine tune the Monteath method.

|	
Latitude Resolution	Defines the resolution of the final gridded Monteath data. It also affects the automatic radial list file, as the density of radials will be affected by the required resolution.
Longitude Resolution	As above, but for longitude.
Interval Distance	The Monteath method is an algorithm based on an integral. The distance between calculation points along a radial (i.e. the interval distance) affects the accuracy and computation time of the calculation. The optimum distance using DTED Level 0 at Datatrak frequencies is 1000m.
Receiver Height	This allows the Monteath method to take into account the height of the receiver above the ground. Usually, this should be set to 0m (i.e. on the ground).
File Count Initialiser	The radials produced from the Monteath method are numbered sequentially. This option allows you to select what number the file count should start from.
Geoid Model	The Monteath method can calculate the phase and field strength over a WGS-84 geoid or over a spherical earth. It is recommended that the calculation is made over WGS-84 geoid to retain the accuracy of the method.

16
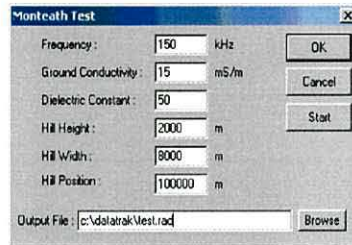
Monteath Test

Fig. 10 – Monteath test dialog box

The Monteath test dialog box (Fig. 10) allows you to test a theoretical path over a spherical earth. You can modify any of the settings detailed below.

Frequency	This is the frequency, in kHz, of the signal you wish to analyse.
Ground Conductivity	The ground is assumed to have a constant value of ground conductivity all along the path. Enter the value in mS/m in this setting.
Dielectric Constant	The dielectric constant is assumed to be constant all along the signal path. Enter the value in this setting.
Hill Height	An optional gaussian hill can be placed anywhere along the path. This value alters the height of the hill. 0m specifies no hill is required.
Hill Width	The gaussian hill width is defined by this setting.
Hill Position	This setting changes the distance of the hill from the transmitter. The value defines the distance from the transmitter to the centre of the hill.
Output File	This is the file the results will be written to.

17

2.1.9   Transmitter Details

Below is a description of the fields in the 'Transmitter Details' section.

Datatrak/Interferer	These radio buttons select what type of transmitter these details represent.
Name	A unique name for the transmitter. This will also be the filename of the attenuation arrays.
Latitude/Longitude	Coordinates of the transmitter location. If the coordinates of a Datatrak transmitter is outside its network window, then the software will warn you, and give you a chance to modify the values.
f1 ERP *ERP*	Effective Radiated Power (ERP). For Datatrak transmitters, this is the f1 signal effective radiated power in Watts. For Interferers, this is the daytime effective radiated power.
f2 ERP *NERP*	(Night-time) Effective Radiated Power. For Datatrak transmitters, this is the f2 signal effective radiated power in Watts. For Interferers, this is the night-time effective radiated power.
Purpose	The purpose of the Datatrak transmitter. It has three values:- f1 Trigger (+ Navigation); f2 Trigger (+Navigation); Navigation Only. *Datatrak Only.*
Network	The network that the transmitter belongs to. *Datatrak Only.*
Station No.	This the transmitter's unique station number in the network. This is *not* the slot number. *Datatrak Only.*
Method	The array creation method to be used for this transmitter. Available options are Monteath method or Millington method. *Datatrak Only.*
Stn. Delay	This the station delay at the station, given in millilanes (millicycles). Each transmitted frequency can have a different delay. This will affect the absolute accuracy and confidence factor plots in CPSCoverage. Average measured values in UK: 30, 28, 36, 33 (millilanes) *Datatrak Only.*
Site Name	The site name of the interferer transmitter. The site name can be different from 'Name' as a site can have several LF transmitters at different frequencies. *Interferer Only.*

18

Bandwidth	The bandwidth of the radio emission from the transmitter in kHz. For CW transmissions, this is ignored. *Interferer Only.*
Emission Class	The 3-5 alphanumeric code use to define the modulation and signal type of the radio emission. Uses standard ITU designations (e.g. A1A). *Interferer Only.*
Frequency	The centre frequency of the radio emission from the transmitter in kHz. *Interferer Only.*

NOTE: The 'radiation pattern' and 'azimuth of maximum value' is no longer required. The interference analysis uses the actual gain values from the interference database.

2.1.10   Array Creation Control

By selecting transmitters in the transmitter list, you can control whether their groundwave or skywave attenuation arrays need to be generated or not by using these two tick boxes. A tick in the appropriate box will mean that the groundwave or skywave attenuation array will be created.

If more than one transmitter is selected, and their attenuation array options are different, then the tick boxes will be greyed out to show this. Clicking on the tick boxes in this state will set all the selected transmitters to the same state.

2.1.11   Find

This tool allows you to find transmitters in the transmitter list.

This is a simple find tool, and will only find the first transmitter name in the list that starts with the search criteria.

To use the find tool, simply type in the transmitter name you wish to find, and click on 'Go'. Details of the first transmitter that matches the search criteria will appear in 'Transmitter Details', and the transmitter list will scroll to show its position in the list. The Find tool will only search the transmitters that appear in the transmitter list, and is therefore dependent on the Filter setting. The search is not case sensitive.

2.1.12   Filter

This useful tool allows you only to view certain transmitters in the list.

You can filter by network, type of transmitter, or the attenuation array status. To change the filter, simply select the filter you require from the drop down box. The transmitter list will then refresh with only the transmitters with the attributes you have specified.

19

2.2 How to create a new network

NOTE: When generating a new network, it is advisable that a non-critical computer system is devoted entirely to the array creation process. On a 1GHz PC, two sets of radials (f1 and f2) for one transmitter at 0.05 degree resolution and an interval distance of 1000m, takes around 9 hours to complete. Several computer systems have been successfully used to generate arrays in parallel, with the data being served from a single computer.

1. Start the ArrayCreate application.
2. Click on 'Options' to make sure that all the settings are correct (you will only need to do this once).
3. Our first task is to create a new network. Click on 'Edit Networks'. This will bring up the network management window.
4. Click on 'Add'. This will allow you to enter the network details into the relevant fields. For more information on this task, see section 2.1.3. For this example, use these values.
    *   Name: United Kingdom
    *   F1:   146.455 (kHz)
    *   F2:   133.2275 (kHz)
    *   Code: 1
    *   Geoid: OSGB
    *   Window dimensions (clockwise, from the top): 65, 10, 45, -15
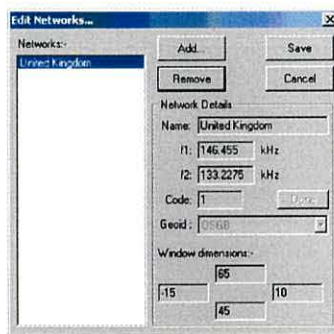5. When you have finished, click on 'Done'. You should now have a window which looks like this:-

Fig. 11 – Edit Network dialog box with example network

6. Click on 'Save' to save the network and close the window. You will return to the main application window. We now have a network ready for transmitters.
7. Click on 'Add Tx'. Fields in 'Transmitter Details' section will become enabled, allowing you to enter the details of a Datatrak transmitter. As an example, here are the details of the UK number 4 transmitter at Kineton.
    *   Name: UK_POS_4
    *   Latitude: 52.146537

20

- Longitude: -1.5056554
- ERP: 40 (W)
- Purpose: fl Trigger
- Network: United Kingdom
- Station No.:   4
- Method: Monteath Method
- Stn. Delay: 18, 16, 23, 19 (measured values in millilanes)

8. When complete, click on 'Done'. The transmitter name will appear in the transmitter list on the left hand side. You will notice that the Gnd/Sky fields have a 'Y' indicating that the attenuation arrays will be generated during the next array creation session.

9. Enter all the UK transmitters into the software using the same method. By the end, you should have a window which looks like this:-
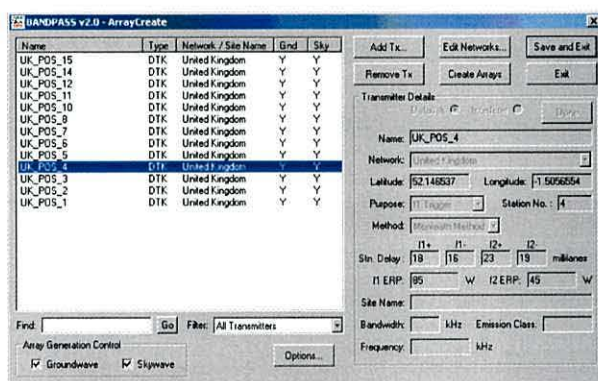

Fig. 12 – ArrayCreate main widow with example transmitters

10. We are now ready to start the attenuation array creation process. Make sure that all the transmitters have a 'Y' in the Gnd and Sky fields. If not, see section 2.1.10. Click on 'Create Arrays'.

11. Since the transmitters require the Monteath method to create the arrays, the Create Monteath arrays dialog box will appear. Make sure that the three main options are checked (Generate radial list, Run Monteath method, and Grid Radial Data), and click on Start.

12. This process will take many hours, possibly days to complete.

13. Once this process is complete, click on Create Arrays once again.

14. The Millington/Skywave array creation window will appear. Before the process starts, it will tell you how many transmitters are going to be processed. You can cancel the operation now, and nothing will happen.

15. Click on 'Start'. The array creation process will start, and it takes approximately 3 minutes per transmitter. In the meantime, the progress bar will inform you of the progress of individual transmitters.
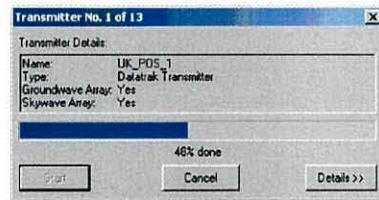
21

Fig. 13 – Create Array dialog box while generating an array

Clicking on 'Details' will expand the window to show more information on the array creation process (e.g. details on which conductivity files are being used). This is useful for diagnosing any problems which might crop up.

16. When all the transmitters have been processed, the 'Cancel' button will change to 'Close'. Click on this button, and the window will close. You will return to the main application window.

17. We have now completed the task of creating a network, and creating the attenuation arrays for all the transmitters in the network. They are now ready for use by the CPSCoverage application.

22

3. CPSCoverage

3.0 Introduction

The purpose of CPSCoverage is to produce coverage/performance plots using the transmitter information and attenuation arrays created in ArrayCreate.

There is a whole host of options available to the user, and instructions on how to use them are given on the following pages.

3.0.1 Main Window Layout

The layout of the CPSCoverage application is shown below. It has three main sections, as shown below.
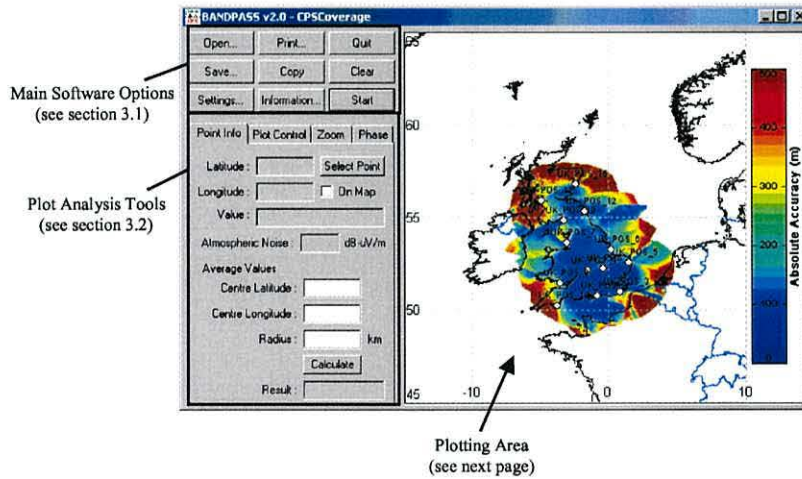

Fig. 14 – CPSCoverage Main Window Layout
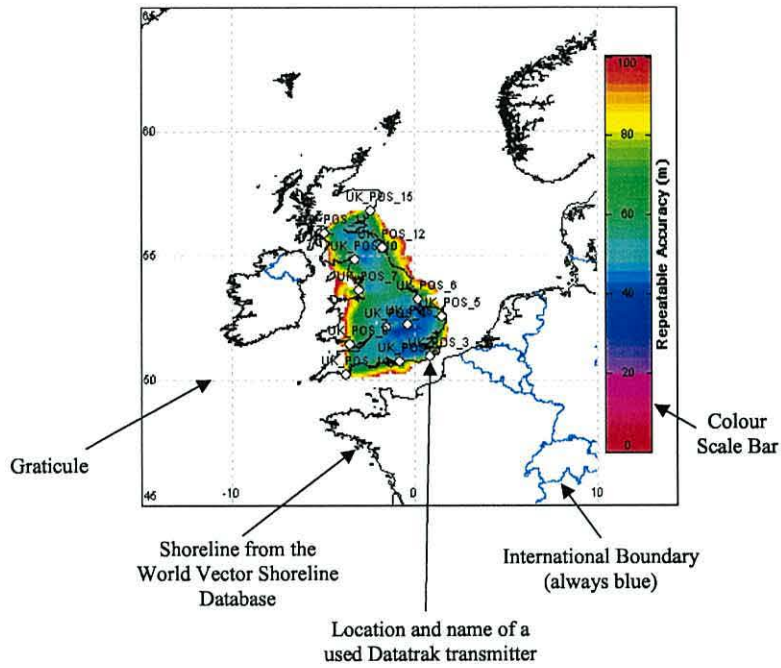
23

3.0.2 Plotting Area Description

Fig. 15 – Plotting Area Layout

The graticule and ticks on the colour scale bar are auto-ranging. Should you zoom into an area of the plot, the graticule will scale itself to a sensible interval.

The shoreline and international boundary are part of the same vector data file. Due to the size of the map file, it takes some time to render the map on the screen.

24

3.1 Main Software Options

3.1.1 Options

The options dialog box provides the settings with which the user can modify to produce different coverage/performance plots. New to version 2.0, the options are now tabbed to provide a cleaner and easier to use interface.
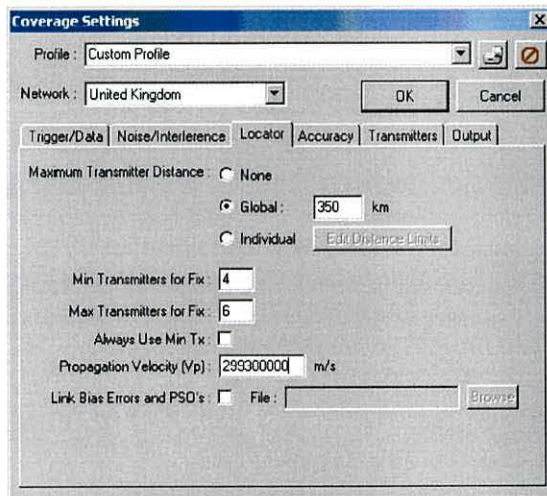

Fig. 16 – Coverage Settings dialog box (example showing the 'Locator' options tab)

3.1.1.1 Trigger/Data Tab

Wanted Groundwave	When ticked, the groundwave signal from the Datatrak transmitters are included in the coverage/performance analysis.
Use Monteath where possible	When ticked, the field strength of the groundwave signal is calculated using arrays generated using the Monteath method. If the Monteath arrays are not available, then the software resorts to the Millington arrays.
Wanted Skywave	When ticked, the skywave signal from the Datatrak transmitters are included in the coverage/performance analysis. If the groundwave and skywave signals are included, then the own-skywave fading will be added to the analysis.

25

Limit to Trigger/Data Coverage	When enabled, the coverage of the plot will be limited to the coverage of the Trigger/Data signal from the trigger transmitters in the network.
Trigger/Data SNR Limit	The lowest signal-to-noise ratio (SNR) the trigger/data signal needs to work correctly. A lower SNR will deem the Locator to be not working at all. The navigation signals do not have a SNR limit.

3.1.1.2 Noise/Interference

Locator Noise Floor	The level of noise in the Locator with no input signal. Given in units of dB-µV/m.
Atmospheric	Selects which atmospheric noise profile to use in the coverage/performance analysis. To modify profiles, click on 'Edit Noise Profiles...'.
Vehicle	The level of vehicle noise to be used in the coverage/performance analysis. Values can be modified using the 'Edit Noise Profiles...' option.

NOTE: During analysis, the software selects the highest value of noise at each receiver location.

Noise – Editing Profiles

Clicking on the 'Edit Noise Profiles...' button allows you to modify the parameters that define the level of atmospheric and vehicle noise.
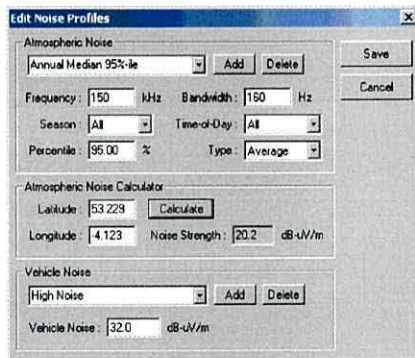

Fig. 17 – Noise Profile Editing Dialog Box

26

Atmospheric Noise

The atmospheric noise profiles are handled in much the same way as the profiles in the main options dialog box. A name is given to a profile, and when all the options are set, click on 'Add' to store the profile. 'Delete' remove the currently selected profile.

Below are the descriptions of the available options.

Frequency	Centre frequency to use when calculating the atmospheric noise.
Bandwidth	Bandwidth of the receiver in Hz.
Season	Selects which season to use. They all can be selected using the 'All' option.
Time-of-Day	Selects which of the six time blocks to use. Again, they all can be selected using the 'All' option.
Percentile	Atmospheric noise varies statistically, and this option allows you select the noise level not exceeded x-% of the time.
Type	This option selects the method with which to combine multiple season or time-of-day blocks. 'Average' averages the values, 'Max Value' takes the strongest noise value, and 'Min Value' takes the weakest noise value at a given location.

Atmospheric Noise Calculator

This handy tool allows you to test the atmospheric noise set-up by entering a location, and clicking 'Calculate'. The atmospheric noise will then be calculated for that location.

Vehicle Noise

Again, vehicle noise is handled using profiles similar to atmospheric noise. A name is given to the profile, and the value is entered into the vehicle noise text box. Clicking on 'Add' adds the profile to the list. 'Delete' removes the current profile from the list.

Save and Cancel

When editing is complete, click on 'Save'. This will save all the changes made to the noise profiles, and update the options dialog box.

Cancelling the dialog box will undo any changes made to the profiles.

27

Interference

The interference analysis requires a text file containing the list of transmitters. The text file is selected in the settings option in ArrayCreate. Please use the Interference Database Access file to amend the transmitter list, remembering to export the data to the relevant file. Refer to the Interference Database instruction manual for more information.

None	No interference will be included in the analysis.
Daytime Interference	Daytime (groundwave only) interference will be included in the analysis.
Night-time Interference	Night-time (groundwave and skywave) interference will be included in the analysis.
Generate Interference Layers	Brings up a dialog box to produce the interference layers needed by the coverage/performance analysis. To start the process, click on 'Start'. You can cancel the analysis by clicking on 'Cancel', but you will lose the interference layers.

The details shown in the 'Generate Interference Layers' window are stored in a text file 'Analysis.Log' in a folder called the same as the network name in the installation folder (e.g. C:\Program Files\BANDPASS\United Kingdom\Analysis.Log'). This information will assist you in discovering any interference problems which might become evident when producing coverage/performance plots.

For each interferer, the following information is given:-
- Site name of the interferer
- Assignment ID of the transmitter (unique ID number of the transmitter)
- Analysis status (see below)
- Centre frequency
- Transmitter location
- Daytime and night time power.

Additional spectral details are given for passband interferers, such as the transmission bandwidth and the emission type. Also, the rejection the Locator when using the navigation and the trigger/data filters is displayed to aid tracking down an interfering problem.

Analysis Status

The analysis status for each transmitter is shown after the assignment ID as a sequence of four letters or dashes.

The first character is either a 'G' or '-'. If a 'G' is displayed in this field, then the interference analysis is taking into account the groundwave field strength of the

28

transmitter. If a '-' is shown, then the groundwave signal is not a problem for the network.

The second letter is either a 'S' or '-'. This is similar to 'G', but it shows the status of the skywave signal in the analysis.

The third letter is either a 'B' or '-'. If it is a 'B', then the transmitter is being considered as a blocker in the analysis.

The last letter is either an 'F' or '-'. If it is an 'F', then the analysis has found the attenuation arrays for the transmitter, and is using them in the analysis.

3.1.1.3 Locator

Max Transmitter Distance	The maximum distance between receiver location and transmitter that the analysis will use to calculate the repeatable accuracy.
	Three options are available:- • None – No limits on the distance between transmitter and receiver. • Global – The specified distance limit is applied to all transmitters • Individual – The individual transmitters have separate distance limits.
	To change the individual transmitter distance limits, select the 'Individual' radio button and then click on 'Edit Distance Limits'. This will bring up a dialog box listing all the transmitters in the network. To change a transmitter's distance limit, click on its current value. You will then be able to edit that value. Click elsewhere or press Enter to finish editing. Click on 'Ok' to commit the changes.
Min Transmitters for Fix	Minimum number of transmitters to use in the repeatable accuracy solution.
Max Transmitters for Fix	Maximum number of transmitters to use in the repeatable accuracy solution.
Always Use Min Tx	When enabled, it allows the receiver to use the nearest 'minimum number of transmitters for fix' even if it's further than the maximum distance limit.
Propagation Velocity (Vp)	This is the propagation velocity assumed by the software to calculate the error in the phase delay. This will affect the absolute accuracy and confidence factor plots.

29

Link biases and PSO's	Required for absolute accuracy and confidence factor plots. The given file contains the standard Locator 'pr', 'stxs' and 'pso' commands so that the software knows how the stations are linked, and is useful to check PSOs. Examples can be installed through the BANDPASS installer, and they will be in the BANDPASS root directory called "pso.txt" and "no pso.txt".

3.1.1.4 Accuracy

Repeatable Accuracy Limit	The maximum value of repeatable accuracy that will be plotted. Value given is in metres not exceeded 95% of the time.
Absolute Accuracy Limit	The maximum value of absolute accuracy that will be plotted. Value is given in metres.
Confidence Factor Limit	The maximum value of confidence factor that will be plotted.

3.1.1.5 Transmitters

This tab controls which transmitters are used in the coverage/performance model. Using the arrow buttons, you can select whether a single transmitter or the whole list is included or excluded from the coverage/performance analysis. The transmitters in the 'Used Transmitters' list will be used in the coverage/performance analysis.

Slot Offsets
To complete the models of the stations, the slot offsets must be included in the phase delay calculation (for absolute accuracy and confidence factor). Clicking on the 'Slot Offsets' button allows the values to be entered on a *slot* basis. To enter a slot offset, simply click on the cell for the appropriate frequency and slot, and type in the new value. When finished, click on 'Ok' for the values to be saved.

3.1.1.6 Output – Plot Options

Trigger/Data Signal Field Strength	Plots the field strength of the trigger/data signal from any trigger/data transmitters that has been selected for use in the analysis.
Atmospheric Noise	Plots the atmospheric noise level across the network area.
Navigation SNR	Plots the SNR/SIR (which ever is lower) of the navigation signal. Use the frequency option below to select f1 or f2.
Repeatable Accuracy	Plots the repeatable accuracy of the network.

30

HDOP	Plots the Horizontal Dilution Of Precision of the network.
Number of Transmitters in Fix	Plots the number of transmitters used in the fix. The upper limit is determined by 'Max Transmitters for Fix'.
Number of Transmitters Available	Plots the maximum number of transmitters available in an area.
Transmitter 'Availability'	Plots where the Locator will select a transmitter. When using this option, only select the transmitter required in 'Select Datatrak Transmitters'. The output will contain three levels. The first level is where the Locator will always select the transmitter. The second level is where the Locator might select the transmitter due to one of the other transmitters being out of action.
Predict Phase Offsets (C-O)	This is a single transmitter plot showing the difference between the calculated distance to the transmitter (C) and the measured distance using the Monteath arrays (O). The 'Phase' tab on the main window allows you to modify the plot units and Vp on-the-fly.
Absolute Accuracy	Plots the absolute accuracy of the network.
Absolute Accuracy Direction	Plots the direction of the error vector (absolute accuracy is the error vector magnitude). Value in degrees.
Confidence Factor	Plots the confidence factor of the network.
Phase Difference	Calculates the phase difference between two stations. The stations are selected using their slot numbers which is entered below the 'Plot' option.

3.1.1.7 Plot – Other Options

Frequency	If a plot option requires a frequency selection (e.g. Navigation SNR), then that selection is made using this option.
Reference Slot	Used for plotting phase differences. This is the reference slot, or 'master' slot.

31

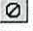|	
Transmitted Slot	Used for plotting phase differences. This is the transmitted slot, or 'slave' slot.
Multi-layer Output	An useful debugging aid. Selecting a file and a position in the network, a large amount of information can be gathered, including the groundwave-to-interference ratio (GIR) and the matrices used in the absolute accuracy calculation.

3.1.1.8 Profiles

The software allows you store settings in the form of profiles. The purpose of this function is to allow common settings to be selected with ease. You can type in any title you wish to represent the settings you've used for the coverage/performance analysis. Profiles are independent of the network, so you can apply the same profiles to any network in the network list.

Adding a Profile

1. Set the settings to the values you require.
2. Type in a name for the profile. For example, "Daytime Repeatable Accuracy".
3. Click on 🖳 to save the profile. The profile is now saved, and will be available in the drop list, ready for use.

Deleting a Profile

1. Select the profile you want to delete.
2. Click on 🗑 to remove the profile.
3. You will be asked to confirm the removal. Click on 'Yes'.

32

3.1.2 Start

Clicking on this button will start the coverage/performance analysis. A box will appear to inform you of the status of the coverage/performance analysis. Progress bars will show how the analysis is progressing. The analysis process takes a few minutes to complete, depending on the specification of your PC.

The status box also has the option of cancelling the analysis. Simply click on 'Cancel', and the analysis will finish. It may take a couple of seconds for the software to react. This is to make sure that the analysis has finished cleanly.

There is also an option to boost the speed of the analysis. However, this will only make a difference if you have other software which is using a lot of processor time.

When the analysis is complete, the software will plot the results, ready for further investigation.

3.1.3 Open

This option allows you to load in three different types of file.

- BANDPASS file
- Attenuation Array file (*.dtk; *.int)
- Interference Array file (*.f1; *.f2)
- Monteath Field Strength Arrays (*.fs1; *.fs2)
- Monteath Phase Delay Arrays (*.ph1; *.ph2)
- Terrain Height Arrays (*.ter)
- Groundwave-to-Interference Ratio Arrays (*.gi1; *.gi2)

Most of the time, you will only need to load in the BANDPASS file type, but occasionally, you may need to check the attenuation/interference array files. The attenuation arrays will be represented as the field strength of a 1kW transmitter.

To Load in a file, simply select the file type from the 'Files of type:' drop down box, and select the file from the file list. Click on 'Open'. The file selected will be loaded into the software, and plotted on the screen. The software is also backward compatible with .BAN files saved using previous versions of the software.

For more information on the BANDPASS file type, see 'Save'.

3.1.4 Save

This option allows you to save in three different formats.

- Bitmap File
- Raw Data File
- BANDPASS file

33

Saving as a bitmap file will save the plot as a standard Windows BMP file which you can open up in any graphics or word-processing package. This will be useful for inserting plots into reports or presentations. The size of the bitmap will be the same size as the plot on the screen. Therefore, to create large bitmaps, maximise the main window.

The raw data file saves the data used to create the plot. The text file produced can then be loaded into MS Excel, for example, for further processing.

The most useful file format to save is the BANDPASS file format. This saves the settings used to create the plot, as well as the actual results produced by the coverage/performance analysis. This means that once the analysis has been completed, you can load the results back in for further investigation. Details of the transmitters used in the plot will also saved.

3.1.5 Copy

This option copies the current plot onto the clipboard as a bitmap. The image is then accessible from any other application by using its Paste function. The size of the copied image is the same size as the plot area.

The copied plot will have a border surrounding it.

3.1.6 Print

This opens a dialog to arrange the printing of the plot onto any installed printer. This is a standard Print dialog, and should be familiar to most Windows users.

The current version of the software will only use the entire area of the page to print out the plots. Future versions of the software will hopefully provide the option to size and position the plot onto the page.

3.1.7 Information

This option opens a window with details of the settings used to produce the current plot. This is useful for checking on conditions under which saved plot were generated. If the current plot was loaded using a non-BANDPASS file type, then this window will only contain the type of file, and its filename.

3.1.8 Clear

This option clears the plot, and resets the settings.

3.1.9 Quit

Exits the application.

34

3.2   Plot Analysis Tools

This area of the software has been updated so that the tools are more conveniently placed. The options are now tabbed to allow easy access.
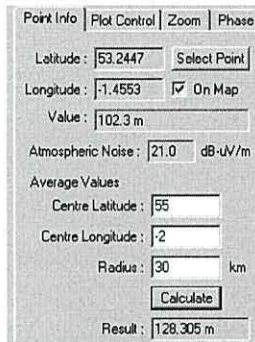

Fig. 18 – Tabbed Plot Analysis Tools

3.2.1 Point Info Tab

This tab provides information on a specific point on the plot. If 'On Map' is selected, then a cross will appear at the selected point. There are two ways in which you can specify a location:-

3.2.1.1 Using the map

1. Use the mouse to click on the point of interest in the plot.
2. The longitude and latitude of the point will be displayed, as well as the value of the plot at that point. Also, if atmospheric noise was in the analysis that produced the plot, its value will also be displayed.

3.2.1.2 Specifying a precise location

1. Click on 'Select Point'.
2. Enter the longitude and latitude of the point of interest. South and West coordinates are negative (e.g. 15°W should be entered as –15).
3. Click on 'Show Point'. The value at the specified location will be displayed.

3.2.1.3 Averaging values

1. Enter the centre latitude and longitude, and the radius of the circle of values you wish to average.
2. Click on 'Calculate'.
3. The software with calculate an average value of values in the given circle, and print out the results.

35

3.2.2 Plot Control Tab

The plot control tab allows you to control what is displayed on the plot. You can also adjust the scale, and quantise it if required.
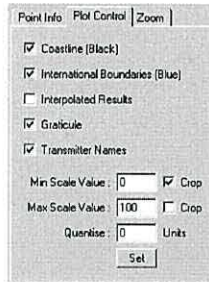

Fig. 19 – Plot Control Settings

Coastline	When enabled, the coastline is shown on the plot in black.
International Boundaries	When enabled, the international boundaries are shown on the plot in blue.
Interpolated Results	When ticked, the data will be plotted at the screen resolution. Any pixels in-between receiver locations will have interpolated data. The result is a less 'blocky' plot. This is especially true for zoomed in areas.
Graticule	When ticked, the graticule is drawn on the plot.
Transmitter Names	When enabled, the names of the transmitters are printed on the plot.
Min Scale Value	The lowest scale value. If the 'crop' option is enabled, then any value below the minimum will not be plotted. Click on 'Set' to update plot.
Max Scale Value	The highest scale value. If the 'crop' option is enabled, then any value above the maximum will not be plotted. Click on 'Set' to update plot.
Quantise	Plots the results at discrete levels. The value entered defines the step size between levels. A value of '0' removes any quantisation. Click on 'Set' to update plot.

36

3.2.3 Zoom Tab

Clicking on the zoom tab will allow you to enter new limits of the area you wish to view. By default, the entire network area defined in the network details section of ArrayCreate is shown. However, you can use this option to view a specific section of the network area.
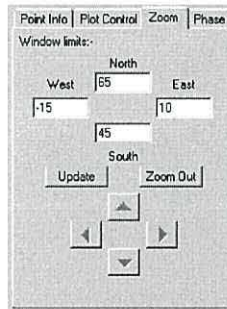

Fig. 20 – Zoom Settings

To set the zoom, enter the new limits for the window, and click on 'Update'. Only the area within the limits given will then be drawn.

Clicking on 'Zoom Out' will restore the entire network limits, and will redraw the plot immediately.

When zoomed in, the arrow buttons towards the bottom of the tab window will be enabled. These allow you to move around the plot without having to type in new window limits.
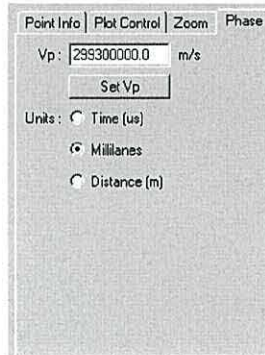
37

3.2.4 Phase Tab

Fig. 21 – Phase (C-O) Control Tab

The phase tab is only available when a phase offset plot is shown. The options available allow you to change the units and the Vp without having to rerun the coverage/prediction algorithm. On changing the units, the plot will be re-plotted immediately. You may have to adjust the minimum and maximum values in the Plot Control tab.
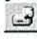
The Vp adjustment allows you to modify the Vp assumed in the phase offset calculation. Once a new Vp has been entered, you must press the 'Set Vp' button in order to re-calculate the new phase offset plot.

38

3.3 How to generate coverage/performance plots

As an example of how to use the software, the following steps will show you how to produce a daytime repeatable accuracy plot with atmospheric and vehicle noise, and interference.

We will assume that the details for the UK network have been entered into the software using ArrayCreate, and the network is called 'United Kingdon'. This will the case if you have followed the tutorial for ArrayCreate.

1. Start the CPSCoverage application.
2. Select 'Options'.
3. In the network drop-down box, select 'United Kingdon'.
4. If you have not already done so, click on 'Generate Interference Layers', and then 'Generate Interference Layers', to produce the interference layers required by the coverage/performance analysis. The process takes around five minutes to complete, depending on the specification of your PC. If this step is ignored, then the software will warn you that the analysis will fail due to missing files.
5. Set the options required for the coverage/performance analysis. The values required for this example are:-
   - Wanted Groundwave – Yes
   - Wanted Skywave – No
   - Limit to Trigger/Data Coverage – No
   - Locator Noise Floor – 5 dB-uV/m
   - Trigger/Data SNR Limit – 0 dB
   - Atmospheric Noise – 95%-ile Annual Median
   - Vehicle Noise – 27dB-uV/m
   - Interference – Daytime
   - Maximum Error Limit – 100m
   - Max Transmitter Distance – Global: 350km
   - Min Transmitters for Fix – 4
   - Max Transmitters for Fix – 6
   - Always Use Min Tx – No
   - Plot – Repeatable Accuracy

   At this point, you may wish to save these settings as a profile. Do this by entering a name for the profile (e.g. 'Daytime Repeatable Accuracy') in the profile drop down box, and clicking on ⬚. The profile will then be saved for future use.
6. Click on the 'Transmitters' tab. Make sure that all the transmitters are in the 'Used Transmitters' list by clicking on '>>'. Click on 'Ok'.
7. Confirm the settings by clicking on 'Ok'. If all is well, you will return to the main window.
8. Click on 'Start', which will start the coverage/performance process. Once this process has begun, it will not stop until it has completed, or there is an error (e.g. a missing file). The analysis takes a few minutes to complete, depending on the specification of the PC. A progress bar will be displayed to show how

39

each part of the coverage/performance analysis is doing. If the progress bar should stop for an unreasonable length of time (say, more than a minute), then assume that the software has crashed, and try to run the software again.

9. As soon as the analysis has finished, the result will be displayed in the plotting area. Due to the large map file used by the software, the coastline and international boundaries may take some time to appear on the screen. The plot is complete when the colour scale has appeared on the right-hand side of the plot. You should now have a window which looks like this:-
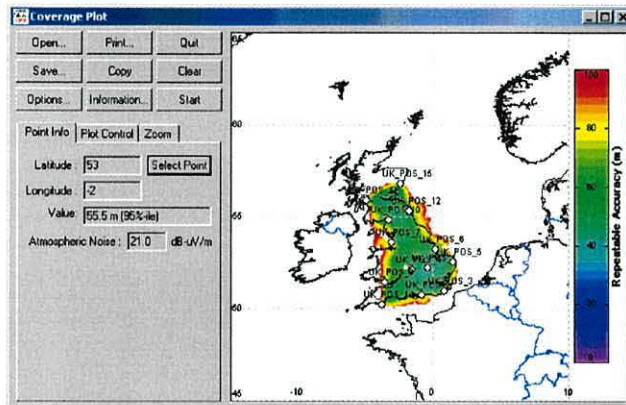

Fig. 22 – CPSCoverage main window with example plot

10. Now would be a good opportunity to save the plot. Click on 'Save', and select 'BANDPASS file' from the Save as type drop down box. Enter a filename, and click on 'Save'. The file will be saved, and a box will appear to confirm that.

11. You can investigate the value of repeatable accuracy by clicking on the coloured area of the map, or by clicking on 'Select Point' to enter a specific location. We find that that at 53°N 2°W the repeatable accuracy is 55.5m (95%-ile).

12. You are able to print/copy or save as a bitmap using the relevant buttons from the cluster of options on the left.

13. Clicking on 'Information…' will bring up information about the settings used to generate the plot, and some information on all the transmitters used.

14. Other plots are available (e.g. absolute accuracy and confidence factor) by selecting the appropriate option in the settings.

40

4. Appendix

4.0 File Type Description

When starting ArrayCreate or CPSCoverage, the following file types are defined, and given icons, allowing you to easily identify the type of file.

.CND   Ground Conductivity Database file. The file holds the ground conductivity data for a 10° x 10° region. The file name contains the coordinates of the south-west point of the 'tile'.

.DTK   Groundwave or skywave attenuation array for the Datatrak transmitter specified in the filename.

.INT   As .DTK, but for interferers instead.

.BAN   BANDPASS File. This file holds the results and settings of a coverage/performance analysis. For more information, see sections 2.1.3 and 2.1.4.

.F1 f_1 Interference Field Strength Layer. This is an array of the interference field strength at the f_1 frequency. There are different layers for trigger/data and navigation (due to different filters being used), and also for day and night.

.F2   As .F1, but for f_2.

.MAP   Vector data for map. The file holds the map data for a 10° x 10° region. The file name contains the coordinates of the south-west point of the 'tile'.

.FS1   Gridded f_1 field strength array generated using the Monteath method.

.FS2   As .FS1 but for f_2.

.PH1   Gridded f_1 phase delay array generated using the Monteath method.

.PH2   As .PH1 but for f_2.

.TER   Gridded terrain height information generated using the Monteath method.

.DT0   DTED Level 0 file.

.RAD   Monteath method radial file. See below for details.

41

4.1 Geoid.dat file format

The Geoid.dat file is used to provide the software with information on the geoids used in the Locator on different networks. It also provides the adjustment parameters to convert from the Locator geoid to WGS84 as used by the Monteath method. This is so that plots dependent on phase delay results are correct. This information below will allow you to add or modify the current geoid list.

Each line represents a different geoid type, and has the following space delimited format.

<Name of Geoid enclosed in double quotes> <Semi-major axis in m> <Flattening> <X offset from WGS84 in m> <Y offset from WGS84 in m> <Z offset from WGS84 in m> <X rotation in radians> <Y rotation in radians> <Z rotation in radians> <Scaling factor in ppm>

4.2 Radial File Format

Once the radial from the Monteath method have passed through the gridding process, they can be stored for later use, or even deleted. However, you may require some more detailed information along a specific path. The format of the space delimited radial file is given below for this purpose.

<Latitude of calculation point> <Longitude of calculation point> <Ground height in m> <Distance from transmitter in m> <ASF (not used)> <Secondary factor in μs> <Field strength in dB-μV/m> <Raw phase value in radians> <Sea water delay (not used)> <Ground conductivity in S/m> <Raw attenuation factor magnitude>

4.3 Monteath Transmitter Directory Structure

The directory structure shown below is relative to the 'Root directory for Transmitter Data' as defined in the Monteath options in ArrayCreate.

<transmitter name>	Root directory for the transmitter
<transmitter name>.fs1	f_1 Gridded field strength data
<transmitter name>.fs2	f_2 Gridded field strength data
<transmitter name>.ph1	f_1 Gridded phase delay data
<transmitter name>.ph2	f_2 Gridded phase delay data
\\height.ter	Gridded terrain height data
\\Radial.lst	Radial list file for transmitter
\\f1	Directory to hold f_1 radial files
\\asf*<number>*.rad	Radial files for f_1 signal
\\f2	Directory to hold f_2 radial files
\\asf*<number>*.rad	Radial files for f_2 signal

42